

PTCOG Report 1 (2010)

**PTCOG Publications Sub-Committee Task Group on
Shielding Design and Radiation Safety of Charged
Particle Therapy Facilities**

RC22 on Ion-Beam Therapy
20 September 2009

PTCOG REPORT 1: (Final version, January 15, 2010)

1
2
3
4
5
6
7
8
9
10
11
12
13
14
15
16
17
18
19
20
21
22
23
24
25
26
27
28
29
30
31
32
33
34
35
36
37
38
39
40
41
42
43
44
45
46
47
48

SHIELDING DESIGN AND RADIATION SAFETY OF CHARGED PARTICLE THERAPY FACILITIES

PTCOG Publications Sub-Committee Task Group:

N.E. Ipe (Leader), Consultant, Shielding Design, Dosimetry & Radiation Protection,
San Carlos, California, U.S.A.
G. Fehrenbacher, G.S.I. Darmstadt, Germany
I. Gudowska, Stockholm University, Sweden
H. Paganetti, Massachusetts General Hospital, Boston, Massachusetts, USA
J.M. Schippers, P.S.I, Villigen, Switzerland
S. Roesler, CERN, Geneva, Switzerland
Y. Uwamino, RIKEN, Saitama, Japan

Advisors

D. T. L. Jones, Proton Therapy Centre, Ružomberok, Slovak Republic
and Department of Human Biology, University Cape Town, South Africa
A. Mazal, Institut Curie, Paris, France
A. Smith, M.D. Anderson Cancer Center, Houston, Texas, U.S.A.

Consultants

S. Ban, Radiation Science Center, High Energy Accelerator Research Organization
(KEK), Japan
H. Yashima, Division of Nuclear Engineering Science, Research Reactor Institute, Kyoto
University, Japan

49	
50	
51	
52	
53	
54	
55	
56	
57	
58	
59	
60	
61	
62	
63	
64	
65	
66	
67	
68	
69	SHIELDING DESIGN AND RADIATION SAFETY OF CHARGED PARTICLE
70	THERAPY FACILITIES
71	

72	CONTENTS		
73			
74	ACKNOWLEDGEMENTS.....		ix
75	PREFACE.....		x
76	1. Introduction		1
77	1.1 Brief Overview of Charged Particle Therapy Facilities		1
78	1.2 Overview of Particle Accelerator Shielding		5
79	1.3 Dose Quantities and Conversion Coefficients		14
80	1.3.1 Protection and Operational Dose Quantities		14
81	1.3.2 Conversion Coefficients		19
82	1.4 Shielding Design and Radiation Safety		23
83	2. Radiological Aspects of Particle Therapy Facilities.....		24
84	2.1 Charged Particle Interactions.....		24
85	2.1.1 Electromagnetic Interactions of Charged Particles		25
86	2.1.1.1 Interaction of Charged Particles with Atomic Electrons		25
87	2.1.1.2 Interaction of Charged Particles with Nucleus		28
88	2.1.2 Nuclear Interactions.....		28
89	2.1.2.1 Nucleon-Nucleus Interactions		28
90	2.1.2.2 Heavy Ion-Nucleus Interactions		30
91	2.1.3 Hadron Interactions		34
92	2.1.3.1 Hadronic or Nuclear Cascade		34
93	2.1.3.2 Proton Interactions.....		37
94	2.1.4 Electromagnetic Cascade.....		39
95	2.2 Secondary Radiation Environment.....		39
96	2.2.1 Neutron Energy Classifications		40
97	2.2.2 Neutron Interactions		41
98	2.2.3 Protons: Neutron Yield, Energy Spectra, and Angular Distributions.....		43
99	2.2.4 Ions: Neutron Yields, Energy Spectra, and Angular Distribution		53
100	2.3 Beam Losses and Sources of Radiation.....		59
101	2.3.1 Cyclotrons.....		59
102	2.3.1.1 Energy Selection System (ESS)		62
103	2.3.2 Synchrotrons.....		64
104	2.3.3 Beam Transport Line		68
105	2.3.4 Treatment Rooms		68
106	2.3.4.1 Fixed Beam Rooms		69
107	2.3.4.2 Gantry Rooms.....		71
108	2.3.5 Beam Shaping and Delivery		71
109	2.4 New Technologies		72
110	2.4.1 Single-Room Systems.....		72
111	2.4.2 FFAG		79
112	2.4.3 Laser Acceleration		79

113	3. Shielding Design Considerations	81
114	3.1 Regulatory Requirements	81
115	3.1.1 Radiological Areas	82
116	3.1.2 Dose Limits for Various Countries	86
117	3.2 Primary and Secondary Shielding Barriers	88
118	3.3 Use Factors	88
119	3.4 Occupancy Factor	89
120	3.5 Workload	90
121	3.5.1 Example for Workload Calculations and Usage Assumptions	92
122	3.5.2 Beam Parameters Used for Shielding Calculations	95
123	3.6 Self-Shielding of Beam Line Components	100
124	3.7 Calculational Methods	100
125	3.7.1 Analytical Methods	100
126	3.7.2 Monte Carlo Calculations	104
127	3.7.3 Monte Carlo Computational Models	105
128	3.7.3.1 Carbon Ions	106
129	3.7.3.2 Protons	116
130	3.7.4 Other codes	118
131	3.8 Shielding Materials and Transmission	118
132	3.8.1 Shielding Materials	118
133	3.8.1.1 Earth	119
134	3.8.1.2 Concrete and Heavy Concretes	119
135	3.8.1.3 Steel	123
136	3.8.1.4 Polyethylene and Paraffin	123
137	3.8.1.5 Lead	124
138	3.8.2 Transmission	124
139	3.8.3 Verification of Density and Composition	132
140	3.8.3.1 Density	132
141	3.8.3.2 Composition	132
142	3.8.4 Joints, Cracks, and Voids	133
143	3.8.5 Rebar and Form Ties	133
144	3.9 Special Topics	134
145	3.9.1 Mazes	134
146	3.9.2 Penetrations and Ducts	137
147	3.9.3 Skyshine and Groundshine	140
148	3.10 Examples for Existing Facilities	144
149	3.10.1 Facilities for Proton Therapy	144
150	3.10.1.1 Loma Linda, CA, USA	144
151	3.10.1.2 Massachusetts General Hospital (MGH), Boston, MA, USA	147
152	3.10.1.3 National Cancer Center (NCC), Republic of Korea	149
153	3.10.1.4 Rinecker Proton Therapy Center, Munich, Germany	151
154	3.10.1.5 Paul Scherrer Institute (PSI), Switzerland	153
155	3.10.1.6 Proton Medical Research Center, Tsukuba, Japan	155
156	3.10.2 Facilities for Proton Therapy and Heavy Ion Therapy	157
157	3.10.2.1 Heavy Ion Medical Accelerator in Chiba (HIMAC), Japan	157
158	3.10.2.2 Gunma University, Japan	161
159	3.10.2.3 CNAO, Pavia, Italy	165
160	3.10.2.4 HIT, Heidelberg, Germany	167

161	3.11 Qualified Expert	170
162	3.11.1 Schematic Design	171
163	3.11.2 Design Development	172
164	3.11.3 Construction Documentation	172
165	3.11.4 Construction Inspection	173
166	3.12 Shielding Report	173
167	3.13 Shielding Integrity Radiation Survey	174
168	4. Radiation Monitoring	176
169	4.1 Introduction	176
170	4.1.1 Operational Quantities	176
171	4.2 Prompt Radiation Monitoring	179
172	4.2.1 Characteristics of Prompt Radiation Field	179
173	4.2.1.1 Mixed Field	179
174	4.2.1.2 Pulsed Field	183
175	4.2.1.3 Noise	184
176	4.2.1.4 Magnetic Field	185
177	4.2.1.5 Radiations Unrelated to Beam Acceleration	185
178	4.2.2 Survey Meters	185
179	4.2.2.1 Neutron Survey Meters	185
180	4.2.2.1.1 Rem Meter	186
181	4.2.2.1.2 Proton Recoil Scintillation Counter	189
182	4.2.2.2 Photon Survey Meters	189
183	4.2.2.2.1 Ionization Chamber	189
184	4.2.2.2.2 NaI(Tl) Scintillator	189
185	4.2.3 Spectrometers	190
186	4.2.3.1 Photon Spectrometer	190
187	4.2.3.2 Neutron Spectrometer	190
188	4.2.3.3 LET Spectrometer	194
189	4.2.4 Area Monitors	194
190	4.2.5 Passive Monitoring	196
191	4.3 Measurement of Residual Radioactivity	198
192	4.3.1 Introduction	198
193	4.3.2 Ionization Chamber	199
194	4.3.3 NaI(Tl) Scintillators	199
195	4.3.4 Geiger-Müller Tube	200
196	4.3.5 Other Survey Meters for Contamination Measurement	200
197	4.4 Individual Monitoring	201
198	4.4.1 Introduction	201
199	4.4.2 Active Dosimeter	202
200	4.4.3 Passive Dosimeter	203
201	4.4.3.1 Thermoluminescence Dosimeter (TLD)	203
202	4.4.3.2 Optically Stimulated Luminescence (OSL) Dosimeter	204
203	4.4.3.3 Glass Dosimeter	204
204	4.4.3.4 Direct Ion Storage (DIS) Dosimeter	204
205	4.4.3.5 Solid State Nuclear Track Detector	205
206	4.4.3.6 Film Dosimeter	205
207	4.5 Calibration	206

208	4.5.1	Introduction	206
209	4.5.2	Calibration of Ambient Dose Monitor.....	207
210	4.5.2.1	Calibration of Photon Monitor	207
211	4.5.2.2	Calibration of Neutron Monitor.....	208
212	4.5.3	Calibration of Individual Monitors.....	209
213	5.	Activation	211
214	5.1	Introduction	211
215	5.1.1	Activation Reactions.....	212
216	5.1.2	Activation and Decay	217
217	5.2	Accelerator Components.....	219
218	5.2.1	Residual Activity Induced by Primary Particles.....	219
219	5.2.1.1	Residual Activities in Al, Cr, Fe, Ni, Cu.....	220
220	5.2.1.2	Mass-Yield Distribution of Residual Activities in Cu.....	222
221	5.2.1.3	Spatial Distribution of Residual Activities with Cu Target Depth	224
222	5.2.1.4	Total Residual Activity Estimation Induced in Cu Target	226
223	5.2.1.5	Gamma-Ray Dose Estimation from Residual Activity in Cu Target	230
224	5.2.2	Residual Activities Induced by Secondary Neutrons	233
225	5.3	Concrete.....	237
226	5.4	Cooling and Groundwater	245
227	5.4.1	Activation Cross Sections.....	245
228	5.4.2	Effects of Water Activation.....	249
229	5.5	Air.....	250
230	5.5.1	Activation Cross Sections.....	250
231	5.5.2	Estimation of Concentration of Air Activation	253
232	5.5.2.1	Radionuclide Concentrations of Exhaust Air	253
233	5.5.2.2	Radionuclide Concentrations of Room Air	254
234	6.	Monte Carlo Codes for Particle Therapy.....	255
235	6.1	General-Purpose Codes	255
236	6.2	Areas of Application.....	256
237	6.2.1	Shielding Studies and Secondary Doses to the Patient.....	256
238	6.2.2	Activation Studies.....	257
239	6.3	Requirements	258
240	6.3.1	Shielding Studies	258
241	6.3.2	Activation Studies.....	260
242	6.3.3	Secondary Doses to Patients.....	261
243	6.3.4	User-Friendliness.....	262
244	6.4	Overview of the Most Commonly Used Codes.....	262
245	6.4.1	FLUKA.....	262
246	6.4.2	GEANT4.....	264
247	6.4.3	MARS15.....	265
248	6.4.4	MCNPX	267
249	6.4.5	PHITS	268
250	6.4.6	SHIELD/SHIELD-HIT.....	269
251	7.	Patient Dose from Secondary Radiation.....	272

252	7.1 Sources of Secondary Radiation	273
253	7.1.1 Secondary Particles Produced in the Beam-Line Elements	273
254	7.1.2 Secondary Particles Produced in the Patient	275
255	7.2 Out of Treatment Field Absorbed Dose to Patients (Secondary Dose)	278
256	7.2.1 Experimental Methods	278
257	7.2.2 Calculation Methods (Monte Carlo Techniques)	279
258	7.2.3 Human Phantoms	282
259	7.3 Results of Measurements of Secondary Doses in Particle Therapy	288
260	7.4 Results for Calculated Secondary Doses to Patients	291
261	7.5 Biological Effects of Secondary Particles (Low- and High-LET Particles, Low Doses)	304
262	7.6 Concept of Equivalent Dose to Patient Due to Secondary Particles	306
263	7.6.1 Radiation Weighting Factors	306
264	7.6.2 Equivalent Dose	308
265	7.7 Early and Late Effects	309
266	7.8 Models	312
267	7.8.1 Model Concepts	313
268	7.8.2 Dose-Response Relationships	317
269	7.9 Risks of Radiation-Induced Secondary Cancers in Particle Therapy	319
270	7.10 Uncertainties and Limitations of Risks Estimations	325
271	7.11 Summary and Conclusion	327
272	8. Safety Systems and Interlocks	329
273	8.1 Introduction	329
274	8.1.1 Safety Requirements	333
275	8.1.2 Safety Standards	334
276	8.1.3 Risk Analysis	335
277	8.1.4 Interlock Analysis and Reset	336
278	8.1.5 Quality Assurance	339
279	8.2 Methods of Turning off the Beam	340
280	8.2.1 Beam Interrupting Components	341
281	8.2.2 Use of the Different Beam Interrupting Components	345
282	8.3 Control Systems, Mastership, and Facility Mode	350
283	8.3.1 Control Concept	351
284	8.3.2 Separation of Systems	353
285	8.3.3 Facility Modes	355
286	8.3.4 Treatment Procedure and Typical Operator Actions	355
287	8.3.5 Hardware	357
288	8.4 Personnel Safety System	358
289	8.4.1 Purpose	359
290	8.4.2 Modes of Operation	360
291	8.4.3 Rules of Beam Turn-Off	363
292	8.4.4 Functional Implementation	363
293	8.4.5 Components	364
294	8.4.5.1 Area Access Control	364
295	8.4.5.2 Detectors	367
296	8.5 Patient Safety System	367
297	8.5.1 Purpose	368
298	8.5.2 Functional Requirements	369

299	8.5.3	Description of System	371
300	8.5.4	Components of the Patient Safety System (PaSS).....	373
301	8.5.4.1	Main Patient Safety Switch and Controller (MPSSC).....	376
302	8.5.4.2	Local PaSS.....	376
303	8.5.4.3	Emergency OR Module.....	377
304	8.5.4.4	Detectors and Safety-Relevant Signals from Various Components.....	377
305	8.5.4.5	Electronics, Hardware, and Firmware.....	378
306	8.5.5	Implementation of the PaSS for Dose Application and Spot Scanning	378
307	8.5.6	Rules for Turning the Beam Off.....	379
308	8.5.7	Quality Assurance.....	383
309	8.6	Machine Safety: Run Permit System.....	384
310	8.6.1	Purpose	384
311	8.6.2	Functional Requirements.....	385
312	8.6.3	Description of System	386
313	8.6.4	Components and Conditions That Are Checked	388
314	8.6.5	High-Reliability Components and Fail-Safe Design.....	388
315	8.6.6	Rules for Turning the Beam Off.....	389
316	8.6.7	Tests and Quality Assurance (QA).....	390
317		Glossary	392
318		References	398
319			
320			

321

ACKNOWLEDGEMENTS

322

323 Dr. Nisy Elizabeth Ipe notes, "Sincere gratitude is expressed to the task group members for all
324 their outstanding work and great efforts in writing the chapters and reviewing the report: to the advisors
325 for reviewing the report; to the consultants for their contribution to Chapter 5; to Kory Stamper for her
326 outstanding and timely editorial assistance; to Al Smith for his unwavering support and encouragement;
327 and to the PTCOG Publications Subcommittee for giving me the opportunity to lead this effort."

328

329 Dr. Yoshitomo Uwamino would like to thank Prof. S. Ban, High Energy Accelerator Research
330 Organization (KEK), and Dr. H. Yashima, Kyoto Univ. Research Reactor Institute, for their invaluable
331 assistance in the writing of Chapter 5.

332

333 Dr. Jacobus Maarten Schippers notes, "At PSI, many people have been involved in the conceptual
334 design and building of the systems described here and in understand the regulations. B. Amrein, A.
335 Coray, G. Dzieglewski, A. Fuchs, C. Hilbes, M. Hofer, T. Korhonen, A. Mezger, and W. Roser are
336 acknowledged for their help with the preparation of this overview and their valuable input and feedback.
337 Based on the pioneering work of E. Pedroni, several of these people, as well as E. Egger, T. Lomax, M.
338 Grossmann, G. Goitein, the group of S. Hirschberg, I. Jirousek, M. Rejzek, J. Verwey, and many others
339 have contributed to the design of the concepts, analysis of risks, and the realization of the now working
340 systems."

341

342

PREFACE

343

344 The current report on shielding and radiation protection for charged particle therapy facilities is
345 the first report produced by the Publications Subcommittee of the Particle Therapy Co-Operative Group
346 (PTCOG). The PTCOG Publications Subcommittee was authorized at the PTCOG 46 Steering
347 Committee meeting in Wanjie, China, and has the following membership:

348

349 Co-Chairpersons: Al Smith and Erik Blomquist

350

351 Members: Masayuki Mumada

352

Takashi Ogino

353

Thomas Delaney

354

Eugen Hug

355

Carl Rossi

356

Thomas Bortfeld

357

358 De Facto Members: Hirohiko Tsujii, PTCOG Steering Committee Chariman

359

Martin Jermann, PTCOG Secretary/Treasurer

360

361 The Publications Subcommittee was charged with defining topics of interest to PTCOG members
362 and establishing Task Groups to develop reports on such topics. The first Task Group to be established
363 was Task Group I: Shielding Design and Radiation Protection of Charged Particle Therapy Facilities.
364 The Task Group has the following members:

365

366 Task Group Leader: Nisy Ipe, Shielding Consultant, San Carlos, CA USA

367

368

Task Group Members:

369

Georg Fehrenbacher, G.S.I., Darmstadt, Germany

370

Irena Gudowska, Stockholm University, Sweden

371

Harald Paganetti, Francis H. Burr Proton Therapy Center, Boston, MA, US

372

Jacobus Maarten Schippers, P.S.I., Switzerland

373

Stefan Roesler, CERN, Switzerland

374

Yoshitomo Uwamino, RIKEN, Japan

375

376

Task Group Advisers

377

Dan Jones, iThema Laboratory, S. Africa

378

Alejandro Mazal, Institut Curie, France

379

Al Smith, M. D. Anderson Cancer Center, USA

380

381

Consultants

382

Shuichi Ban, Radiation Science Center, High Energy Accelerator Research

383

Organization (KEK), Japan

384

Hiroshi Yashima, Division of Nuclear Engineering Science, Research Reactor

385

Institute, Kyoto University, Japan

386

387

The topic of shielding and radiation protection was proposed by a number of PTCOG members

388

and was deemed to be important to all particle therapy facilities. The topic is, however, somewhat

389

difficult to address due to the variety of particle accelerators, treatment delivery systems, and regulations

390

encountered throughout the world. Because of these differences, some of the material in the report is, by

391

necessity, more general than would have been the case if specific circumstances were being addressed.

392

393 We have tried, as far as possible, to describe modern and up-to-date methodology, procedures,
394 and instrumentation used in shielding calculations and radiation measurements. That said, we have not
395 attempted to be exhaustive and therefore have not covered every possible technique and every new
396 technology. We have focused on the “tried and proven” with the assumption that this approach would
397 provide the most useful document for particle therapy users and developers. It is our intent, however, to
398 periodically update the document in order to keep it current with the latest thinking experience and
399 technologies. The document is being published electronically and is available on the PTCOG web site:
400 <http://ptcog.web.psi.ch>.

401

402 We encourage PTCOG members, and others, to send comments, critiques, and corrections to the
403 address specified in the PTCOG Publication Subcommittee link on the PTCOG web site. We will
404 attempt to address corrections in a timely manner. Comments and critiques will be addressed as time
405 permits.

406

407 I am greatly appreciative of the work done by each of the Task Group members, consultants, and
408 reviewers. Everyone involved in the production of this document has been a volunteer and therefore has
409 not received any tangible compensation for their work. Everyone reading the document will realize that a
410 tremendous amount of work went into each individual effort. I especially want to thank Nisy Ipe who
411 organized and led this tremendous effort. The document was brought to conclusion on time and on zero
412 budget (except for the services of the editorial assistant), in spite of the demands of her private consulting
413 business. I would also like to acknowledge Kory Stamper for the editorial assistance.

414

415 Now that this initial effort has been brought to a successful conclusion, the Publications
416 Subcommittee intends to identify other topics of general interest to the PTCOG community and publish
417 additional reports. We look forward to your feedback and assistance.

418

419

Al Smith

420

September 2009

421

1. Introduction

422

Nisy Elizabeth Ipe

423

424

1.1 Brief Overview of Charged Particle Therapy Facilities

425

426 Charged particle therapy facilities might use protons and various ions such as helium, lithium,
427 boron, carbon, nitrogen, oxygen, neon, and argon to treat malignant and nonmalignant diseases. Particle
428 energies are required that allow penetration of 30 cm or more in tissue. In this report, the primary
429 emphasis will be on protons and carbon ions. There are currently about thirty operational particle therapy
430 facilities (both proton and carbon) worldwide (PTCOG, 2009). Another twenty-three facilities or so are
431 in the planning, design, or construction stage at the time of writing this report.

432

433 A typical large particle therapy (PT) facility might consist of an injector, a cyclotron or a
434 synchrotron to accelerate the particles, a high-energy beam transport line, several treatment rooms
435 including fixed beam and 360° gantry rooms, and, often, a research area (ICRU, 2007). Recently, single-
436 room therapy systems with a synchrocyclotron integrated in the treatment room have also become
437 available. These and other novel technologies are discussed in Chapter 2. Several vendors offer single-
438 room systems with the accelerator outside the treatment room; such facilities usually have the ability to
439 add additional treatment rooms in future facility expansions. For both cyclotron- and synchrotron-based
440 systems, dose rates of 1 to 2 Gy/min are typically used for patient treatment using “large” fields in the
441 order of 30 cm x 30 cm. Special beam lines devoted to eye treatments use dose rates in the order of 15 to
442 20 Gy/min but for smaller fields of about 3 cm diameter. There are a few systems used specifically for
443 radiosurgery techniques that use dose rates and field sizes intermediate to those for large field treatments
444 and eye treatments.

445

446 During the operation of particle therapy facilities, secondary radiation is produced at locations
447 where beam losses occur. Such losses may occur in the synchrotron and cyclotron along the beam line
448 during injection, acceleration, extraction, energy degradation, and transport of the particles in the beam
449 line to the treatment room, and in the beam shaping devices in the treatment nozzle. In addition, the
450 deposition of beam proton interactions in the patient, beam stop, or dosimetry phantom also results in
451 radiation production. Thus, the entire facility requires shielding. The interaction of protons and carbon
452 ions with matter results in “prompt” and “residual” radiation. Prompt radiation persists only during the
453 time that the beam is present. Residual radiation from activation continues after the beam is shut off. For
454 charged particle therapy facilities, neutrons dominate the prompt radiation dose outside the shielding.

455

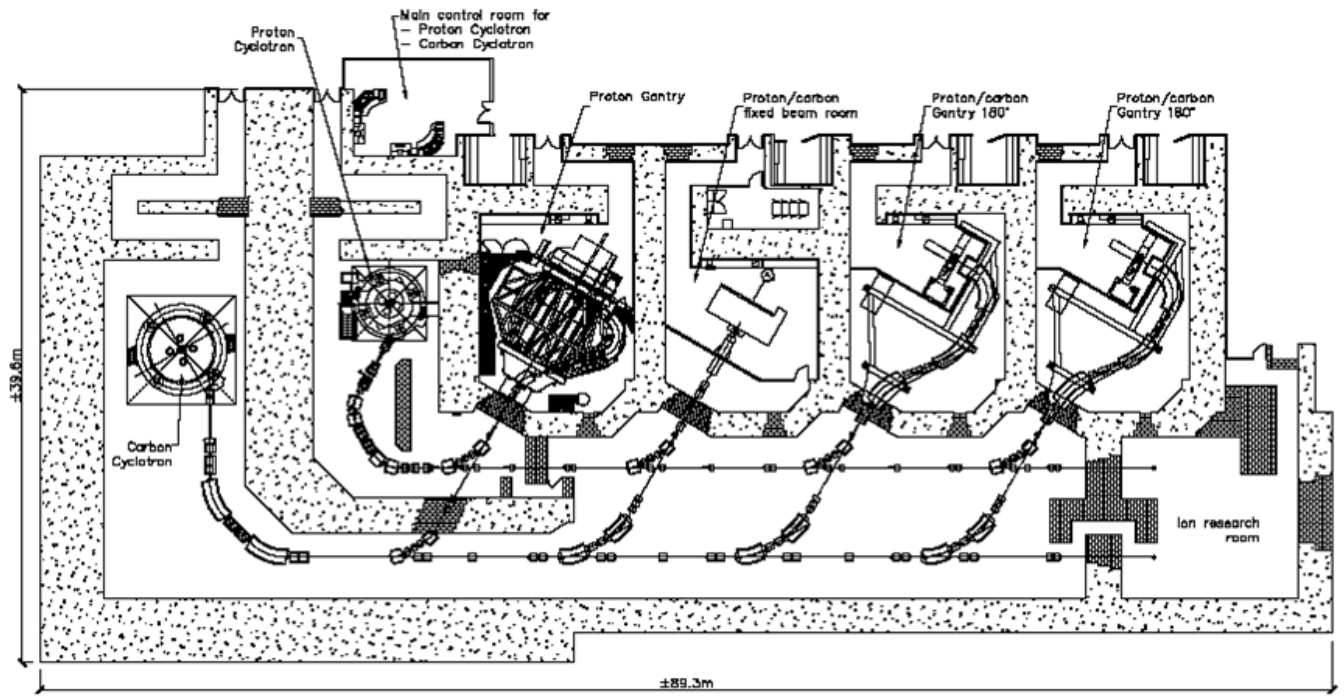
456 Proton energies in therapy facilities typically range from about 230 MeV to 250 MeV, while
457 carbon ions may have maximum energies of 320 MeV u^{-1} to 430 MeV u^{-1} . For ions, it is customary to use
458 the specific energy defined as the ratio of the total energy to the atomic mass number (MeV amu^{-1} or
459 MeV u^{-1}) (NCRP, 2003). The specific energy is generally considered equivalent to the kinetic energy per
460 nucleon. Because there are 12 carbon nucleons the total energy available for interactions is 5.16 GeV for
461 430 MeV u^{-1} carbon ions. Thus, the maximum neutron energy will exceed 430 MeV in this case. For
462 carbon ion beams, the maximum energy of the neutrons is approximately two times the energy of the
463 carbon ion (Kurosawa *et al.*, 1999). For proton beams, the neutron energies extend to a maximum, which
464 is the energy of the incident proton.

465

466 Figure 1.1 shows a schematic of a cyclotron-based PT facility capable of accelerating protons or
467 carbon ions. Figure 1.2 shows an example of a synchrotron-based PT facility.

468

469



470

471

472 Figure 1.1. Schematic of a cyclotron-based particle therapy facility (Courtesy of IBA¹)

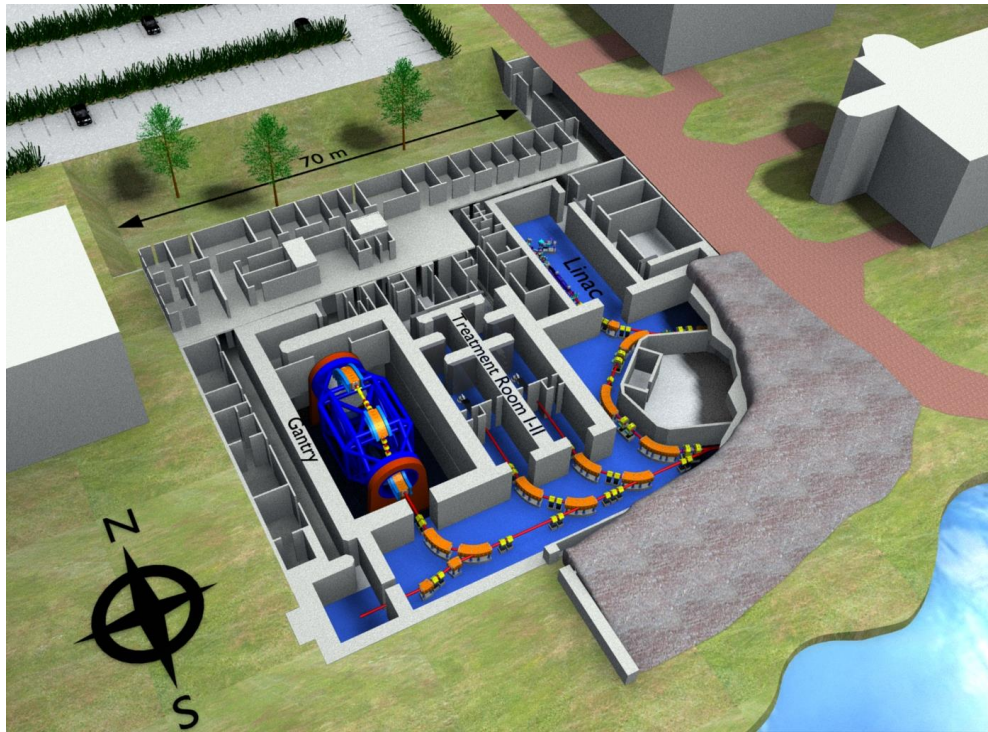
473

¹ Ion Beam Applications, Belgium

474

475

476



477

478 Figure 1.2. Heidelberg Ion Therapy Center (Courtesy of G. Fehrenbacher)

479

480

1.2 Overview of Particle Accelerator Shielding

481

482 The history of particle accelerator shielding dates back to the 1930s, with the construction and
483 operation of particle accelerators at Cambridge by Cockroft and Walton, and at Berkeley by Lawrence
484 and Livingstone (Stevenson, 1999; IAEA, 1988). The early accelerators were of low energy and
485 intensity, and many of them were constructed underground. However, as larger accelerators producing
486 particles with much higher energies were developed (*e.g.*, the Cosmotron at Brookhaven and the
487 Bevatron at Berkeley), knowledge of the prompt radiation fields and the requirements for effective
488 shielding design became necessary. An understanding of the generation of prompt and residual radiation
489 requires knowledge of the nuclear reactions that occur in the energy range of interest. These are
490 discussed in Chapter 2.

491

492 The prompt radiation field produced by protons (67 MeV to 250 MeV) encountered in proton
493 therapy is quite complex, consisting of a mixture of charged and neutral particles as well as photons.
494 When these protons react with matter, a hadronic or nuclear cascade (spray of particles) is produced in
495 which neutrons have energies as high as the proton energy (ICRU, 2000). Further discussion can be
496 found in Chapter 2. This high-energy component with neutron energies (E_n) above 100 MeV propagates
497 the neutrons through the shielding; and continuously regenerates lower-energy neutrons and charged
498 particles at all depths in the shield *via* inelastic reactions with the shielding material (Moritz, 2001).
499 Thus, the neutron energy distribution consists of two components, high-energy neutrons produced by the
500 cascade and evaporation neutrons with energy peaked at ~ 2 MeV. The high-energy neutrons are forward
501 peaked but the evaporation neutrons are isotropic. The highest-energy neutrons detected outside the
502 shielding are those that arrive without interaction, or that have undergone only elastic scattering or direct
503 inelastic scattering with little loss of energy, and a small change in direction. Low-energy neutrons and
504 charged particles detected outside the shielding are those that have been generated at the outer surface of

505 the shield. Thus, the yield of high-energy neutrons ($E_n > 100$ MeV) in the primary collision of the
506 protons with the target material determines the magnitude of the prompt radiation field outside the shield
507 for intermediate-energy protons. The high-energy neutrons are anisotropic and are forward peaked. In the
508 therapeutic energy range of interest, the charged particles produced by the protons will be absorbed in
509 shielding that is sufficiently thick to protect against neutrons. Thus, neutrons dominate the radiation field
510 outside the shielding. Degraded neutrons might undergo capture reactions in the shielding, giving rise to
511 neutron-capture gamma rays.

512

513 The prompt radiation field produced by carbon ions is also dominated by neutrons with much
514 higher energies than is the case with protons. Dose contributions from pions, protons, and photons are
515 significantly lower than from neutrons. Additional information is provided in Chapter 2.

516

517 The goal of shielding is to attenuate secondary radiation to levels that are within regulatory or
518 design limits for individual exposure, and to protect equipment from radiation damage, which should be
519 done at a reasonable cost and without compromising the use of the accelerator for its intended purpose
520 (Stevenson, 2001). This requires knowledge of the following parameters (Ipe, 2008), some of which are
521 discussed in detail in Chapter 3.

522

- 523 1. Accelerator type, particle type, and maximum energy
- 524 2. Beam losses and targets
- 525 3. Beam-on time
- 526 4. Beam shaping and delivery
- 527 5. Regulatory and design limits
- 528 6. Workload, including number of patients to be treated, energies for treatment, field sizes,
529 dose per treatment

530 7. Use factors

531 8. Occupancy factors

532

533 There are several powerful computer codes discussed in Chapter 6 that are capable of providing
 534 detailed spatial distributions of dose equivalent outside the shielding. However, it is often desirable to
 535 perform simpler calculations, especially during the schematic design of the facility. Shielding can be
 536 estimated over a wide range of thicknesses by the following equation for a point source, which combines
 537 the inverse square law and an exponential attenuation through the shield, and is independent of geometry
 538 (Agosteo *et al.*, 1996a):

$$539 \quad H(E_p, \theta, d/\lambda(\theta)) = \frac{H_0(E_p, \theta)}{r^2} \exp\left[-\frac{d}{\lambda(\theta)g(\theta)}\right] \quad (1.1)$$

540 where:

541 H is the dose equivalent outside the shielding;

542 H_0 is source term at a production angle θ with respect to the incident beam and is assumed
 543 to be geometry independent;

544 E_p is the energy of the incident particle;

545 r is the distance between the target and the point at which the dose equivalent is scored;

546 d is the thickness of the shield;

547 $d/g(\theta)$ is the slant thickness of the shield at an angle θ ;

548 $\lambda(\theta)$ is the attenuation length for dose equivalent at an angle θ and is defined as the
 549 penetration distance in which the intensity of the radiation is attenuated by a factor of e ;

550 $g(\theta) = \cos\theta$ for forward shielding;

551 $g(\theta) = \sin\theta$ for lateral shielding;

552 $g(\theta) = 1$ for spherical geometry.

553

554 Approximation of the radiation transmission by an exponential function works well over a limited
555 range of thickness (NCRP, 2003). The attenuation length is usually expressed in cm (or m) and in g cm^{-2}
556 (or kg m^{-2}) when multiplied by the density (ρ) and will be referred to hereafter as λ . For thicknesses (ρd)
557 that are less than $\sim 100 \text{ g cm}^{-2}$, the value of λ changes with increasing depth in the shield because the
558 “softer” radiations are more easily attenuated, and the neutron spectrum hardens. Figure 1.3 shows the
559 variation of attenuation length ($\rho\lambda$) for monoenergetic neutrons in concrete as a function of energy. The
560 attenuation length increases with increasing neutron energy at energies greater than $\sim 20 \text{ MeV}$. In the
561 past, it has typically been assumed that the attenuation length reaches a high-energy limiting value of
562 about 120 g cm^{-2} , even though the data in Fig. 1.3 show a slightly increasing trend above 200 MeV .

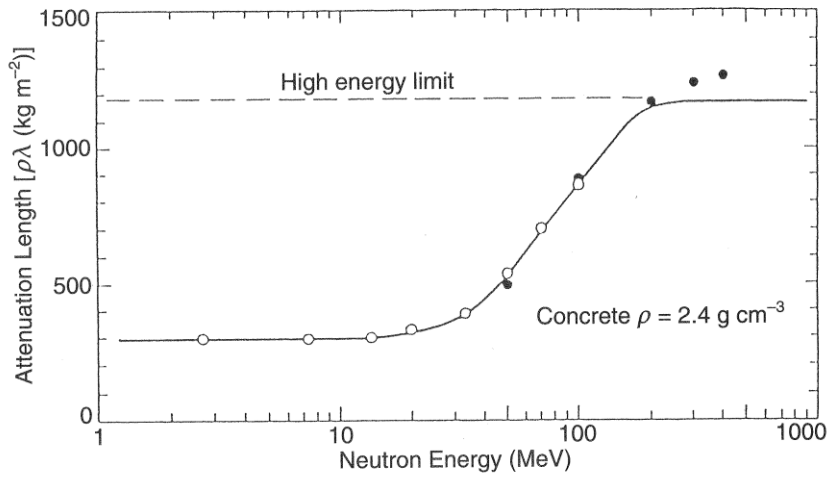
563
564 Figures 1.4a and 1.4b show the comparison of neutron dose attenuation lengths measured at
565 various facilities, for concrete and iron, respectively, as a function of the effective maximum energy
566 (E_{max}) of the source neutrons, for neutrons with energies from thermal to maximum. Figures 1.5a and
567 1.5b show the comparison of neutron dose attenuation lengths measured at various facilities, for concrete
568 and iron, respectively, as a function of the effective maximum energy (E_{max}) of the source neutrons, for
569 neutrons with energies greater than 20 MeV . As expected, the attenuation lengths in the latter case are
570 larger than for neutrons with energies greater than thermal energy. The experiments are described in a
571 paper by Nakamura and include measurements for E_{max} ranging from 22 MeV to 700 MeV , and various
572 production angles for a variety of neutron sources (Nakamura, 2004). Table 1.1 summarizes the site and
573 properties of the neutron source, shielding material, and the detectors. According to Nakamura, the
574 measured neutron dose attenuation length (thermal to maximum energy) for concrete lies between 30 g
575 cm^{-2} and 40 g cm^{-2} from about 22 MeV to 65 MeV in the forward direction and then gradually increases
576 above 100 MeV to a maximum value of about 130 g cm^{-2} , which may be the high-energy limit. For 400
577 MeV u^{-1} carbon ions, the measured attenuation length in the forward direction for concrete (0°
578 production angle) for a maximum neutron energy of 700 MeV is $126 \pm 9 \text{ g cm}^{-2}$, while the calculated

579 value is $115.2 \pm 9 \text{ g cm}^{-2}$. The corresponding measured and calculated attenuation lengths for iron in the
580 forward direction were $211 \pm 9 \text{ g cm}^{-2}$, and $209.2 \pm 1.5 \text{ g cm}^{-2}$, respectively. Monte Carlo calculations by
581 Ipe and Fasso (Ipe and Fasso, 2006) yielded a total dose (from all particles) attenuation length in the
582 forward direction of $123.8 \pm 0.5 \text{ g cm}^{-2}$ for 430 Mev u^{-1} carbon ions in concrete. Steel is much more
583 effective than concrete for the shielding of high-energy neutrons. It is important to note that, in addition
584 to energy and production angle (θ), λ also depends upon the material composition and density. Monte
585 Carlo calculations by Ipe indicate that, for concrete, shielding for 250 MeV protons in the forward
586 direction can differ by about 30 cm for shielding thicknesses of the order of 2 m to 3 m when two
587 concretes with the same density but differing compositions are used. Thus, all concretes will not have the
588 same λ at a given angle and energy, and the differences can be quite pronounced, especially in the
589 forward direction for concretes with different compositions and densities. More information on shielding
590 is provided in Chapter 3.

591

592

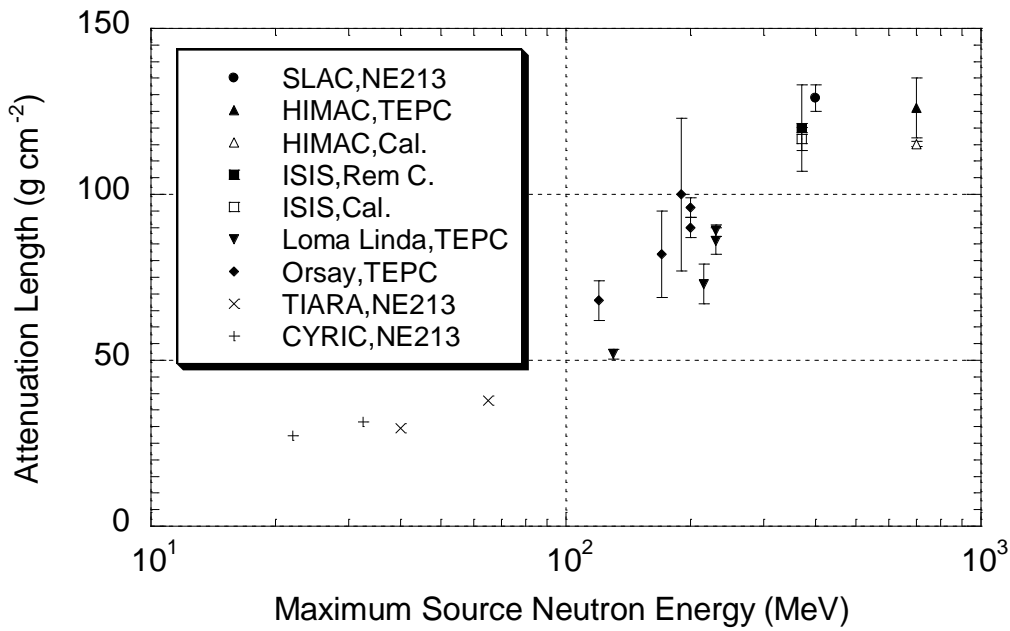
593



594

595 Figure 1.3. The variation of attenuation length ($\rho\lambda$) for monoenergetic neutrons in concrete of density ρ
596 = 2400 kg m^{-3} (NCRP, 2003). Reprinted with permission of the National Council on Radiation Protection
597 and Measurements, <http://NCRPonline.org>

598

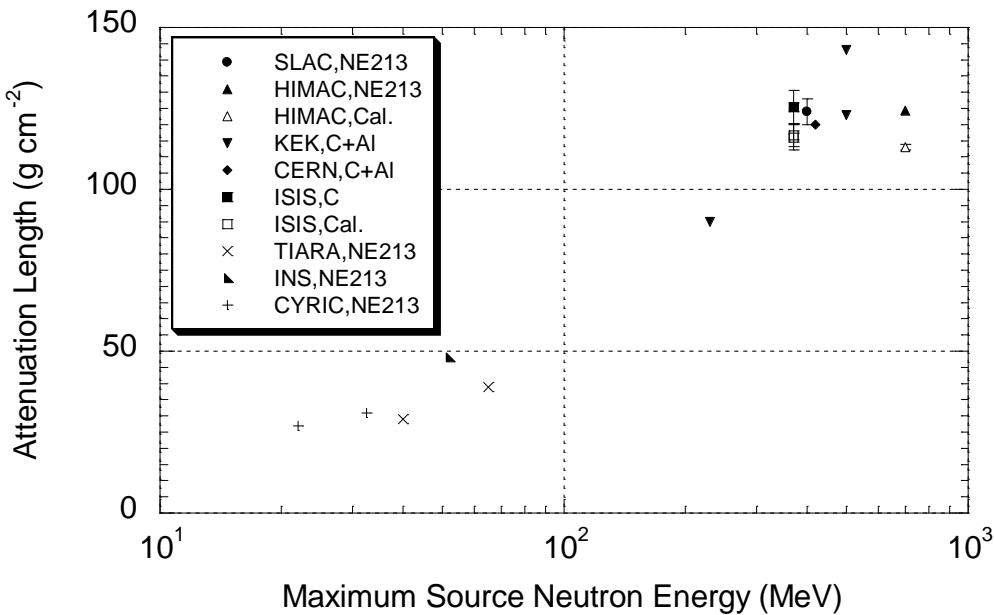


599

600 Figure 1.4a. Comparison of measured neutron dose attenuation lengths in concrete for neutrons of
 601 energy from thermal to maximum source energy (Nakamura, 2004)

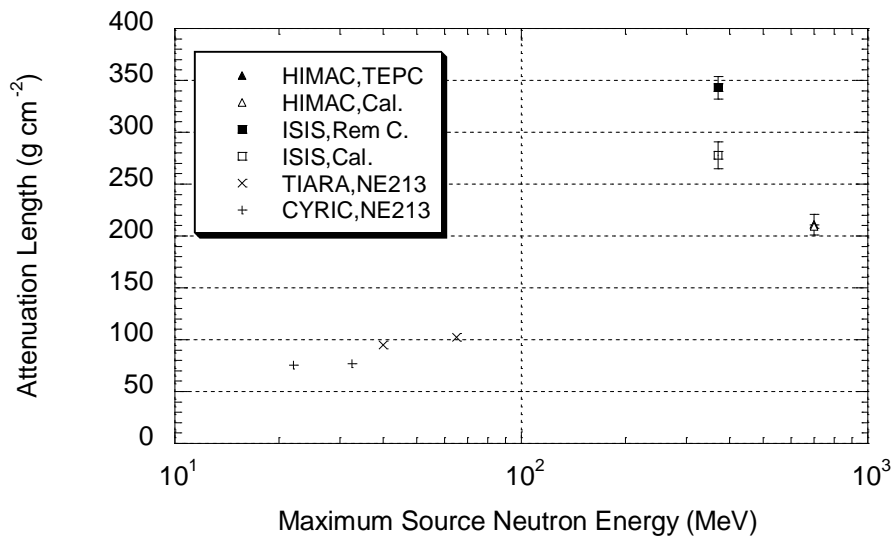
602

603



604

605 Figure 1.4b. Comparison of measured neutron dose attenuation lengths in concrete for neutrons of energy
 606 greater than 20 MeV (Nakamura, 2004)

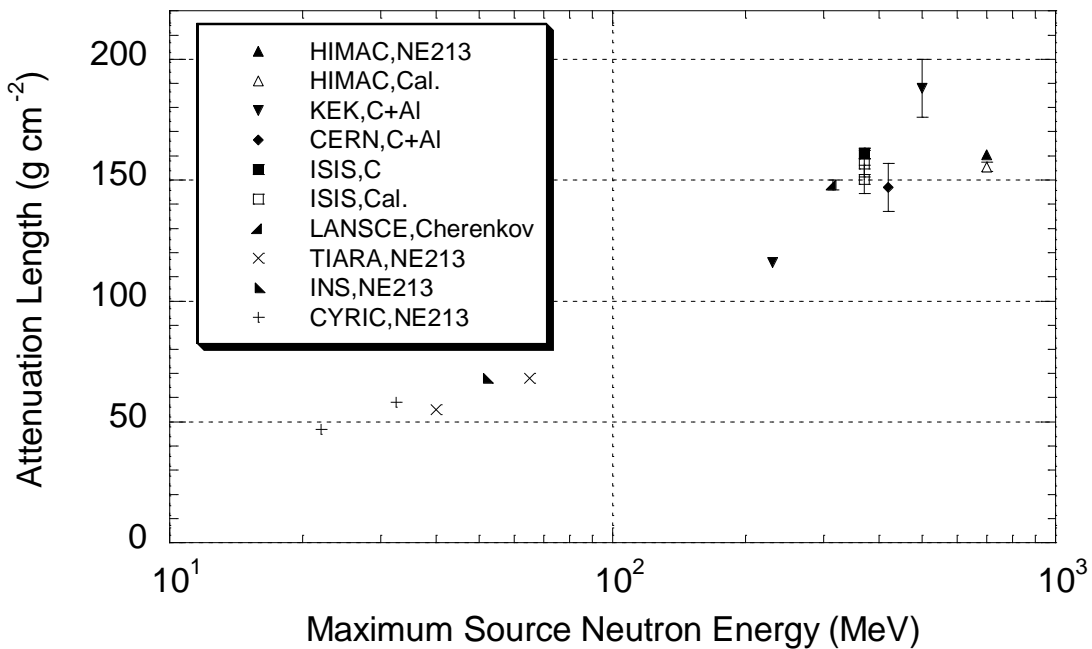


607

608 Figure 1.5a. Comparison of measured neutron dose attenuation lengths in iron for neutrons with energy
 609 from thermal to maximum source energy (Nakamura, 2004)

610

611



612

613 Figure 1.5b. Comparison of measured neutron dose attenuation lengths in iron for neutrons with energy
 614 greater than 20 MeV (Nakamura, 2004)

615

616

617 Table 1.1. Summary of site, neutron source, shielding material, and detector properties

618

Site	Projectile	Target (thickness)	Neutron source and measured angle	Shield material (thickness)	Detector
Cyclotron and Radioisotope Center (CYRIC), Tohoku University, Japan	25 , 35 MeV proton	Li (2 mm)	Quasi-monoenergetic collimated beam at 0°	Concrete (10 cm to 40 cm) Iron (25 cm to 100 cm)	NE213 proton recoil proportional counter Bonner Ball with ³ He counter
TIARA proton cyclotron facility, Japan Atomic Energy Research Institute (JAERI), Japan	43 MeV proton	Li (3.6 mm)	Quasi-monoenergetic collimated beam at 0°	Concrete (25 cm to 200 cm) Iron (10 to 30 cm)	BC501A Bonner Ball with ³ He counter
	68 MeV proton	Li (5.2 mm)			
Loma Linda University Medical Center, U.S.A.	230 MeV proton	Al, Fe, Pb (stopping length, 10.2- cm diameter)	White spectrum (0°, 22°, 45°, 90°)	Concrete (39 g cm ⁻² 515 g cm ⁻² , 1.88 g cm ⁻³ density)	Tissue Equivalent Proportional Counter (TEPC)
Orsay Proton Therapy Center, France	200 MeV proton	Al (15 cm long, 9 cm diameter) Water (20 cm x 20 cm x 32 cm)	White spectrum (0°, 22°, 45°, 67.5°, 90°)	Concrete (0 cm to 300 cm)	Ion chamber TEPC Rem counter Rem counter with lead (LINUS) LiF TLD with moderators
HIMAC, National Institute of Radiological Sciences (NIRS), Japan	400 MeV u ⁻¹ C	Cu (10 cm x 10 cm x 5 cm)	White spectrum (0°)	Concrete (50 cm to 200 cm) Iron (20 cm to 100 cm)	TEPC NE213 Activation detectors (Bi, C) Self-Time of Flight (TOF) detector
National Superconducting Cyclotron Laboratory (NSCL), U.S.A.	155 MeV u ⁻¹ He, C, O	Hevimet (5.08 cm x 5.093 cm)	White spectrum (44°-94°)	Concrete (308 to 1057 g cm ⁻² , 2.4 g cm ⁻³ density)	Bonner Ball with LiI (Eu)
TRIUMF, Canada	500 MeV proton		White spectrum	Concrete	Bonner Ball with LiI (Eu) ¹¹ C activation of NE102A
KENS, High Energy Accelerator Research Organization (KEK), Japan	500 MeV proton	W (stopping length)	White spectrum (0°)	Concrete (0 m to 4 m)	Activation detectors (Bi, Al, Au)
LANSCE, Los Alamos National Laboratory (LANL), U.S.A.	800 MeV proton	Cu (60 cm long, 21 cm diameter)	White spectrum (90°)	Iron (4 to 5 m)	6 ton water Cherenkov detector
ISIS, Rutherford Appleton Laboratory (RAL), U.K.	800 MeV proton	Ta (30 cm long, 9 cm diameter)	White spectrum (90°)	Concrete (20 cm to 120 cm) Iron (10 cm to 60 cm) After 284 cm thick iron and 97 cm thick concrete	Bonner Ball with LiI (Eu) Rem counter
AGS, Brookhaven National Laboratory, U.S.A.	1.6, 12, 24 GeV proton	Hg (130 cm long, 20 cm diameter)	White spectrum (0°)	Steel (0 m to 3.7 m)	Activation detectors (Bi, Al, Au)
			White spectrum (90°)	Concrete (0 m to 5 m) Steel (0 to 3.3 m)	
SLAC, Stanford National Accelerator Laboratory, U.S.A.	28.7 GeV electron	Al (145 cm long, 30 cm diameter)	White spectrum (90°)	Concrete (274, 335, 396 cm)	NE213 Bonner Ball with LiI (Eu)
CERN, Switzerland	120, 205 GeV/c proton	Cu (50 cm long, 7 cm diameter)	White spectrum (90°)	Iron (40 cm) Concrete (80 cm)	TEPC (HANDI) Bonner Ball with LiI (Eu) LINUS ²⁰⁹ Bi and ²³² Th fission chambers
	160 GeV u ⁻¹ lead	Pb	White spectrum	Concrete	

619

620 The attenuation length of neutrons in the shielding material determines the thickness of shielding
621 that is required to reduce the dose to acceptable levels. Shielding for neutrons must be such that
622 sufficient material is interposed between the source and the point of interest, and neutrons of all energies
623 must be attenuated effectively (Moritz, 2001). Dense material of high-atomic mass such as steel meets
624 the first criterion, and hydrogen meets the second criterion because of effective attenuation by elastic
625 scattering. However, steel is transparent to neutrons of energy ~ 0.2 MeV to 0.3 MeV. Therefore, a layer
626 of hydrogenous material must always follow the steel. Alternatively, large thicknesses of concrete or
627 concrete with high-z aggregates can be used as discussed in Chapter 3.

628

629 **1.3 Dose Quantities and Conversion Coefficients**

630

631 **1.3.1 Protection and Operational Dose Quantities**

632

633 The interaction of radiation with matter is comprised of a series of events (collisions) in which
634 the particle energy is dissipated and finally deposited in matter. The dose quantities that are used in
635 shielding calculations and radiation monitoring are discussed below.

636

637 Shielding calculations and radiation monitoring are performed solely for radiation protection. The
638 former are performed to ensure that the facility is designed so that exposures of personnel and the public
639 are within regulatory limits. The latter is performed to demonstrate compliance with design or regulatory
640 limits (NCRP, 2003). Thus, the calculations and measurements must be expressed in terms of quantities
641 in which the limits are defined. The International Commission on Radiological Protection (ICRP)
642 defines dose limits. They are expressed in terms of protection quantities measured in the human body.
643 Compliance with these limits can be demonstrated by measurement of the appropriate operational
644 quantity defined by the International Commissions on Radiological Units and Measurements (ICRU).

645 ICRP Publication 60 (ICRP, 1991) recommended the use of equivalent dose (H_T) and effective dose (E)
646 as protection quantities. However, these quantities are not directly measurable. For external individual
647 exposure the accepted convention is the use of operational quantities, ambient dose equivalent $H^*(d)$, the
648 directional dose equivalent $H(d, \Omega)$, and personal dose equivalent $H_p(d)$, defined by ICRU. The two sets
649 of quantities might be related to the particle fluence and, in turn, by conversion coefficients to each other.
650 Note that the term “dose” might be used in a generic sense throughout this document to refer to the
651 various dose quantities. The definitions of protection and operational quantities taken from ICRU Report
652 51 (ICRU, 1991), ICRP Publication 60 (ICRP, 1991) and ICRP Publication 103 (ICRP, 2007) are as
653 follows:

654
655 The **absorbed dose**, D , is the quotient of $D = \frac{d\bar{\varepsilon}}{dm}$ where $d\bar{\varepsilon}$ is the mean energy imparted by
656 ionizing radiation to matter of mass dm . The unit is $J\ kg^{-1}$. The special name for the unit of
657 absorbed dose is the gray (Gy).

658
659 The **dose equivalent**, H , is the product of Q and D at a point in tissue, where D is the absorbed
660 dose and Q is the quality factor at that point. Thus, $H = Q D$. The unit of dose equivalent in the SI
661 system of units is joules per kilogram ($J\ kg^{-1}$) and its special name is the sievert (Sv).

662
663 The dose equivalent was specified in ICRP Publication 21 (ICRP, 1973). ICRP Publication 60
664 (ICRP, 1991) introduced the concept of equivalent dose. ICRP Publication 103 (ICRP, 2007)
665 modified the weighting factors.

666

667 The **equivalent dose**, H_T , in a tissue or organ is given by $H_T = \sum_R w_R D_{T,R}$, where $D_{T,R}$ is the
668 mean absorbed dose in the tissue or organ, T , due to radiation, R , and w_R is the corresponding
669 radiation weighting factor. The unit of equivalent dose is the sievert (Sv).

670

671 The weighting factor, w_R for the protection quantities recommended by ICRP Publication 103
672 (ICRP, 2007) is shown in Table 1.2. In the case of neutrons, w_R varies with energy and therefore
673 the computation for the protection quantities is made by integration over the entire energy
674 spectrum.

675

676

677 Table 1.2. Radiation weighting factors recommended by ICRP Publication 103

678

Radiation Type	Energy Range	w_R
Photons, electrons and muons	All energies	1
Neutrons	< 1 MeV	$w_R = 2.5 + 18.2 \exp\left[-\frac{(\ln(E))^2}{6}\right]$
Neutrons	1 MeV to 50 MeV	$w_R = 5 + 17 \exp\left[-\frac{(\ln(2E))^2}{6}\right]$
Neutrons	> 50 MeV	$w_R = 2.5 + 3.5 \exp\left[-\frac{(\ln(0.04E))^2}{6}\right]$
Protons, other than recoil protons	> 2 MeV	2
Alpha particles, fission fragments and heavy nuclei	All energies	20

679

680

681

682 The **effective dose**, E , is given by $E = \sum_R w_T H_T$, where H_T is the equivalent dose in the tissue or
683 organ, T , and w_T is the corresponding tissue weighting factor. The effective dose is expressed in
684 Sv.

685

686 The **ambient dose equivalent**, $H^*(d)$, at a point in a radiation field, is the dose equivalent that
687 would be produced by the corresponding expanded and aligned field, in the ICRU sphere
688 (diameter = 30 cm, 76.2 % O, 10.1 % H, 11.1 % C and 2.6 % N) at a depth, d , on the radius
689 opposing the direction of the aligned field (ICRU, 1993). The ambient dose equivalent is
690 measured in Sv. For strongly penetrating radiation, a depth of 10 mm is recommended. For
691 weakly penetrating radiation, a depth of 0.07 mm is recommended. In the expanded and aligned
692 field, the fluence and its energy distribution have the same values throughout the volume of
693 interest as in the actual field at the point of reference, but the fluence is unidirectional.

694

695 The **directional dose equivalent**, $H'(d, \Omega)$, at a point in a radiation field, is the dose equivalent
696 that would be produced by the corresponding expanded field in the ICRU sphere at a depth, d , on
697 the radius in a specified direction, Ω (ICRU, 1993). The directional dose equivalent is measured
698 in Sv. For strongly penetrating radiation, a depth of 10 mm is recommended. For weakly
699 penetrating radiation, a depth of 0.07 mm is recommended.

700

701 The **personal dose equivalent**, $H_p(d)$, is the dose equivalent in soft tissue, at an appropriate
702 depth, d , below a specified point on the body. The personal dose equivalent is measured in Sv.
703 For strongly penetrating radiation, a depth of 10 mm is recommended. For weakly penetrating
704 radiation, a depth of 0.07 mm is recommended.

705

706 **1.3.2 Conversion Coefficients**

707

708 **Conversion coefficients** are used to relate the protection and operational quantities to physical
709 quantities characterizing the radiation field (ICRU, 1998). Frequently radiation fields are characterized in
710 terms of absorbed dose or fluence. The **fluence**, Φ , is the quotient of dN by dA where dN is the number
711 of particles incident on a sphere of cross-sectional area dA . The unit is m^{-2} or cm^{-2} . Thus, for example, the
712 effective dose can be obtained by multiplying the fluence with the fluence-to-effective dose conversion
713 coefficient.

714

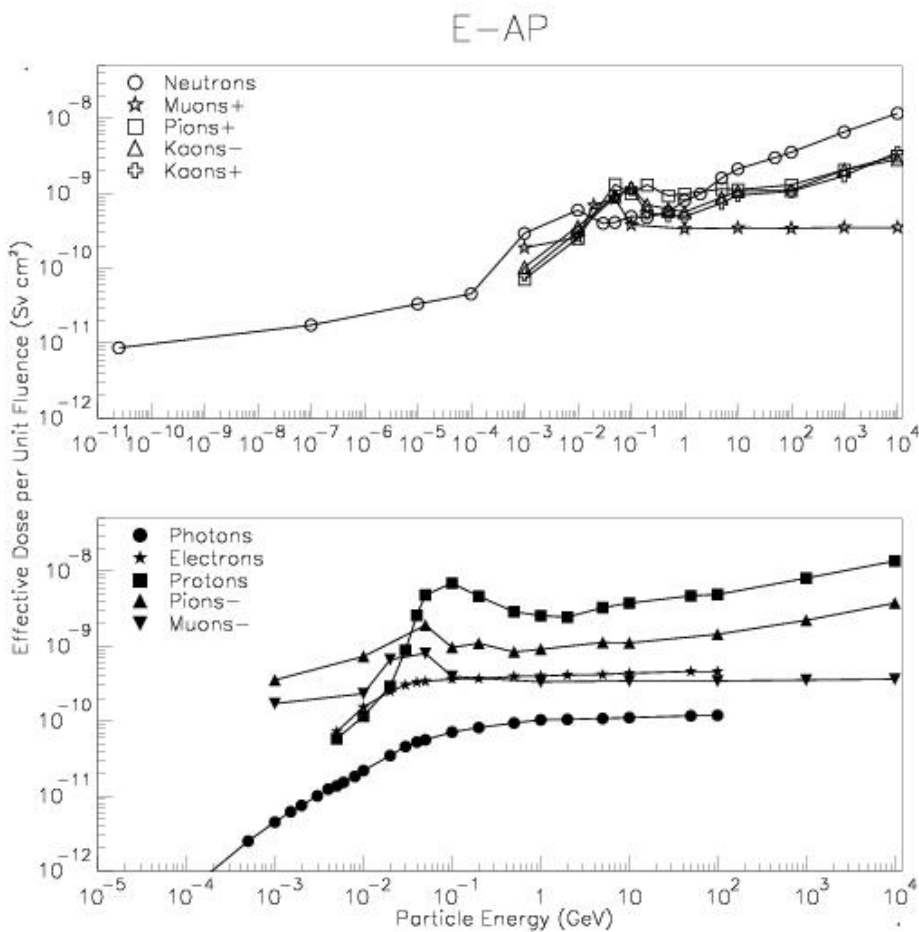
715 The fluence-to-dose conversion coefficients at high energies are the basic data for shielding
716 calculations. Conversion coefficients for electrons with energies up to 45 MeV, photons with energies up
717 to 10 MeV and neutrons with energies up to 180 MeV can be found in ICRU Report 57 (ICRU, 1998).
718 Fluence-to-effective dose and fluence-to-ambient dose equivalent conversion coefficients have been
719 calculated by the Monte Carlo transport code FLUKA (Ferrari, 2005; Battistoni *et al.*, 2007) for many
720 types of radiation (photons, electrons, positrons, protons, neutrons, muons, charged pions, kaons) and
721 incident energies (up to 10 TeV). The data are summarized in a paper by Pelliccioni (Pelliccioni, 2000).
722 Conversion coefficients for high-energy electrons, photons, neutrons, and protons have also been
723 calculated by others using various Monte Carlo codes. These references are cited in ICRU Report 57
724 (ICRU, 1998) and Pelliccioni (2000). Figure 1.5 shows the fluence-to effective dose conversion
725 coefficients for anterior-posterior (AP) irradiation for various particles as a function of particle energy
726 (Pelliccioni, 2000). Figure 1.6 shows the fluence-to ambient dose equivalent conversion coefficients.
727 Figure 1.7 shows the fluence-to effective dose conversion coefficients for isotropic (ISO) irradiation.

728

729

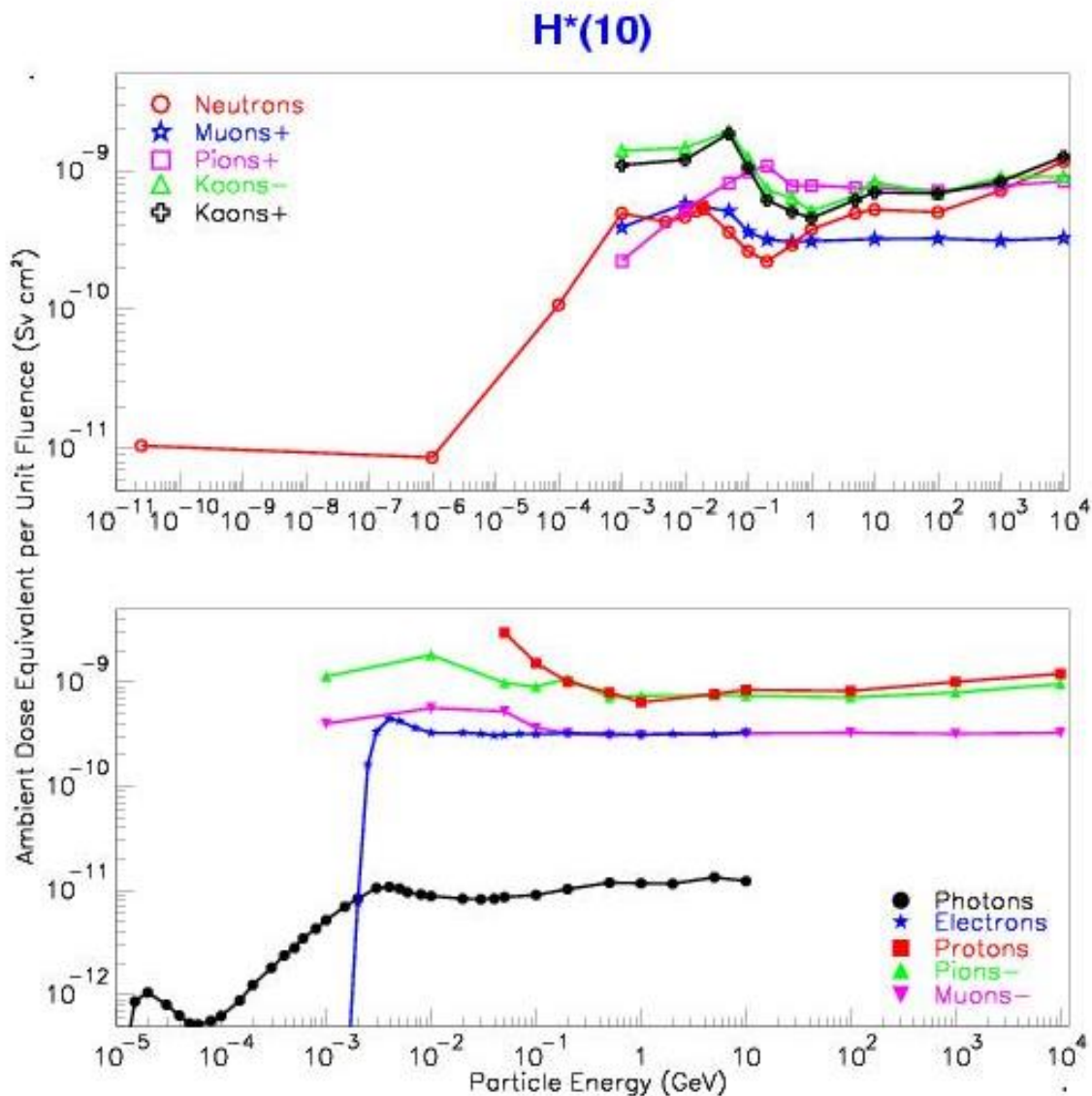
730

731

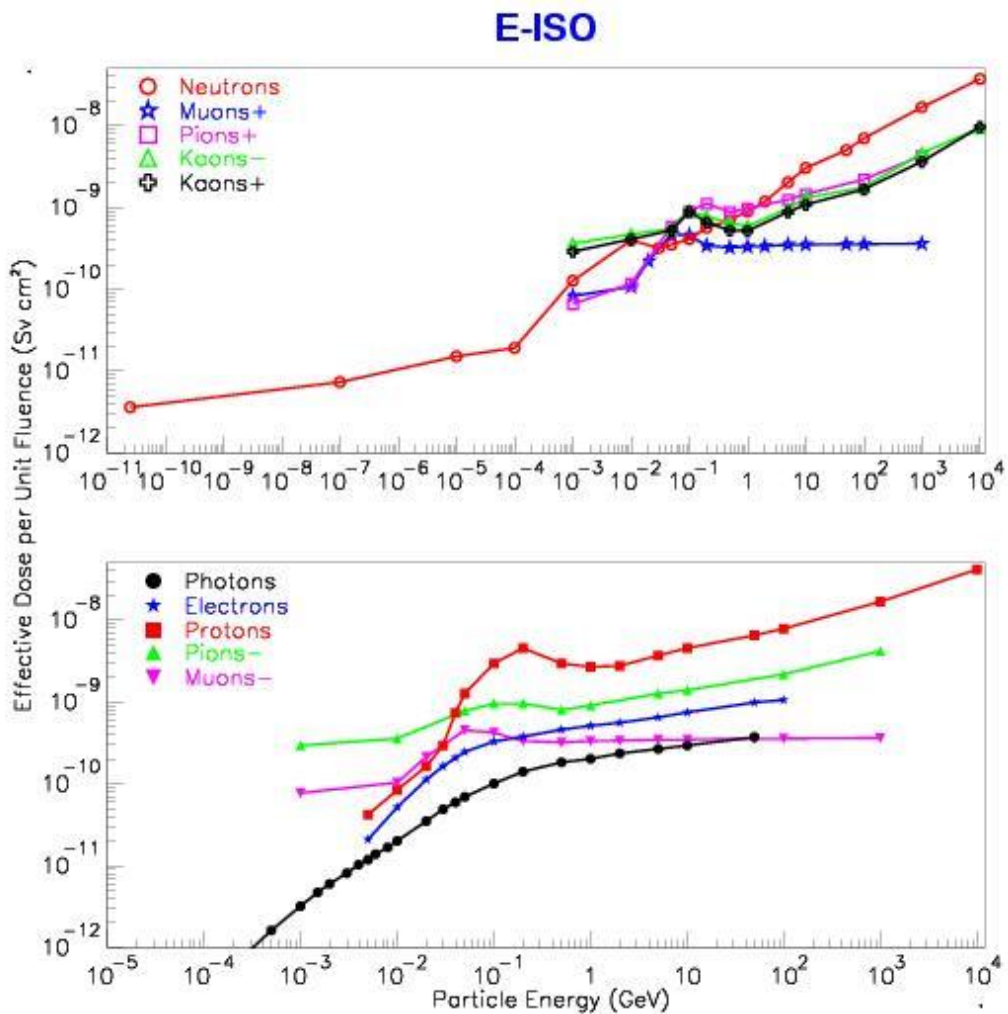


732

733 Figure 1.5. Fluence-to-effective dose conversion coefficients for AP irradiation as a function of energy
734 for various types of radiation (Pelliccioni, 2000)



735
736 Figure 1.6. Fluence-to-ambient dose conversion coefficients as a function of energy for various types of
737 radiation (Courtesy of M. Pellicioni; Pellicioni, 2000)
738



739
740 Figure 1.7. Fluence-to-effective dose conversion coefficients for ISO (isotropic) irradiation as a
741 function of energy for various types of radiation (Courtesy of M. Pelliccioni)
742

743

1.4 Shielding Design and Radiation Safety

744

745 The remainder of this report is devoted to shielding design (Chapters 2 and 3) and radiation safety
746 (chapters 4-6) of charged particle therapy accelerators. The literature is replete with data and information
747 for high-energy proton accelerators (> 1 GeV); however, such information is sparse for intermediate-
748 energy protons and carbon ions. The purpose of this report is to provide sufficient information for the
749 design of new facilities; therefore, it does not necessarily provide a comprehensive citation of all related
750 references for proton and carbon ion.

751

752

2. Radiological Aspects of Particle Therapy Facilities

753

Nisy Elizabeth Ipe

754

755

2.1 Charged Particle Interactions

756

757

758

759

760

761

762

763

764

765

766

767

768

769

770

771

772

773

774

775

776

The literature is replete with the physics of high-energy particle accelerator shielding, but there is a dearth of related information for intermediate energy charged particle accelerators. The first section of this chapter provides a summary of the particle interactions with the emphasis placed mainly on the interactions pertaining to shielding of charged particle therapy facilities.

The interaction of an accelerated beam of charged particles with matter results in the production of different types of radiation (NCRP, 2003). The yield (number of secondary particles emitted per incident primary particle) and types of secondary radiation generally increase with increasing kinetic energy of the incident particle. The processes that are important in energy deposition include the strong (or nuclear) interaction, the electromagnetic interaction, and the weak interaction (ICRU, 1978). The electromagnetic interaction is comprised of the direct interactions that are long range and that occur between particles that carry charge or have a magnetic moment, and the interactions in which photons are emitted or absorbed. The strong interaction occurs only between hadrons or between photons and hadrons. It is the strongest of all the interactions but occurs over a short range ($<10^{-13}$ cm). It is responsible for the binding of protons and neutrons in the atomic nucleus.

Hadrons comprise the majority of all known particles and interact *via* strong interactions (ICRU, 1978). They consist of baryons and mesons. Baryons are particles with mass equal to or greater than that of the proton and have a half-integral spin. They include protons and neutrons. Mesons are particles that have an integral or zero spin, and include pions (pi-mesons, π) and kaons (k-mesons, K). Pions are

777 produced in high-energy reactions and charged pions play a dominant role in the propagation of the
778 hadronic cascade (described in section 2.1.2). They decay to muons in air or a vacuum, but have a high
779 probability of stopping in condensed matter. Positive pions will decay and negative pions will be
780 captured, forming pi-mesic atoms. In the latter case, the atoms will quickly de-excite and emit
781 characteristic x rays, while the pions will be captured by the nucleus. The interactions of pions with
782 nuclei lead to nuclear break-up and the subsequent emission of low-energy protons (p), alpha particles
783 (α) and high-LET nuclear fragments. Heavier mesons and baryons are also produced, but the probability
784 of their production is significantly lower than that of pions. Hadrons interact with each other *via* strong
785 interactions when their distance of separation is less than 10^{-13} cm. At distances larger than this, they can
786 interact *via* electromagnetic interactions such as proton scattering and proton energy-loss by ionization.

787

788 The interactions of charged particles include electromagnetic interactions with atomic electrons
789 and the nucleus, nuclear reactions and the production of secondary hadrons, nuclear reactions of
790 secondary hadrons, and the electromagnetic cascade. These are described in the following sections.

791

792 **2.1.1 Electromagnetic Interactions of Charged Particles**

793

794 Interaction of charged particles with atomic electrons and the nucleus are briefly described in the
795 following sections.

796

797 **2.1.1.1 Interaction of Charged Particles with Atomic Electrons.** A heavy charged particle
798 loses energy mainly through ionization and excitation of atoms as it traverses matter. Except at low
799 velocities, it loses a negligible amount of energy in nuclear collisions. Its encounters with atomic
800 electrons can be divided into two categories: hard collisions, where the energy imparted is much greater
801 than the binding energy of the electron; and soft collisions, where the energy imparted to the electron is

802 similar in magnitude to its binding energy (ICRU, 1978). In the derivation of the formulae for energy
 803 loss, it is assumed that the incident particle is moving at a speed v that is much greater than the mean
 804 velocity of the electrons in their atomic orbits.

805

806 For hard collisions, the energy transferred is very large compared to the electron binding energy.
 807 Thus, the atomic electrons are considered initially at rest and free (unbound). The maximum energy T_{\max}
 808 that can be imparted by a charged particle to an electron in a head-on collision is given by:

$$809 \quad T_{\max} = 2mc^2 \frac{p^2 c^2}{m^2 c^4 + M^2 c^4 + 2mc^2 E} \quad (3.1)$$

810 where m is the electron rest mass, c is the speed of light in vacuum, p is the momentum of the incident
 811 particle, M is the rest mass of the particle, and E is the total energy of the particle.

812

813 When M is much greater than m , as in the case of mesons or protons, and when $pc \ll (M/m)Mc^2$,

$$814 \quad T_{\max} \approx 2mc^2 \frac{\beta^2}{1 - \beta^2} \quad (3.2)$$

815 where $\beta = v/c$ is the relative velocity of the particle.

816

817 At very high energies, T_{\max} approaches pc or E , and does not depend on the value of M . Thus,
 818 there is a small probability that the knock-on electron can carry off almost all the kinetic energy of the
 819 incident particle.

820

821 The linear rate of energy loss to atomic electrons along the path of a heavy charged particle in a
 822 medium (expressed as MeV/cm or MeV/m) is the basic physical quantity that determines the dose
 823 delivered by the particle in the medium (Turner, 1980). This quantity referred to as $-dE/dx$ is called the
 824 stopping power of the medium for the particle and is given by the Bethe formula:

825
$$-\frac{dE}{dx} = \frac{4\pi z^2 e^4 n}{mc^2 \beta^2} \left[\ln \frac{2mc^2 \beta^2}{I(1-\beta^2)} \right] - \beta^2 \quad (3.3)$$

826 where z is the atomic number of the heavy particle, e is the magnitude of electron charge, n is the number
827 of electrons per unit volume in the medium, and I is the mean excitation energy of the medium.

828

829 The stopping power depends only on the charge ze and the relative velocity β of the heavy
830 particle, and on the relevant properties of the medium such as its mean excitation energy I and the
831 electronic density n .

832

833 The range of a charged particle is the distance that it travels before coming to rest. The distance
834 traveled per unit energy loss is given by the reciprocal of the stopping power. Thus, the range $R(T)$ of a
835 particle of kinetic energy (T) is the integral of the reciprocal of the stopping power down to zero energy,
836 and can be written in the following form (Turner, 1980):

837
$$R(T) = \frac{M}{z^2} f(\beta) \quad (3.4)$$

838

839 It is important to note that the mean range of particles of a given speed is proportional to the mass
840 and varies as the inverse square of their charge. The dependence of the Bethe formula on z^2 implies that
841 particles with the same mass and energy but opposite charge (such as pions and muons) have the same
842 stopping power and range. However, departures from this prediction have been measured and
843 theoretically explained by the inclusion of higher powers of z in the Bethe formula. Statistical
844 fluctuations in the energy-loss process can also result in an r.m.s. (root mean square) spread in the actual
845 range of individual monoenergetic particles, resulting in “range straggling.”

846

847 **2.1.1.2 Interaction of Charged Particles with Nucleus.** A charged particle is also scattered
848 when it passes near a nucleus (ICRU, 1978). The scattering process is generally considered an elastic
849 one, because of the relatively small probability of a photon being emitted with an energy comparable to
850 the kinetic energy of the charged particle. When a charged particle penetrates an absorbing medium,
851 most of the scattering interactions lead to small deflections. Small net deflections occur because of a
852 large number of very small deflections and are referred to as multiple scattering. Large net deflections
853 are the result of a single large-angle scatter plus many very small deflections and are referred to as single
854 scattering. The intermediate case is known as plural scattering.

855

856 **2.1.2 Nuclear Interactions**

857

858 Nuclear interactions include nucleon-nucleus interactions and heavy ion-nucleus interactions.

859

860 **2.1.2.1 Nucleon-Nucleus Interactions.** The incident nucleon enters the nucleus, is deflected by
861 the nuclear potential, and emerges again at a different angle but with the same energy (Moritz, 2001).
862 This is known as direct elastic scattering. The nucleon can also directly collide with a target nucleon and
863 excite it to form a compound state. There are two possibilities:

864

- 865 • Either one or both nucleons have energy greater or less than their separation energy. In the
866 former case, the nucleon with energy greater than the separation energy leaves the nucleus
867 without further interaction, other than being deflected. If the change in mass is zero, the
868 reaction is either an inelastic scattering or a charge-exchange reaction. This is considered a
869 direct reaction. When the change in mass is not zero, the reactions are either transfer or
870 knock-out reactions. The angular distribution of the scattered particles is anisotropic and
871 forward peaked.

872 • The nucleons will undergo further collisions in the compound nucleus, thus spreading the
873 excitation energy over the entire nucleus. The nuclear state becomes complex during the pre-
874 equilibrium phase but eventually attains statistical equilibrium. Sufficient energy is
875 concentrated on one nucleon, which may escape the nucleus or “boil off.” Similarly, the
876 kinetic energy may be concentrated on a group of nucleons, and deuterons, tritons, and alpha
877 particles may be emitted. Heavy fragments may also be emitted. The emission of the particles
878 is described by an evaporation process similar to the evaporation of a molecule from the
879 surface of a liquid. For example, the spectrum of the emitted neutrons may be described by a
880 Maxwellian distribution of the form:

$$881 \quad \frac{dN}{dE_n} = B E_n^{-1} \exp(-E_n / T) \quad (3.4)$$

882 where E_n is the energy of the neutron, B is a constant, and T is the nuclear temperature. The
883 nuclear temperature is characteristic of the target residual nucleus and its excitation energy,
884 and has dimensions of energy. Its value lies between 2 and 8 MeV. When the spectra are
885 plotted as $\ln(E_n^{-1} \times dN/dE)$ versus E_n , the Maxwellian distribution appears on a semi
886 logarithmic scale as a straight line with a slope of $-1/T$. The evaporated particles are emitted
887 isotropically and the energy distribution of the neutrons extends up to about 8 MeV.
888 Compound reactions may also occur during the pre-equilibrium phase, in which case the
889 angle of emission will be strongly correlated with the direction of the incident particle. After
890 statistical equilibrium has been attained, the emitted particles will have an isotropic
891 distribution.

892
893 All the scattered and emitted particles can interact again resulting in an intra-nuclear cascade.
894 Above the pion production threshold (135 MeV), pions also contribute to the nuclear cascade. Neutral

895 pions decay into a pair of gamma rays after traversing a short distance. Charged pions will decay into
896 muons and then electrons if they have a clear flight path (*i.e.*, no further interactions), resulting in an
897 electromagnetic cascade. Neutrons or protons can also induce fission in high-atomic-mass nuclei.

898

899 **2.1.2.2 Heavy Ion-Nucleus Interactions.** Nuclear interactions of heavy ions as they pass through
900 matter arise from grazing or head-on collisions (Raju, 1980). In grazing collisions, fragmentation of
901 either the incident heavy ion or the target nucleus occurs. Fragmentation is the major nuclear interaction.
902 Head-on collisions are less frequent, but in such collisions, large amounts of energy are transferred
903 compared to grazing collisions. In heavy-ion interactions, many secondary particles are created from
904 nucleus-nucleus interactions. Nucleus-nucleus interactions have features that are different from typical
905 hadron-nucleus interactions at either the same total energy or energy per nucleon (ICRU, 1978). The
906 cross section for nuclear collisions between two nuclei is larger than that between a single hadron and
907 either nucleus. When two high-energy nuclei interact, only the segments that interpenetrate each other
908 undergo a significant interaction and mutual disintegration. The remainder of each nucleus is uninvolved
909 even though each is likely to have become highly excited, as is evidenced by the fact that a substantial
910 fragment is usually observed traveling in the same direction and at a similar speed to the incident primary
911 ion. Even though the part of the nucleus that escapes the severe interaction becomes highly excited, it
912 does not undergo evaporation to the extent that it breaks up into fragments with $Z < 3$ (ICRU, 1978). It is
913 only in a head-on collision that the projectile breaks up into many small pieces, so that no high-velocity
914 fragment survives. The residual nucleus and the alpha particles that evaporate from the primary fragment
915 are concentrated about the incident direction.

916

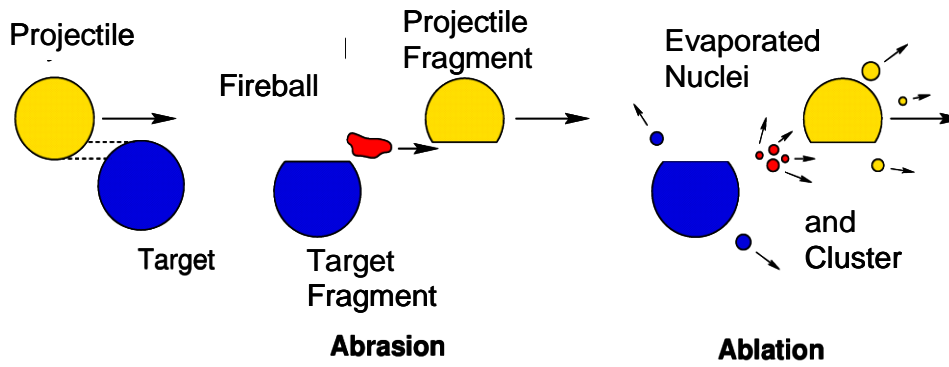
917 The process of fragmentation is frequently described as an abrasion-ablation process and is
918 schematically illustrated in Fig. 2.1 (Gunzert-Marx, 2004). The first step is known as abrasion. In grazing
919 collisions, a small fraction of the nuclear material overlaps and this overlapping zone is known as the

920 fireball. The abraded projectile pre-fragment keeps most of its initial energy while the abraded pre-
921 fragment target remains at rest. The fireball recoils with an intermediate velocity. During ablation, the
922 second step of fragmentation, the pre-fragments and the highly excited fireball evaporate nucleons and
923 light clusters.

924

925

926



927

928 Figure 2.1. Schematic illustration of fragmentation in a target (Courtesy of GSI)
929

930
931 The average number of mesons produced in a nucleus-nucleus interaction is larger than that
932 produced in a proton collision. The number of mesons produced in a single collision between heavy
933 nuclei fluctuates significantly due to the varying degree of overlap between the two nuclei. At high
934 energies ($> \sim 200$ MeV/nucleon), the probability and type of fragmentation does not depend on the
935 incident energy. At low energies, the cross sections for fragmentation decrease significantly. At still
936 lower energies, there is a higher probability that the nuclei come to rest without any interaction. At very
937 low energies ($\sim [1 \text{ to } 2]$ MeV/nucleon) the colliding nuclei may interact as a whole, resulting in the
938 production of a compound nucleus.

939
940 At high energies (Moritz, 1994), heavy ion interactions may be treated as interactions between
941 individual nucleons, *i.e.*, Z protons and $(A-Z)$ neutrons acting independently approximate a heavy ion
942 (Moritz, 1994). Most of the ion interactions occur at a finite impact parameter (the perpendicular distance
943 between the velocity vector of a projectile and center of the target that it is approaching). Therefore, part
944 of the ion may shear off and continue forward as a nuclear fragment. Thus, less than A nucleons are
945 available for further interactions. However, interaction cross sections are large. Therefore the fragmented
946 ion may interact very close to the initial interaction point. Thus, it may appear that all nucleons interact at
947 a single point.

948
949 Agosteo *et al.* (2004a; 2004b) point out that the approach of considering an ion of mass A
950 equivalent to A protons is not a good approximation in shielding calculations for ions in the therapeutic
951 range of interest, but is correct at ultra-relativistic energies, *i.e.*, hundreds of GeV/nucleon. At low
952 energies, the above-mentioned approach leads to an underestimate of shielding thicknesses, with the
953 underestimation increasing with larger shielding thicknesses especially in the forward direction. This can

954 be attributed to the fact that secondary neutrons generated from ion interactions have energies that extend
955 to a maximum of about two times the specific energy of the ion.

956

957 Experimental data from heavy ion reactions for ions with specific energy greater than 100
958 MeV/nucleon have been tabulated in a handbook (Nakamura and Heilbron, 2006). This handbook
959 includes thick-target secondary neutron yields, thin-target secondary neutron production cross sections,
960 measurements of neutron penetration behind shielding, spallation product cross sections and yields, and
961 parameterizations of neutron yields.

962

963 **2.1.3 Hadron Interactions**

964

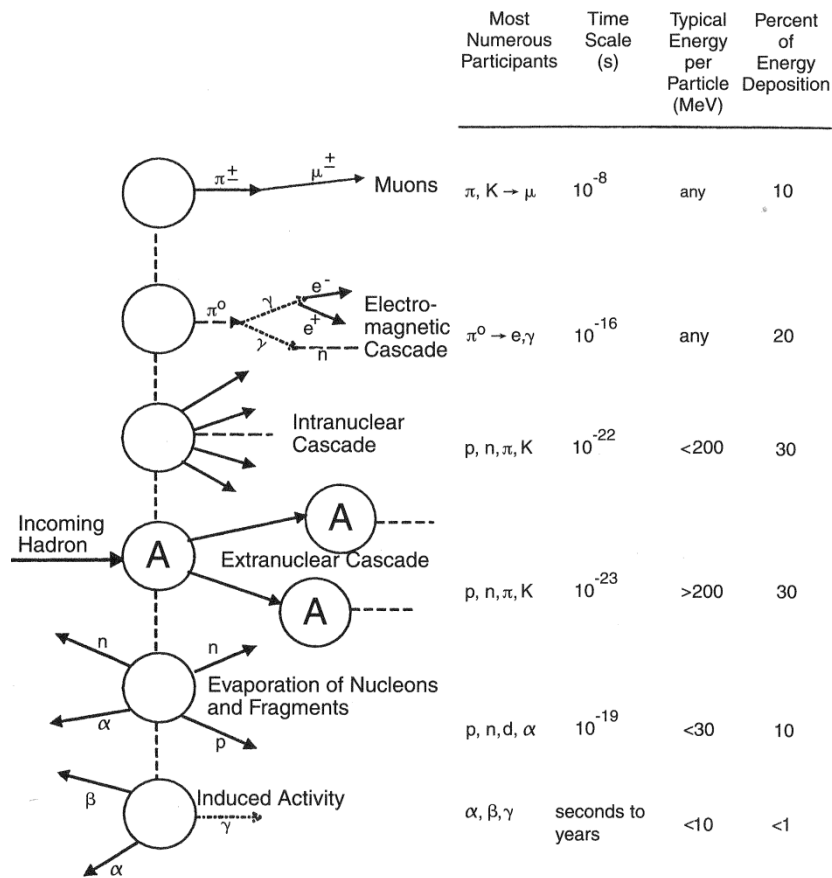
965 The hadronic cascade and proton interactions are discussed in the following sections.

966

967 **2.1.3.1 Hadronic or Nuclear Cascade.** Figure 2.2 provides a schematic representation of the
968 hadronic or nuclear cascade (ICRU, 1978; NCRP, 2003). The typical energy per particle in the figure
969 refers to the energy of the outgoing particle, and not the energy of the incoming particle.

970

971



972

973

974

975 Figure 2.2. Six levels of hadronic cascade (NCRP, 2003). Reprinted with permission of the National
 976 Council on Radiation Protection and Measurements, <http://NCRPonline.org>.

977

978

979 Six distinct and independent processes characterize the hadronic cascade. The extra-nuclear
980 cascade is the most important process and feeds all other processes. The hadrons (p , n , π^\pm , etc) propagate
981 this cascade. When a baryon or a meson interacts with a nucleus as a whole, it will release fast forward-
982 directed baryons and mesons, which will propagate the shower by collisions with other nuclei. With each
983 interaction the number of particles increases.

984

985 An intra-nuclear cascade may also occur when the particles in the extra-nuclear cascade interact
986 with individual nucleons inside the struck nucleus. This gives rise to similar reaction products, but of
987 lower energy, and emitted at wider angles. These particles may also contribute to the extra-nuclear
988 cascade, but to a much lesser extent. The intra-nuclear cascade process occurs within $\sim 10^{-22}$ s.
989 Above the pion production threshold (135 MeV), pions also contribute to the nuclear cascade. The
990 neutral pions (π^0) from the extra- and intra-cascades decay into two photons, which in turn can initiate an
991 electromagnetic cascade. The energy transferred is deposited by ionization losses within a distance of
992 several radiation lengths. The radiation length X_0 is the mean path length required to reduce the energy of
993 a relativistic charged particle by a factor of e . The neutral pion decay occurs within $\sim 10^{-16}$ s.
994 Some of the charged pions and kaons (π^\pm , K^\pm) will decay before they have dissipated all their energy,
995 releasing one muon (μ^\pm) from each meson decay. Muons are very penetrating particles and deposit their
996 energy mainly by ionization. Muon photonuclear reactions are also possible. The charged pion and kaon
997 decays occur within $\sim 10^{-8}$ s.

998

999 After interaction with the incoming hadron, the prefragment, *i.e.*, what remains of the original
1000 nucleus, is left in an excited state. It de-excites by emitting particles, mainly neutrons and protons, that
1001 do not contribute to the cascade or are involved with any of the other processes. These low-energy
1002 neutrons travel long distances, continuously depositing energy. The proton energy is deposited locally.

1003 The evaporation of nucleons takes place within $\sim 10^{-19}$ s. The de-excited nucleus may be radioactive,
1004 thus leading to residual radiation.

1005

1006 Thus, the interaction of a high-energy hadron with a nucleus results in the production of a large
1007 number of particles, mainly nucleons, pions, and kaons. A large fraction of the incident energy may be
1008 transferred to a single nucleon, that can be considered the propagator of the cascade. Energy transfer
1009 mainly occurs by the interaction of high-energy nucleons with energies greater than ~ 150 MeV, and
1010 these particles propagate the cascade. Nucleons with energies between 20 MeV and 150 MeV also
1011 transfer their energy by nuclear interactions, but the energy is transferred to a large number of nucleons
1012 instead of to a single nucleon. Therefore, each nucleon receives on average only a fraction of the total
1013 energy transferred and therefore has a low kinetic energy of ~ 10 MeV. Charged particles at these
1014 energies are quickly stopped by ionization. Thus, neutrons predominate at low energies. Charged pions
1015 and kaons decay into muons and neutrinos. Because muons are not subject to the strong interaction, they
1016 are primarily stopped in matter by ionization energy losses. Energetic gamma rays produced by the decay
1017 of neutral pions initiate electromagnetic cascades. However, the attenuation length (defined in Chapter 1)
1018 of these cascades is much shorter than the absorption length (distance traveled in which the intensity of
1019 the particles is reduced by a factor of e due to absorption) of strongly interacting particles; therefore, they
1020 do not contribute significantly to the energy transport. Thus, with increasing depth in the shield, neutrons
1021 are the principal propagators of the cascade because protons and pions with energies less than ~ 450
1022 MeV have a high rate of energy loss.

1023

1024 **2.1.3.2 Proton Interactions.** The interactions of protons with matter result in the degradation of
1025 the energy of the protons, and the production of a spray or cascade of secondary particles known as the
1026 hadronic or nuclear cascade, as described in the previous section. The extra-nuclear cascade occurs at
1027 primary proton energies above a few GeV (Moritz, 1994), and is followed by an intra-nuclear cascade.

1028 The intra-nuclear cascade takes place at proton energies between 50 MeV and 1000 MeV. Therefore, the
1029 intra-nuclear cascade is of importance for shielding in the proton therapeutic energy range of interest (67
1030 to 250 MeV), and the yield of low-energy neutrons increases as the primary proton energy increases
1031 (ICRU, 1978). However, the greater yield is more than compensated for by greater attenuation in the
1032 shield due to a higher cross section at low energy. Shielding studies indicate that the radiation field
1033 reaches an equilibrium condition beyond a few mean-free paths within the shield. Neutrons with energies
1034 greater than 150 MeV regenerate the cascade even though they are present in relatively small numbers.
1035 They are accompanied by numerous low-energy neutrons produced in the interactions. The shape of the
1036 neutron spectrum observed at the shield surface is very similar to that which exists in the shield. The
1037 presence of holes or penetrations in the shielding may perturb the shape of the neutron spectrum, with an
1038 increased number of low-energy neutrons in the vicinity of the penetrations. Both experiments and
1039 calculations confirm that for a well-developed cascade the shape of the spectrum is rather independent of
1040 the location within the shield, the incident energy, or even the shielding material, as long as the hydrogen
1041 content is essentially the same (ICRU, 1978). The typical neutron spectrum observed outside a thick
1042 concrete shield consists of peaks at a few MeV and at ~ 100 MeV.

1043

1044 At proton energies below 10 MeV, the proton is absorbed into the target nucleus and creates a
1045 new compound nucleus, as explained in section 2.1.2.1 (IAEA, 1988).

1046

1047 Photons are produced by inelastic neutron scattering and neutron capture by hydrogen within the
1048 concrete wall, and the inelastic scattering of evaporation neutrons in the target. The contribution of dose
1049 from photons produced in the shield is important only for primary neutrons with energies below 25 MeV
1050 and for thick concrete shields. The total photon dose is much lower than the neutron dose for proton
1051 energies higher than 150 MeV and for a sufficiently thick shield.

1052

1053 The energy loss at the lowest proton energy is mainly due to ionization of the material in which
1054 the protons are stopped. The lowest-energy proton produces the greatest specific ionization resulting in
1055 the formation of the Bragg peak at the end of the proton range. This property has been exploited in
1056 proton therapy. Protons can penetrate the Coulomb barrier when their kinetic energy is sufficiently high.
1057 In this case, nuclear reactions are also possible in addition to Coulomb scattering. As the energy of the
1058 protons increase, the nuclear reactions compete with the electromagnetic interactions.

1059

1060 **2.1.4 Electromagnetic Cascade**

1061

1062 Electromagnetic cascades are initiated by pion decay as shown in Fig. 2.2; however, the intra-
1063 nuclear cascade dominates for protons in the therapeutic range of interest. When a high-energy electron
1064 interacts with matter, only a small fraction of the energy is dissipated as a result of collision processes. A
1065 large fraction is spent in the production of high-energy photons or bremsstrahlung. These photons
1066 interact through pair production or Compton collisions resulting in the production of electrons. These
1067 electrons radiate more photons, which in turn interact to produce more electrons. At each new step, the
1068 number of particles increases and the average energy decreases. This process continues until the
1069 electrons fall into the energy range where radiation losses can no longer compete with collision losses.
1070 Eventually, the energy of the primary electron is completely dissipated in excitation and ionization of the
1071 atoms, resulting in heat production. This entire process resulting in a cascade of photons, electrons, and
1072 positrons is called an electromagnetic cascade. A very small fraction of the bremsstrahlung energy in the
1073 cascade is utilized in the production of hadrons such as neutrons, protons, and pions.

1074

1075 **2.2 Secondary Radiation Environment**

1076

1077 The secondary radiation environment for charged particle therapy accelerators is comprised of:

1078

1079

1. Neutrons; charged particles like pions, kaons, ions; and nuclear fragments emitted in inelastic hadronic interactions;

1080

1081

2. Prompt gamma radiation from the interaction of neutrons or ions with matter;

1082

3. Muons and other particles;

1083

4. Characteristic x rays due to transfer of energy from the charged particle to an electron in the bound state and the subsequent emission of a photon from the decay of the excited state;

1084

1085

1086

5. Bremsstrahlung radiation produced by the transfer of energy from the accelerated charged particle to a photon in the electromagnetic field of an atom; and

1087

1088

6. Residual radiation from radioactivation produced by nuclear reactions of the particle with atomic nuclei.

1089

1090

1091

Neutrons dominate the prompt radiation field for proton and ion accelerators outside the

1092

shielding. In general, the radiation dose outside the shielding depends upon the energy, type of incident particle, the beam-on time, the target material and dimensions, and the shielding itself.

1093

1094

1095

2.2.1 Neutron Energy Classifications

1096

1097

For radiation protection purposes the neutrons can be classified as follows:

1098

Thermal: $\bar{E}_n = 0.025$ eV at 20° C, typically $E_n \leq 0.5$ eV (cadmium resonance)

1099

Intermediate: 0.5 eV $< E_n \leq 10$ keV

1100

Fast: 10 keV $< E_n \leq 20$ MeV

1101

Relativistic or high-energy: $E_n > 20$ MeV

1102

where \bar{E}_n is the average energy of the neutrons and E_n is the energy of the neutrons.

1103

1104 **2.2.2 Neutron Interactions**

1105

1106 Because neutrons are uncharged, they can travel appreciable distances in matter without
1107 undergoing interactions. When a neutron collides with an atom, it can undergo an elastic or an inelastic
1108 reaction (Turner, 1986). An elastic reaction is one in which the total kinetic energy of the incoming
1109 particle is conserved. In an inelastic reaction, the nucleus absorbs some energy and is left in an excited
1110 state. The neutron can also be captured or absorbed by a nucleus in reactions such as (n,p), (n,2n), (n, α)
1111 or (n, γ).

1112

1113 Thermal neutrons (n_{th}) are in approximate thermal equilibrium with their surroundings and gain
1114 and lose only small amounts of energy through elastic scattering. They diffuse about until captured by
1115 atomic nuclei. Thermal neutrons undergo radiative capture, *i.e.*, neutron absorption followed by the
1116 immediate emission of a gamma ray, such as in the $^1H(n_{th},\gamma)^2H$ reaction. The gamma ray has an energy
1117 of 2.22 MeV. The capture crosssection is $0.33 \times 10^{-24} \text{ cm}^2$. This reaction occurs in shielding materials
1118 such as polyethylene and concrete. Borated polyethylene is used because the cross section for capture in
1119 boron is much higher ($3480 \times 10^{-24} \text{ cm}^2$) and the subsequent capture gamma ray from the $^{10}B(n_{th},\alpha)^7Li$ is
1120 much lower energy (0.48 MeV). The capture cross sections for low-energy neutrons ($< 1 \text{ keV}$) decrease
1121 as the reciprocal of the velocity or as the neutron energy increases.

1122

1123 Intermediate energy neutrons lose energy by scattering and are absorbed.

1124

1125 Fast neutrons include evaporation neutrons from charged particle accelerators. They interact with
1126 matter mainly through a series of elastic and inelastic scattering, and are finally absorbed after giving up
1127 their energy (ICRU, 1978). On the average, approximately 7 MeV is given up to gamma rays during the

1128 slowing down and capture process. Above 10 MeV, inelastic scattering is the dominant process in all
1129 materials. At lower energies elastic scattering dominates. Below 1 MeV, elastic scattering is the principle
1130 process by which neutrons interact in hydrogenous materials such as concrete and polyethylene. When
1131 high-Z material such as steel is used for shielding, it must always be followed by hydrogenous material
1132 because the energy of the neutrons may be reduced by inelastic scattering to an energy where they may
1133 be transparent to the non-hydrogenous material. For example, as stated in Chapter 1, steel is transparent
1134 to neutrons of energy ~ 0.2 MeV to 0.3 MeV.

1135

1136 Relativistic neutrons arise from cascade processes in proton accelerators, and nuclear and
1137 fragmentation processes at ion accelerators, and are important in propagating the radiation field. This
1138 high-energy component with neutron energies (E_n) above 100 MeV propagates the neutrons through the
1139 shielding; and continuously regenerates lower-energy neutrons and charged particles at all depths in the
1140 shield *via* inelastic reactions with the shielding material (Moritz, 2001). For neutrons with energies
1141 between 50 and 100 MeV, reactions occur in three stages (NCRP, 1971). An intra-nuclear cascade
1142 develops in the first stage. The incident high-energy neutron interacts with an individual nucleon in the
1143 nucleus. The scattered and recoiling nucleons from the interaction proceed through the nucleus. Each of
1144 these nucleons may in turn interact with other nucleons in the nucleus, leading to the development of a
1145 cascade. Some of the cascade particles that have sufficiently high energy escape from the nucleus, while
1146 others do not. In the second stage, the energy of those particles that do not escape is assumed to be
1147 distributed among the remaining nucleons in the nucleus, leaving it in an excited state. The residual
1148 nucleus evaporates particles such as alpha particles and other nucleons. In the third stage, after particle
1149 emission is no longer energetically possible, the remaining excitation energy is emitted in the form of
1150 gamma rays.

1151

1152 2.2.3 Protons: Neutron Yield, Energy Spectra, and Angular Distributions

1153

1154 As stated in Chapter 1, the prompt radiation field produced by protons of energies up to 250 MeV
1155 encountered in proton therapy is quite complex, consisting of a mixture of charged and neutral particles
1156 as well as photons. Neutrons dominate the prompt radiation field. As the proton energy increases, the
1157 threshold for nuclear reactions is exceeded and more nuclear interactions can occur. At energies above
1158 200 MeV, the nuclear cascade process occurs. Between proton energies of 50 and 500 MeV the neutron
1159 yields increase as approximately E_P^2 where E_P is the energy of the incident proton (IAEA, 1988).

1160 Calculations and measurements of neutron yields, energy spectra, and angular distributions for protons of
1161 various energies incident on different types of materials can be found in the literature (Agosteo *et al.*,
1162 1995; Agosteo *et al.*, 1996; Agosteo *et al.*, 2007; Kato *et al.*, 2002; Nakashima *et al.*, 1995; NCRP, 2003;
1163 Tayama *et al.*, 2002; Tesch, 1985). Comparisons between calculations and measurements can be found in
1164 the papers by Kato *et al.* (2000), Nakashima *et al.* (1995), and Tayama *et al.* (2002).

1165

1166 Thick targets are targets in which the protons or ions are stopped, *i.e.*, the thickness is greater
1167 than or equal to the particle range. Thin targets are targets with thicknesses that are significantly less than
1168 the particle range. Thus, for example, the protons lose an insignificant amount of energy in the target,
1169 and the kinetic energy available for neutron production in the target is the full incident proton energy
1170 (IAEA, 1988).

1171

1172 The neutron yield of a target is defined as the number of neutrons emitted per incident primary
1173 particle. Table 2.1 shows the neutron yield (integrated over all angles) from 100 MeV to 250 MeV
1174 protons impinging on a thick iron target, based on calculations with the Monte Carlo code, FLUKA
1175 (Agosteo *et al.*, 2007; Ferrari, 2005). FLUKA is described in Chapter 6. The total yield (n_{tot}), and yields

1176 for neutron energy (E_n) less than, and greater than 19.6 MeV are shown. As expected, the neutron yield
1177 increases with increasing proton energy.
1178

1179 Table 2.1. Neutron yields for 100 MeV to 250 MeV protons incident on a thick iron target (Agosteo *et*
 1180 *al.*, 2007)

Proton Energy E_P (MeV)	Range (mm)	Iron Target Radius (mm)	Iron Target Thickness (mm)	Neutron Yield (neutrons per proton)		
				$E_n < 19.6$ MeV	$E_n > 19.6$ MeV	n_{tot}
100	14.45	10	20	0.118	0.017	0.135
150	29.17	15	30	0.233	0.051	0.284
200	47.65	25	50	0.381	0.096	0.477
250	69.30	58	75	0.586	0.140	0.726

1181

1182

1183 The average neutron energies (\bar{E}_n) for various emission angles are shown in Table 2.2 for the
1184 targets described in Table 2.1. As the proton energy increases, the spectra in the forward direction (0° to
1185 10°) hardens as is evidenced by the increasing average neutron energy. However, at very large angles
1186 (130° to 140°) the average energy does not change significantly with increasing proton energies.
1187

1188 Table 2.2. Average neutron energies for various emission angles as a function of proton energy (Agosteo
 1189 *et al.*, 2007)

Proton Energy (MeV)↓	Average Neutron Energy, \bar{E}_n (MeV)				
	Emission Angles→	0° to 10°	40° to 50°	80° to 90°	130° to 140°
100		22.58	12.06	4.96	3.56
150		40.41	17.26	6.29	3.93
200		57.73	22.03	7.38	3.98
250		67.72	22.90	8.09	3.62

1190

1191

1192 Table 2.3 shows the neutron yield as a function of target dimensions for 250 MeV protons. As the
1193 target radius increases, the total neutron yield increases, but the yield for $E_n > 19.6$ MeV decreases. Thus,
1194 the average neutron energy also decreases, as seen in Table 2.4. The total neutron yield increases with
1195 increasing target thickness, but the yield for $E_n > 19.6$ MeV decreases. The data shows that the average
1196 energy increases at the 0° to 10° and 40° to 50° emission angles, but decreases for emission angles larger
1197 than 80° to 90° . As the target thickness increases, the proton interactions increase and the secondary
1198 neutron yield increases. Initially the yield is dominated by the high-energy neutrons. As the thickness is
1199 further increased, the high-energy neutrons interact, producing more low-energy neutrons. Thus, the
1200 high-energy neutron yield decreases and the low-energy neutron yield increases, while the overall
1201 neutron yield increases. With further increasing thickness, the low-energy neutrons get attenuated in the
1202 target. The net result of this competing process is an increase in total neutron yield with increasing target
1203 thickness until it reaches a maximum and then it is expected to decrease due to the attenuation of low-
1204 energy neutrons in the target material.

1205

1206

1207 Table 2.3. Neutron yield for 250 MeV protons as a function of iron target dimensions (Agosteo *et al.*,
1208 2007)

1209

Iron Target Radius (mm)	Iron Target Thickness (mm)	Neutron Yield (neutrons per proton)		
		$E_n < 19.6$ MeV	$E_n > 19.6$ MeV	η_{tot}
37.5	75.0	0.567	0.148	0.715
58.0	75.0	0.586	0.140	0.726
75.0	75.0	0.596	0.136	0.732
75.0	150.0	0.671	0.111	0.782

1210

1211

1212

1213 Table 2.4. Average neutron energies at 250 MeV for various emission angles as a function of iron target
 1214 dimensions (Agosteo *et al.*, 2007)

1215

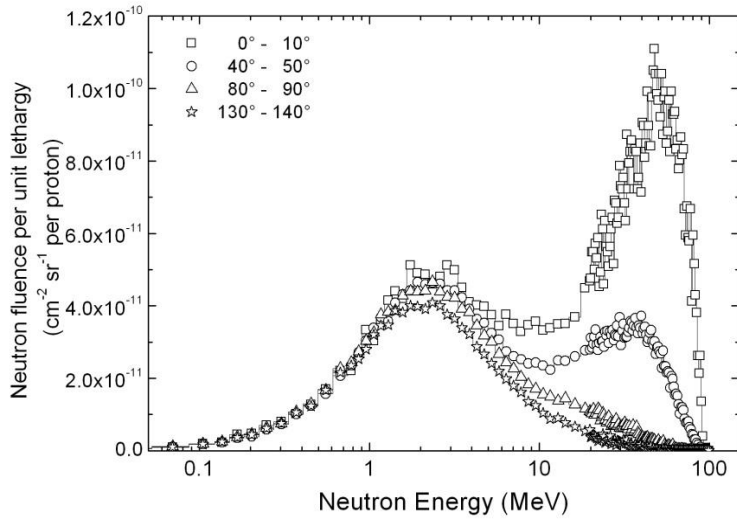
Iron Target Radius (mm) ↓	Iron Target Thickness (mm)	Average Neutron Energy, \bar{E}_n (MeV)			
		Emission Angles →	0° to 10°	40° to 50°	80° to 90°
37.5	75.0	73.6	25.9	8.1	3.9
58.0	75.0	67.7	22.9	8.1	3.6
75.0	75.0	64.7	21.3	8.1	3.5
75.0	150.0	70.3	23.5	6.9	3.2

1216

1217

1218 Figures 2.3 and 2.4 show the double differential neutron spectra as lethargy (logarithm of energy
1219 decrement) plots calculated with FLUKA for neutrons at various emission angles, produced by 100 MeV
1220 and 250 MeV protons incident on thick iron targets (without any concrete shielding) described in Table
1221 2.1 (Agosteo *et al.*, 2007). The energy distributions in these figures are typically characterized by two
1222 peaks: a high-energy peak (produced by the scattered beam particle) and an evaporation peak at ~ 2
1223 MeV. As the proton energy increases, the high-energy peaks shift to higher energies, which are
1224 particularly evident in the forward direction (0° to 10°). The high-energy peak for the unshielded target is
1225 not the usual 100 MeV peak that is observed outside thick concrete shielding as described in Section
1226 2.1.3.2. Thus, it is important to use wide-energy range instruments for neutron monitoring, as discussed
1227 in Chapter 4.

1228

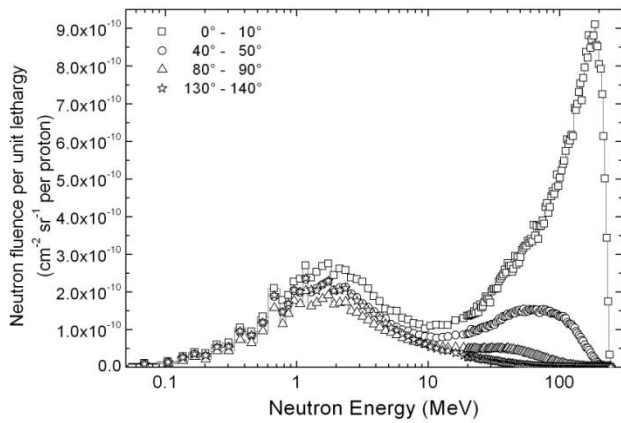


1229

1230 Figure 2.3. Double differential neutron spectra for 100 MeV protons incident on a thick iron target
1231 (Courtesy of S. Agosteo, Agosteo *et al.*, 2007)

1232

1233



1234

1235 Figure 2.4. Double differential neutron spectra for 250 MeV protons incident on a thick iron target
1236 (Courtesy of S. Agosteo, Agosteo *et al.*, 2007)

1237

1238 **2.2.4 Ions: Neutron Yields, Energy Spectra, and Angular Distribution**

1239

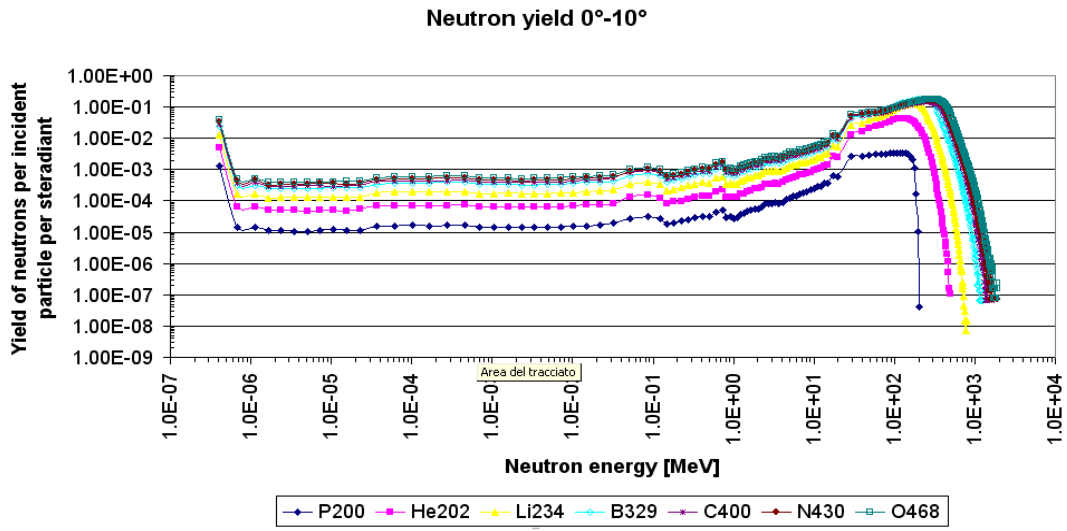
1240 Neutrons dominate the radiation field of ion accelerators. The contributions from photons,
1241 protons, and pions are small, as discussed in Chapter 3. Calculations and measurements of neutron
1242 yields, energy spectra, and angular distribution for ions of various energies incident on different types of
1243 materials can be found in the literature (Gunzert-Marx, 2004; Kato *et al.*, 2002; Kurosawa *et al.*, 1999;
1244 Nakamura, 2000; Nakamura *et al.*, 2002; Nakamura *et al.*, 2006; NCRP, 2003; Porta *et al.*, 2008; Shin *et*
1245 *al.*, 1997).

1246

1247 Figure 2.5 shows the total secondary neutron yield produced in tissue as a function of kinetic
1248 energy of the projectile (kinetic energy per nucleon \times number of nucleons) for various ions; protons (200
1249 MeV), helium (202 MeV/nucleon), lithium (234 MeV/nucleon), boron (329 MeV/nucleon), carbon (400
1250 MeV/nucleon), nitrogen (430 MeV/nucleon), and oxygen (468 MeV/nucleon) (Porta *et al.*, 2008). The
1251 results are based on calculations with FLUKA for ions incident on an International Commission on
1252 Radiation Units and Measurements (ICRU) tissue phantom (composition: 76.2 % O, 10.1 % H, 11.1 % C
1253 and 2.6 % N). The phantom was 40 cm in height and 40 cm in diameter, and the beam diameter was 10
1254 mm. The energy of each ion was chosen so that the range in water was 26.2 cm.

1255

1256



1257

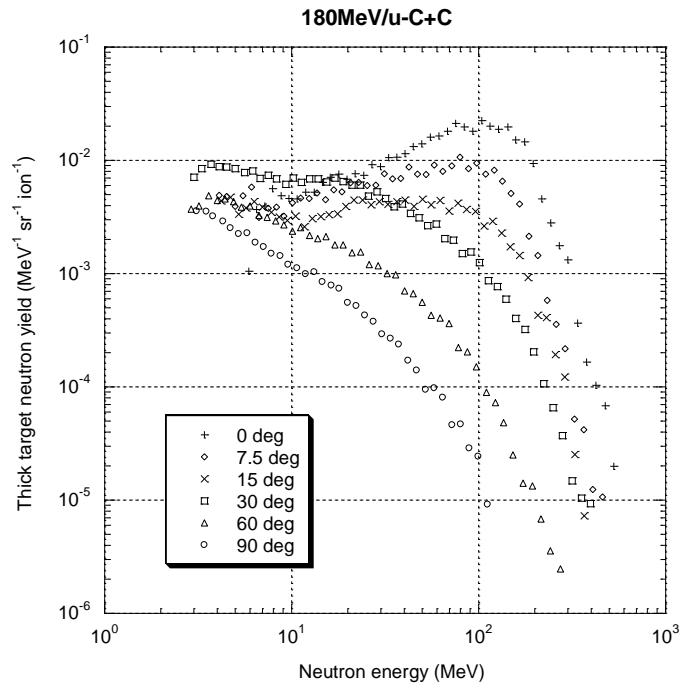
1258

1259 Figure 2.5. Total neutron yield expressed as neutrons per unit of solid angle and per incident particle in
1260 the 0° to 10° angular bin (Courtesy of A. Porta, Porta *et al.*, 2008).

1261

1262 Only carbon ions will be discussed in this section. Figures 2.6, 2.7, and 2.8 show the measured
1263 neutron spectra from 180 MeV/nucleon and 400 MeV/nucleon carbon ions incident on copper and
1264 carbon targets (Kurosawa *et al.*, 1999). The dimensions of the carbon target were 10 cm × 10 cm × 2 cm
1265 for 180 MeV/nucleon and 10 cm × 10 cm × 20 cm for 400 MeV/nucleon carbon ions, respectively. The
1266 dimension of the copper target was 10 cm × 10 cm × 1.5 cm. The spectra in the forward direction have a
1267 peak at the high-energy end that broadens with angle of emission. The peak energy is ~ 60 % to 70 % of
1268 the specific energy (140 MeV for 180 MeV/nucleon and 230 MeV for 400 MeV/nucleon). This data
1269 together with other data in the paper by Kurosawa *et al.* indicate that the high-energy neutron component
1270 produced in the forward direction by a break-up process and the momentum transfer from projectile to
1271 target nuclei are higher for both lighter target nuclei and higher projectile energy than for heavier target
1272 nuclei and lower projectile energy.
1273

1274



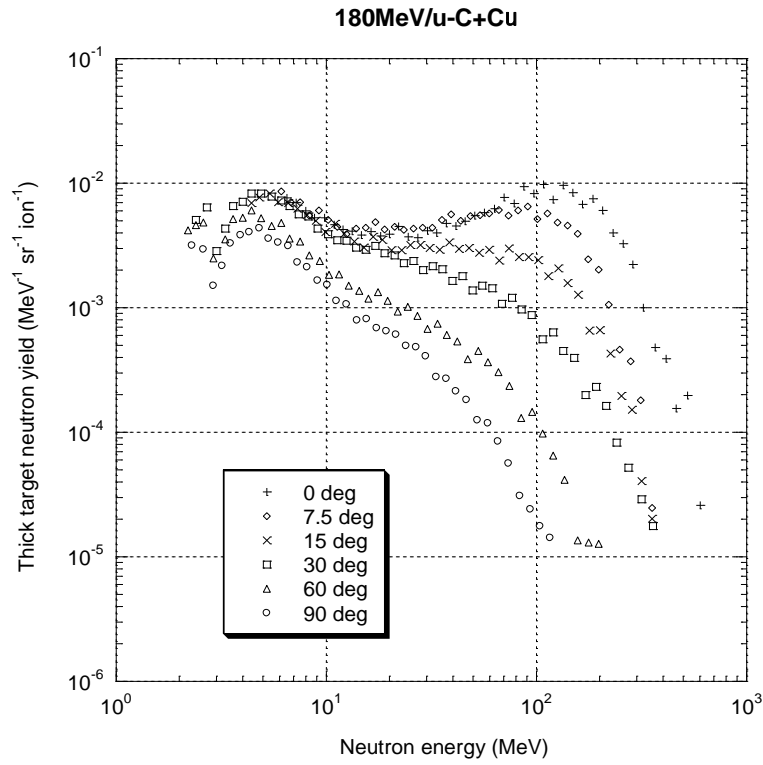
1275

1276

1277 Figure 2.6. Neutron spectra from 180 MeV/nucleon C ions incident on a C target (Kurosawa *et al.*,
1278 1999)

1279

1280

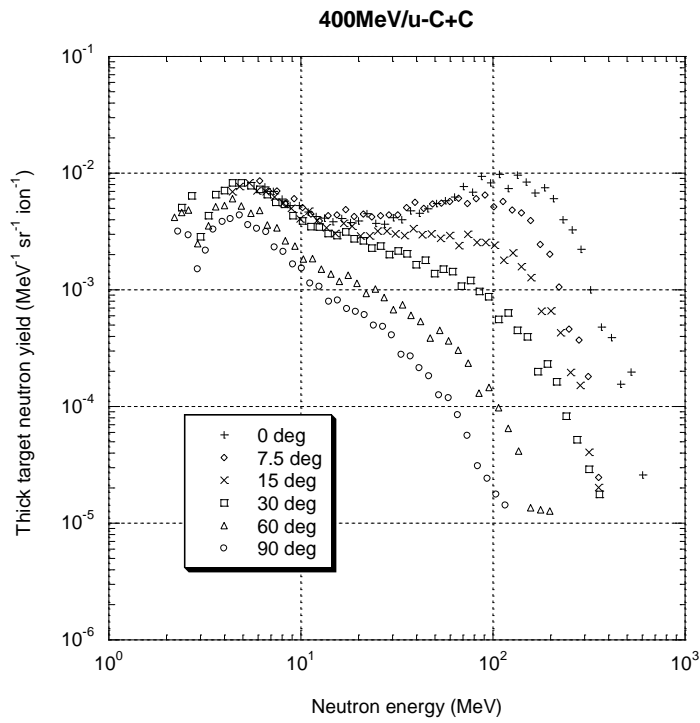


1281

1282 Figure 2.7. Neutron spectra from 180 MeV/nucleon C ions incident on a Cu target (Kurosawa *et*
1283 *al.*,1999)

1284

1285



1286

1287

1288 Figure 2.8. Neutron spectra from 400 MeV/nucleon C ions incident on a C target (Kurosawa *et al.*,

1289 1999)

1290

1291

1292

2.3 Beam Losses and Sources of Radiation

1293

1294 During the operation of particle therapy facilities, the interaction of the particles with beam-line
1295 components and the patient results in the production of radiation with neutrons being the dominant
1296 component. Typically the shielding thicknesses for various parts of the facility may range from about 60
1297 cm to about 7 m of concrete. Effective shielding can only be designed if the beam losses and sources of
1298 radiation for the charged particle therapy facilities are well understood. This requires knowledge of how
1299 the accelerators operate and deliver beam to the treatment rooms. Specific details of beam losses,
1300 duration, frequency, targets, and locations should be provided by the equipment vendor so that all
1301 sources of radiation are considered in the shielding design. It is important to note that higher beam losses
1302 will occur during start-up and commissioning as the beam is tuned and delivered to the final destination,
1303 and should be planned for. Both cyclotrons and synchrotron-based systems are discussed below.

1304

1305 2.3.1 Cyclotrons

1306

1307 Cyclotrons are used for both proton and ion acceleration and produce essentially continuous
1308 beams. Fixed-energy machines are used for therapy and are designed to operate at energies required to
1309 reach deep-seated tumors (Coutrakron, 2007). The principle of operation for a proton cyclotron is as
1310 follows: protons are extracted from the ion source located at the center of the and are injected into the
1311 cyclotron. The cyclotron is comprised of a large magnet (or several sector magnets) with an internal
1312 vacuum region located between the poles of the magnet(s). The maximum radius of a commercial room-
1313 temperature therapy cyclotron is about 1 m. There are large D-shaped electrodes commonly referred to as
1314 “dees.” A sinusoidal-alternating voltage with a frequency equal to the revolution frequency of the
1315 protons (or a multiple thereof) is applied across the dees as the protons travel in their orbit. Thus, as the

1316 protons cross a gap between the electrodes, they are further accelerated and begin to spiral outwards. The
1317 orbit radius is determined by the magnetic field. Figure 2.8 shows the inside view of the C-230 IBA
1318 cyclotron, which has four spiral-shaped electrodes. The protons are injected from the ion source below
1319 into the center of the cyclotron. The magnetic field of the cyclotron increases as the orbit radius increases
1320 to compensate for the relativistic mass increase, and the turn-by-turn separation decreases at higher
1321 energies. All the particles travel at the same revolution frequency, regardless of their energy or orbit,
1322 because the cyclotron is isochronous. The protons exit the cyclotron through a hole in the return yoke
1323 after passing through the electrostatic extraction plates.

1324

1325 During acceleration, continuous beam losses occur in the cyclotron. Depending upon the beam
1326 optics, about 20 % to 50 % of the accelerated beam particles can be lost in the cyclotron. The magnet
1327 yoke is made of steel and provides significant self-shielding, except in regions where there are holes
1328 through the yoke. These holes need to be considered in the shielding design. Losses at very low proton
1329 energies are not of concern for prompt radiation shielding, but can contribute to activation of the
1330 cyclotron. The beam losses of concern in the shielding design are those that occur at higher energies, and
1331 those due to protons that are close to their extraction energy (230 MeV to 250 MeV depending upon the
1332 cyclotron type) striking the dees and the extraction septum which are made of copper. These beam losses
1333 also result in activation of the cyclotron.

1334

1335



1336

1337

1338

1339 Figure 2.9. Inside view of C-230 IBA cyclotron (Courtesy of IBA)

1340

1341 **2.3.1.1 Energy Selection System (ESS).** For the treatment of tumors at shallow depths, the
1342 proton energy extracted from the cyclotron has to be lowered. This is typically achieved by using an
1343 energy selection system (ESS) after extraction. Figure 2.10 shows an ESS that is comprised of an energy
1344 degrader, a tantalum collimator, nickel energy slits and collimator, and a nickel beam stop. The energy
1345 degrader consists of a variable-thickness material, typically graphite, arranged in a wheel that is rotated
1346 into position, thus reducing the proton energy down to the energy of interest. In principle, the proton
1347 beam energy can be reduced to 75 MeV in the equipment described here. However, sometimes range
1348 shifters are used inside the nozzles in treatment rooms to achieve these lower energies. The intensity
1349 from the cyclotron has to be increased as the degraded energy is decreased in order to maintain the same
1350 dose rate at the patient. Thus, large amounts of neutrons are produced in the degrader, especially at the
1351 lower energies, resulting in thicker local shielding requirements in this area. The degrader scatters the
1352 protons and increases the energy spread. Most of the scattered beam from the degrader is collimated in a
1353 tantalum collimator, in order to reduce the beam emittance. A magnetic spectrometer and energy slits are
1354 used to reduce the energy spread. Beam stops are used to tune the beam. Neutrons are also produced in
1355 the collimator and slits. Losses in the ESS are large, and they also result in activation.
1356

1361 2.3.2 Synchrotrons

1362

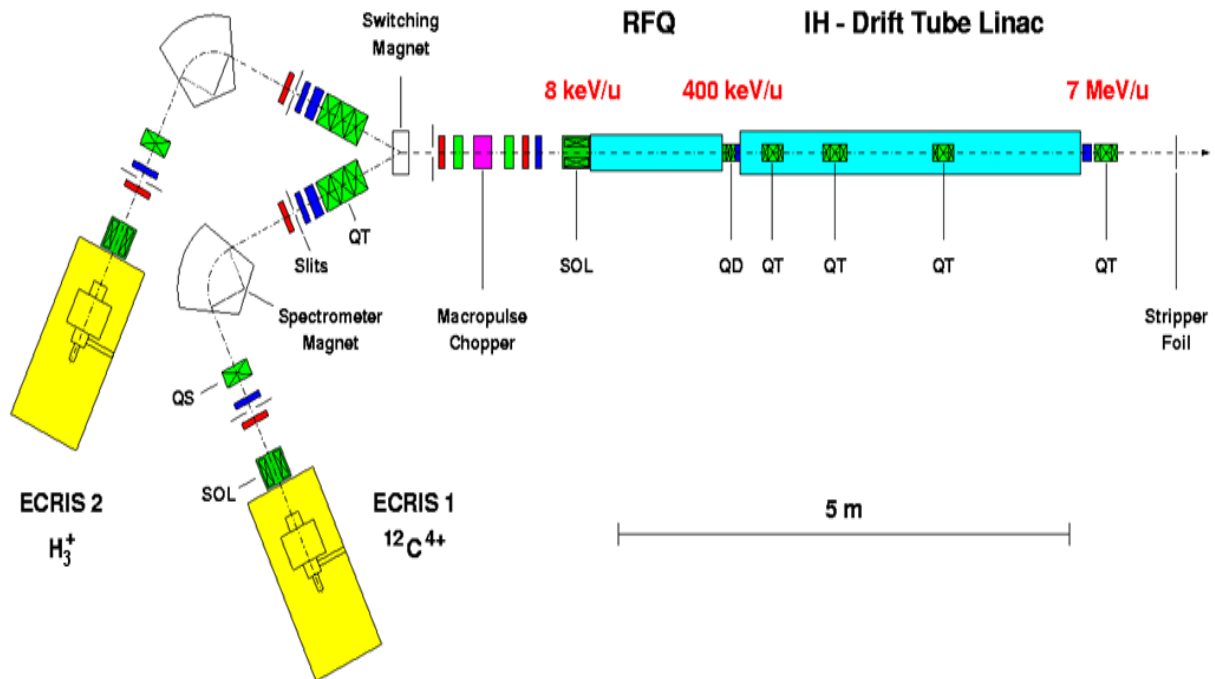
1363 Synchrotrons are designed to accelerate protons and ions to the exact energy needed for therapy,
1364 thus eliminating the need for energy degraders. This in turn results in less local shielding and activation
1365 of beam-line components. Synchrotrons however, are pulsed machines. For synchrotrons, the orbit radius
1366 is held constant and the magnetic field is increased as the particle energy increases. Maximum proton
1367 energy for therapy is ~ 250 MeV with about 10^{11} protons/spill, while maximum carbon energies range
1368 from (320 to 430) MeV/nucleon with $(0.4 \text{ to } 1.0) \times 10^9$ ions/spill. A spill typically lasts from 1 s to 10 s.
1369 Thus, proton intensities can be up to 250 times higher than carbon intensities.

1370

1371 Figure 2.11 shows a typical injector system for a synchrotron. There are two ion sources
1372 (ECRIS), one for protons and one for carbon. Proton facilities, of course, have only one ion source. A
1373 switching magnet allows the selection of either carbon ions or protons. The particles are then accelerated
1374 from 8 keV/nucleon by the RFQ (radiofrequency quadrupole) and by the IH (inter digital H-type
1375 structure) drift tube linear accelerator (linac) combination to 7 MeV/nucleon. The stripper foil produces
1376 fully stripped ions, thus eliminating all contamination, and the beam is delivered to the synchrotron.
1377 Sources of radiation include x rays from the ion source, x rays produced by back-streaming electrons
1378 striking the linac structure; and neutrons produced by the interaction of the ions with the linac structure
1379 at the end of the linac. The target material is typically copper or iron. The production of x rays from
1380 back-streaming electrons will depend upon the vacuum conditions and the design of the accelerator
1381 (NCRP, 1977). The use of a Faraday cup to intercept the beam downstream of the linac must also be
1382 considered in the shielding design.

1383

1384



1385

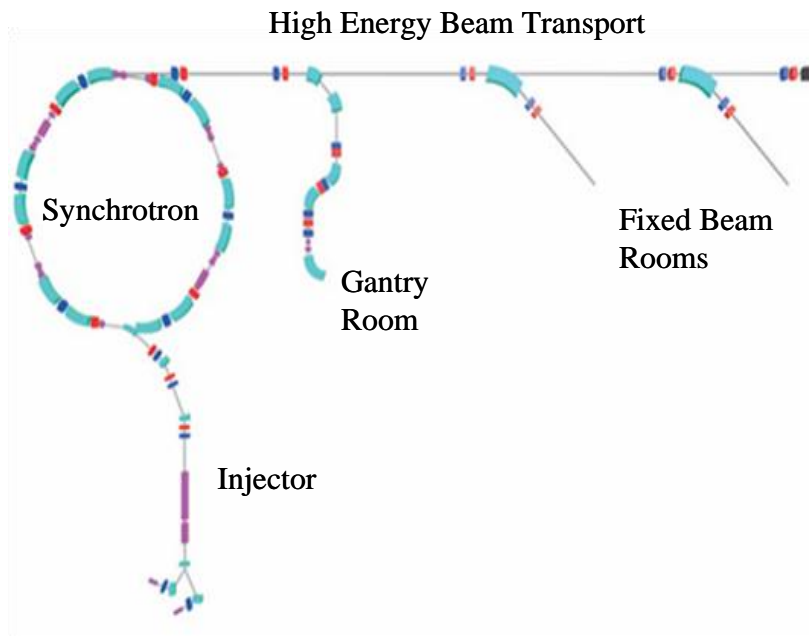
1386 Figure 2.11. Typical injector for synchrotron (Courtesy of *Gesellschaft für Schwerionenforschung*)

1387

1388 Figure 2.12 shows the synchrotron , high energy beam transport (HEBT), and transport to
1389 treatment rooms for a typical Siemens particle therapy facility. The synchrotron is capable of
1390 accelerating carbon ions to 430 MeV/nucleon and protons to 250 MeV. The synchrotron is filled using a
1391 multi-turn injection scheme. The beam is accelerated to the desired energy in less than 1 s. More than
1392 200 beam energies can be requested from cycle to cycle. A slow extraction technique is used to extract
1393 the beam and the extraction time varies from 1 s to 10 s.

1394

1395



1396

1397

1398

1399 Figure 2.12. Synchrotron, HEBT, and transport to treatment rooms (Courtesy of Siemens Medical
1400 Systems)

1401

1402 For synchrotrons in general, beam losses can occur during the injection process, RF capture and
1403 acceleration, and during extraction. Some of these losses may occur locally while others may be
1404 distributed around the synchrotron. The target material is typically copper or iron. Losses will be
1405 machine-specific and therefore the equipment vendor should provide this information. Particles that are
1406 not used in a spill may be deflected on to a beam dump or stopper and will need to be considered in the
1407 shielding design and activation analysis. In some cases these particles are decelerated before being
1408 dumped and therefore are not of concern in the shielding design or activation analysis.

1409

1410 X rays are produced at the injection and extraction septa due to the voltage applied across
1411 electrostatic deflectors, and may need to be considered in the exposure to personnel working in the
1412 vicinity of the synchrotron components during commissioning.

1413

1414 **2.3.3 Beam Transport Line**

1415

1416 For both cyclotron- and synchrotron-based systems losses occur in the beam transport line. These
1417 losses are usually very low (~ 1 %) and distributed along the beam line, but need to be considered for
1418 shielding design. The target material is typically copper or iron. During operation, the beam is steered
1419 onto Faraday cups, beam stoppers, and beam dumps, all of which need to be considered in the shielding
1420 design.

1421

1422 **2.3.4 Treatment Rooms**

1423

1424 The radiation produced from the beam impinging on the patient (or phantom) is a dominant
1425 source for the treatment rooms. Thus, a thick-tissue target should be assumed in computer simulations
1426 for shielding calculations. In addition, losses in the nozzle, beam-shaping, and range-shifting devices

1427 must also be considered in the shielding design. The contributions from adjacent areas, such as the
1428 HEBT and other treatment rooms, should also be considered

1429

1430 Typically, the treatment rooms do not have shielded doors, and therefore the effectiveness of the
1431 maze design is critical. A full computer simulation for the maze is recommended. Mazes are discussed in
1432 more detail in Chapter 3. Treatment rooms either have fixed beams rooms or gantries.

1433

1434 **2.3.4.1 Fixed Beam Rooms.** In fixed beam rooms, either a single horizontal fixed beam or dual
1435 (horizontal and vertical or oblique) beams are used. For a facility with both protons and carbon ions, both
1436 particles have to be considered for shielding design. Although the proton intensity is much higher than
1437 the carbon intensity for synchrotron-based facilities, the neutron dose rate in the forward direction is
1438 higher for the carbon ions. Shielding walls in the forward direction are much thicker than the lateral
1439 walls and the walls in the backward direction. At large angles and at the maze entrance, the neutron dose
1440 from protons is higher than that from carbon ions. Figure 2.13 shows a fixed beam room with a
1441 horizontal and a 45° vertical beam. The Use Factor (U) is defined as the fraction of time that the primary
1442 proton or carbon ion beam is directed towards the barrier. For rooms with dual beams the Use Factor for
1443 the wall in the forward (0°) direction for each beam should be considered. This may be either 1/2 for
1444 both beams or 2/3 for one beam and 1/3 for the other. For a single beam, the Use Factor is one for the
1445 wall in the forward direction.

1446

1447

1448



1449

1450 Figure 2.13. Fixed beam room with dual beams (Courtesy of Siemens Medical Systems)

1451

1452 **2.3.4.2 Gantry Rooms.** In gantry rooms, the beam is rotated about the patient. On average, it can
1453 be assumed that the Use Factor for each of the four barriers (two walls, floor and ceiling) is 0.25. In some
1454 designs, the gantry counterweight (made of large thicknesses of steel) acts as a stopper in the forward
1455 direction, but it covers a small angle and is asymmetric. The ceiling, lateral walls, and floor are exposed
1456 to the forward-directed radiation. However, because of the lower Use Factor, walls in the forward
1457 direction can be thinner than for fixed beam rooms.

1458

1459 **2.3.5 Beam Shaping and Delivery**

1460

1461 Various methods are used to shape and deliver the beam to the patient. They can be divided
1462 primarily into two categories: passive scattering and pencil beam scanning.

1463

1464 In passive scattering, a range modulation wheel or a ridge filter located in the nozzle is used to
1465 produce a spread-out Bragg peak (SOBP) (Smith, 2009). Scatterers located downstream spread the beam
1466 out laterally. A single scatterer is usually used for small fields and a double scatterer is used for large
1467 fields. Between the nozzle exit and the patient, a collimator (specific to the treatment field) is used to
1468 shape the field laterally, while a range compensator is used to correct for the shape of the patient surface,
1469 inhomogeneities in the tissues traversed by the beam, and the shape of the distal target volume. Since
1470 there are losses due to the incidence of the primary beam on the various delivery and shaping devices, a
1471 much higher beam current is required at the nozzle entrance when compared to the other delivery
1472 techniques. The efficiency of a passive scattering system is typically about 45 %. Therefore, more
1473 shielding is required for passive scattering as compared to pencil beam scanning. This technique also
1474 results in higher secondary dose to the patient as discussed in Chapter 7.

1475

1476 In pencil beam scanning, horizontal and vertical magnets are used to scan the beam in a plane
1477 perpendicular to the beam axis. The range of the beam in the patient is adjusted by changing the beam
1478 energy. In synchrotrons, this is achieved by changing the accelerator energy. In cyclotrons, the ESS is
1479 used to change the energy. Additionally, energy absorbers can also be used in the nozzle for range
1480 shifting and/or range modulation. However, and unlike in passive scattering, there are fewer scatterers
1481 and therefore fewer beam losses; thus, the resulting production of secondary radiation is minimized.

1482

1483

2.4 New Technologies

1484

1485 There have been several advances in accelerator technology and some of these are summarized in
1486 a paper by Smith (2009). They include single-room systems: cyclotron- or synchrotron-based; Dielectric
1487 Wall Accelerator (DWA); Fixed-Field Alternating-Gradient Accelerators (FFAG); and Laser Accelerated
1488 Protons.

1489

1490 2.4.1 Single-Room Systems

1491

1492 Figure 2.14 shows a schematic of the proton gantry of a single-room synchrocyclotron-based
1493 system that is now commercially available. The maximum proton energy at the exit of the cyclotron is
1494 250 MeV. The 250 MeV beam is scattered or spread in the treatment room by the field shaping system,
1495 comprised of the first and second scatterers, energy degrader, and range modulator, which are located in
1496 the gantry. Since the cyclotron is super-conducting, it is small and incorporated into the gantry head. The
1497 gantry is capable of rotating ± 90 degrees about the patient plane. Therefore only the ceiling, one lateral
1498 wall, and the floor intercept the forward-directed radiation, and each of these barriers can be assumed to
1499 have a Use Factor of 1/3.

1500

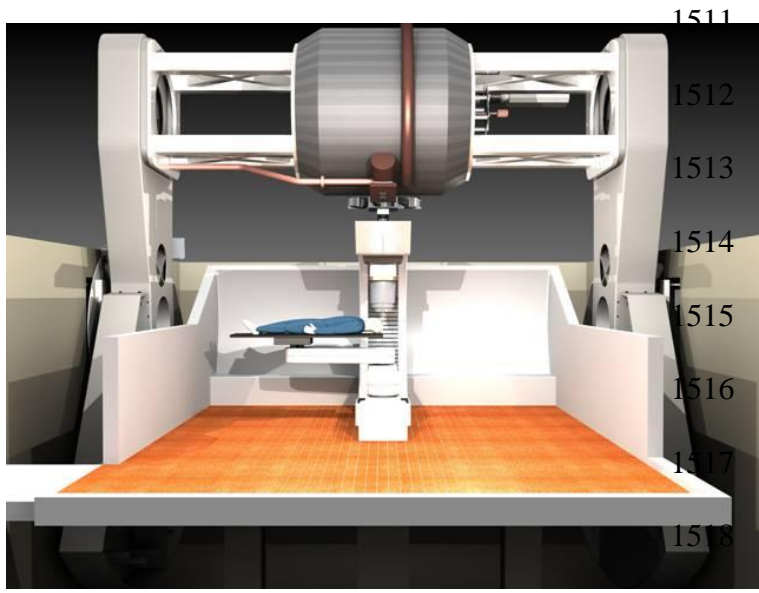
1501 Figure 2.15 shows a 3-D rendition of a single-room cyclotron based facility. The room has two
1502 levels with entrances: a patient treatment level, and a sub-level. Thus, there are two entrance mazes, one
1503 at each level. Both mazes will require shielded doors due to maze-scattered neutrons and neutron-capture
1504 gamma rays. The beam losses to be considered include the primary beam stopped in the patient or
1505 phantom, and leakage from the cyclotron and field shaping systems located in the gantry head. The
1506 thicknesses of the barriers range from about 1.5 m to 4.0 m of concrete .

1507

1508 Figure 2.16 shows a synchrotron-based single room facility.

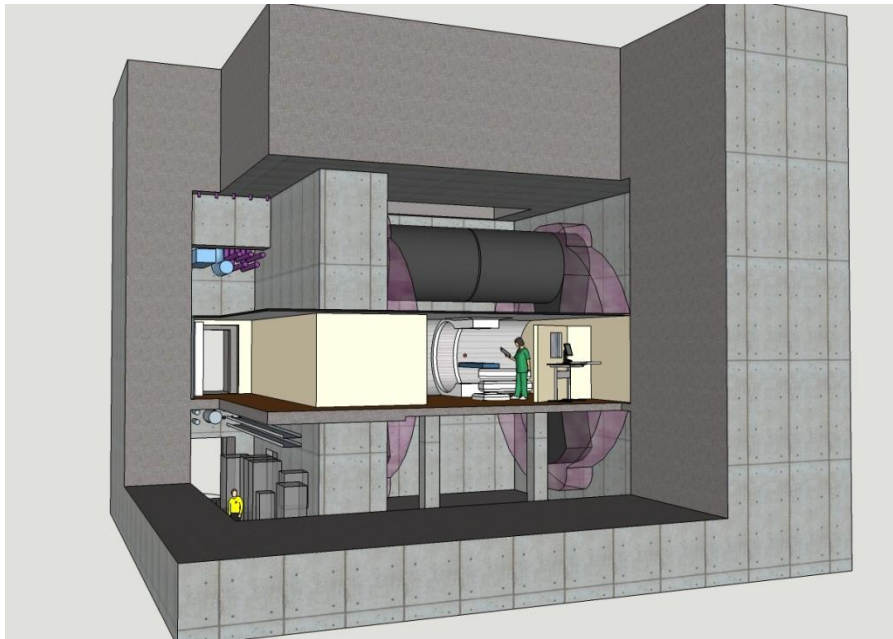
1509

1510



1519
1520 Figure 2.14. Proton therapy gantry including a synchrotron (Courtesy of Still River Systems,
1521 Littleton, MA)
1522

1523



1524

1525

1526 Figure 2.15. Architect’s 3-D rendition of a synchrotron-based single-room facility (Courtesy of The
1527 Benham Companies, An SAIC Company, Oklahoma City, Oklahoma)

1528

1529

1530

1531

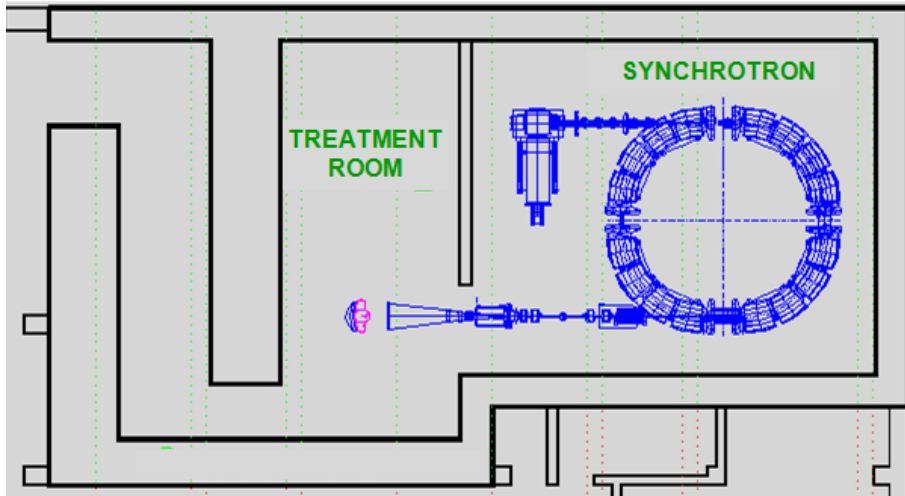
1532

1533

1534

1535

1536



1537

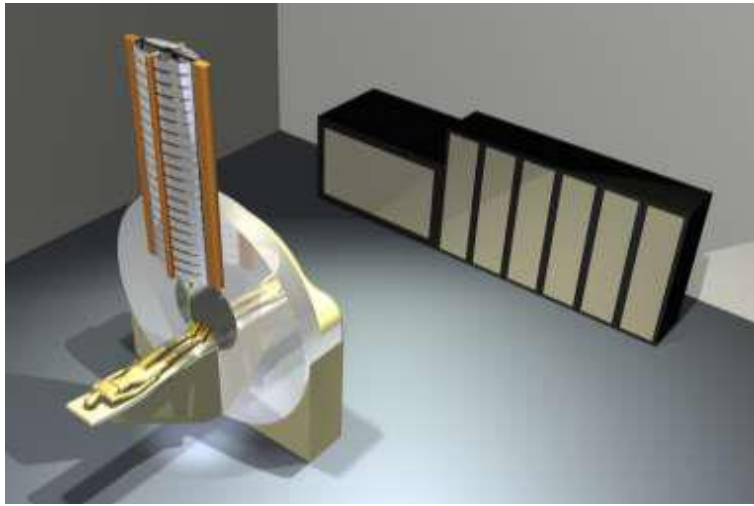
1538 Figure 2.16. Schematic layout of single-room synchrotron-based proton therapy system (Courtesy of
1539 ProTom International, Flower Mound, Texas)

1540

1541 Conventional accelerator cavities have an accelerating field only in their gaps, which occupy only
1542 a small fraction of the cavity length, and have an accelerating gradient of approximately 1 MeV/m to 2
1543 MeV/m. In contrast, dielectric wall accelerators (DWA) have the potential of producing gradients of
1544 approximately 100 MeV/m (Caporasa, 2009). In a DWA, the beam line is replaced by an insulating wall
1545 so that protons can be accelerated uniformly over the entire length of the accelerator. Figure 2.17 shows
1546 the schematic of a compact proton DWA. Protons can be accelerated to 200 MeV in 2 m. The linac is
1547 modular and hence the energy of the protons can be changed easily. The energy, intensity, and spot width
1548 can be varied from pulse to pulse with pulse widths of the order of nanoseconds at a repetition rate of 50
1549 Hz. Losses along the linac are minimal since the linac aperture is much larger than the beam size. The
1550 primary source of secondary radiation is from the proton beam incident on the patient or the phantom.
1551 Since it is a traveling wave linac, bremsstahlung from back-streaming electrons is also not an issue. The
1552 linac has the capability of being rotated through at least 200°.

1553

1554



1555

1556

1557 Figure 2.17. Compact proton dielectric wall accelerator (Caporaso, 2009)

1558

1559 2.4.2 FFAG

1560
1561 FFAG accelerators have fixed magnetic fields (as in cyclotrons) and pulsed acceleration (as in
1562 synchrotrons). For these accelerators, beam losses discussed in previous sections for synchrotrons and
1563 cyclotrons will apply.

1564

1565 2.4.3 Laser Acceleration

1566

1567 A laser pulse interacting with high-density hydrogen-rich material ionizes it, and subsequently
1568 interacts with the created plasma. Protons are accelerated by focusing a high-power laser ($\sim 10^{21}$ W cm⁻²)
1569 on a very thin target (~ 0.5 μ m to 1 μ m thick) with electron densities $n_e = 5 \times 10^{22}$ cm⁻³ (Fan, 2007;
1570 Smith, 2009). The resulting high peak power intensity produced by the extremely short pulse width (~ 50
1571 fs) creates a huge burst of ionization in the target, thus expelling a large number of relativistic electrons.
1572 The sudden loss of electrons results in a high positive charge on the target. The transient positive field
1573 accelerates protons to high energies, resulting in a broad energy spectrum and a large angular
1574 distribution. Protons with energies of 200 MeV or higher can be produced. Special particle selection and
1575 collimation devices are needed to generate the desired proton beams for treatment. Thus, a large number
1576 of unwanted protons and electrons are produced during laser acceleration. For a laser-proton therapy
1577 unit, the target foil assembly and the beam selection device are placed inside the rotating gantry. The
1578 laser is transported to the gantry directly and to the target foil through a series of mirrors. The electron
1579 and proton emission from the target foil are forward-peaked along the axis of the laser beam and have a
1580 wide angular spread. Most of the primary charged particles are stopped in the primary collimator. A small
1581 fraction passes into the particle selection system. The interaction of these high-energy protons with the
1582 selection and collimation devices results in the production of neutrons. The neutrons can further interact
1583 with the shielding to produce neutron capture gamma rays. Bremsstrahlung radiation from electrons must

1584 also be considered in the shielding design since nearly half of the incident laser energy transfers to
1585 electrons, which have a maximum energy that is almost the same as protons. Thus, the leakage radiation
1586 consists of neutrons and photons. In addition to leakage, the deposition of the proton beam in the patient,
1587 phantom or beam stop must also be considered for room shielding.

1588

1589

3. Shielding Design Considerations

1590

Georg Fehrenbacher and Nisy Elizabeth Ipe

1591

1592

3.1 Regulatory Requirements

1593

1594

1595

1596

1597

1598

1599

1600

1601

1602

1603

1604

1605

1606

1607

1608

1609

1610

1611

1612

1613

The use of charged particle beams for therapy purposes is associated with the generation of ionizing radiation which might expose the facility personnel or the public. Patients can also be exposed to unintended radiation. As stated in previous chapters, neutrons are the main source of secondary radiation to be considered in the shielding design of such facilities. The protection of the following different groups of individuals exposed to secondary radiation has to be considered:

- Occupationally exposed workers
- Members of the public (visitors to the clinic and the public in the vicinity of the facility)
- Patients

Most of the national radiation protection regulations are based on international guidelines or standards. For example, standards are formulated by the International Commission on Radiological Protection ICRP (ICRP, 1991; 2007), which are adapted into international rules such as the EURATOM regulations (EURATOM, 1996) and then incorporated into the European national regulations. The international regulations set a minimum level of standards that can be surpassed by the corresponding national laws. Thus, the national radiation protection regulations are comparable for the countries of the European Union.

In some countries, such as Germany, occupationally exposed workers are further classified into categories depending upon the annual effective dose that they receive: Category A (6 mSv per year)

1614 and Category B (20 mSv per year). In this chapter, only the radiation protection for occupational
1615 workers and the public are considered. Chapter 7 covers patients. Dose limits are defined for the
1616 exposure by external radiation and for the intake of radionuclides leading to an internal exposure.

1617

1618 In the U.S., medical facilities are subject to state regulations. These regulations are based on
1619 standards of protection issued by the U.S. Nuclear Regulatory Commission (USNRC, 2009).

1620

1621 The dose limits enforced by national radiation protection regulations are specified in the quantity,
1622 effective dose (defined in Chapter 1). Further limits are applied for the exposure of single organs or
1623 tissues like the lens of the eye or the skin (ICRP, 1991). Because regulations vary from country to
1624 country, it is not possible to list all of them. *However, it is up to each facility to comply with their local,*
1625 *state, or national regulations.* A few examples are given in the sections below.

1626

1627 **3.1.1 Radiological Areas**

1628

1629 In the U.S., radiological areas are defined as shown below (USNRC, 2009):

1630

1631 *Radiation Area* means any area accessible to individuals, in which radiation levels could
1632 result in an individual receiving a dose equivalent in excess of 0.05 mSv in 1 hour at 30
1633 centimeters from the source of radiation or from any surface that the radiation penetrates.

1634

1635 *High Radiation Area* means an area accessible to individuals, in which radiation levels from
1636 radiation sources external to the body could result in an individual receiving a dose equivalent
1637 in excess of 1 mSv in 1 hour at 30 centimeters from any source of radiation or 30 centimeters
1638 from any surface that the radiation penetrates.

1639

1640 *Very High Radiation Area* means an area accessible to individuals, in which radiation levels
1641 from radiation sources external to the body could result in an individual receiving an absorbed
1642 dose in excess of 5 Gy in 1 hour at 1 meter from a source of radiation or 1 meter from any
1643 surface that the radiation penetrates

1644

1645 In addition, radiological areas in the U.S. are classified as *Controlled Areas* when the access,
1646 occupancy, and working conditions are controlled for radiation protection purposes (NCRP, 2005). The
1647 personnel working in the areas are those who have been specifically trained in the use of ionizing
1648 radiation and who are individually monitored. *Unrestricted Area* (or *Uncontrolled Area*) means an area,
1649 access to which is neither limited nor controlled by the licensee are areas that have no restriction of
1650 access, occupancy or working conditions. These areas are often referred to as *Public Areas*. Individuals
1651 who occupy *Uncontrolled Areas* include patients, visitors, service personnel, and employees who do not
1652 work routinely with or around radiation sources. Therefore, these individuals do not require individual
1653 monitoring. *Restricted Area* means an area, access to which is limited for the purpose of protecting
1654 individuals against undue risks from exposure to radiation and radioactive materials.

1655

1656 In Germany, Italy, and Switzerland, the classification of radiological areas is based on the
1657 concepts formulated in the IAEA Safety Series No. 115 (IAEA, 1996). A *Controlled Area* is any area in
1658 which specific protection measures and safety provisions are or could be required for controlling normal
1659 exposures or preventing the spread of contamination during normal working conditions, and preventing
1660 or limiting the extent of potential exposures. A *Supervised Area* is any area not designated as a controlled
1661 area, but for which occupational exposure conditions are kept under review even though specific
1662 protective measures and safety provisions are not normally needed (IAEA, 1996; 2006). The *Interdicted*
1663 *Area* or *Restricted Area* is defined as a part of the controlled area where an increased dose rate level or

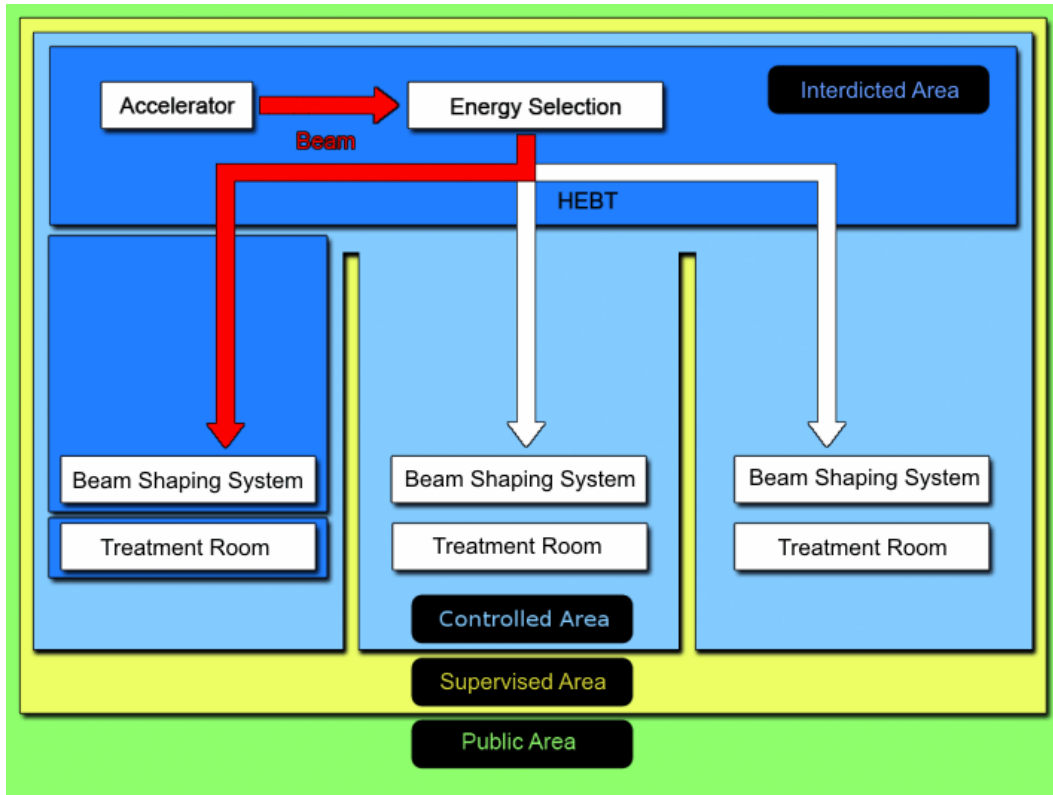
1664 contamination must be considered. Only in some countries is there an explicit definition of these areas in
1665 the radiation protection legislation. Interdicted areas are usually determined by the local radiation safety
1666 management. In some countries the concept of *Intermittent Area* is used for the situations where the
1667 same area changes the status; for example, the treatment rooms (*Interdicted* during use of the beam, and
1668 *Controlled or Supervised* the rest of the time).

1669

1670 The radiological areas for a particle therapy facility (in Germany, Italy, and Switzerland) are
1671 shown in Figure 3.1. All parts of the accelerator where the particle beam is transported are inaccessible
1672 areas (shown in dark blue) while there is beam in the areas. Areas surrounding the accelerator are
1673 controlled areas (shown in light blue) or supervised areas (shown in yellow). The dose limits for the
1674 public may be applied outside the building (shown in green), which is usually accessible to the public.

1675

1676



1677

1678

1679 Figure 3.1. Radiological areas for a particle therapy facility (Courtesy of G. Fehrenbacher, J. Goetze, T.

1680 Knoll, GSI (2009)).

1681

1682

1683 **3.1.2 Dose Limits for Various Countries**

1684

1685 Table 3.1 shows the radiological areas and the dose limits for a few countries as an example. The
1686 dose limits for the countries in the European Union (Italy and Germany) are similar for controlled,
1687 supervised and public areas. In Germany, areas with dose rates > 3 mSv/h are defined as restricted areas.
1688 France further classifies the restricted areas as shown in the table. In the U.S., controlled areas have dose
1689 limits which are much lower than the dose limits for other countries. Thus, for example, while in the U.S.
1690 the control room adjacent to the treatment room has a design dose limit of 5 mSv/yr, dose limits for
1691 controlled areas in other countries are much higher. Therefore, a cookie-cutter design originating in one
1692 country could potentially underestimate or overestimate the shielding in some areas for a charged particle
1693 therapy facility in another country assuming similar patient workload, usage, and beam parameters.

1694

1695 Table 3.1. Examples of classification of radiological areas in some countries. Data sources are cited for
 1696 each country.

Area	USA (USNRC, 2009)	Japan (JRPL, 2004)	South Korea (Lee, 2008)	Italy (IRPL, 2000)	Switzerland (BfG, 2004)	Germany (GRPO, 2005)	France (JORF, 2006)
Restricted	-	-	-	No general regulation (RSO ¹ judgement)	-		Forbidden: >100mSv/h Orange: <2 to100 mSv/h Yellow: < 25 μ Sv to 2 mSv/h
Controlled	≤ 5 mSv/y	<1 mSv/week	-		<20 mSv/y	<3 mSv/h	Green: 7.5 to 25 μ Sv /h
Supervised (area near controlled area)		<1.3 mSv/3 months at boundary of controlled area	<0.4 mSv/week (based on 20 mSv/y for radiation workers)	< 6 mSv/y	<5 mSv/y	< 6 mSv/y	< 7.5 μ Sv /h
Public	≤ 1 mSv/y, 20 μ Sv in 1 h with T=1	<250 μ Sv/3 months (outside of site boundary)	< 1 mSv/y	<1mSv/y Recommended operational limit = 0.25 mSV/y	<1mSv/y	<1 mSv/y	< 80 μ Sv /month

1697

1698 ¹(RSO=Radiation Safety Officer)

1699

1700

3.2 Primary and Secondary Shielding Barriers

1701

1702 In photon therapy, the radiation consists of primary and secondary radiation (NCRP, 2005). The
1703 primary radiation (also referred to as the useful beam) is the radiation emitted directly from the
1704 equipment that is used for patient therapy. The primary barrier is a wall, ceiling, floor, or other structure
1705 that will intercept the primary radiation emitted directly from the equipment. The secondary barrier
1706 intercepts the leakage radiation from the protective housing of the source, as well as any radiation
1707 scattered by the patient or other objects.

1708

1709 For the purposes of this report, for charged particle therapy facilities, we will refer to the protons
1710 or carbon ions as the “primary beam.” The “secondary radiation” will include all the radiation produced
1711 by the interaction of the primary beam with any target including the patient, leakage radiation from the
1712 machine, as well as any scattered radiation. Hence, a primary barrier is defined as a shielding wall,
1713 ceiling, floor, or other structure toward which the primary proton or carbon beam is directed. The
1714 primary barrier intercepts the 0° secondary radiation produced by the interaction of the primary beam
1715 with any target, including the patient. If the primary beam is directed toward the corner of a wall, then
1716 the corner becomes the primary barrier. The secondary barrier is defined as any wall, floor, or ceiling
1717 which is not the primary barrier, *i.e.*, it does not intercept the 0° secondary radiation.

1718

1719

3.3 Use Factors

1720

1721 For photon therapy, the “use factor” as a function of gantry angle [U(G)] gives the fraction of the
1722 weekly workload for which the gantry or beam is oriented in an angular interval centered about angle G
1723 (NCRP, 2005). The IAEA defines the use factor for photon therapy as the fraction of the time during
1724 which the radiation under consideration is directed at a particular barrier (IAEA, 2006). For charged

1725 particle therapy facilities, the use factor (U) may be defined as the fraction of beam operation time during
1726 which the primary proton or carbon ion beam is directed toward a primary barrier. For a gantry room
1727 where the beam rotates 360° about an isocenter, the distribution of gantry treatment angles will be
1728 symmetrical and therefore one can assume a use factor of $1/4$ for each of the primary barriers, *i.e.*, two
1729 walls, ceiling, and floor which directly intercept the primary beam. For a gantry that rotates $\pm 90^\circ$ about
1730 the isocenter, a use factor of $1/3$ can be assumed for each of the primary barriers, *i.e.*, one wall, ceiling,
1731 and floor. For a horizontal fixed beam room, the primary beam direction is fixed, and the use factor is 1
1732 for the barrier toward which the primary beam is directed. Thus, the shielding thickness of each of the
1733 four primary barriers for a gantry room will be less than the thickness required for a fixed beam
1734 primary barrier, because the use factor is only $1/4$.

1735

1736

3.4 Occupancy Factor

1737

1738 The occupancy factor (T) for an area is the average fraction of the time that the maximally
1739 exposed individual is present in the area while the beam is on (NCRP, 2005). If the use of the machine is
1740 spread out uniformly during the week, the occupancy factor is the fraction of the working hours in the
1741 week during which the individual occupies the area. For instance, corridors, stairways, bathrooms, or
1742 outside areas have lower occupancy factors than offices, nurse's stations, wards, staff, or control rooms.
1743 The occupancy factor for controlled areas is typically assumed to be 1, and is based on the premise that a
1744 radiation worker works 100 % of the time in one controlled area or another. However, there can be
1745 exceptions where access to a controlled area is restricted for a radiation worker when radiation is being
1746 produced. In such a case, a lower occupancy factor may be deemed appropriate by the qualified expert
1747 (defined in Section 3.11). The NCRP and IAEA list occupancy factors for various areas (IAEA 2006,
1748 NCRP 2005).

1749

1750

3.5 Workload

1751

1752 The concept of workload (W) for photon radiotherapy is defined as the time integral of the
1753 absorbed dose rate determined at the depth of the maximum absorbed dose in the patient, at a distance of
1754 1 m from the source (NCRP, 2005). It is usually specified as the absorbed dose from photons delivered to
1755 the isocenter in a week, is based on the projected use, and is estimated from the average number of
1756 patients (or fields) treated in a week and the absorbed dose delivered per patient (or field). It also
1757 includes the average weekly absorbed dose delivered during calibrations, quality controls, and physics
1758 measurements. This concept of workload cannot be directly applied to charged particle therapy facilities
1759 for the following reasons:

1760

- 1761 1. In photon therapy, the workload is defined in terms of the primary beam photon dose rate
1762 at the isocenter in a treatment room. Photoneutrons are produced only when the incident
1763 photon energy is higher than about 6 MV. The average energies of the photoneutrons are
1764 1 MeV to 2 MeV. (NCRP, 2005). Photoneutrons are produced mainly in the accelerator
1765 head and any external high-Z target such as lead shielding, *etc.* The photoneutron dose
1766 equivalent rate (from neutrons produced in the accelerator head) is less than 0.1 % of the
1767 primary beam photon dose at the isocenter. The photon leakage dose rate from the
1768 accelerator head is also less than 0.1 % of the primary photon beam dose rate at the
1769 isocenter. The tenth value layer of the primary photons and leakage photons is
1770 significantly greater than tenth value layer of the photonneutrons. Therefore, if the
1771 facility is shielded for photons with concrete, it will be more than adequately shielded for
1772 photoneutrons. For charged particle therapy, any target that intercepts the primary beam
1773 becomes a source of secondary high-energy radiation which must be shielded. For

1774 example, during treatment the proton or ion beam (primary beam) is completely stopped
1775 in the patient tissue, and that then becomes a source of secondary radiation. Further,
1776 secondary radiation production can also occur in beam shaping devices and the beam
1777 nozzle. The secondary radiation dominated by high-energy neutrons determines the
1778 shielding of the treatment room.

1779

1780 2. An important distinction needs to be made when comparing photon therapy and charged
1781 particle therapy. For example, in a gantry room, even though the dose is delivered to the
1782 patient (located at the isocenter of a gantry room), the secondary radiation dose is defined
1783 at 1 m from the isocenter and not at the isocenter, as in photon therapy. Furthermore, in
1784 charged particle therapy the distribution of secondary radiation dose is forward-peaked
1785 and has an angular profile and spectra, unlike in photon therapy, where the photon neutrons
1786 have an almost isotropic distribution.

1787

1788 3. Depending upon the chosen irradiation technique, the energy of the ion beam changes
1789 (*e.g.*, the energy selection system (ESS) for protons from cyclotrons or the use of
1790 synchrotrons for protons and heavy ions).

1791

1792 4. For photon therapy there is only one shielded treatment room. For charged particle
1793 therapy, in addition to shielded treatment rooms, the cyclotron or synchrotron, the beam
1794 transport lines, and the research rooms are also shielded. These areas may have beam
1795 when there is no beam in the treatment room.

1796

- 1797 5. For charged particle therapy facilities, the distinction of the type of primary particle type
1798 is important, because the different energy-angular distributions of the secondary neutrons
1799 influence the shielding design.
1800
- 1801 6. The time structure of the charged particle therapy beam can be rather complicated in
1802 comparison to a photon therapy linear accelerator. Therefore, one has to take into account
1803 the fact that the produced radiation may have a highly discontinuous time structure.
1804
- 1805 7. In charged particle therapy, the patient dose is expressed in the unit Gy equivalent, with
1806 RBEs which have values higher than 1 for heavier ions (like carbon). The shielding
1807 design is essentially based on the (averaged) spectral neutron energy fluence weighted
1808 with dose conversion coefficients (spectral dose distribution). The same dose value for the
1809 irradiated tissue can be associated with significant differing spectral dose distributions.
1810

1811 Thus, the workload must be used in a generic sense to include for each treatment room, each
1812 particle type, each energy, the beam shaping method, the number of fractions per week and the time per
1813 fraction, the dose per fraction, and the proton or carbon ion current required to deliver a specific dose
1814 rate. Once the workload for the treatment room has been established, one must work backwards to
1815 determine the energies and currents from the cyclotron or the synchrotron. The workload for the
1816 cyclotron or synchrotron can then be determined. The workload for each facility will be site-specific.
1817 Further the beam losses, targets and their locations, and associated currents are equipment-specific and
1818 will vary from one equipment vendor to the other.

1819

1820 **3.5.1 Example for Workload Calculations and Usage Assumptions**

1821

1822 An example for workload calculations and usage assumptions, assuming 100 % uniform scanning
1823 for a proton cyclotron facility with a maximum proton energy of 230 MeV, is shown below. The reader
1824 is cautioned against blindly using the example below because it may not be applicable to his or her
1825 facility.

1826

1827 In the following example, we assume a proton cyclotron facility with one gantry room, one
1828 inclined beam room, and one fixed beam room. In each of the three rooms, we assume a total of 25
1829 treatments or fractions per 8 hour day. Treatments are performed at different energies, and 100 %
1830 uniform scanning is assumed. For each energy, the proton current (in nA) required for a 2 Gy/min dose
1831 rate in the patient is provided by the equipment vendor. We assume that each treatment delivers a dose of
1832 2 Gy, which corresponds to a 1 minute irradiation time. A stopping tissue target is assumed in each
1833 treatment room. Based on the treatments, we determine the fraction of time the cyclotron operates at each
1834 energy. The beam losses and targets in the cyclotron, energy selection system and target, and beam
1835 transport line are provided by the equipment vendor.

1836

1837 1. Gantry room and inclined beam rooms:

1838 a) Beam-on time for 2 Gy = 25 fractions/8 h x 40 h/week x 1 min/fraction = 125 min/week

1839 b) Treatments and beam parameters

1840 i. 20 % of treatments at 180 MeV, 3.3 nA at 2 Gy/min

1841 ii. 60 % of treatments at 130 MeV, 2.3 nA at 2 Gy/min

1842 iii. 20 % of treatments at 88.75 MeV, 3.09 nA at 2 Gy/min

1843

1844 2. Horizontal beam room:

1845 a) Beam-on time for 2 Gy = 25 fractions/8 h x 40 h/week x 1 min/fraction = 125 min/week

- 1846 b) Treatments and beam parameters
- 1847 i. 80 % of treatments at 216 MeV, 4 nA at 2 Gy/min
- 1848 ii. 20 % of treatments at 180 MeV, 3.3 nA at 2 Gy/min
- 1849
- 1850 3. Cyclotron
- 1851 a) Beam-on time = 20 h/week
- 1852 b) Beam energies
- 1853 i. 20 % at 216 MeV
- 1854 ii. 20 % at 180 MeV
- 1855 iii. 45 % at 130 MeV
- 1856 iv. 15 % at 130 MeV (88.75 MeV at patient)
- 1857 c) Beam losses in cyclotron
- 1858 i. Transmission efficiency = 35 %
- 1859 ii. Losses at 10 MeV (20 %), ignored because of low energy (10 MeV)
- 1860 iii. 4 counter dees (20 % loss), 10 % at 230 MeV, 10 % at 150 MeV
- 1861 iv. Septum (35 % loss), all at 230 MeV
- 1862 v. 5 % loss between cyclotron and degrader
- 1863
- 1864 4. ESS (Energy selection system)
- 1865 a) Energies
- 1866 i. Carbon degrader: 230 MeV
- 1867 ii. Tantalum collimator: 216 MeV, 180 MeV, 130 MeV
- 1868 b) Beam loss varies depending upon energies requested. Maximum beam loss occurs at ESS.
- 1869
- 1870 5. BTL (Beam transport line)

- 1871 a) Beam-on time = 20 h/week
- 1872 b) Beam Loss = 5 %
- 1873 c) Beam Energies
- 1874 i. 20 % operation at 230 MeV
- 1875 ii. 20 % operation at 180 MeV
- 1876 iii. 45 % operation at 130 MeV
- 1877 iv. 15 % operation at 130 MeV (88.75 MeV at patient)

1878

1879 **3.5.2 Beam Parameters Used for Shielding Calculations**

1880

1881 Table 3.2 shows, for the above example, the beam parameters as provided by the equipment
1882 vendor and the calculated parameters using the vendor's data that are required for shielding calculations.
1883 Column 1 shows the energy of the proton beam at the degrader. Column 2 shows the thickness of the
1884 carbon degrader in the ESS. Column 3 shows the degrader energy. Column 4 shows the thickness of the
1885 carbon range shifter in the nozzle. The range shifter is used only to degrade 130 MeV to 88.75 MeV in
1886 the nozzle. Column 5 shows the proton beam energy at the nozzle exit. Column 6 shows the range in
1887 patient. Column 7 shows the beam size. Column 8 shows the beam current at the cyclotron exit. Column
1888 9 shows the ESS transmission obtained by interpolating data from the equipment vendor for uniform
1889 scanning. Column 10 shows the beam currents at the nozzle entrance. Column 11 shows the beam
1890 current in the BTL calculated backwards, *i.e.* dividing the currents in Column 10 by 0.95 to account for 5
1891 % loss in the BTL. The columns in italics show information provided by the vendor.

1892

1893 For shielding calculations, the currents shown in Column 8 are used for the cyclotron
1894 calculations, while the currents shown in Column 10 are used for treatment rooms and the currents

1895 shown in Column 11 are used for BTL. All the losses in the carbon degrader occur at 230 MeV but with
1896 varying thicknesses as shown in Table 3.2. For the septum and the counter dees, a copper stopping target
1897 is assumed. For losses in the counter dees, 50 % of the losses occur at 230 MeV, while the remaining 50
1898 % occur at 150 MeV.

1899

1900 The contribution of multiple sources to dose at any given location must be considered in the
1901 shielding design. For example, a room in the vicinity of one treatment room may also see dose from the
1902 adjacent treatment room.

1903 Table 3.2. An example of beam parameters used for shielding calculations.

1904

Beam Energy at Cyclotron Exit and Degrader (MeV)	ESS Carbon Degrader Thickness (mm)	Beam Energy at Tantalum Collimator and Nozzle Entrance (MeV)	Carbon Range Shifter Thickness in Nozzle (g/cm^2)	Beam Energy at Nozzle Exit (MeV)	Range in Patient (g/cm^2)	Beam Size (cm x cm)	Beam Current at Cyclotron Exit (nA)	ESS Transmission	Beam Current at Nozzle Entrance (nA)	Beam Current in BTL Calculated Backwards Assuming 5 % Loss in Iron Target
230		130	4.1	88.75	6.24	30 x 30	90.35	0.0068	3.09	3.25
230	130	130		130	21.3	30 x 30	51.0	0.0068	2.3	2.42
230	74.4	180		180		30 x 30	15.83	0.0455	3.3	3.47
230	26.51	216		216	22	30 x 30	7.5	0.1916	4	4.21
230	0.0	230		230	31.8	30 x 30	4.72	0.446	3.77	3.97

1905

1906

1907 Table 3.3 shows a summary of a survey of beam losses at various synchrotron and cyclotron
1908 particle therapy facilities.
1909

1910

1911 Table 3.3. Survey of beam losses at various synchrotron and cyclotron particle therapy facilities. Data

1912 sources are given for each survey.

1913

Accelerator Type	Synchrotron		Cyclotron
Particle Type	Carbon		Proton
Injection LINAC-	60 % (Noda, 2004)		-
Synchrotron			
Loss in the accel.	36 % (Noda, 2004)		50 % (Avery, 2008)
	5 % (Agosteo, 2001)		55 % (Geisler, 2007)
			65 % (Newhauser, 2002)
Extraction	10 % (Noda, 2004)		50 % (Avery, 2008)
	5 % (Agosteo, 2001)		20 % (Geisler, 2007) or higher
HEBT (High	~ 5 % (Noda, 2004)		~ 5 %
Energy Beam	~ 4 to 7 % (Agosteo, 2001)		1% (Newhauser, 2002)
Transport)			
Beam Shaping	Active	Passive	Passive
ESS (Energy	-	70 % (Noda,	> 55 % (99 %)
Selection System)		2004)	(Geisler, 2007), (Rinecker, 2005)
			63 % (Newhauser, 2002)

1914

1915

1916

3.6 Self-Shielding of Beam Line Components

1917

1918 The beam lines are comprised of massive beam optics elements such as dipoles, quadrupoles,
1919 sextupoles, *etc.* As expected, beam losses may occur in these magnets when the particles deviate from
1920 their predetermined path. The elements are typically made of materials such as steel and copper which
1921 provide a large amount of self-shielding. The exact amount of beam losses in these magnets is usually
1922 unknown, and the details of these magnets are not usually provided by the equipment vendor. Self-
1923 shielding of accelerator components can be taken into account by using known beam losses and a
1924 (simplified) model of the magnets in Monte Carlo calculations. When self-shielding is neglected in
1925 shielding calculations, the measured radiation doses are significantly lower than calculated doses. The
1926 cyclotron and the gantry also have a large amount of self-shielding. The self-shielding of the cyclotron is
1927 usually considered in the shielding design, except at the location where there are openings in the magnet
1928 yoke.

1929

1930

3.7 Calculational Methods

1931

3.7.1 Analytical Methods

1933

1934 Most analytical models can be described as line-of-sight (also called point kernel) models which
1935 incorporate the following parameters and assumptions:

1936

1937

1. Point loss;

1938

2. Distance of the point source to reference point (r);

1939

3. Angle of the incident beam (line) and the direction to the reference point (θ);

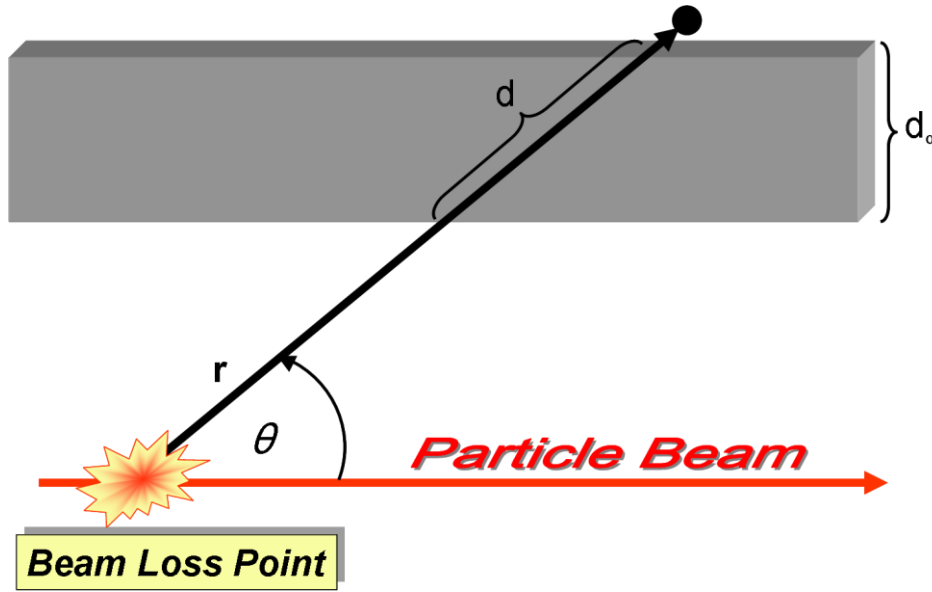
- 1940 4. Angular specific source term $H_0(E_p, \theta)$ which depends on the ion type and target type, as
1941 well as E_p , the particle energy;
- 1942 5. Exponential attenuation in shielding material of thickness d_0 , where d ($d_0/\sin(\theta)$) is the
1943 slant thickness, and $\lambda(\theta)$ is the attenuation length. λ depends on the angle θ , because the
1944 neutron energy distribution changes with the angle θ .

1945

1946 Figure 3.2 shows the geometry for the line-of-sight-model.

1947

1948



1949

1950

1951 Figure 3.2. Application of the line-of-sight models to simple bulk shielding geometries (Courtesy of G.

1952 Fehrenbacher, J. Goetze, T. Knoll, GSI (2009)).

1953

1954 The dose (rate) at the reference point is derived from the source term H_0 and geometrical
1955 quantities. The dose $H(E_p, d, \theta)$ at the reference point can then be estimated as follows:

1956

$$1957 \quad H(E_p, d, \theta) = H_0(E_p, \theta) \cdot \frac{1}{r^2} \cdot \exp\left(-\frac{d}{\lambda(\theta)}\right) \quad (3.1)$$

1958

1959 In 1961, Burton Moyer developed a semi-empirical method for the shield design of the 6 GeV
1960 proton Bevatron (NCRP, 2003). Design studies of the proton synchrotron at Fermi National Accelerator
1961 Laboratory (FNAL, Batavia, Illinois) and the Super Proton Synchrotron (SPS, CERN, Geneva) led to the
1962 improvement of the Moyer model. This model is only applicable to angles close to 90° and the transverse
1963 shielding for a high-energy proton accelerator is determined using the following simple form of the
1964 Moyer model (Thomas, 1993):

1965

$$1966 \quad H = \frac{H_0}{r^2} \left[\frac{E_p}{E_0} \right]^\alpha \exp\left[-\frac{d}{\lambda}\right] \quad (3.2)$$

1967

1968 where H = maximum dose equivalent rate at a given radial distance (r) from the target, d = shield
1969 thickness, E_p = proton energy, $E_0 = 1$ GeV, $H_0 = 2.6 \times 10^{-14}$ Sv m^2 , and α is about 0.8.

1970

1971 This model is effective in the GeV region because the neutron dose attenuation length (λ) is
1972 nearly constant regardless of energy (see Fig. 1.3). However, the model is restricted to the determination
1973 of neutron dose equivalent produced at an angle between 60° to 120° . At proton energies in the
1974 therapeutic range of interest, the neutron attenuation length increases considerably with energy as shown
1975 in Fig. 1.3. Clearly, such empirical models are limited in their use because they are limited to transverse
1976 shielding, and do not account for changes in energy, angle of production, target material and dimensions,

1977 and concrete material composition and density. In the past, the Moyer model has been used in the
1978 shielding design of some proton therapy facilities; however, it is not appropriate for such use.

1979

1980 Kato and Nakamura have developed a modified version of the Moyer model which includes
1981 changes in attenuation length with shield thickness, and also includes a correction for oblique penetration
1982 through the shield (Kato, 2001). Tesch has also developed a model for proton energies from 50 MeV to 1
1983 GeV (Tesch, 1985). In the past, high-energy accelerators were shielded using analytical methods.
1984 However, with the advent of powerful computers and sophisticated Monte Carlo codes, computational
1985 methods have superseded analytical methods. Analytical methods may be used for the planning of the
1986 bulk shielding, but do not provide a very precise prediction of the dose rate levels outside the shielding.
1987 The advantages of analytical methods are their ease of use and the comparatively high efficiency in
1988 obtaining results. Their drawbacks are the very simplistic assumptions, limited applicability to simple
1989 planar geometries, and limitations of target materials and geometry.

1990

1991 **3.7.2 Monte Carlo Calculations**

1992

1993 Monte Carlo codes are described in detail in Chapter 6, and are used extensively for shielding
1994 calculations. These codes can be used to do a full simulation, modeling the accelerator or beam line and
1995 the room geometry in its entirety. They can also be used to derive computational models as discussed in
1996 the next section. Monte Carlo codes have been used for shielding design of rooms or mazes at several
1997 facilities (Agosteo *et al.*, 1996b; Avery *et al.*, 2008; Dittrich and Hansmann, 2006; Hofmann and
1998 Dittrich, 2005; Kim *et al.*, 2003; Porta *et al.*, 2005; Stichelbaut, 2009). Monte Carlo codes can be used
1999 to generate isodose curves (dose contours), which provide a visualization of the secondary radiation field
2000 that helps facilitate the shielding design (Hofmann and Dittrich, 2005). It is important to note that when

2001 comparing Monte Carlo calculations to experimental data, the actual experimental configuration should
2002 be modeled, including the instrument response and the concrete composition. Further, the experiment
2003 should have been performed using the appropriate instrumentation. If there are any deviations from the
2004 above conditions, there will be large discrepancies between measurements and simulations.
2005 Unfortunately, there is hardly any published data for charged particle therapy facilities that meets all
2006 these conditions.

2007

2008 **3.7.3 Monte Carlo Computational Models**

2009

2010 Monte Carlo computational models that are independent of geometry typically consist of a source
2011 term and an exponential term that describes the attenuation of the radiation. Both the source term and the
2012 attenuation length are a dependent on particle type and are a function of energy and angle. Agosteo *et al.*
2013 (1996b) first derived such models using experimental double differential neutron spectra, but the data is
2014 now obsolete (Agosteo, 2007). Ipe and Fasso (2006) have published source terms and attenuation lengths
2015 for composite barriers with 430 MeV carbon ions incident on a 30 cm ICRU sphere. As discussed in
2016 Chapter 1, computational models are useful especially during the schematic phase of the facility design,
2017 when the design undergoes several changes, to determine the bulk shielding. In this case, the entire room
2018 geometry is not modeled but usually spherical shells of shielding material are placed around the target,
2019 and dose is scored at given angular intervals and in each shell of shielding material. The dose at each
2020 angle can be plotted as a function of shielding thickness and the data can be fitted to obtain source terms
2021 and attenuation lengths as a function of angle, and at the energies of interest, with the appropriate target
2022 using Monte Carlo methods. The source terms and attenuation lengths will depend upon the composition
2023 and density of the shielding material. A stopping target can be used to determine dose rates from the
2024 beam incident on the patient. However, the use of a stopping target is not necessarily conservative in all

2025 cases, because for a thin target, the hadron cascade may propagate in the downstream shielding. Ray
2026 traces can be performed at various angles and the source terms and attenuation lengths can be used for
2027 dose calculations. These models are also useful in identifying thin shielding and facilitates improved
2028 shield design. The qualified expert should not rely on published models but should derive computational
2029 models for energies, targets and concrete composition that are site specific.

2030

2031 **3.7.3.1 Carbon Ions.** Ipe and Fasso (2006) describe Monte Carlo calculations performed using
2032 FLUKA to derive computational models for 430 MeV/u carbon ions incident on tissue. The simulations
2033 were performed so that source terms and attenuation lengths in concrete and composite barriers (concrete
2034 plus iron) could be determined for 430 MeV/u carbon ions incident on an ICRU tissue sphere (15 cm
2035 radius, 76.2 % O, 10.1 % H, 11.1 % C, and 2.6 % N). The concrete was assumed to be Portland cement
2036 with a density of 2.35 g cm^{-3} .

2037

2038 Figure 3.3 shows the total ambient dose equivalent from all particles in picosieverts per carbon
2039 ion normalized to a distance of 1 m from the target ($\text{pSv}\cdot\text{m}^2$) as a function of shielding thickness. The
2040 dose at any distance d from the tissue target is obtained by dividing the dose at 1 m by d^2 . Also shown is
2041 the dose equivalent in vacuum. It is important to note that there is a dose build-up in the first few layers
2042 of the shielding before attenuation takes place. Therefore, dose equivalent rates in vacuum should not be
2043 used to determine shielding thicknesses. The errors are not shown but are typically within 20 %. The
2044 attenuation length, λ , changes with shielding depth and reaches equilibrium after about 1.35 m of
2045 shielding thickness. The data in Figure 3.3 were fitted with the classical two parameter formula as shown
2046 in Equation 1.1. The equilibrium attenuation length, λ_e , is given by the reciprocal of the exponent. The
2047 results are shown in Table 3.4 together with the parameters for two other polar angles (10° to 30° and
2048 40° to 50°). The source terms and attenuation lengths are valid for shielding thicknesses greater than 1.35

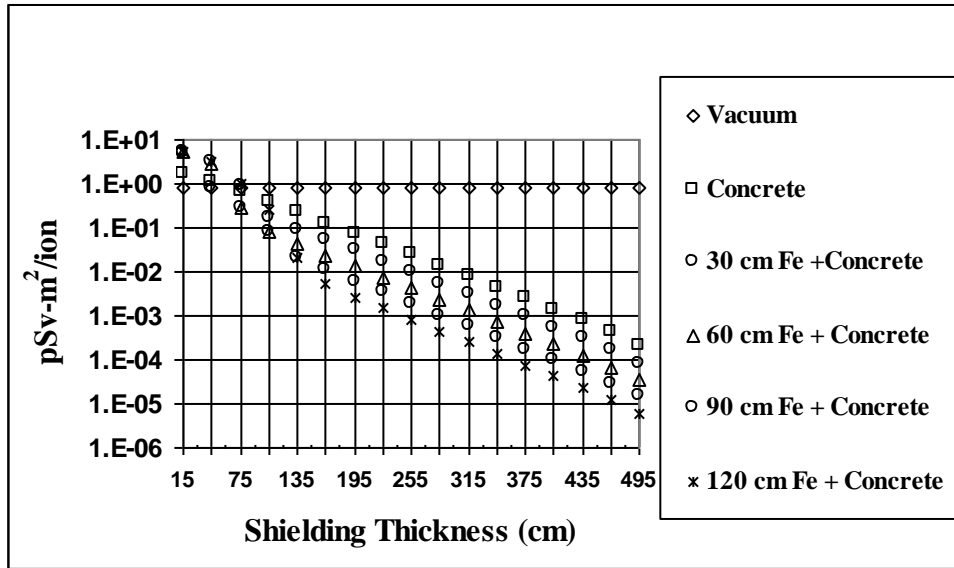
2049 m. The attenuation lengths shown are the dose equivalent attenuation lengths for all particles and not just
2050 for neutrons. The attenuation length in the 10° to 30° range is higher than in the forward direction. A
2051 similar observation was made by Agosteo *et al.* (1996b) for 400 MeV/u carbon ion data. This may be
2052 attributed to the fact that head-on collisions for carbon ions are less frequent than grazing collisions
2053 (Raju, 1980).

2054

2055 In general, it can be observed that the addition of 30 cm of iron provides a reduction in the
2056 source term by a factor of about 2. In the forward direction (0° to 30°), there is a softening of the
2057 spectrum with the addition of iron, as can be observed by the change in attenuation length. At large
2058 angles (40° to 60°), the iron does not appear to provide any significant softening of the spectrum. It is
2059 important to note that the source terms and attenuation lengths will depend upon the particle energy, the
2060 material and dimensions of the target, the angle of production, the fluence to dose equivalent conversion
2061 factors, and the composition and density of the shielding material. Additionally the source terms and
2062 attenuation lengths will also depend on how good the fit is. There is no other published data on source
2063 terms and attenuation lengths (computational or experimental) for 430 MeV/u carbon ions.

2064

2065



2066

2067

2068 Figure 3.3. Dose equivalent per carbon ion (0° to 10°) as a function of shielding thickness for 430 MeV/u
2069 carbon ions incident on ICRU tissue sphere for composite shield (Ipe and Fasso, 2006).

2070

2071 Table 3.4 Computational models for concrete and composite shield (concrete and iron) for 430 MeV/u
2072 carbon ions incident on ICRU tissue sphere (15 cm radius) valid for shielding thickness > 1.35 m (Ipe
2073 and Fasso, 2006).

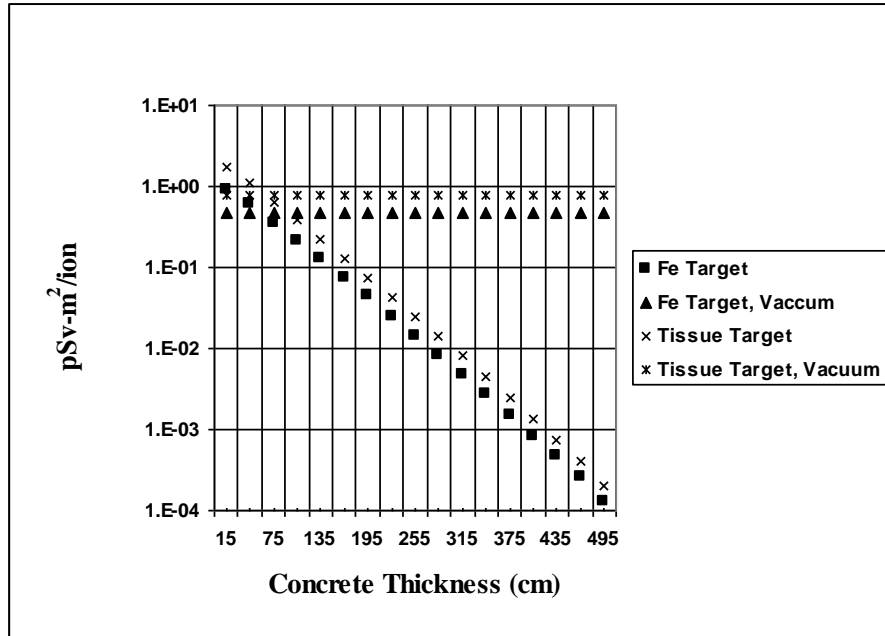
2074

Iron Thickness (cm)	0° to 10°		10° to 30°		40° to 60°	
	H ₀ (Sv-m ² /ion)	λ _e (g/cm ²)	H ₀ (Sv-m ² /ion)	λ _e (g/cm ²)	H ₀ (Sv-m ² /ion)	λ _e (g/cm ²)
0	(3.02 ± 0.04) x 10 ⁻¹²	123.81 ± 0.48	(4.81 ± 0.06) x 10 ⁻¹³	133.09 ± 0.74	(4.71 ± 0.21) x 10 ⁻¹⁴	117.64 ± 1.32
30	(1.25 ± 0.02) x 10 ⁻¹²	123.12 ± 0.38	(2.44 ± 0.03) x 10 ⁻¹³	129.64 ± 0.36	(1.91 ± 0.08) x 10 ⁻¹⁴	119.38 ± 0.48
60	(6.05 ± 0.03) x 10 ⁻¹³	120.32 ± 0.46	(1.11 ± 0.04) x 10 ⁻¹³	128.66 ± 0.70	(8.29 ± 0.66) x 10 ⁻¹⁵	118.5 ± 0.80
90	(2.77 ± 0.09) x 10 ⁻¹³	119.58 ± 1.25	(5.27 ± 0.29) x 10 ⁻¹⁴	126.09 ± 0.80	(3.29 ± 0.69) x 10 ⁻¹⁵	119.14 ± 1.34
120	(1.33 ± 0.05) x 10 ⁻¹³	117.68 ± 0.91	(2.48 ± 0.24) x 10 ⁻¹⁴	124.29 ± 0.94	(1.34 ± 0.68) x 10 ⁻¹⁵	118.83 ± 2.89

2075

2076

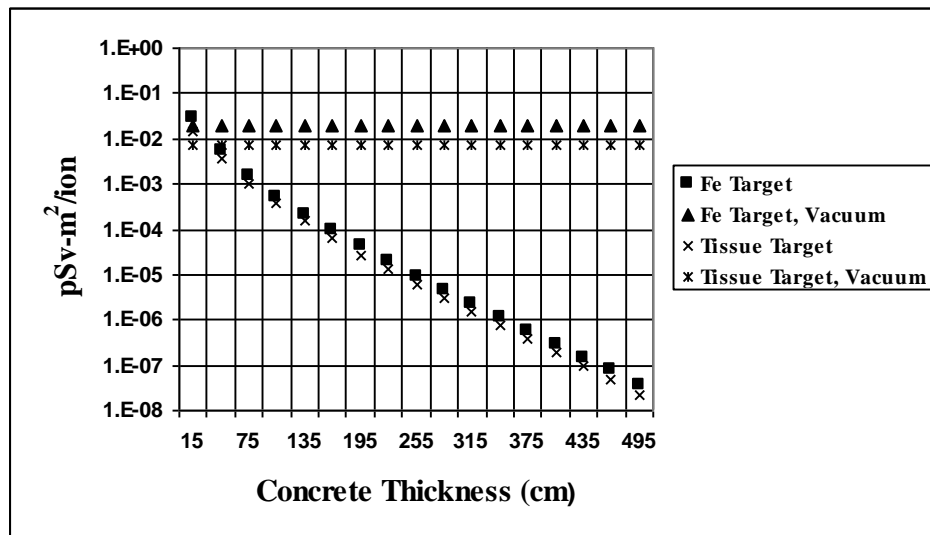
2077 Figures 3.4 and 3.5 show the dose per carbon ion in picosieverts per particle normalized to 1 m
2078 (pSv-m²) as a function of concrete thickness for both iron (Fe) target and tissue targets in the 0° to 10°
2079 and 80° to 100° directions. In the forward direction, the doses in vacuum and concrete are higher for the
2080 tissue target when compared to the iron target, whereas at the large angles, the doses are lower for the
2081 tissue target when compared to the iron target. This is because the high-energy neutron components
2082 produced in the forward direction by a break-up process and the momentum transfer from projectile to
2083 target nuclei are higher for both lighter nuclei targets and higher projectile energy than for heavier
2084 nuclei targets and lower projectile energy (Gunzert-Marx *et al.*, 2004). Thus, more forward-directed
2085 neutrons will be produced in a stopping tissue target than in a stopping iron target. For both targets, there
2086 is a build up in dose in the first few layers of the concrete shield. The attenuation lengths reach
2087 equilibrium only after about a meter or more of concrete in the forward direction.
2088



2089

2090 Figure 3.4. Dose equivalent per carbon ion (0° to 10°) as a function of concrete thickness for 430 MeV/u
2091 carbon ions incident on ICRU tissue and iron targets (Ipe and Fasso, 2006).

2092

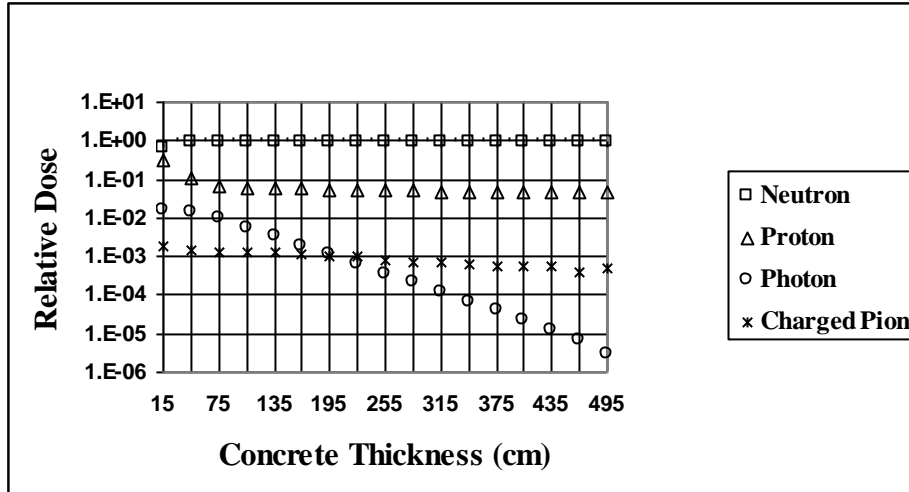


2093

2094 Figure 3.5. Dose equivalent per carbon ion (80° to 100°) as a function of concrete thickness for 430
2095 MeV/u carbon ions incident on ICRU tissue and iron targets (Ipe and Fasso, 2006).

2096

2097 Figure 3.6 shows the relative dose equivalent contributions of the various particles for 0° to 10° at
2098 1 m from the target. Neutrons are the largest contributor to the total dose. At a depth of 15 cm in
2099 concrete, about 66 % of the dose is from neutrons, about 32 % from protons, less than 2 % from photons,
2100 and less than 0.2 % from charged pions. The neutron contribution increases to about 95 % at greater
2101 depths. At large angles (not shown in the figure), the neutron contribution remains fairly constant at all
2102 depths (96 %), while the proton contribution increases from less than 1 % to about 2 % with increasing
2103 depths. Thus, neutrons dominate the dose outside the shielding at all angles.
2104



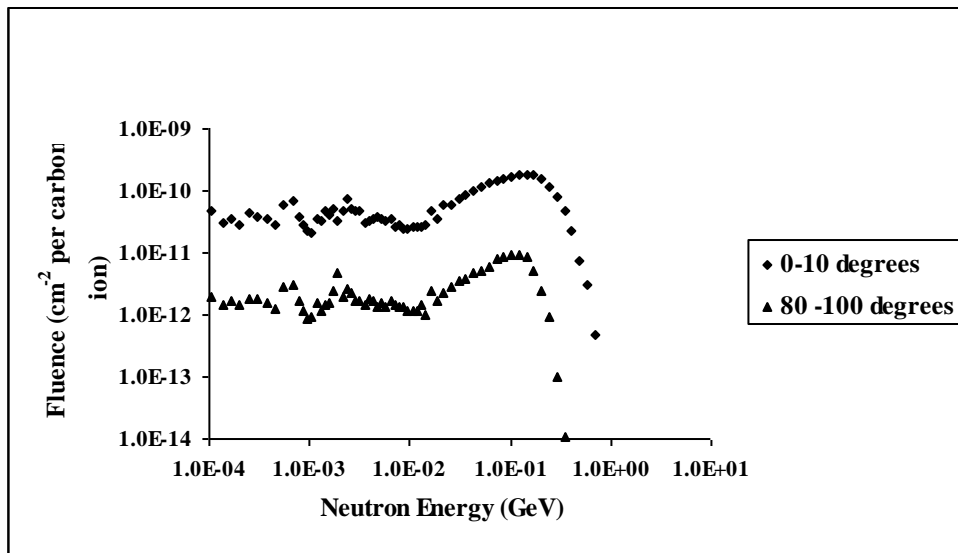
2105

2106 Figure 3.6. Relative dose equivalent contributions at 0° to 10° per carbon ion at 1 m from ICRU tissue
2107 sphere (Ipe and Fasso, 2006).

2108

2109 Figure 3.7 shows the neutron spectra from 430 MeV/u carbon ions incident on tissue at the
2110 concrete surface, for 0° to 10° and for 80° to 90° . The errors are not shown but are typically within 20 %.
2111 The fluence is in lethargy units, *i.e.*, $E \times d\phi/dE$, where E is the neutron energy and $d\phi/dE$ is the
2112 differential fluence. The neutron fluence in the forward direction (0° to 10°) is much greater than the
2113 neutron fluence at the large angles (80° to 100°) at the concrete surface. The neutron spectrum in the
2114 forward direction extends up to about 1 GeV in energy, while the spectrum at the large angle extends to
2115 about 0.4 GeV. In both spectra, the oxygen resonance peaks (from concrete) at 500 keV and the
2116 evaporation neutron peaks at about 2.3 MeV are observed. A high-energy neutron peak is observed at
2117 about 340 MeV in the forward direction, while a broad peak is observed between about 20 and 50 MeV
2118 at the large angles.
2119

2120



2121

2122 Figure 3.7. Neutron energy spectra incident at concrete surface for 430 MeV/u carbon ions incident on

2123 ICRU tissue sphere (Ipe and Fasso, 2006).

2124

2125 **3.7.3.2 Protons.** Agosteo *et al.* (2007) have derived computational models for concrete for 100,
2126 150, 200, and 250 MeV protons incident on a thick iron target using the Monte Carlo code FLUKA,
2127 using the TSF 5.5 concrete with a density of 2.31 g cm^{-3} and a water content of 5.5 %. A single
2128 exponential fit was used for the data in the forward direction, and a double exponential fit was used at
2129 large angles ($> 40^\circ$). The results are shown in Table 3.5. They have also made an extensive comparison
2130 of their Monte Carlo computational data with published experimental and computational data and
2131 conclude that “there is wide range of variability in the results, which reflects the large differences in the
2132 geometrical configurations (experimental or computational), material composition and techniques used.
2133 The concrete composition may have a substantial impact on the attenuation properties of a barrier”
2134 (Agosteo *et al.*, 2007). Teichmann (2006) has published computational models for 72 MeV and 250 MeV
2135 protons incident on a thick iron target, using the Monte Carlo code MCNPX (Pelowitz, 2005) for the
2136 TSF 5.5 concrete. Attenuation lengths calculated with FLUKA and MCNPX agree to within 10 %,
2137 whereas the source terms are significantly different. For example, MCNPX source term is 1.5 times
2138 lower than the FLUKA source term at 250 MeV in the 0° to 10° interval. Ipe (2008) has published the
2139 equilibrium attenuation lengths for 250 MeV protons incident on a tissue target for composite (iron plus
2140 concrete) barriers. Tayama *et al.* (2002) have published source terms and attenuation lengths based on
2141 MCNPX for concrete, for 52 MeV, 113 MeV and 256 MeV protons incident on a thick iron target.
2142 Tayama *et al.* (2002) also compare experimental source terms and attenuation lengths measured by
2143 Siebers (1993) for 230 MeV with MCNPX calculations. The calculated source term and attenuation
2144 length are within a factor of 2 and 35 %, respectively, of the measured values.

2145

2146 Table 3.5. Source term parameter and attenuation length for proton beams stopped in a thick iron target.

2147 The attenuation is computed for normal concrete (TSF-5.5) (Agosteo, 2007).

2148

Energy (MeV)	Angular Bin	H ₁ (10) per proton (Sv m ²)	λ ₁ (g cm ⁻²)	H ₂ (10) per Proton (Sv m ²)	λ ₂ (g cm ⁻²)
100	0° to 10°			(8.9 ± 0.4) x 10 ⁻¹⁶	59.7 ± 0.2
	40° to 50°	(5.9 ± 1.3) x 10 ⁻¹⁶	47.5 ± 2.7	(1.5 ± 0.1) x 10 ⁻¹⁶	57.2 ± 0.3
	80° to 90°	(5.3 ± 0.8) x 10 ⁻¹⁶	33.7 ± 1.2	(1.1 ± 0.3) x 10 ⁻¹⁷	52.6 ± 0.7
	130° to 140°	(4.7 ± 0.4) x 10 ⁻¹⁶	30.7 ± 0.5	(8.0 ± 5.1) x 10 ⁻¹⁸	46.1 ± 2.8
150	0° to 10°			(3.0 ± 0.2) x 10 ⁻¹⁵	80.4 ± 0.5
	40° to 50°	(1.2 ± 0.2) x 10 ⁻¹⁵	57.8 ± 3.4	(3.3 ± 0.8) x 10 ⁻¹⁶	74.3 ± 1.4
	80° to 90°	(10.0 ± 2.2) x 10 ⁻¹⁶	37.4 ± 2.7	(1.2 ± 0.3) x 10 ⁻¹⁷	70.8 ± 1.3
	130° to 140°	(7.8 ± 2.0) x 10 ⁻¹⁶	32.1 ± 1.5	(2.1 ± 0.6) x 10 ⁻¹⁸	61.8 ± 1.1
200	0° to 10°			(5.6 ± 0.4) x 10 ⁻¹⁵	96.6 ± 0.8
	40° to 50°	(1.9 ± 0.3) x 10 ⁻¹⁵	68.3 ± 5.9	(6.8 ± 0.5) x 10 ⁻¹⁶	86.4 ± 0.5
	80° to 90°	(1.3 ± 0.4) x 10 ⁻¹⁵	43.8 ± 4.4	(3.7 ± 0.8) x 10 ⁻¹⁷	78.3 ± 1.3
	130° to 140°	(1.3 ± 0.3) x 10 ⁻¹⁵	32.8 ± 1.6	(2.8 ± 2.4) x 10 ⁻¹⁸	70.0 ± 4.1
250	0° to 10°			(9.8 ± 1.0) x 10 ⁻¹⁵	105.4 ± 1.4
	40° to 50°	(2.3 ± 0.5) x 10 ⁻¹⁵	77.0 ± 7.9	(1.2 ± 0.1) x 10 ⁻¹⁵	93.5 ± 0.5
	80° to 90°	(1.4 ± 0.4) x 10 ⁻¹⁵	49.7 ± 5.7	(9.0 ± 2.5) x 10 ⁻¹⁷	83.7 ± 2.0
	130° to 140°	(1.9 ± 0.6) x 10 ⁻¹⁵	34.4 ± 3.4	(6.5 ± 2.6) x 10 ⁻¹⁸	79.1 ± 3.4

2149

2150

2151 **3.7.4 Other codes**

2152

2153 The ANISN code (Engle, 1967) was used for the design of the Hyogo (HIBMC) and Gunma
2154 University facilities.

2155

2156 The BULK-I code is a Microsoft Excel application and developed at the accelerator laboratory
2157 KEK in Japan (Tayama, 2004). The tool is applicable for proton beams in the energy range from 50 MeV
2158 to 500 MeV. The shielding can be computed not only for concrete but also for iron or combinations of
2159 both.

2160

2161 The BULK C-12 code, developed at the University of Applied Science in Zittau, Germany, in
2162 cooperation with AREVA, Erlangen, Germany (Norosinski, 2006), is capable of estimating neutron and
2163 photon effective dose rates from medium energy protons (50 MeV to 500 MeV) or carbon ions (155
2164 MeV/u to 430 MeV/u). Shielding materials considered in the code are concrete walls or a combination of
2165 iron and concrete. The code is available from the Nuclear Energy Agency (NEA) (Norosinski, 2006).

2166

2167 **3.8 Shielding Materials and Transmission**

2168

2169 **3.8.1 Shielding Materials**

2170

2171 Earth, concrete, and steel are typically used for particle accelerator shielding (NCRP, 2003).
2172 Other materials such as polyethylene and lead are used to a limited extent. As previously stated, neutrons
2173 are the dominant secondary radiation, and when using steel a layer of hydrogenous material, must be
2174 used in conjunction with the steel.

2175

2176 **3.8.1.1 Earth.** Earth is often used as shielding material at underground accelerator facilities and
2177 must be compacted to minimize cracks and voids. Earth is primarily composed of silicon dioxide (SiO_2),
2178 which makes it suitable for shielding of both gamma radiation and neutrons (NCRP, 2003). It contains
2179 water which improves the shielding of neutrons. Because the water content (0% to 30%) of the earth and
2180 its density (1.7 g/cm^3 to 2.2 g/cm^3) can vary quite a bit, the soil characteristics of the site must be
2181 determined to ensure effective shielding design. The activation of the ground water must also be
2182 considered for underground facilities. Partial earth shielding is used at some particle therapy facilities
2183 (HIT facility in Heidelberg, CNAO in Pavia, Italy, and Gunma University in Japan). The only cost
2184 associated with earth is its transportation offsite.

2185

2186 **3.8.1.2 Concrete and Heavy Concretes.** Concrete is a mixture of cement, coarse and fine
2187 aggregates, water, and sometimes supplementary cementing materials and/or chemical admixtures (see
2188 http://www.cement.org/tech/faq_unit_weights.asp). The density of concrete varies depending on the
2189 amount and density of the aggregate, the amount of air that is entrapped or purposely entrained, and the
2190 water and cement contents (which in turn are influenced by the maximum size of the aggregate).
2191 Ordinary concrete has a density that varies between 2.2 and 2.4 g cm^{-3} .

2192

2193 Concrete has many advantages compared to other shielding materials (NCRP, 2005). It can be
2194 poured in almost any configuration and provides shielding for both photons and neutrons. It is relatively
2195 inexpensive. Because of its structural strength, poured-in-place concrete can be used to support the
2196 building and any additional shielding. Concrete blocks are also available. Water exists in concrete in the
2197 free and bound form. The water content of concrete plays a significant role in the shielding of neutrons.
2198 With time, the free water evaporates, but the concrete also hydrates (absorbs moisture from the

2199 surrounding environment) until it reaches some equilibrium. About 3 % of the water may evaporate in
2200 the first 30 days or so. For neutron shielding, a water content of about 5 % is recommended.

2201

2202 In the U.S., ordinary concrete is usually considered to have a density of 2.35 g cm^{-3} (147 lb feet
2203 3). Concrete used for floor slabs in buildings are typically lightweight with a density that varies between
2204 1.6 and 1.7 g cm^{-3} .

2205

2206 The poured-in-place concrete is usually reinforced with steel rebar, which makes it more effective
2207 for neutrons. Because the steel rebar is not included in the concrete composition, measured radiation
2208 doses with heavily reinforced concrete will be lower than calculated doses. The disadvantage of concrete
2209 is that takes months to pour. The typical compositions of various types of concrete are shown in Table
2210 3.6.

2211

2212 High-Z aggregates or small pieces of scrap steel or iron are sometimes added to concrete to
2213 increase its density and effective Z. These concretes are known as heavy concretes. Densities of up to
2214 about 4.8 g cm^{-3} can be achieved. However, the pouring of such high-Z enhanced concrete is a special
2215 skill and should not be undertaken by an ordinary concrete contractor because of settling, handling, and
2216 structural issues (NCRP, 2005). Ordinary concrete pumps are not capable of handling such dense
2217 concrete. The high-Z aggregates could sink to the bottom resulting in a non-uniform composition and
2218 density. Concrete trucks with greater capacity will be required for transportation. Heavy concretes made
2219 locally at the construction site may not be subject to industrial standards and will need to be checked.
2220 Prefabricated heavy concretes are subject to rigorous standards and are available as blocks or
2221 interlocking blocks. The high-Z aggregate enhanced concrete is also sold in the form of either
2222 interlocking or non-interlocking modular blocks. It is preferable to use the interlocking blocks to avoid

2223 the streaming of radiation. Concrete enhanced with iron ore is particularly effective for the shielding of
2224 relativistic neutrons. .

2225

2226 Ledite® is manufactured by Atomic International, Frederick, Pennsylvania, and is a modular pre-
2227 engineered interlocking high density block which has a high iron content. It is currently used in the
2228 shielding of photon therapy linear accelerators. It can be placed in existing structures and can be
2229 relocated and reused. Its use results in considerable time savings. Pouring of concrete takes months,
2230 whereas Ledite can be stacked in weeks. In order to study the space savings that could result from the use
2231 of Ledite, the transmission of three different compositions were investigated: Proshield Ledite 300 ($\rho =$
2232 4.77 g cm^{-3}) which is was marketed by the manufacturer for particle therapy, and two previous
2233 compositions referred to as Ledite 293² ($\rho = 4.77 \text{ g cm}^{-3}$) and Ledite 247³ ($\rho = 3.95 \text{ g cm}^{-3}$). The results
2234 are discussed in Section 3.8.2.

2235

2236 An important consideration in the choice of shielding materials is their susceptibility to
2237 radioactivation by neutrons, which can last for decades. Activation of concrete is discussed in Chapter 4.
2238 It has been observed that for short-lived radioactivity, ²⁴Na ($T_{1/2} = 15 \text{ h}$) is dominant, and for longer-lived
2239 radioactivity, ²²Na ($T_{1/2} = 2.6 \text{ a}$) and ¹⁵²Eu ($T_{1/2} = 12 \text{ a}$) are dominant. The steel rebars can also get
2240 activated. Higher activation may occur with some heavy concrete like barites (which are barium
2241 containing). Radioactive isotopes such as ¹³³Ba ($T_{1/2} = 10.7 \text{ a}$), ¹³⁷Cs ($T_{1/2} = 30.0 \text{ a}$), ¹³¹Ba ($T_{1/2} = 12 \text{ d}$),
2242 and ¹³⁴Cs ($T_{1/2} = 2.1 \text{ a}$) can contribute significantly to the external dose rates (Sullivan, 1992). Studies by
2243 Ipe (2009b) indicate that activation in Ledite is not significantly greater than activation in concrete.

2244

² Marketed as XN-288

³ Marketed as XN-240

2245 Table 3.6. Typical compositions of various types of concrete after curing (Chilton *et al.*, 1984; NCRP,
 2246 2003). The sum of partial densities is not exact the entire density of concrete due to missing element
 2247 proportions.

2248

Concrete Type	Ordinary	Barytes^a	Magnetite-Steel
Density (g/cm³)	2.35	3.35	4.64
Element	Partial Density (g/cm³)		
Hydrogen	0.013	0.012	0.011
Oxygen	1.165	1.043	0.638
Silicon	0.737	0.035	0.073
Calcium	0.194	0.168	0.258
Carbon	-	-	-
Sodium	0.04	-	-
Magnesium	0.006	0.004	0.017
Aluminum	0.107	0.014	0.048
Sulfur	0.003	0.361	-
Potassium	0.045	0.159	-
Iron	0.029	-	3.512
Titanium	-	-	0.074
Chromium	-	-	-
Manganese	-	-	-
Vanadium	-	-	0.003
Barium	-	1.551	-

2249 ^aBarytes with BaSO₄ ore as aggregate

2250

2251 **3.8.1.3 Steel.** Steel is an iron alloy and is useful for shielding photons and high-energy neutrons.
2252 The high density of steel ($\sim 7.4 \text{ g/cm}^3$) together with its physical properties leads to tenth-value thickness
2253 for high-energy neutrons of about 41 cm (Sullivan, 1992). Therefore, steel is often used when space is at
2254 a premium. Steel or iron are usually available in the form of blocks (NCRP, 2003). Natural iron is
2255 comprised of 91.7 % ^{56}Fe , 2.2 % of ^{57}Fe , and 0.3 % of ^{58}Fe . The lowest inelastic energy level of ^{56}Fe is
2256 847 keV. Neutrons above 847 keV will lose their energy by inelastic scattering, while neutrons below
2257 847 keV can lose their energy only by elastic scattering which is a very inefficient process for iron.
2258 Therefore, there is a build up of neutrons below this energy. This is also the energy region where the
2259 neutrons have the highest weighting factor. Natural iron also has two energy regions where the minimum
2260 cross section is very low because of the resonance in ^{56}Fe . They are at 27.7 keV (0.5 barn) and at 73.9
2261 keV (0.6 barn). Thus, the attenuation length in this region is about 50 % higher than the high-energy
2262 attenuation length. Therefore, large fluxes of neutrons can be found outside steel shielding. For lower
2263 energy neutrons, only the elastic scattering process causes neutron energy degradation. As stated in
2264 Chapter 1, if steel is used for the shielding of high-energy neutrons, it must be followed by a
2265 hydrogenous material for shielding the low-energy neutrons which are generated.

2266
2267 Due to the large variety of nuclear processes, including neutron capture reactions of thermalized
2268 neutrons, steel can be highly activated. It is reported that the following radionuclides are produced in
2269 steel or iron by protons and neutrons: $^{52,54,56}\text{Mn}$, $^{44,46}\text{Sc}$, $^{56,57,58,60}\text{Co}$, ^{48}V , $^{49,51}\text{Cr}$, $^{22,24}\text{Na}$, and ^{59}Fe
2270 (Freytag, 1972; Numajiri, 2007). Thermal neutrons cause ^{59}Fe and ^{60}Co activation. It is obvious that steel
2271 with less cobalt can reduce the production of cobalt isotopes.

2272
2273 **3.8.1.4 Polyethylene and Paraffin.** Polyethylene $(\text{CH}_2)_n$ and paraffin have the same percentage
2274 of hydrogen. Paraffin is less expensive but has a lower density and is flammable (NCRP, 2005).

2275 Therefore, polyethylene is preferred for neutron shielding even though it is more expensive. Attenuation
2276 curves in polyethylene of neutrons from 72 MeV protons incident on a thick iron target are reported by
2277 Teichmann (2006). The thermal neutron capture in polyethylene yields a 2.2 MeV gamma ray which is
2278 quite penetrating. Therefore, boron-loaded polyethylene can be used. Thermal neutron capture in boron
2279 yields a 0.475 MeV gamma ray. Borated polyethylene can be used for shielding of doors and ducts and
2280 other penetrations.

2281

2282 **3.8.1.5 Lead.** Lead has a very high density (11.35 g cm^{-3}) and is used mainly for the shielding of
2283 photons. Lead is available in bricks, sheets, and plates. Lead is malleable (NCRP, 2005) and therefore
2284 cannot be stacked to large heights because it will not support its own weight. Therefore, it will require a
2285 secondary support system. Lead is transparent to fast neutrons and it should not be used for door sills or
2286 thresholds for particle therapy facilities where secondary neutrons dominate the radiation field. However,
2287 it does decrease the energy of higher energy neutrons by inelastic scattering down to about 5 MeV.
2288 Below this, the inelastic cross section for neutrons drops sharply. Lead is toxic and should be encased in
2289 steel or other materials, or protected by paint.

2290

2291 **3.8.2 Transmission**

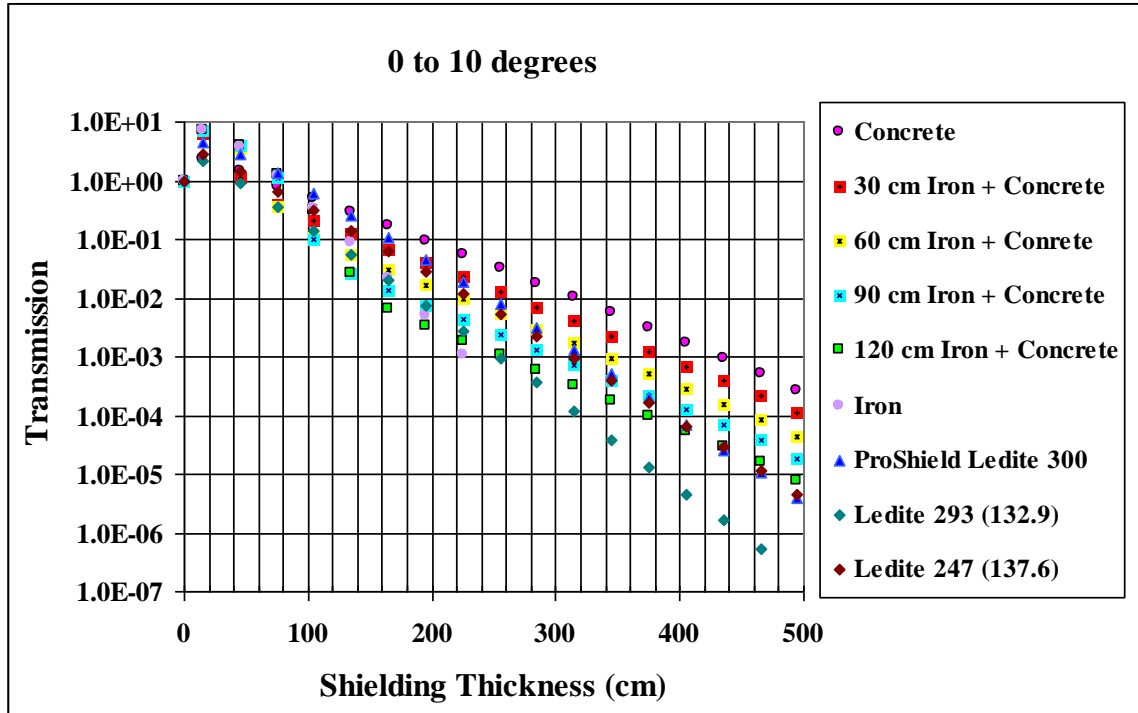
2292

2293 The transmission of a given thickness of shielding material is defined as the ratio of the dose at a
2294 given angle with shielding to the dose at the same angle without shielding. Transmission curves can also
2295 be used to determine shielding thicknesses.

2296

2297 Figures 3.8 through 3.10 show the total particle dose equivalent transmission (based on FLUKA
2298 calculations) of three different compositions of Ledite®, composite shields, and iron and concrete as a

2299 function of shielding thickness for various angles when for 430 MeV/u carbon ions incident on a 30 cm
2300 ICU tissue sphere (Ipe, 2009). Figures 3.11 through 3.13 show similar data for 250 MeV protons. These
2301 transmission curves can be used to determine the composite shielding thickness that can be used to
2302 replace large concrete thicknesses in the forward direction in the treatment room and thus save space. For
2303 example, from Fig. 3.8 it can be observed that 4.65 m of concrete provides about the same attenuation as
2304 about 2.6 m of Ledite 293 or 3.3 m of Proshield Ledite or 120 cm of iron plus 165 cm of concrete (total
2305 shielding thickness = 2.85 m). Thus, a space savings of 2.05 m is obtained with Ledite 293; 1.65 m is
2306 obtained with Proshield Ledite 300; and 1.85 m is obtained with composite shielding of 120 cm of iron
2307 plus concrete. From the figures it can also be observed that Ledite 293 is more effective than Ledite 247
2308 and Proshield Ledite 300 in the forward direction, even though Proshield Ledite has a higher density than
2309 Ledite 293. Thus, both composition and density of shielding material impact transmission.
2310

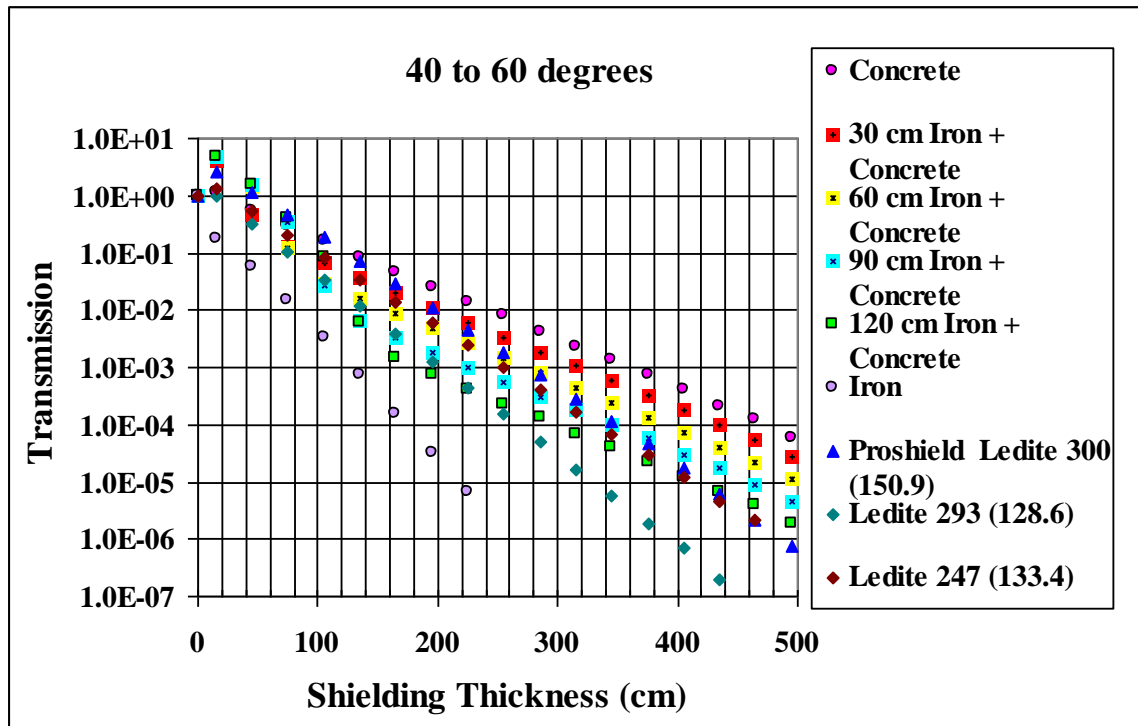


2311

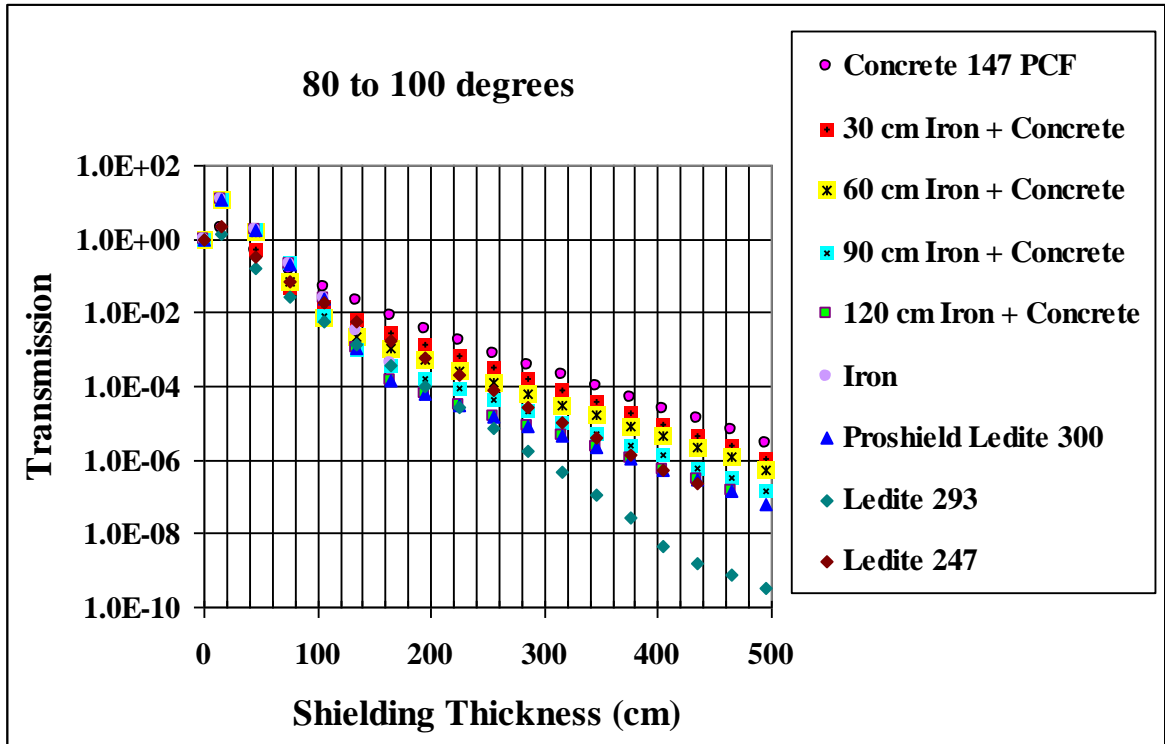
2312 Figure 3.8. Transmission curves for 430 MeV/u carbon incident on 30 cm ICRU sphere (0° to 10°) (Ipe,
2313 2009a) (Copyright 8 September 09 by the American Nuclear Society, La Grange Park, Illinois).

2314

2315



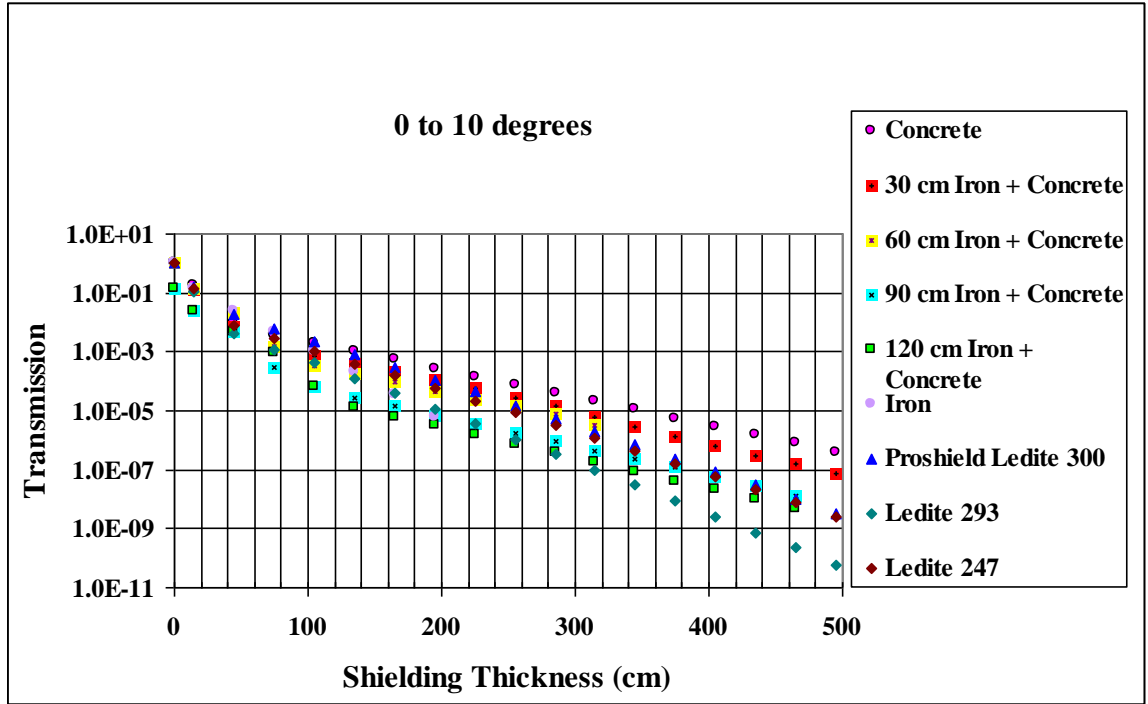
2316
2317 Figure 3.9. Transmission curves for 430 MeV/u carbon incident on ICRU sphere (40° to 60°) (Ipe,
2318 2009a) (Copyright 8 September 09 by the American Nuclear Society, La Grange Park, Illinois).
2319



2320

2321 Figure 3.10. Transmission curves for 430 MeV/u carbon incident on ICRU sphere (80° to 90°) (Ipe,
2322 2009b).

2323



2324

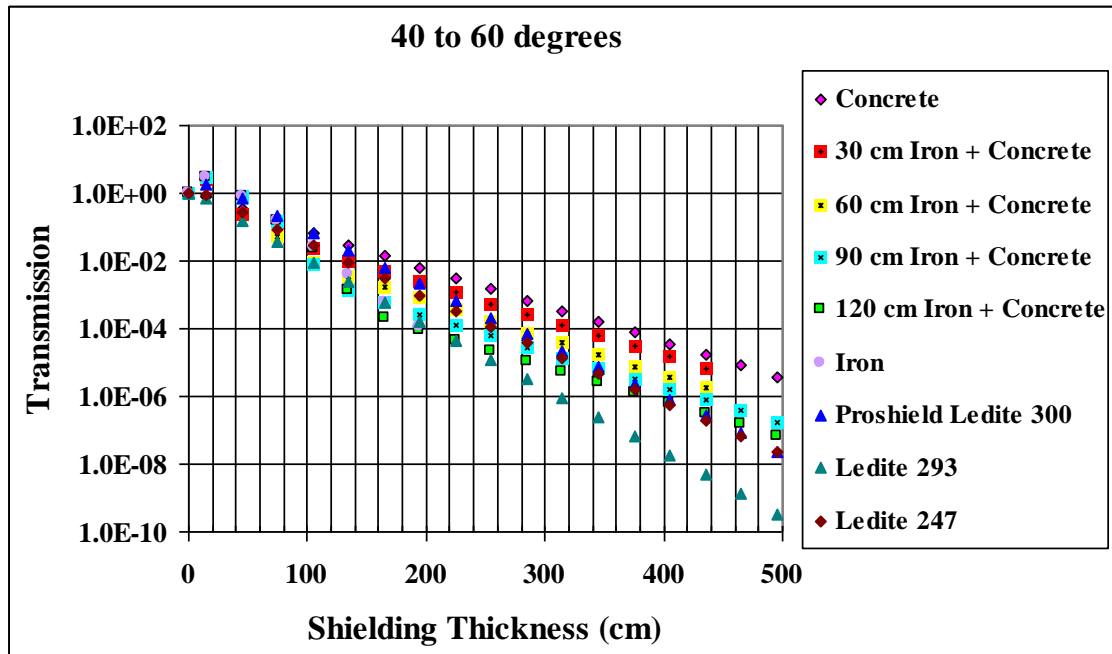
2325 Figure 3.11. Transmission curves for 250 MeV protons incident on ICRU sphere (0° to 10°) (Ipe, 2009a)

2326 (Copyright 8 September 09 by the American Nuclear Society, La Grange Park, Illinois.)

2327

2328

2329



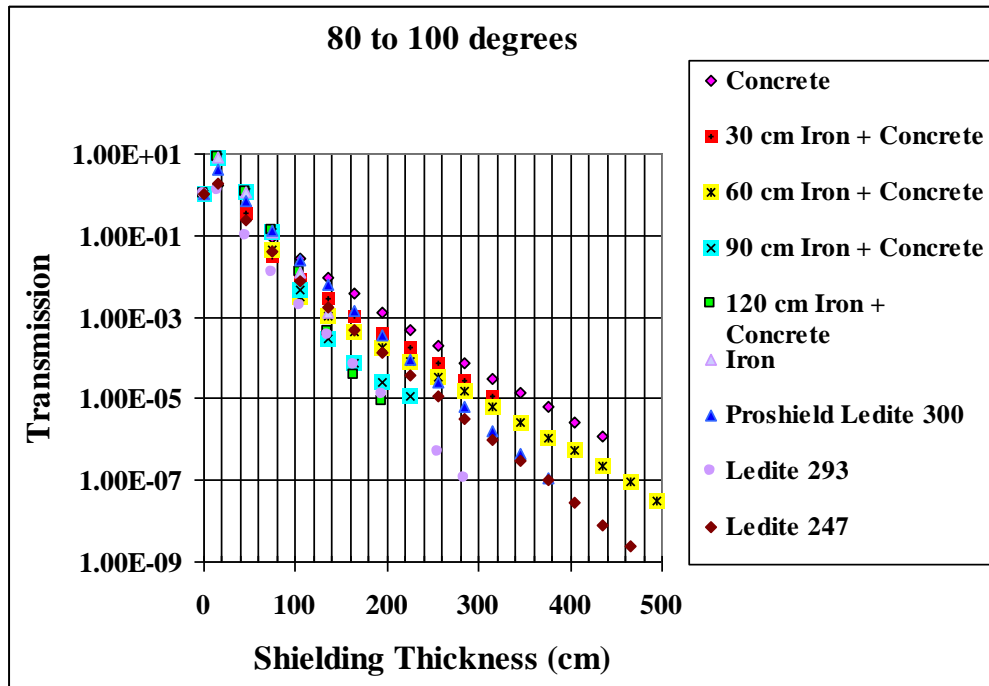
2330

2331 Figure 3.12. Transmission curves for 250 MeV protons incident on ICRU sphere (40° to 60°) (Ipe, 2009a)

2332 (Copyright 8 September 09 by the American Nuclear Society, La Grange Park, Illinois).

2333

2334



2335

2336 Figure 3.13. Transmission curves for 250 MeV protons incident on ICRU sphere (80° to 100°) (Ipe,
2337 2009b).

2338

2339 **3.8.3 Verification of Density and Composition**

2340

2341 The transmission of the shielding material depends upon both density and composition.

2342 Therefore, it is important to determine density and composition.

2343

2344 **3.8.3.1 Density.** The density of concrete is a function of mixture proportions, air content, water
2345 demand, and the specific density and moisture content of the aggregate (ASTM, 2003). Decrease in
2346 density is due to moisture loss that, in turn, is a function of aggregate moisture content, ambient
2347 conditions, and the ratio of the surface area to the volume of the concrete member. For most concretes,
2348 equilibrium density is approached at about 90 to 180 days. Extensive tests demonstrate that despite
2349 variations in the initial moisture content of lightweight aggregate, the equilibrium density will be
2350 approximately 0.05 g cm^{-3} (3.0 lb ft^{-3}) greater than the oven-dry density. Therefore, determination of
2351 oven-dry density will be the most conservative approach. Because the water in concrete does evaporate
2352 with time, the use of “wet” density is not conservative. On-site density testing should be performed.

2353

2354 **3.8.3.2 Composition.** The composition of concrete is usually determined using x-ray
2355 fluorescence (XRF). Fourteen elements can be analyzed (Si, Al, Fe, Ca, Mg, S, Na, K, Ti, P, Mn, Sr, Zn,
2356 and Cr). However, this method does not identify elements below sodium, which require combustion
2357 tests. The hydrogen content is of great importance in neutron shielding; therefore, additional tests need to
2358 be performed. Other tests include the determination of carbon, hydrogen, and nitrogen with the Perkin-
2359 Elmer 2400 CHN Elemental Analyzer (ASTM, 2003). Oxygen can be determined with the Carlo Erba
2360 1108 or LECO 932 analyzer. Elements which interfere with oxygen analysis are silicon, boron, and
2361 fluorine (high content). Oxygen can also be analyzed with the ICP (inductive coupled plasma) method.
2362 Carbon and sulfur can be analyzed using a LECO analyzer. In the XRF test results, the elements are

2363 usually reported as oxides. Therefore, a special request must be made up front in order to get the fraction
2364 by weight of the raw elements.

2365

2366 **3.8.4 Joints, Cracks, and Voids**

2367

2368 Joints between the same shielding materials should be staggered to ensure integrity of the
2369 shielding. If shielding blocks are used, they should be interlocking. If grout is used, it should have the
2370 same density as the shielding material.

2371

2372 For concrete pours, vibration of concrete should be used to ensure that there are no voids in the
2373 concrete. Continuous pours are preferred for the concrete walls and ceiling. For non-continuous
2374 concrete, appropriate measures (such as sandblasting of poured surface before pouring the next portion,
2375 use of keyways, staggered joints, *etc.*) should be in place to ensure that there are no thin spots at the cold
2376 joint. For non-continuous pours, the ceiling should be notched into lateral walls.

2377

2378 **3.8.5 Rebar and Form Ties**

2379

2380 Rebar is made of steel and while its use varies, typically it occupies less than 5 % of the barrier
2381 area. The density of steel (7.8 g cm^{-3}) is much higher than concrete (2.35 g cm^{-3}) and its mass
2382 attenuation coefficient for photons below $\sim 800 \text{ keV}$ and above $\sim 3 \text{ MeV}$ is greater than that of concrete.
2383 But because of its higher density, in all cases it is a better photon shield. As stated before, steel followed
2384 by concrete is also effective for the shielding of neutrons.

2385

2386 Form ties completely penetrate the shielding, and typically they are heavy double wires or steel
2387 rods with a diameter of about 2.5 cm. Thus, the form tie acts as a very long duct, but most of the neutrons
2388 will scatter out of the steel. Sometimes cones are used at the end of the form ties. The holes left by the
2389 cones should be filled with grout of the same density as the concrete.

2390

2391

3.9 Special Topics

2392

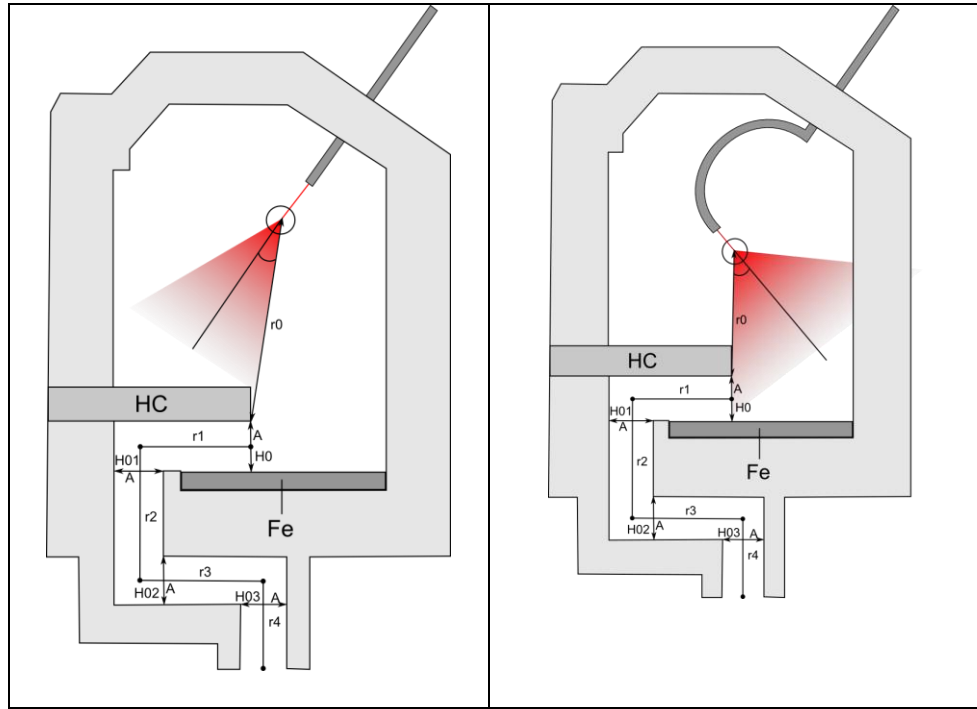
2393 3.9.1 Mazes

2394

2395 Mazes are used to reduce the radiation dose at the entrance to the shielded room so that a massive
2396 shielded door is not required. Depending upon the effectiveness of the maze, either no door may be
2397 required, or a thin shielded door may be required. The typical approach is to avoid the direct propagation
2398 of radiation to the entrance of the maze as shown in Figure 3.14.

2399

2400



2401

2402 Figure 3.14. Example for the maze of a treatment room with fixed beam geometry (left) and for a gantry
2403 geometry with a rotating radiation cone (right). The shielding walls are made of normal concrete, heavy
2404 concrete (HC), and concrete reinforced with steel layers (Fe). The maze for the attenuation of secondary
2405 radiation has four legs. The legs are most effective when the bends are 90 degrees as shown (Courtesy of
2406 G. Fehrenbacher, J. Goetze, T. Knoll, GSI (2009)).

2407

2408

2409 Two basic rules must be considered in the design of a maze: the forward-directed radiation from
2410 the target should never be directed toward the maze; and the sum of the thicknesses of each maze wall
2411 should be equal to the thickness of the direct-shielded wall. The effectiveness of a maze depends upon
2412 the following characteristics:

2413

- 2414 • As the number of legs increases, the attenuation increases. The legs are normally
2415 perpendicular to each other. The effect of the reduction of the radiation levels in the first
2416 leg is less pronounced than in the consecutive legs.
- 2417 • Because the forward-directed radiation does not enter the maze, only the attenuation of
2418 scattered radiation, with an energy distribution shifted toward lower energies in
2419 comparison to the forward-directed spectrum coming directly from the target, should be
2420 considered for the planning of the single maze walls.
- 2421 • During the propagation of neutron radiation along the maze and the continuous production
2422 of thermal neutrons, a permanent source of gamma radiation is present because it is
2423 caused by (n,γ) reactions. Therefore, the attenuation of gamma radiation must be taken
2424 into account.

2425

2426 Radiation levels inside a maze can be estimated with analytical methods, Monte Carlo
2427 calculations, or experimental data. Tesch (1982) provides an approximation that is easy to use and based
2428 on experimental data from an Am-Be neutron source and a concrete-lined labyrinth. The equations are
2429 defined for the first leg (Equation 3.3) and separately for the second leg and all further legs (Equation
2430 3.4):

2431

2432
$$H(r_1) = 2 \cdot H_0(r_0) \cdot \left(\frac{r_0}{r_1}\right)^2, \text{ for the first leg} \quad (3.3)$$

2433

$$2434 \quad H(r_i) = \left(\frac{\exp\left(-\frac{r_i}{0.45}\right) + 0.022 \cdot A_i^{1.3} \cdot \exp\left(-\frac{r_i}{2.35}\right)}{1 + 0.022 \cdot A_i^{1.3}} \right) \cdot H_{oi}, \text{ for the } i^{\text{th}} \text{ leg } (i > 1) \quad (3.4)$$

2435

2436 where :

2437 H_0 = dose at the first mouth of the maze;

2438 r_0 = distance from the source to the first mouth in the maze (unit in m);

2439 r_1 = center line distance of first leg (m);

2440 r_i = center line distance of i^{th} leg (m);

2441 A_i = cross sectional area of the i^{th} mouth of the i^{th} leg (m^2);

2442 H_{oi} = dose equivalent at the entrance to the i^{th} leg.

2443

2444 The measured dose rates and the corresponding calculated values with Equations 3.3 and 3.4

2445 agree reasonably well. Increasing the length of the maze and decreasing its cross-sectional area increases

2446 the attenuation. Other methods can be found in the literature (Dinter, 1993; Göbel *et al.*, 1975; Sullivan,

2447 1992).

2448

2449 **3.9.2 Penetrations and Ducts**

2450

2451 Ducts and penetrations in the shielding wall are required for the routing of air conditioning,

2452 cooling water, electrical conduits, physicist's conduits, *etc.* Direct penetration of the shielded walls must

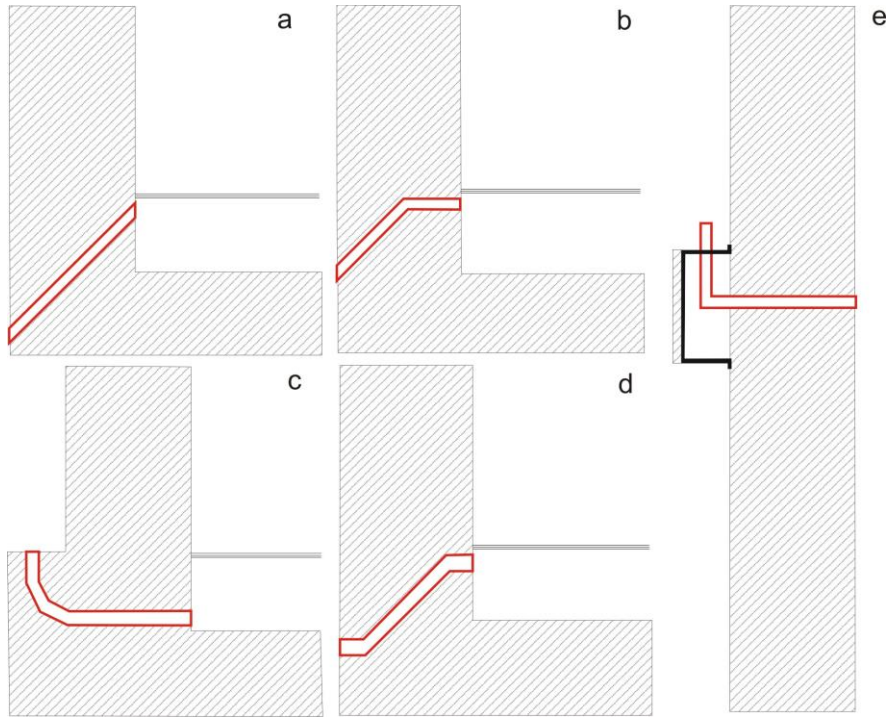
2453 be avoided. Oblique penetrations as shown in Figure 3.15a increase the radiation path length, and hence,

2454 the attenuation. However the forward-directed radiation should not point in the direction of the

2455 penetration. Another effective method is the introduction of bends and arcs, as shown in Figures 3.15b,

2456 3.15c, and 3.15d. The reduction of the radiation along the duct is accomplished at the bends where the
2457 radiation is scattered. In some cases when an oblique penetration of the duct is not feasible, shadow mask
2458 shielding such as shown in Figure 3.15d can be used. Usually the cables filling the penetrations provide
2459 some minimal shielding.
2460

2461



2462

2463 Figure 3.15. Various types of ducts and penetrations with different methods for the reduction of radiation
2464 propagation along the duct: a) Extension of the duct length, b) and c) use of a bend, d) use of two bends,
2465 and e) covering of the penetration with a shield (Courtesy of G. Fehrenbacher, J. Goetze, T. Knoll, GSI
2466 (2009)).

2467

2468 The DUCT III (Tayama *et al.*, 2001) code, based upon a semi-empirical method, is suitable for
2469 duct calculations (cylindrical, rectangular, annular, and slit) for gamma radiation and neutrons with
2470 energies up to 10 MeV and 3 GeV, respectively. The DUCT III code is available through the NEA.

2471

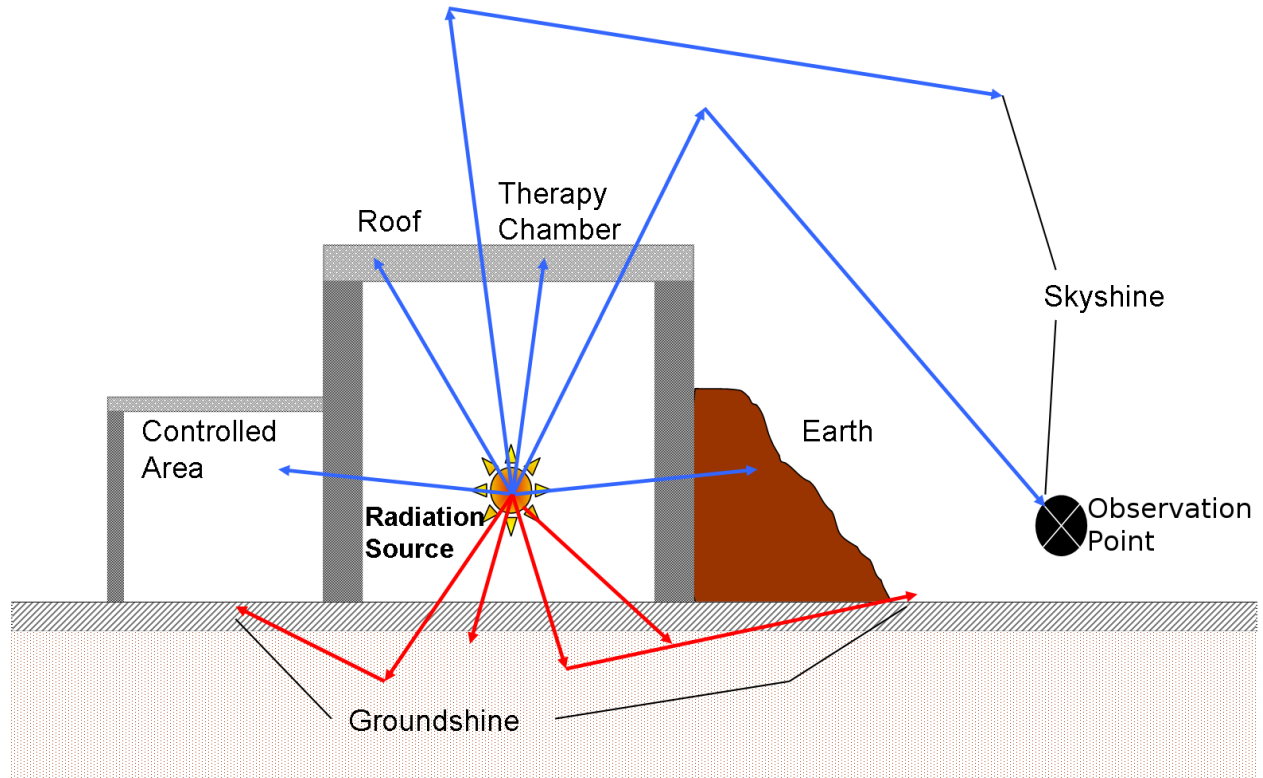
2472 **3.9.3 Skyshine and Groundshine**

2473

2474 Some facilities may be designed with little shielding in the ceiling above the accelerator or
2475 treatment room when the area above the ceiling is not occupied. Secondary radiation may then be
2476 scattered down by the atmosphere to the ground level. This is referred to as “skyshine” and illustrated in
2477 Figure 3.16. A treatment room is shown with substantial beam depositions in a target, *e.g.*, the tissue of
2478 the patient. Similarly, “groundshine” refers to radiation escaping the floor slab, reaching the earth, and
2479 scattering upwards.

2480

2481



2482

2483 Figure 3.16. Examples of skyshine and groundshine . Secondary radiation produced in a treatment room
2484 can partially escape through the roof (or the floor slab) and cause non negligible dose rates at the
2485 observation point (Courtesy of G. Fehrenbacher, J. Goetze, T. Knoll, GSI (2009)).

2486

2487 Skyshine results from the scattering of lower-energy neutrons (NCRP, 2003). High-energy
2488 neutrons that penetrate the ceiling shielding undergo inelastic collisions with the air to generate more
2489 low-energy neutrons. Therefore, it is necessary to know the intensities as well as the energy and angular
2490 distributions of neutrons entering the sky above the ceiling of the shielded room. Stevenson and Thomas
2491 (Stevenson, 1984) developed a method for the calculation of skyshine that are valid at distances of ~
2492 100 m to 1000 m from the source. The following assumptions and simplifications were made:

- 2493
- 2494 • A differential neutron energy spectrum of the form $1/E$ (where E is the energy)
2495 extending up to a maximum neutron energy (called upper energy of the neutron
2496 spectrum) is used. The highly penetrating neutron component is overestimated in this
2497 assumption.
 - 2498 • The neutrons are emitted into a cone with a semi-vertical angle of about 75° . This
2499 assumption leads to an overestimation of the dose at large distances for neutron
2500 emissions with small semi-vertical angles.

2501

2502 The neutron dose equivalent per source neutron escaping the roof shielding is given by:

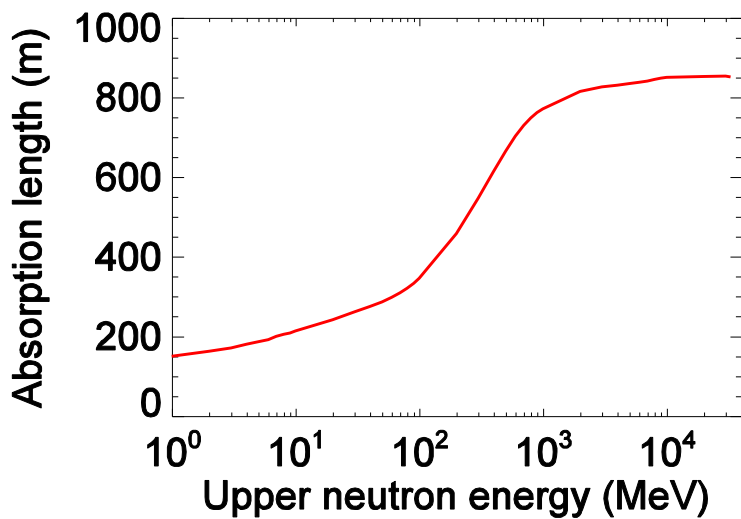
2503

2504
$$H(r) = \frac{\kappa}{r^2} \cdot \exp\left(-\frac{r}{\lambda}\right), \quad (3.5)$$

2505

2506 where r is the distance from the source to the observation point (m), κ is a constant with a value
2507 between $1.5\text{E-}15 \text{ Sv}\cdot\text{m}^2$ and $3\text{E-}15 \text{ Sv}\cdot\text{m}^2$, and λ is the effective absorption length in the air of the
2508 maximum neutron energy. The values of λ are given in Figure 3.17 for the energy range from 1 MeV to
2509 10 GeV.

2510



2511

2512 Figure 3.17. Absorption length of neutrons escaping from the ceiling and causing skyshine. Calculated
2513 by G. Fehrenbacher based on formula cited in NCRP 144 (NCRP, 2003).

2514

2515 Equation 3.5 was further modified by Stapleton *et al.* (1994) with the introduction of more
2516 realistic neutron spectra, the angular dependency of the neutron emission, and weighting of the high-
2517 energy neutrons. The modified expression is given by:

2518

$$2519 \quad H(r) = \frac{\kappa'}{(h+r)^2} \cdot \exp\left(-\frac{r}{\lambda}\right) \quad (3.6)$$

2520

2521 where $\kappa' = 2 \times 10^{-15}$ Sv m² per neutron and h = 40 m. Equation 3.5 is an empirical summary of
2522 experimental and theoretical data, and may used with some constraints.

2523

2524 **3.10 Examples for Existing Facilities**

2525

2526 This section provides examples of the shielding design of various facilities.

2527

2528 **3.10.1 Facilities for Proton Therapy**

2529

2530 **3.10.1.1 Loma Linda, CA, USA.** The Loma Linda University Medical Center (LLUMC) is the
2531 first hospital-based proton treatment facility built in the world. Figure 3.18 shows a layout of the facility
2532 which is comprised of a 7-m diameter synchrotron (with a 2 MeV RFQ for pre-acceleration), three gantry
2533 rooms, and one fixed beam room. The energy range of the synchrotron is 70 MeV to 250 MeV. The
2534 design intensity is 10¹¹ protons/sec. The beam extraction efficiency is higher than 95 % (Coutrakon,
2535 1990; Scharf, 2001; Slater, 1991). The beam-shaping passive systems include ridge filters, scattering
2536 foils, and a wobbler. A total of 1000 to 2000 patients can be treated per year, with a maximum of 150
2537 treatments per day.

2538

2539 Awschalom (1987) collected shielding data for 250 MeV proton beams in preparation for
2540 construction planning. The facility was built below ground level, which allowed relatively thin outer
2541 walls. The main radiation safety calculations were performed by Hagan *et al.* (1988). Secondary
2542 radiation production by protons with energies from 150 MeV to 250 MeV was computed with the Monte
2543 Carlo code HETC (Cloth, 1981) for iron and water targets. The subsequent transportation of the
2544 produced neutron radiation was performed with the ANISN code (Engle, 1967) for a spherical geometry.
2545 Attenuation curves were derived for concrete thicknesses in the range up to 650 cm. An experimental
2546 assembly of the synchrotron was set up at the Fermi National Accelerator Laboratory. Holes were drilled
2547 in the concrete shielding and TEPC detectors (described in Chapter 4) were positioned outside the holes.
2548 Experimental attenuation curves were derived for the angular range from 0° to 90° and served as a
2549 benchmark for the theoretical attenuation curves (Siebers, 1990; 1993).
2550

2551



2552

2553 Figure 3.18. Proton therapy facility at the Loma Linda University Medical Center. The installation has a
2554 synchrotron, three rooms for treatments with a gantry, and a fixed beam branch with two beam lines (1)
2555 and a fixed beam line for calibration measurements (2) (Courtesy of G. Fehrenbacher, J. Goetze, T.
2556 Knoll, GSI (2009)).

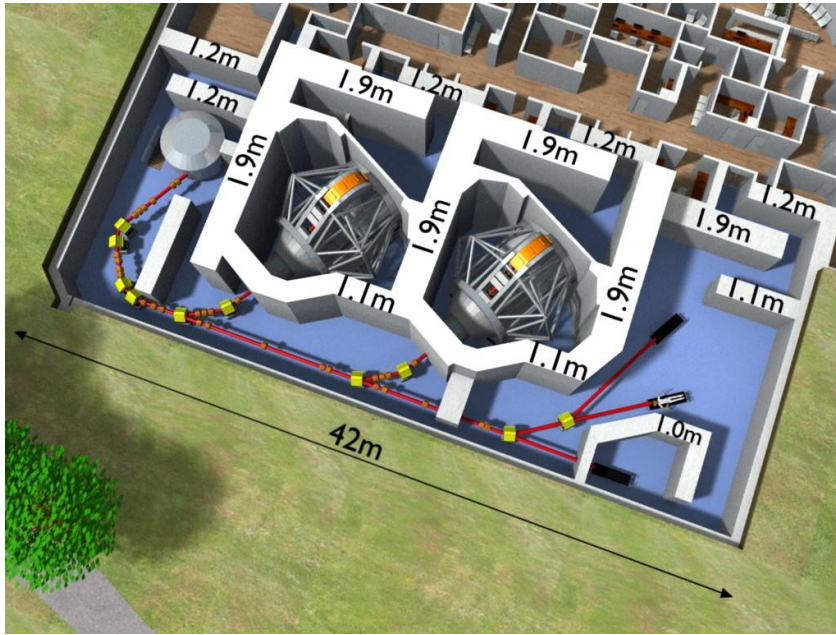
2557

2558 **3.10.1.2 Massachusetts General Hospital (MGH), Boston, MA, USA.** Figure 3.19 shows a
2559 layout of Massachusetts General Hospital (MGH). The accelerator is an IBA 230 MeV cyclotron. There
2560 are two gantry rooms, a horizontal beam line for ocular treatments, and an experimental beam line. The
2561 beam-shaping system consists of a passive scattering system and a wobbler. The accelerator and the
2562 treatment floor are underground. About 500 patients are treated per year.

2563
2564 The basic layout was designed using analytical models from Tesch for both the bulk shielding
2565 (Tesch, 1985) and the mazes (Tesch, 1982). Self-shielding of the beam conducting elements was
2566 neglected except for the cyclotron. The facility was built below ground, which allowed relatively thin
2567 outer walls. The final design was verified after construction using MCNPX (Newhauser, 2005; Titt,
2568 2005).

2569

2570



2571

2572 Figure 3.19. Northeast Proton Therapy Center (NPTC) at the Massachusetts General Hospital (MGH) in
2573 Boston. The facility is comprised of two gantry rooms, one with a horizontal geometry, and an
2574 experimental room (Courtesy of G. Fehrenbacher, J. Goetze, T. Knoll, GSI (2009)).

2575

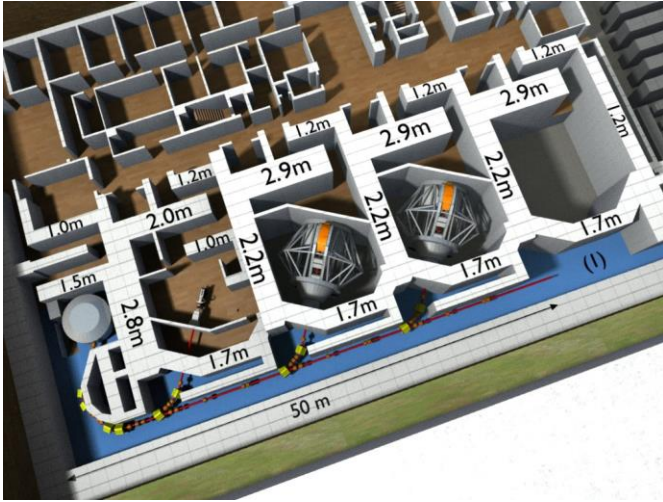
2576 **3.10.1.3 National Cancer Center (NCC), Republic of Korea.** Figure 3.20 shows the National
2577 Cancer Center (NCC) in Korea. The accelerator is an IBA 230 MeV cyclotron. The facility is comprised
2578 of three treatment rooms: two gantry rooms and one fixed beam room. An area is planned for
2579 experiments. Initially, the scattering method was used and the wobbling method was expected to be used
2580 in the later stages. The raster scan technique will be used in the future.

2581

2582 Shielding calculation were performed initially using Tesch's analytical model (Tesch, 1985) and
2583 later using MCNPX. The facility is shielded with concrete of density 2.3 g/cm^3 . The assumptions used
2584 for shielding calculations are a maximum beam-on time of 30 min per hour, 2 Gy/fraction, and 50 h
2585 treatment time per week for 50 weeks per year. The legal dose limits are shown in Table 3.1. It is
2586 interesting to note that the maze walls for this facility are 2.9 m thick, compared to the NPTC maze walls
2587 which are only 1.9 m thick. As stated previously workloads, usage assumptions, and regulatory
2588 requirements vary from facility to facility; therefore, shield designs differ.

2589

2590



2591

2592 Figure 3.20. Layout of the proton therapy facility in Kyonggi, South Korea. The facility comprises three
2593 treatment rooms and an area for experiments (1). The accelerator is a cyclotron from IBA in Belgium.

2594 (Courtesy of G. Fehrenbacher, J. Goetze, T. Knoll, GSI (2009)).

2595

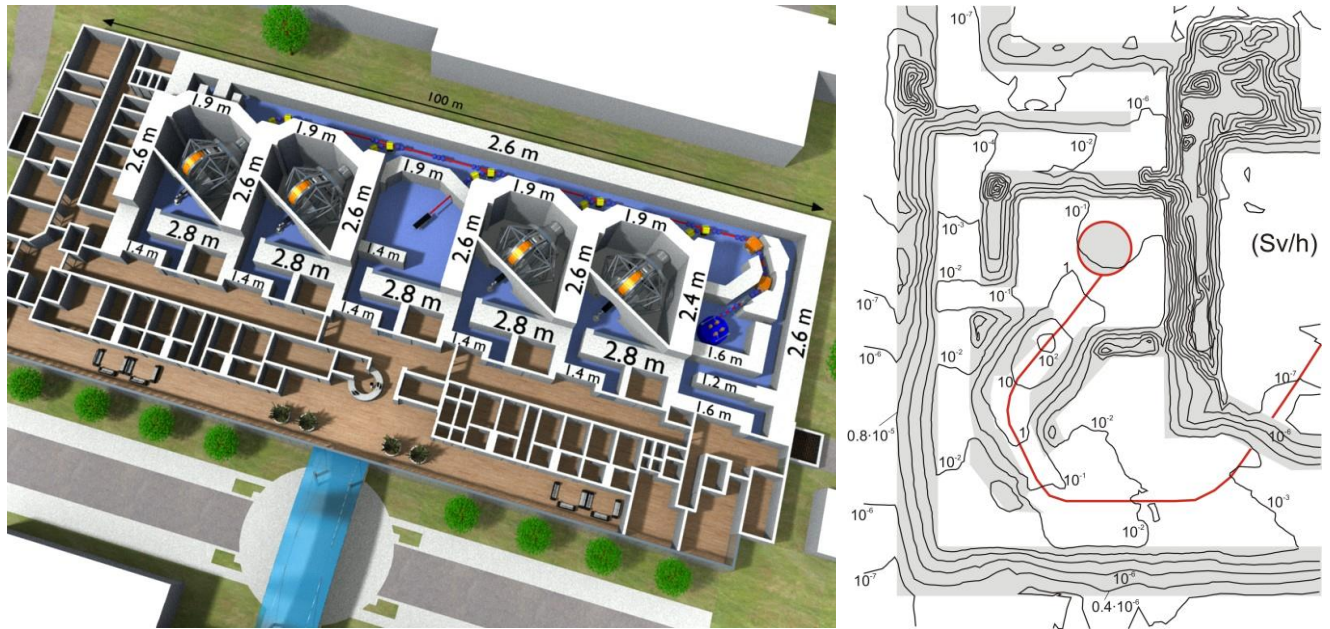
2596 **3.10.1.4 Rinecker Proton Therapy Center, Munich, Germany.** Figure 3.21 shows the
2597 Rinecker Proton Therapy Center in Munich. The facility consists of a 250 MeV superconducting
2598 cyclotron with a maximum proton current of 500 nA. There are four gantry rooms and one fixed beam
2599 room.

2600

2601 Shielding calculations were based on a 250 MeV proton beam incident on a graphite degrader
2602 thick enough to reduce the energy to 70 MeV (Hofmann and Dittrich, 2005). Annual dose limits of 5
2603 mSv and 1 mSv were used for occupationally exposed workers and the public, respectively. Ordinary
2604 concrete and heavy concrete (mainly for the degrader area) were used for shielding the facility. Shielding
2605 calculations were performed with MCNPX. The introduction of variance reduction techniques was
2606 necessary to obtain results with comparable statistical errors for all considered regions. Optimization
2607 studies for the degrader shielding were performed. Figure 3.21 (right side) shows the isodose curves
2608 and the spatial development of the radiation propagation in and around the shielding walls and rooms.

2609

2610



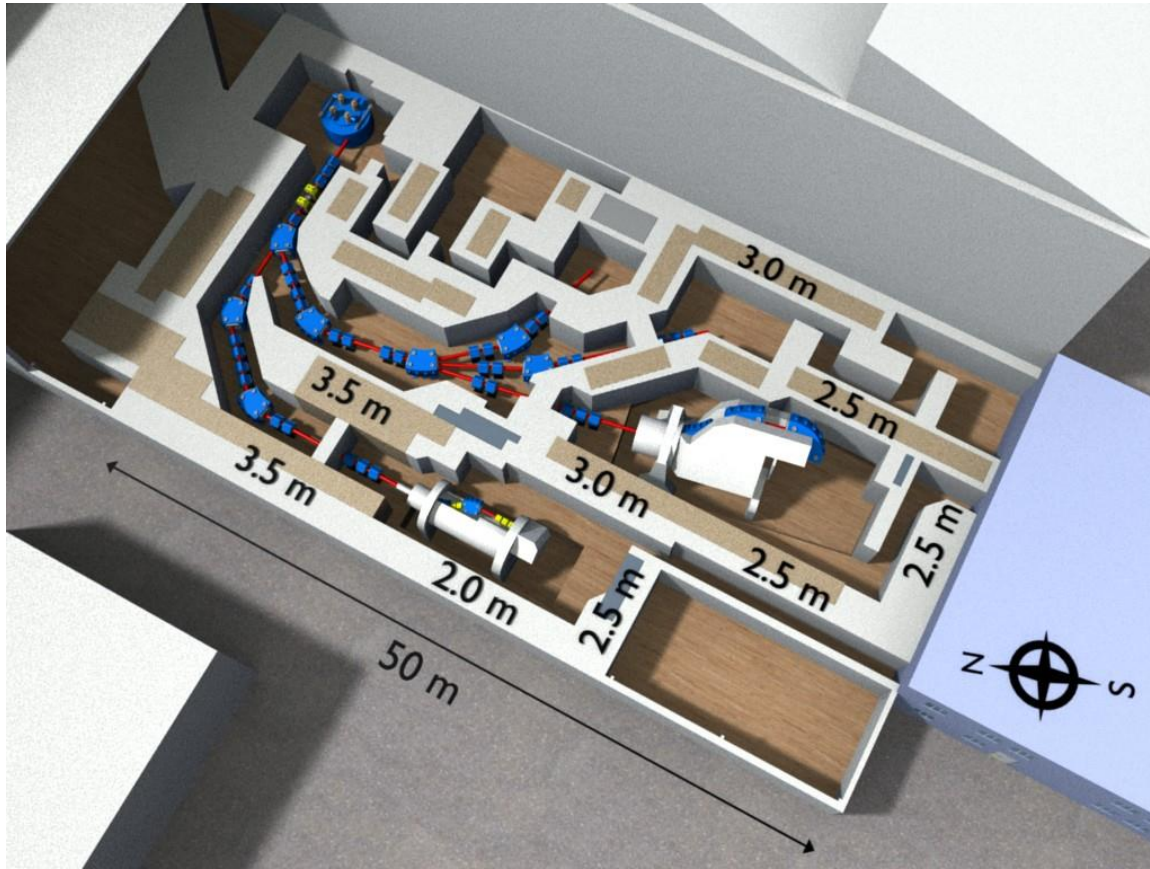
2611 Figure 3.21. Left: Building of the Rinecker Proton Therapy Center in Munich. Right: The dose
2612 distribution of the area near the cyclotron and the energy selection system is shown here. The highest
2613 dose rates occur in this area (Hofmann and Dittrich, 2005).

2614

2615 **3.10.1.5 Paul Scherrer Institute (PSI), Switzerland.** Figure 3.22 shows the proton treatment
2616 facility at the Paul Scherrer Institute (PSI). The facility is comprised of a 250 MeV ($I_{\max} \leq 500$ nA)
2617 superconducting cyclotron, two gantry rooms, a fixed beam room, and a research room. The shielding
2618 design is essentially based on computational models (Teichmann, 2006). Concrete, heavy concrete, and
2619 steel were used for shielding. The design goals were a) dose rates less than 1 $\mu\text{Sv/h}$ for lateral walls, b)
2620 dose rates less than 10 $\mu\text{Sv/h}$ on top of the roof shielding, and c) dose rates less than 1 to 10 $\mu\text{Sv/h}$ in
2621 accessible areas adjacent to the areas with beam. Because existing concrete blocks were used, and due to
2622 structural issues, walls are in some cases are thicker than necessary from a shielding point of view. The
2623 thickness of the roof of the degrader area is about 3.5 m; of the cyclotron area it is about 2.5 m; and the
2624 gantry rooms have a roof of about 1 m.

2625

2626



2627

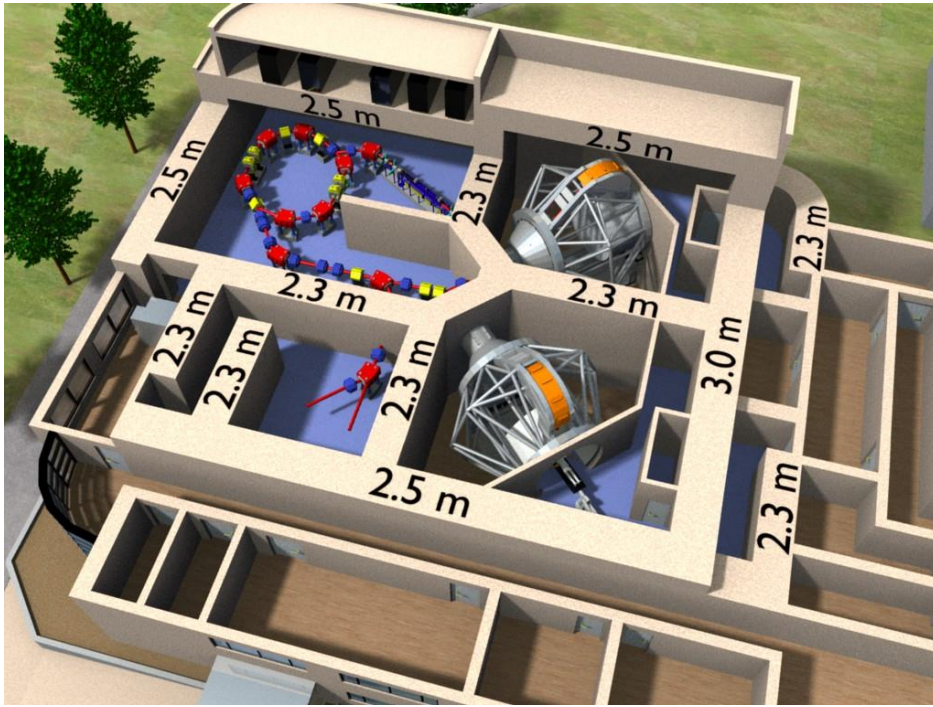
2628 Figure 3.22. Treatment facility at PSI, Switzerland, with two gantry rooms and a fixed beam room

2629 (Courtesy of G. Fehrenbacher, J. Goetze, T. Knoll, GSI (2009)).

2630

2631 **3.10.1.6 Proton Medical Research Center, Tsukuba, Japan.** Figure 3.23 shows the proton
2632 medical research center in Tsukuba. The facility is comprised of a 23 m circumference synchrotron, two
2633 gantry rooms, and a research room. The injector consists of a Duoplasmatron ion source (30 keV beam
2634 energy), a radiofrequency quadrupole RFQ (3.5 MeV), and an Alvarez unit (7 MeV). The synchrotron
2635 accelerates protons to energies that range from 70 MeV to 250 MeV. The proton beam intensity is $6.1 \times$
2636 10^{10} particles per second (pps), and the total accelerated charge per week is 258 μC . The shielding design
2637 was developed on the basis of experimental data measured at the Los Alamos Meson Physics Facility
2638 (Meier, 1990). Double differential distributions for the produced neutron radiation in thick target
2639 approximation (carbon, iron, and others) were measured by means of the time-of-flight technique. Proton
2640 beams with energy of 256 MeV were used. The angular ranges of the measured neutrons were 30° , 60° ,
2641 120° and 150° . The transport of the source neutrons was performed by using the ANISN code (Engle,
2642 1967) in combination with DLC-119B/HILO86R/J3 group constants of the cross sections.
2643

2644



2645

2646 Figure 3.23. Layout of the Proton Medical Research Center at the University of Tsukuba (Courtesy of G.
2647 Fehrenbacher, J. Goetze, T. Knoll, GSI (2009)).

2648

2649

2650 **3.10.2 Facilities for Proton Therapy and Heavy Ion Therapy**

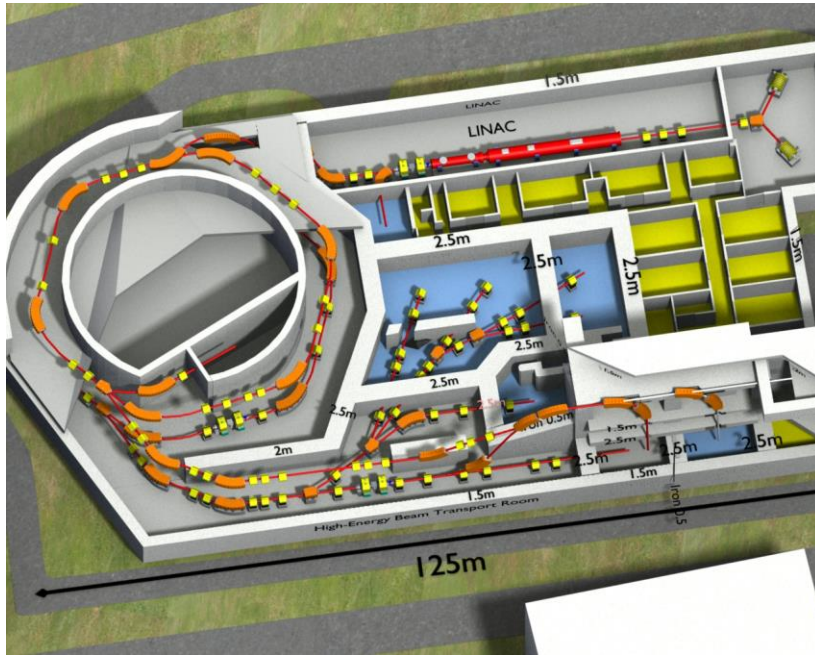
2651

2652 **3.10.2.1 Heavy Ion Medical Accelerator in Chiba (HIMAC), Japan.** At HIMAC (Hirao *et*
2653 *al.*, 1992) a large variety of ions can be accelerated, such as p, He, C, Ne, Si and Ar ions. However,
2654 carbon ions are mainly used for patient treatment. The facility is shown in Figure 3.24 and is comprised
2655 of two synchrotrons, one horizontal (H) treatment room, one vertical (V) treatment room, one horizontal
2656 and vertical combination treatment room (H&V), a physics and general-purpose irradiation room, a
2657 medium energy beam irradiation room, and a room for biological irradiations. The combination treatment
2658 room can be operated with two different beams from both synchrotrons (see the red beam lines in Fig.
2659 3.24).

2660

2661

2662



2663

2664 Figure 3.24. Schematic of the HIMAC facility (Courtesy of G. Fehrenbacher, J. Goetze, T. Knoll, GSI
2665 (2009)).

2666

2667

2668 The extracted beam intensity for carbon ions from the synchrotron is 2×10^8 ions per second
2669 (Uwamino, 2007). Beam loss distributions are reported for 500 MeV/u He ions (energy higher than
2670 needed for therapy) (Uwamino, 2007). About 5 % beam losses occur during extraction, 10 % beam
2671 losses occur during the acceleration along the ring, 15 % beam losses occur at the ring scrapers, and 10
2672 % beam losses at the vertical beam transfer lines. This beam loss data and the estimated time period of
2673 weekly operation per week (synchrotron, 108 h/week; treatment rooms, 11 to 18 h/week) served as a basis
2674 for the shielding calculations. The results of HETC-KFA calculations (Cloth, 1981) were used to
2675 develop an approximate formula for the calculation of secondary neutron fluence produced by He ions
2676 and other ion types with the capability to compute the neutron fluence as a function of the ion energy
2677 (Ban, 1982). The attenuation of the neutron radiation in the bulk shield is calculated and the
2678 corresponding dose values are derived (Ban, 1982). The results for the shielding calculations are given in
2679 Table 3.7 for some essential areas in HIMAC. The shielding walls are partially augmented by iron. In
2680 Table 3.7 (3rd column), the values for the thicknesses of the combined concrete-iron shields are
2681 converted into effective values for concrete layers. The thickness of the shielding around the synchrotron
2682 is 1.5 m. At the extraction area there is an additional 2.5 m of shielding (Figure 3.24 left). The effective
2683 shield thicknesses for the treatment rooms in the forward and lateral direction are 3.2 m and 2.5 m,
2684 respectively. Shielding thicknesses for the high-energy beam transfer line, the roof shielding, and the
2685 floor shield are also given in Table 3.7.

2686

2687 Table 3.7: Shielding measures of the HIMAC facilities for some areas: synchrotron, therapy A, B, C,
2688 roof, floor, HEBT and Linac (Fehrenbacher, 2007).

Area	Shield Thickness (m)	Effective Concrete Thickness (m)
	Forward Direction /Lateral	Forward Direction /Lateral
	Direction	Direction
Synchrotron	1.5 (Additional 2.5 m local shielding inside)	-
A. Horizontal treatment room (H)	2.5 (0.5 Fe) / 2.5	3.22 / 2.5
B. Combination treatment room (H&V)	2.5 (0.5 Fe) / 1.6, Maze 1.6 (0.8 Fe)	3.22 / 1.6 Maze 2.75
C Vertical treatment room V	2.5 / 1.6, Maze 1.2	-
Roof	1.5	-
Floor	2.4	-
HEBT	1.5 – 2.0	-
Linac	1.5	-

2689

2690

2691 **3.10.2.2 Gunma University, Japan.** Figure 3.25 shows a layout of the Gunma facility, which is
2692 comprised of a synchrotron and three treatment rooms (one horizontal beam line, one vertical beam line,
2693 and one H&V beam line). A fourth room with a vertical beam line is provided for the development of
2694 new irradiation methods (Noda *et al.*, 2006a). The maximum carbon ion energy is 400 MeV/u. About
2695 600 patients are expected to be treated per year.

2696

2697 The desired beam intensity at the irradiation port is 1.2×10^9 pps, which yields 3.6×10^8 ions per
2698 second for patient treatment (Noda *et al.*, 2006a). An overview on beam intensities and beam loss
2699 distributions is given in Table 3.8 at different stages of the acceleration process. For the shielding design,
2700 it was assumed that unused ion beams are decelerated in the accelerator before being dumped (Noda *et*
2701 *al.*, 2006a) and consequently, the neutron production radiation is reduced. The dose rates are calculated
2702 as follows:

2703

- 2704 • The source distributions of the produced neutron radiation are taken from the Kurosawa
2705 measurements (Kurosawa, 1999; Uwamino, 2007).
- 2706 • The beam loss distributions were determined by Noda *et al.* (2006a) and are listed in
2707 Table 3.8.
- 2708 • The dose rates outside the shielding were computed using the ANISN code (Engle, 1967)
2709 and the cross sections from the JAERI (Kotegawa *et al.*, 1993).
- 2710 • It is also reported that certain areas of the facility are designed using the PHITS-code
2711 (Iwase, 2002; Uwamino, 2007) described in Chapter 6.

2712

2713 The shielding thicknesses are shown in Figure 3.25. At some locations, the concrete shielding is
2714 augmented by iron shielding. The synchrotron walls are 3 m to 5 m thick. The horizontal treatment

2715 rooms are shielded with 3 m thick walls in the forward direction (1.9 m concrete and 1.1 m iron, which
2716 results in an effective thickness of 4.6 m concrete) and 1.5 m to 2.5 m in the lateral direction.. The linac
2717 walls are 1.0 m to 2.5 m thick. The floor slab has a thickness of 2.5 m. The roof shielding thickness
2718 varies from 1.1 m to 2.2 m thickness. The wall thicknesses of the fourth irradiation room (V) range from
2719 1.1 m to 1.7 m, and are obviously reduced in comparison to the other treatment rooms due to shorter
2720 estimated irradiation time periods. Table 3.8 summarizes beam loss distributions and absolute beam
2721 intensities..
2722

2723 Table 3.8. Beam loss distributions and absolute beam intensities for the Gunma facility, calculated by
2724 Noda *et al.* (2006a). Efficiency η gives the ion beam transfer efficiency at different stages of the
2725 acceleration and transfer process. The beam intensity is given in the quantity particles per pulse (ppp) or
2726 in the quantity particles per sec (pps).

2727

Section	Efficiency η	Beam Intensity
Injection	0.4	2E10 ppp
Synchrotron	0.64	5E9 ppp
Extraction	0.9	1.3E9 pps
HEBT	0.95	1.2E9 pps
Treatment Room	0.3	3.6E8 pps

2728

2729

2730



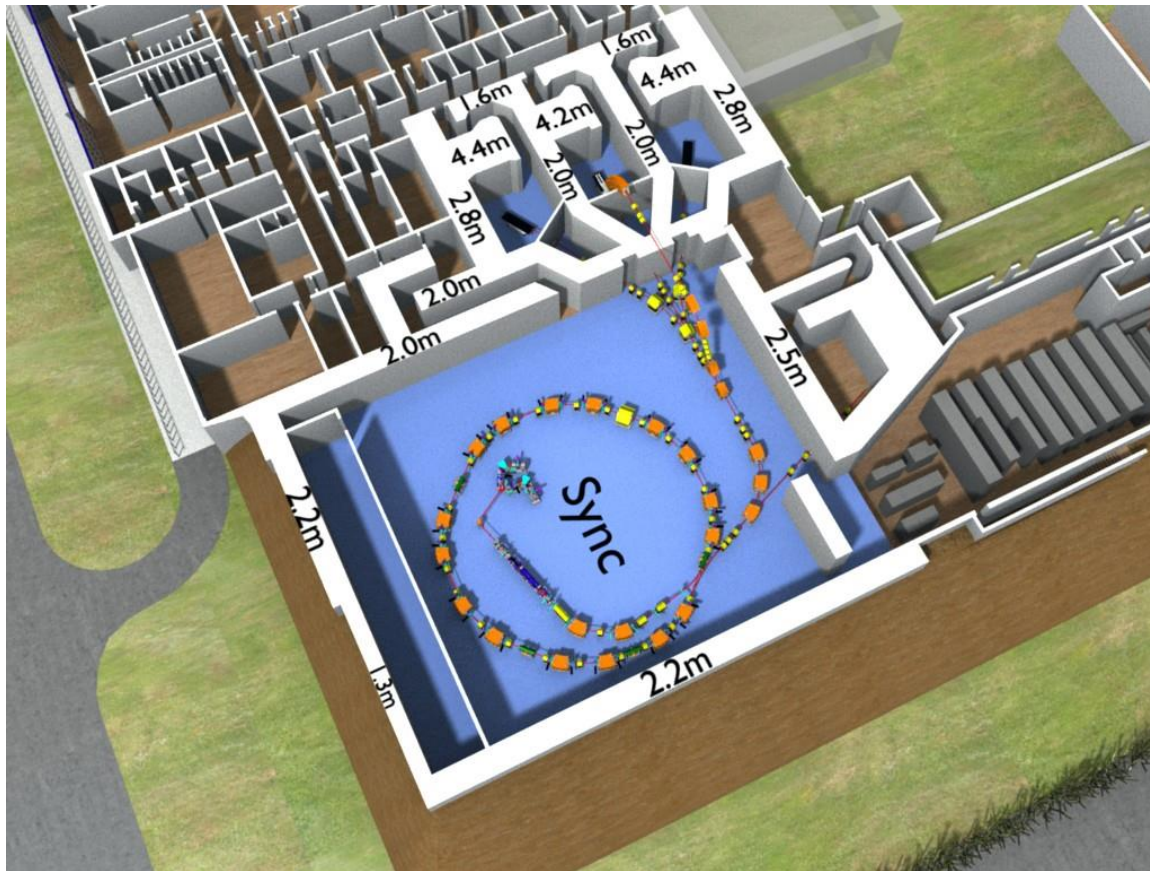
2731

2732 Figure 3.25. Layout of the Gunma ion irradiation facility with the LINAC, the synchrotron (ring
2733 accelerator), and the treatment rooms (Courtesy of G. Fehrenbacher, J. Goetze, T. Knoll, GSI (2009)).

2734

2735 **3.10.2.3 CNAO, Pavia, Italy.** Figure 3.26 shows the first stage of the CNAO facility which is
2736 comprised of a synchrotron, two horizontal beam treatment rooms, and one horizontal-vertical
2737 combination treatment room. Two gantry rooms will be added in the second stage. The facility is capable
2738 of accelerating protons to 250 MeV and carbon ions to 400 MeV. Preliminary shielding studies were
2739 performed by Agosteo (1996b). The most recent shielding design was carried by Porta *et al.* (2005) and
2740 Ferrarini (2007). The synchrotron is shielded by a 2 m thick concrete wall (for the most part) which is
2741 augmented by earth layers (5 m to 7 m for the public area). Inside the synchrotron there are additional
2742 local concrete shields. The treatment rooms are shielded such that the adjoining rooms are kept at dose
2743 rate levels lower than 0.5 $\mu\text{Sv/h}$ (annual dose less than 2 mSv, including the radiation sources from the
2744 synchrotron). The lateral shield thicknesses range from 2 m to 3.1 m and the forward shield walls have
2745 thicknesses of 4.2 m to 4.8 m with an effective thickness of up to 8 m because of the oblique incidence of
2746 the neutrons relative to the shielding walls. The floor shielding is 3.1 m and the roof shielding ranges
2747 from 1.1 m to 2 m.
2748

2749



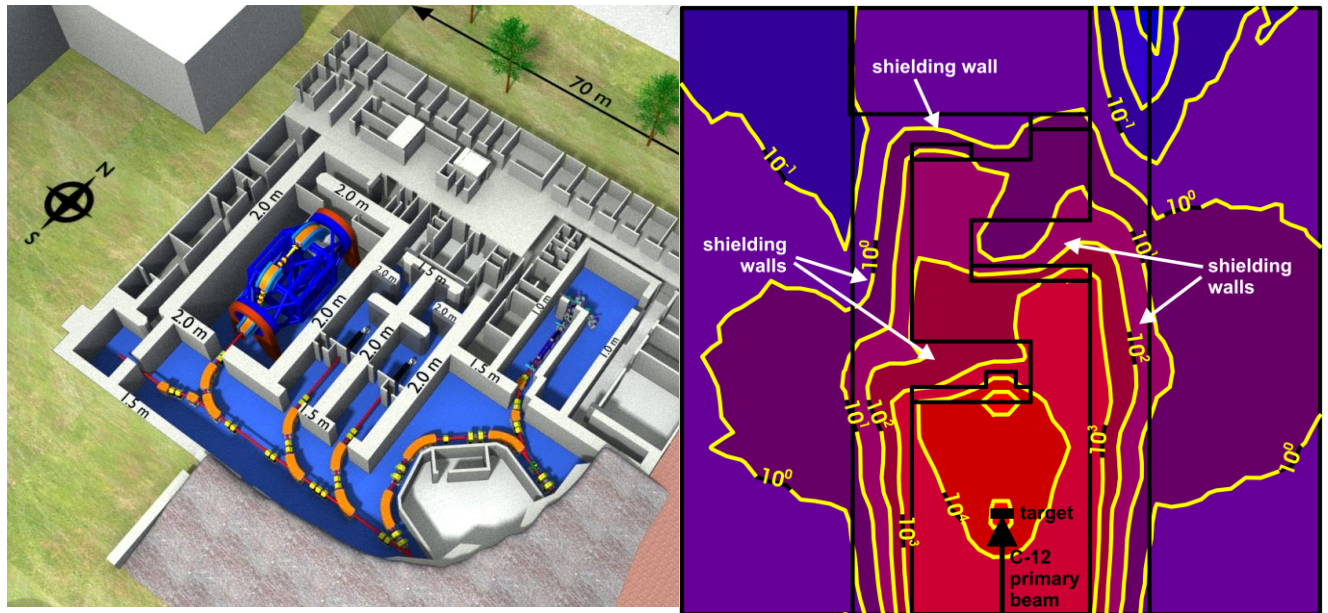
2750

2751 Figure 3.26. Overview of the CNAO facility (Courtesy of G. Fehrenbacher, J. Goetze, T. Knoll, GSI
2752 (2009)).

2753

2754 **3.10.2.4 HIT, Heidelberg, Germany.** Figure 3.27 shows part of the HIT facility which is
2755 comprised of a synchrotron, two horizontal treatment rooms (H), a carbon ion gantry room, and a
2756 research room. The facility is capable of accelerating protons as well as carbon, oxygen, and helium ions.
2757 The energies of the ions are so adapted that the maximum range in water is about 40 cm for protons and
2758 helium ions, 30 cm for carbon ions, and 23 cm for oxygen ions. The beam parameters for HIT are 4 x
2759 10^{10} ppp for protons (220 MeV) or 1×10^9 ppp for carbon ions (430 MeV/u).
2760

2761



2762 Figure 3.27. Left: Part of the HIT facility in Heidelberg. Right: The dose distribution in the horizontal
2763 beam treatment rooms are also shown for carbon ion beams (Fehrenbacher, 2007). The isodose values
2764 (yellow) are given in the units of $\mu\text{Sv/h}$. The values range from $10^5 \mu\text{Sv/h}$ (red) over $10^2 \mu\text{Sv/h}$ to 10^{-1}
2765 $\mu\text{Sv/h}$ (blue) with increments of a factor of 10 (Courtesy of G. Fehrenbacher, J. Goetze, T. Knoll, GSI
2766 (2009)).

2767

2768 The shielding design was developed on the basis of the Kurosawa neutron spectra of the 400
2769 MeV/u of carbon ions (Kurosawa *et al.*, 1999). A line-of-sight model was used to determine dose rates of
2770 the neutron radiation outside the shield (Fehrenbacher *et al.*, 2001). The model considers the angular
2771 dependence of the neutron production (0° to 90°), the angular dependent neutron energy distribution (E_n
2772 > 5 MeV), the neutron energy dependent absorption (removal cross section), and the build-up effect of
2773 the neutron radiation in matter. For angles greater than 90° relative to the incoming ion beam, the
2774 neutron source distribution at 90° was used. Monte Carlo calculations with FLUKA (Fasso *et al.*, 1997)
2775 were also performed for the horizontal treatment rooms using the 2000 version of FLUKA and the
2776 Kurosawa neutron spectra (Fehrenbacher *et al.*, 2002a; Kurosawa, 1999) as well as for the gantry room
2777 (Fehrenbacher *et al.*, 2002b). The results of the treatment room calculations are shown on the right in
2778 Figure 3.27 for carbon ion beams with 400 MeV/u and 3×10^8 ions/sec deposited in a graphite target
2779 (Fehrenbacher, 2007). Further specific studies were performed with FLUKA to study the impact of
2780 recesses in the floor shielding for the horizontal treatment rooms for the installation of robots. When the
2781 heavy ion version of FLUKA (Fasso *et al.*, 2005) was released, a full simulation was performed with
2782 FLUKA and the results were compared with the simulation using the Kurosawa neutron source spectra
2783 as the input for FLUKA. Reasonable agreement (within 26 %) was obtained for the simulations.

2784
2785 The shielding design is based on the annual dose limits given in the Table 3.1 of Section 3.1.2.
2786 An additional dose rate guideline of $3 \mu\text{Sv/h}$ was used outside the interlocked area for 10-min irradiation
2787 periods. The shielding design is based on a 10 % beam losses at local (specific) areas, such as the beam
2788 extraction point, and a 10 % beam losses in the dipole magnets. Additional local concrete shielding was
2789 added in the synchrotron and beam transfer lines because the exact beam loss distribution in these areas
2790 was unknown.

2791

2792 For the horizontal beam treatment rooms, the shielding of the three walls in the entrance maze,
2793 perpendicular to the beam direction that intercept the 0° beam, is comprised of 1.5 m steel and 5.5 m
2794 concrete (total effective concrete thickness of 7.66 m). The lateral concrete thickness is 2 m. The gantry
2795 room has a wall thickness of 2 m. For the gantry room calculations, the iron counterweight of 1 m
2796 thickness was taken into account, because this attenuates the main neutron cone substantially in the
2797 angular range $\pm 25^\circ$ relative to the ion beam line. Application of the use factor for the gantry room
2798 reduces the thickness. The roof shielding (2 m) of the horizontal treatment rooms is partially augmented
2799 with 0.5 m of steel (total effective concrete thickness of 2.72 m). The synchrotron is shielded by a 1.5 m
2800 thick concrete wall and partially by earth on the exterior. Earth (and other bulk materials) covers the
2801 concrete roof of the synchrotron and treatment rooms. The floor slab is 1.5 m to 1.8 m thick and reduces
2802 the activation of soil and ground water.

2803

2804 **3.11 Qualified Expert**

2805

2806 In the case of charged particle therapy facilities, a qualified expert is a physicist who has
2807 expertise and proven experience in the shielding design and radiological aspects of high-energy particle
2808 accelerators, particularly in the shielding of relativistic neutrons. The individual must also be capable of
2809 performing Monte Carlo calculations. Various countries may have different requirements for qualified
2810 experts. In the U.S., most of the states require that the qualified expert is either registered or licensed in
2811 the state.

2812

2813 The qualified expert should be involved in the following phases of the facility design and
2814 construction, so that costly mistakes can be prevented and an optimum and cost effective shielding
2815 design can be implemented.

2816

2817 **3.11.1 Schematic Design**

2818

2819 During this phase, the architect organizes the rooms, the layout of the facility is determined, and a
2820 preliminary design is generated. The qualified physicist should be invited to attend meetings with the
2821 owner and architect. Occupancy factors should be established. Adjacent buildings and multi-storied
2822 structures should be identified. The use of space must be evaluated. The highest radiation levels occur
2823 near the treatment rooms and the accelerator. Therefore, high occupancy rooms such as nurse's stations,
2824 offices, and examination rooms should be located as far away as possible, while low occupancy rooms
2825 such as storage areas may be located closer. Typically, control rooms, patient preparation rooms, *etc.* are
2826 in the immediate vicinity of the treatment rooms.

2827

2828 Workloads should be established. The owner should provide information on the types of particles
2829 to be used, the energies of the particles, the number of treatments per hour, the beam-shaping methods
2830 that are to be used, *etc.* If an equipment vendor has been selected, the vendor should provide the
2831 information regarding beam losses, locations and targets, and currents for various beam-shaping
2832 methods, as well as other information requested by the expert. The concrete composition and density
2833 should be provided at this phase so that the physicist can perform Monte Carlo calculations. The
2834 architect should provide the expert with scaled drawings including both plans and sections. All
2835 dimensions and details must be called out on the drawings. The drawings should show the equipment in
2836 place and the location of the isocenter. The qualified expert should work with the owner and architect,
2837 suggesting the most cost-effective and space-optimizing design, shielding configurations and materials,
2838 and preliminary thicknesses. The preliminary thicknesses will be based on site-specific workload, local
2839 regulations, and other assumptions. The architect should incorporate the shielding thicknesses into the

2840 drawings, and the revised drawings should be sent to the expert for review. A few iterations may take
2841 place. The qualified expert should carefully review the architect's drawings. The qualified expert should
2842 write a preliminary shielding report that includes all the assumptions and specifies the required shielding.

2843

2844 **3.11.2 Design Development**

2845

2846 In this phase, rooms, sizes, and locations will be determined to a greater detail (NCRP, 2005),
2847 and the design will be finalized. The mechanical, electrical, and plumbing details will be worked out, and
2848 sizes of penetration, conduits, ducts, *etc.* will be determined. The architect should incorporate all the new
2849 information into the drawings so that the expert can determine the required shielding for all the
2850 penetrations. Once the shielding has been finalized, the expert should write the final shielding report
2851 which can be submitted to the pertinent regulatory agency. The report should show doses at all locations
2852 and verify regulatory dose compliance. Contents of the report are discussed in Section 3.12.

2853

2854 **3.11.3 Construction Documentation**

2855

2856 During this phase, all the construction drawings are prepared. Details of the project are finalized
2857 in preparation for construction. The shielding in the construction drawings should be identical to that
2858 which is shown in the shielding report. The qualified expert should review all drawings and all
2859 submittals (drawings and information submitted by subcontractors) related to concrete density and
2860 composition, door shielding, penetration shielding, and other special shielding materials. The qualified
2861 expert will also respond to request for information (RFI) from the contractor. Prior to construction, the
2862 qualified expert should participate in a meeting with the owner, architect, contractor, and all other trades

2863 to finalize the shielding items. During this phase there may be changes in shielding configuration due to
2864 constructability issues. The qualified expert should review all such changes.

2865

2866 **3.11.4 Construction Inspection**

2867

2868 During construction, the qualified expert should perform site visits and inspections to ensure that
2869 the shielding is implemented as specified in the shielding report. The qualified expert should carefully
2870 review the shielding to ensure that there are no cracks or thin spots. The dimensions, materials, and
2871 configuration of the room shielding, as well as door and penetration shielding, should be verified.
2872 Inspection reports should be provided by the expert. Any instances of noncompliance should be reported
2873 and corrected by the contractor or subcontractor.

2874

2875 **3.12 Shielding Report**

2876

2877 A copy of the shielding report should be maintained by the facility. The shielding report should
2878 include but is not limited to:

- 2879 1. Names and contact information for qualified physicist, architect, and responsible person at
2880 the facility
- 2881 2. Name and address of facility
- 2882 3. A brief description of accelerator, beam transport lines, treatment rooms
- 2883 4. Beam parameters, loss scenarios, targets, and location
- 2884 5. Workload and usage assumptions
- 2885 6. Occupancy factors
- 2886 7. Regulatory and design limits

- 2911 4. Machine conditions and beam operating parameters
- 2912 5. Details of phantoms used in treatment room
- 2913 6. Instruments used, including type, model, serial number, and calibration certificate
- 2914 (calibration must be current)
- 2915 7. Beam parameters, loss scenarios, targets, and location
- 2916 8. Workload and usage assumptions
- 2917 9. Occupancy factors
- 2918 10. Doses in occupied areas
- 2919 11. Compliance with design and regulatory limits.
- 2920
- 2921

4. Radiation Monitoring

Yoshitomo Uwamino and Georg Fehrenbacher

4.1 Introduction

The different types of radiation which are of concern for individual exposure at a particle therapy facility are prompt radiation during beam operation and residual radiation after the beam is turned off. The prompt radiation is comprised of neutrons and photons behind thick shields of treatment rooms or accelerator vaults, while the residual radiation consists of photons and beta rays from induced radioactivity. Neutron and photon exposure of the patient in the treatment room are also of interest (see Chapter 7).

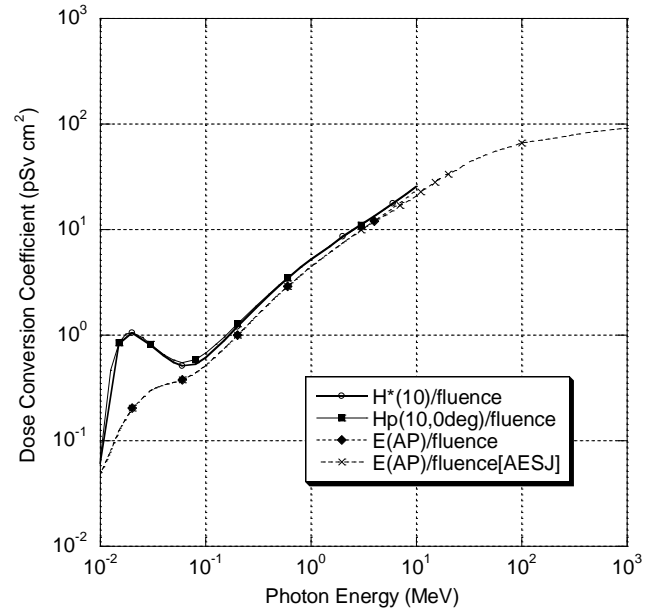
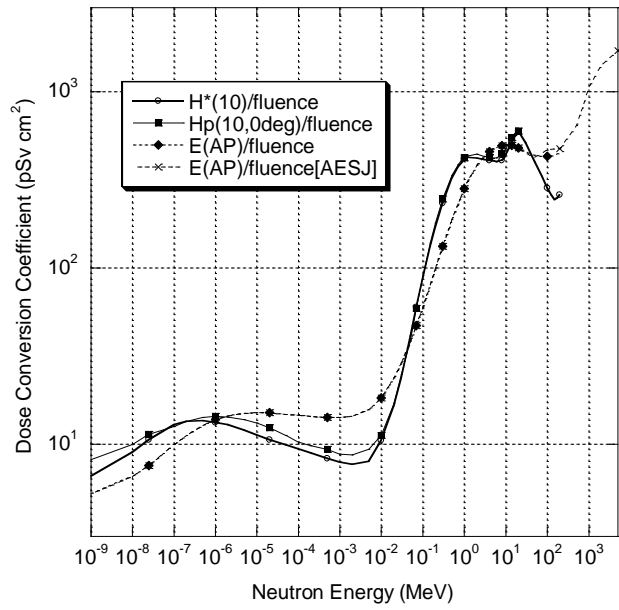
Many valuable references on the basics and principles of radiation detection are available in the literature (Ahmed, 2007; Knoll, 1999; Leroy and Rancoita, 2005; Tsoulfanidis, 1995). ICRU Report 47 (ICRU, 1992a) provides details on the measurements of photon and electron dose equivalents, while ICRU Report 66 (ICRU, 2001) covers neutron measurements. This chapter provides an overview of radiation monitoring and commercially available instrumentation for particle therapy facilities. Since radiation protection regulations vary from country to country, and in some countries from state to state, each facility must ensure that radiation surveys are performed in compliance with the regulations applicable to their specific facility.

4.1.1 Operational Quantities

2945 The quantities to be measured are ambient dose equivalent at 10 mm depth, $H^*(10)$, for area
2946 monitoring, and personal dose equivalent at 10 mm depth, $H_p(10)$, for individual monitoring. The
2947 shallow doses $H_p(0.07)$ and $H_p(3)$, at a depths of 0.07 mm, and 3 mm, respectively, are usually not as
2948 important at particle therapy facilities when compared to the strongly penetrating radiation which
2949 dominates the dose outside the shielding. Figure 4.1 shows the fluence-to-dose-equivalent conversion
2950 coefficients (see Section 1.2.2 for details) as a function of particle energy (ICRP, 1996). Also shown are
2951 the fluence-to-effective-dose conversion coefficients for Anterior–Posterior irradiation geometry, $E(AP)$,
2952 including the recommended data of $E(AP)$ by the Atomic Energy Society of Japan (AESJ, 2004) for
2953 high-energy particles. The neutron data provided by the ICRP are limited to energies of 20 MeV and
2954 below for $H_p(10)$ and 180 MeV and below for $H^*(10)$, respectively. The photon data is limited to
2955 energies of 10 MeV and below. Because the conversion coefficient for $H^*(10)$ for neutrons becomes
2956 smaller than that for $E(AP)$ above 50 MeV, measurement of $E(AP)$ may be considered appropriate for
2957 high-energy neutrons. $H^*(10)$ is not always a conservative estimate for the effective dose, especially for
2958 $E(AP)$. This argument also applies for photons. The results of several studies performed for high-energy
2959 neutrons and photons are reported in the literature (Ferrari *et al.*, 1996; 1997; Mares *et al.*, 1997;
2960 Sakamoto *et al.*, 2003; Sato *et al.*, 1999; Sutton *et al.*, 2001). The conversion coefficient for $E(AP)$
2961 becomes smaller than that for Posterior–Anterior irradiation geometry, $E(PA)$, at neutron energies above
2962 50 MeV. However, the integrated dose from thermal neutrons to high-energy neutrons is highest for AP
2963 geometry, and therefore only $E(AP)$ is considered here.

2964

2965



2966

2967 Figure 4.1. Dose conversion coefficients from particle fluence to ambient dose equivalent, $H^*(10)$,

2968 personal dose equivalent, $H_p(10)$, and effective dose with AP geometry, $E(AP)$.

2969

4.2 Prompt Radiation Monitoring

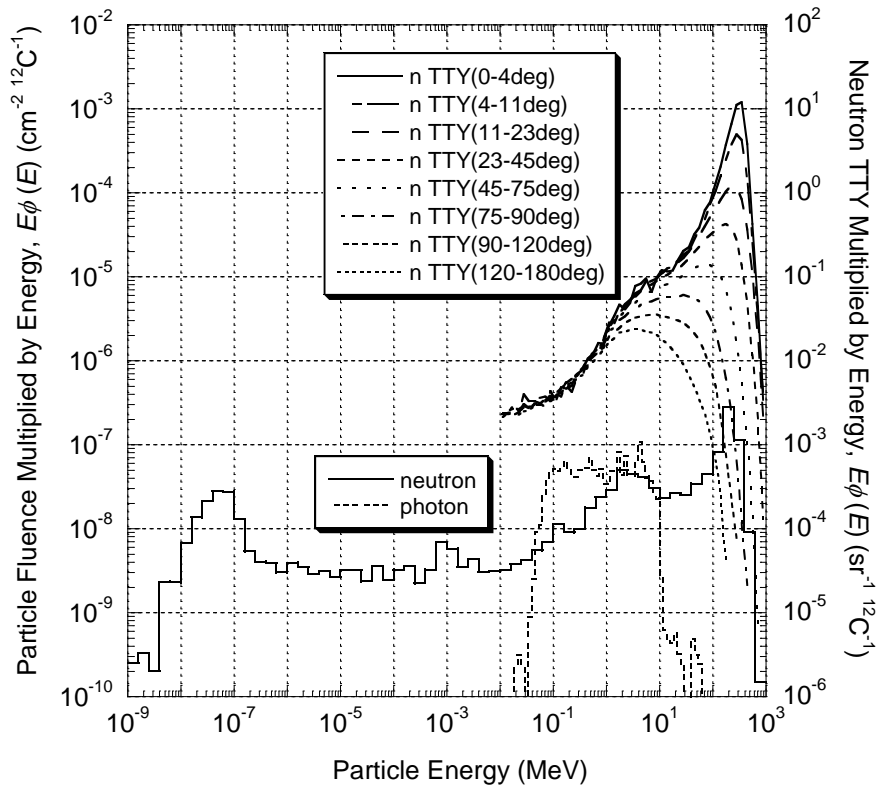
4.2.1 Characteristics of Prompt Radiation Field

4.2.1.1 Mixed Field. High-energy protons and ions produce high-energy neutrons and photons through nuclear interactions with the components of the accelerator and the energy selection system, beam delivery nozzle, and the patient tissue. Several kinds of light ions are produced by the fragmentation process of the primary heavy ions, and these light ions also produce neutrons and photons. High-energy neutrons are slowed down by nuclear scattering and are finally absorbed by matter. Photon emissions accompany these nuclear reactions.

Photons produced by primary charged particles are easily absorbed by the thick room shielding; however, high-energy neutrons can penetrate the shielding. These neutrons produce secondary photons during transmission, resulting in neutrons and photons outside of the shielded area. Neutrons having energies lower than several tens of MeV are easily absorbed. Peaks at about 100 MeV and several MeV appear in the neutron energy spectrum at the outer surface of the shielding. Figure 4.2 shows the angular and energy distributions of neutrons produced in a water phantom of 10 cm diameter and 25 cm thickness irradiated by 400 MeV/nucleon ^{12}C ions, and the neutron and photon spectra in the beam direction behind a 2 m thick ordinary concrete shielding.

Figure 4.3 shows the ratio of the cumulative dose as a function of energy to the total dose calculated with the spectra shown in Fig. 4.2. For photons, almost 100 % of the dose can be measured with a detector, which is sensitive up to 10 MeV, and most conventional detectors meet this criterion. For neutrons, however, typical dosimeters, which are sensitive up to about 15 MeV, may give only one third

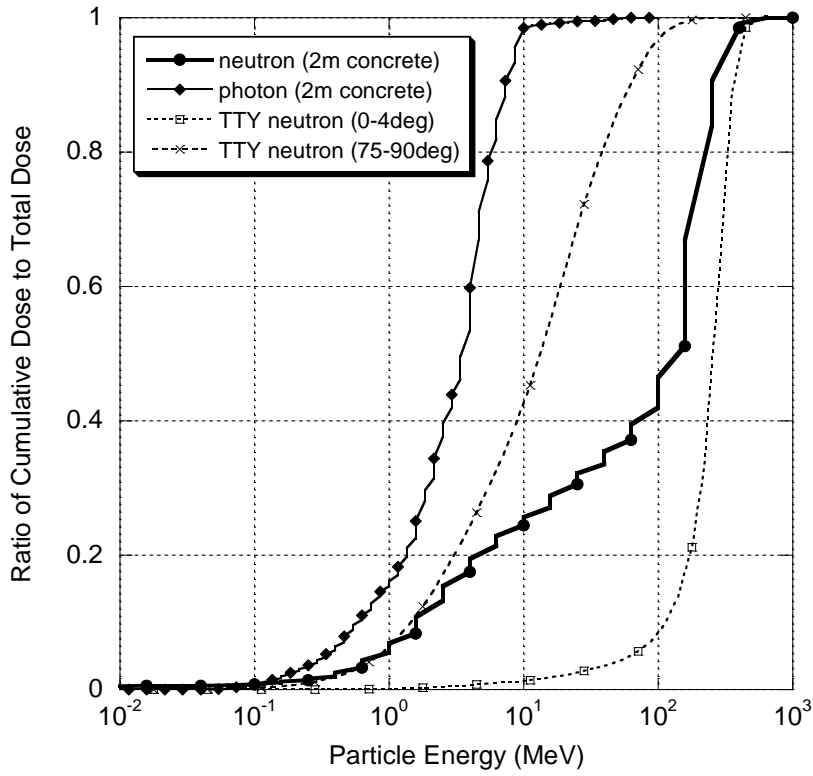
2994 of the true value dose in the forward beam direction outside a thick concrete shield. In the lateral
2995 directions, their readings are more reliable.
2996



2997

2998 Figure 4.2. Angular and energy distributions of TTY (Thick Target Yield) neutrons from a 10 cm
2999 diameter by 25 cm thickness water phantom irradiated by 400 MeV/nucleon ^{12}C ions are shown on the
3000 upper right with the right ordinate. Neutron and photon spectra behind a 2 m thick ordinary concrete
3001 shield in the beam direction are also shown with the left ordinate. These spectra were calculated using
3002 the heavy ion Monte Carlo code, PHITS (Iwase *et al.*, 2002).

3003



3004

3005 Figure 4.3. The ordinate is $\left(\int_0^E E \phi_{\phi}(AP) \phi(E) dE / \int_0^{E_{\max}} E \phi_{\phi}(AP) \phi(E) dE \right)$ where E is particle energy, $E_{\phi}(AP)$ is the
3006 dose conversion coefficients from particle fluence to effective dose for AP geometry (AESJ, 2004), and
3007 $\phi(E)$ is the particle energy fluence shown in Fig. 4.2.

3008

3009 Since a neutron detector, such as a rem meter, has very low sensitivity to photons, it is considered
3010 photon insensitive for charged particle therapy facilities. Photon detectors are also somewhat sensitive to
3011 neutrons, but the estimation of the neutron contribution is difficult. Because neglecting this contribution
3012 results in conservative measurements, the neutron sensitivity is usually ignored for the purpose of
3013 radiation protection.

3014

3015 Primary charged particles are stopped in the patient. Heavy ions, however, produce lighter
3016 particles such as protons and deuterons through fragmentation reactions before stopping. These lighter
3017 particles have longer ranges, and some of them penetrate the patient. When detectors are placed in the
3018 vicinity of a phantom to estimate the neutron and photon exposure to a patient, veto counters operated in
3019 anticoincidence mode may be necessary to eliminate these lighter particles from being recorded.

3020

3021 **4.2.1.2 Pulsed Field.** A detector that counts pulsed signals has an insensitive period after
3022 counting, and this period is called dead time or resolving time, which usually lies between about 10^{-8} s
3023 and 10^{-4} s.

3024

3025 A cyclotron accelerates particles every 10^{-8} s or so, and this acceleration interval is near or shorter
3026 than the dead time, and, therefore, the cyclotron beam is considered to be continuous.

3027

3028 The acceleration interval of a synchrotron, on the other hand, is between 10^{-2} s and 10 s, and thus
3029 its beam has the characteristics of pulsed radiation. During a pulse, a very large amount of radiation is
3030 delivered in a very short time period. Even if several particles of radiation hit a detector within its dead
3031 time, the detector produces only one pulsed signal. This counting loss is a serious problem in a pulsed
3032 radiation field.

3033

3034 The effect of pulsed field is serious near a radiation source because there is hardly any time delay
3035 between the irradiation of primary particles and the detection of secondary neutrons and photons. The
3036 time structure of the neutrons outside the shielding, on the other hand, spreads owing to the different
3037 time-of-flight, *e.g.*, the time-of-flight for 1 m distance is 8 ns for 100 MeV neutrons and 0.5 ms for
3038 thermal neutrons.

3039

3040 If one observes the characteristics of pulsed signals from a detector placed in a pulsed field, on an
3041 oscilloscope, it can be determined whether the reading is correct or not. That is, if the pulse repetition
3042 rate is coincident with the beam extraction rate, the reading of the detector is not correct. A detector
3043 measuring an electric current such as an ionization chamber is not usually affected by the pulsed field.
3044 However, saturation effects due to the recombination of the dense electrons and ions at high peaked dose
3045 rate may become important.

3046

3047 In a particle therapy synchrotron, however, the accelerated particles are extracted slowly because
3048 the irradiation dose must be precisely controlled. The extracted beam, therefore, usually has the
3049 characteristics of continuous radiation. For example, at the HIMAC (Heavy Ion Medical Accelerator in
3050 Chiba) of the National Institute of Radiological Sciences, the acceleration period is 3.3 s and the duration
3051 of extraction is about 2 s.

3052

3053 **4.2.1.3 Noise.** An accelerator uses high-power, high-frequency voltage for acceleration, which is
3054 a very strong source of background noise, thus affecting measurements with active detectors. The signal
3055 cables of the detectors should be separated from the accelerator power cables. Wiring in a grounded
3056 metal pipe is effective for noise reduction. Use of optical fibers is costly but very reliable for

3057 discrimination against noise. Optical fibers, however, are susceptible to mechanical shock and bending,
3058 and lose transparency at high radiation exposures.

3059

3060 **4.2.1.4 Magnetic Field.** Accelerators and beam transport systems use high magnetic fields for
3061 bending and focusing the beam. Magnetic fields strongly affect photomultiplier tubes, thus a usual
3062 scintillation survey meter cannot be used around the magnetic apparatus. Even if the electric current is
3063 switched off, the residual magnetic field due to hysteresis may affect detectors located near magnets.
3064 However, a scintillator coupled to a photo diode is hardly affected by a magnetic field. An analog
3065 indicator using an ammeter does not respond correctly in a magnetic field. A liquid crystal indicator is
3066 much more reliable.

3067

3068 **4.2.1.5 Radiations Unrelated to Beam Acceleration.** Devices operating under high-
3069 radiofrequency power, such as an acceleration cavity and a klystron, emit intense x rays even if the beam
3070 is not accelerated. Leakage of radiation occurs at glass windows and bellows, which are made of low
3071 atomic number materials or thin metal. X-ray leakage from an Electron Cyclotron Resonance (ECR) ion
3072 source is also significant.

3073

3074 **4.2.2 Survey Meters**

3075

3076 Handheld survey meters are typically used to measure instantaneous dose rates and to map the
3077 dose rate distribution outside the shielding. Since the radiation field around a particle therapy facility is
3078 comprised of neutrons and photons, the simultaneous use two types of survey meters is required.

3079

3080 **4.2.2.1 Neutron Survey Meters**

3081

3082 **4.2.2.1.1 Rem Meter.** A rem meter (or a rem counter) is the most popular neutron dose-
3083 equivalent survey meter. It consists of a thermal neutron detector such as a BF_3 (boron trifluoride) or ^3He
3084 (helium) proportional counter or a ^6Li (lithium) glass scintillation counter that is surrounded by a
3085 specially designed polyethylene neutron moderator. The moderator slows down fast and intermediate
3086 energy neutrons, which are then detected by the thermal neutron detector. Because an ordinary rem meter
3087 is practically insensitive to neutrons of energies above 15 MeV, it underestimates the result by as much
3088 as a factor of 3 when used outside a shield of a particle therapy facility as shown in Fig.4.3. Improved
3089 rem meters are also available. These consist of high-atomic number inserts such as lead or tungsten in the
3090 polyethylene moderator (Birattari *et al.*, 1990; Olsher *et al.*, 2000). The interaction of high-energy
3091 neutrons with this inserted material causes neutron multiplication and energy degrading reactions such as
3092 $(n, 2n)$, thus improving the sensitivity to high-energy neutrons. These improved rem meters are too heavy
3093 to be handheld, but give reliable results. An example of such a commercially available rem meter, FHT
3094 762 Wendi-2, is shown in Fig. 4.4. This instrument has an excellent energy response from thermal to 5
3095 GeV, and the response function is shown in Fig. 4.5.

3096

3097



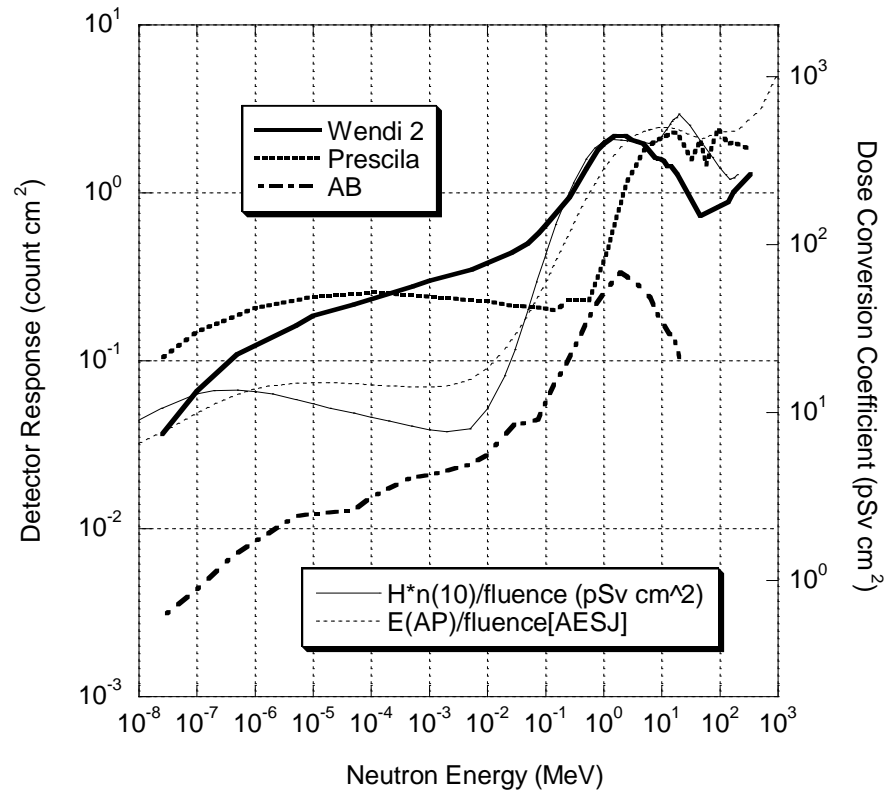
3098

3099 Figure 4.4. FHT 762 Wendi-2 rem meter has an improved energy response to high-energy neutrons.

3100 (Courtesy of Thermo Scientific⁴)

3101

⁴ Thermo Scientific, 27 Forge Parkway, Franklin, Massachusetts 02038 U.S.A.



3102
 3103 Figure 4.5. The response function of the Wendi-2 rem meter is shown with the left side vertical axis.
 3104 The response functions of the Prescila rem meter described in Section 4.2.2.1.2 and the conventional
 3105 Andersson-Braun rem meter (AB) are also shown (Olsher *et al.*, 2000; 2004; courtesy of R.H. Olsher).
 3106 The dose conversion coefficients of $H^*(10)$ and $E(AP)$ are shown for the reference with the right side
 3107 vertical axis (AESJ, 2004; ICRP, 1996).
 3108

3109 **4.2.2.1.2 Proton Recoil Scintillation Counter.** A complex detector consisting of two types of
3110 sensors for fast neutrons and thermal neutrons is available as Prescila rem meter (Olsher *et al.*, 2004).
3111 The fast-neutron sensor consists of a mixture of ZnS(Ag) scintillation powder and epoxy glue and a
3112 Lucite-sheet light guide. The thermal-neutron sensor is a ${}^6\text{Li}+\text{ZnS}(\text{Ag})$ scintillator. By using filters of
3113 cadmium and lead, this counter has a response function whose shape is similar to the conversion
3114 coefficient for neutron fluence-to-dose equivalent, and is sensitive to neutrons above 20 MeV. Its
3115 sensitivity is about 10 times higher than the conventional moderator-based rem meter, and its weight is
3116 about 2 kg.

3117

3118 **4.2.2.2 Photon Survey Meters**

3119

3120 **4.2.2.2.1 Ionization Chamber.** The ionization chamber is the most useful photon survey meter
3121 because it almost energy-independent (usually within $\pm 10\%$ of unity) between 30 keV and a few MeV.
3122 The lower detection limit is about $1\ \mu\text{Sv/h}$; thus, one cannot measure the dose rates close to the
3123 background level. Some types of ionization chambers have removable caps that enable the measurements
3124 of very soft x rays. Since the ionization chamber survey meter measures a very weak current of the order
3125 of femtoamperes (fA) when placed in a field of several $\mu\text{Sv/h}$, it takes several minutes until the detector
3126 becomes stable after being switched on.

3127

3128 **4.2.2.2.2 NaI(Tl) Scintillator.** Scintillators of high atomic number, such as sodium iodide (NaI)
3129 and cesium iodide (CsI), have poor energy response for the measurement of dose equivalent. However,
3130 some scintillation survey meters that have compensation circuits show good energy response similar to
3131 ionization chambers. Scintillation survey meters are mostly insensitive to photons of energies below 50

3132 keV and not appropriate for low-energy x-ray fields. However, an instrument of NHC5,⁵ which is
3133 sensitive down to about 8 keV, is currently available.

3134

3135 **4.2.3 Spectrometers**

3136

3137 **4.2.3.1 Photon Spectrometer.** High purity germanium (Ge) detectors have an excellent energy
3138 resolution and are commonly used for photon spectrometry in research work. Since the Ge detector must
3139 be cooled down to liquid-nitrogen temperature, it is not suitable for routine measurements. Handheld
3140 scintillation survey meters designed for photon spectral measurements are commercially available, such
3141 as InSpectorTM 1000⁶ and identiFINDERTM.⁷ Handheld survey meters with cerium-doped lanthanum
3142 bromide (LaBr₃(Ce)) scintillators are also available. The latter has better energy resolution than the
3143 conventional thallium-doped sodium iodide (NaI(Tl)) scintillator. An unfolding process is required for
3144 the conversion from the light-output distribution obtained by the detector to the photon energy spectrum.

3145

3146 **4.2.3.2 Neutron Spectrometer.** Measurements of light-output or time-of-flight distributions are
3147 common techniques for obtaining high-energy neutron spectra with good energy resolution. For a simple
3148 measurement, a set of neutron detectors with moderators of different thicknesses, the so-called Bonner
3149 spheres, can be used (Awschalom and Sanna, 1985; Wiegel and Alevra, 2002). Wiegel and Alevra used
3150 copper and lead in the moderators, and their spectrometer, NEMUS,⁸ can be used to measure high-energy
3151 neutrons up to 10 GeV. Figures 4.6 and 4.7 show the responses of the NEMUS spheres as a function of

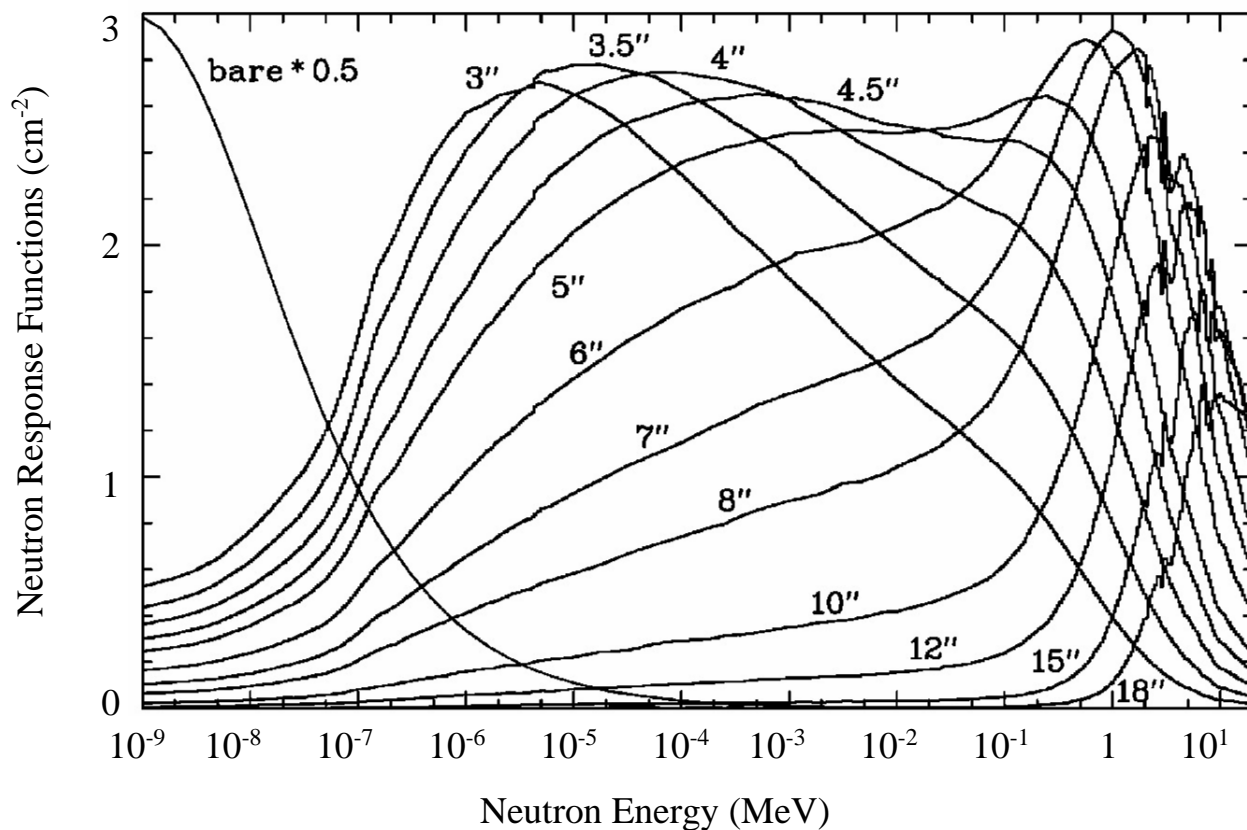
⁵ Fuji Electric Systems Co. Ltd., 1-11-2, Osaki, Shinagawa, Tokyo 141-0032 Japan

⁶ Canberra Industries, Inc., 800 Research Parkway, Meriden, Connecticut 06450 U.S.A.

⁷ ICx Radiation Inc., 100 Midland Road, Oak Ridge, Tennessee 37830 U.S.A.

⁸ Centronic Limited, King Henry's Drive, Croydon, Surrey CR9 0BG, UK

3152 neutron energy. The difference of the important neutron energies of each sphere gives the spectrum
3153 information. The set of the results of these detectors is converted to the neutron energy spectrum with an
3154 unfolding computer program. An initial assumed spectrum that is properly obtained by calculations or
3155 theories is necessary to initiate the unfolding process.
3156



3157

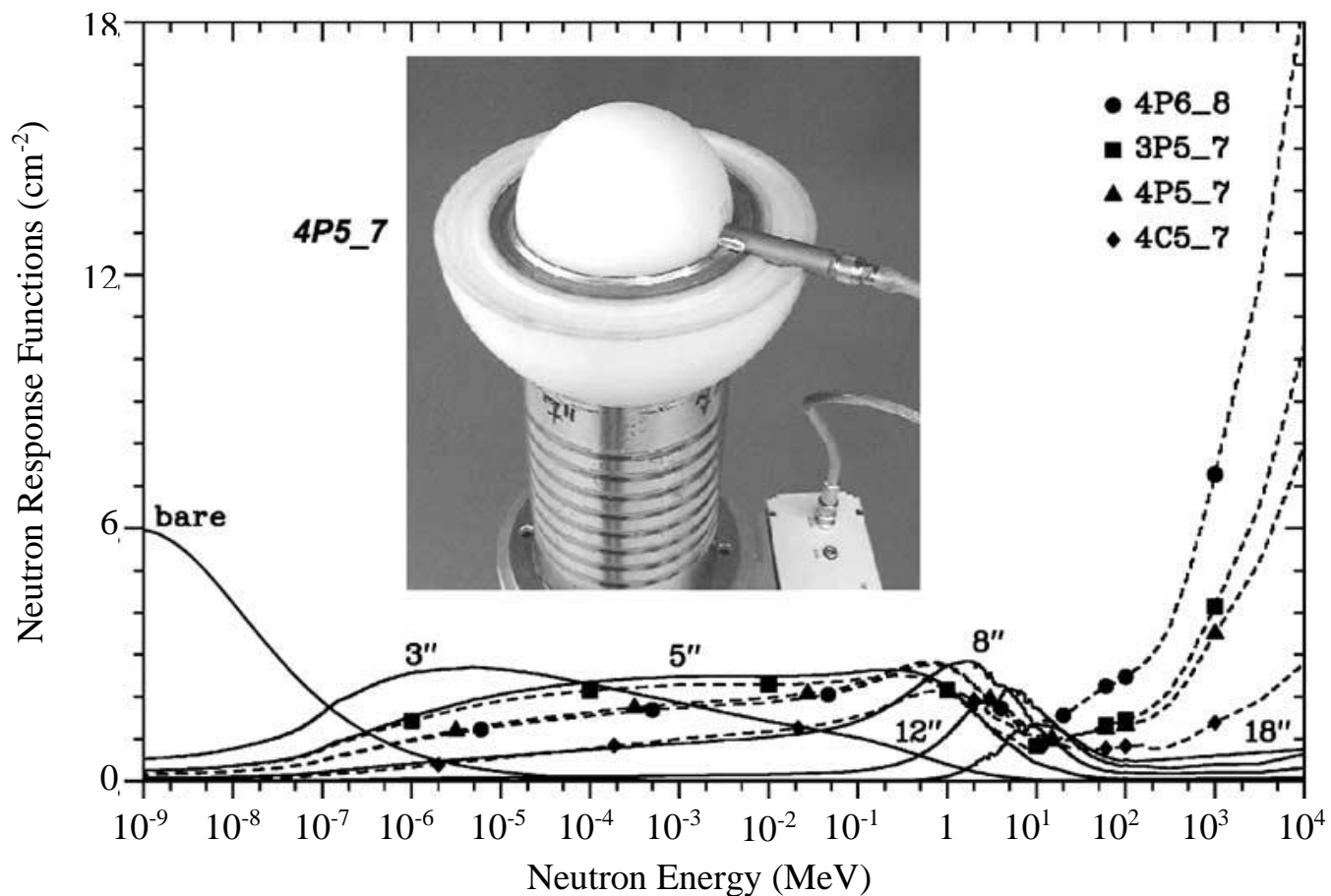
3158

3159

3160 Figure 4.6. Responses of the NEMUS Bonner spheres. The lengths in inches show the diameters of

3161 polyethylene moderators (Wiegel and Alevra, 2002).

3162



3163

3164 Figure 4.7. Responses of the extended NEMUS Bonner spheres. “4P5_7”, for example, means that the
3165 ³He counter is placed in a 4-inch polyethylene sphere covered by a 0.5-inch-thick Pb shell (the diameter
3166 therefore is 5 in) and all are imbedded in a 7-inch polyethylene sphere. The photo shows the opened
3167 configuration. “4C5_7” means that the inserted shell is of 0.5-inch-thick Cu. Six response functions of
3168 the pure polyethylene moderators are also shown (Wiegel and Alevra, 2002).

3169

3170 **4.2.3.3 LET Spectrometer.** The tissue-equivalent proportional counter (TEPC) measures an LET
3171 (linear energy transfer) spectrum of secondary charged particles produced by neutrons and photons, and
3172 the spectrum is converted into dose equivalent or effective dose for both types of radiation. The TEPC is
3173 applicable to any type of radiation because of its measurement principle, and the total dose in a mixed
3174 field is obtained. Several systems have been developed and used (Alberts, 1989; Mazal *et al.*, 1997). The
3175 TEPC, however, has the disadvantage of susceptibility to mechanical shocks, thus preventing its
3176 widespread use for routine measurements as a survey meter.

3177

3178 **4.2.4 Area Monitors**

3179

3180 An area monitoring system consists of pairs of neutron and photon dosimeters and a central control
3181 unit. For neutron detection, rem meters are usually used. Ionization chambers, scintillation detectors, or
3182 semiconductor detectors are selected for photon detection depending upon the radiation intensities.
3183 Stations having local radiation level indicators are also available. The central control unit shows trend
3184 graphs of radiation levels of each station, and records data in a server. The system is of high performance
3185 and expensive (see Fig. 4.8).

3186



3187

3188

3189

3190

3191

Figure 4.8. An example of a monitoring station (a) and a central control unit, MSR-3000, (b). The station has a neutron rem meter and a photon detector.(Courtesy of ALOKA⁹)

⁹ ALOKA Co., Ltd., 6-22-1, Mure, Mitaka, Tokyo 181-8622 Japan

3192 Before determining the monitoring locations, the dose distribution in and around the facility must
3193 be thoroughly studied. Monitoring stations are located where high radiation dose rates are expected or
3194 where radiation levels are important for safety reasons. However, high dose-rate radiation inside the
3195 irradiation room, for example, sometimes causes a breakdown of an intelligent monitoring station.

3196

3197 At accelerator facilities for physics research, area monitors are typically included in safety systems
3198 and are interlocked so that they turn the beam off when measured radiation levels outside shielded areas
3199 exceed a preset value, either considering instantaneous or integrated values. However, at particle therapy
3200 facilities, interruption of the beam is not desirable because the beam is used to treat the patients.
3201 Therefore the systems must be designed robustly enough that no false alarms are given. It depends on the
3202 local regulations what type of action needs to be performed when an alarm is given.

3203

3204 As the above monitoring system is expensive, it is difficult to distribute many stations. Because the
3205 neutron dose is usually dominant around a particle therapy facility, it is possible to place many neutron
3206 rem meters, described in Section 4.2.2.1.1, whose analog outputs are read by a programmable logic
3207 controller (PLC) of a safety system (Uwamino *et al.*, 2005). When the analog output is logarithmic, the
3208 PLC reads the dose rate with a wide dynamic range of more than 5 decades. If the analog output is a
3209 voltage signal, it can be converted into a current signal for a reliable transmission.

3210

3211 **4.2.5 Passive Monitoring**

3212

3213 Passive detectors that were originally developed for individual monitoring, described in Section
3214 4.4.3, can be also used for environmental radiation monitoring. Though real-time results cannot be
3215 obtained with passive detectors, they are very useful because of their low cost. They directly give

3216 integrated doses over an appropriate time period. Furthermore, passive monitors are hardly influenced by
3217 the time structure of a pulsed radiation field, electric noise from lightning, and mechanical shocks.

3218

3219 Since individual monitors are calibrated on a phantom, they cannot be used directly for
3220 environmental measurements. The monitors must be calibrated in free air as described in Section 4.5.2.

3221

3222 Hranitzky *et al.* (2002) developed an $H^*(10)$ photon dosimeter with a LiF thermoluminescence
3223 dosimeter (TLD) and filters. It showed good energy dependence, with less than 5 % deviation between
3224 30 keV and 2.5 MeV.

3225

3226 For x-ray dose measurements near linacs and ECR ion sources, an $H^*(10)$ dosimeter was
3227 developed using LiF TLD chips (Fehrenbacher *et al.*, 2008). Each dosimeter has four TLD chips, and
3228 two chips are covered with copper filter. The weighted average of readings of these tips gives good
3229 responses over the energy range from 10 keV to about 4 MeV; *i.e.*, the deviations of the relative
3230 sensitivity from the $H^*(10)$ response are lower than 25 %.

3231

3232 By using a pair of thermoluminescence dosimeters of ^6LiF and ^7LiF and a specially designed
3233 moderator, Fehrenbacher *et al.* (2007b; 2007c) developed an $H^*(10)$ dosimeter for a wide spectrum of
3234 neutrons ranging up to several hundreds of MeV.

3235

3236 In high-intensity neutron fields, activation foils are also applicable. Capture reactions of Mn, Co,
3237 Ag, In, Dy, and Au are useful for thermal neutron measurement. For fast neutrons, threshold reactions of
3238 $^{12}\text{C}(n, 2n)^{11}\text{C}$, $^{27}\text{Al}(n, \alpha)^{24}\text{Na}$, $^{27}\text{Al}(n, 2n\alpha)^{22}\text{Na}$, $^{59}\text{Co}(n, \alpha)^{56}\text{Mn}$, $^{197}\text{Au}(n, 2n)^{196}\text{Au}$, $^{209}\text{Bi}(n, xn)^{210-x}\text{Bi}$
3239 ($x=4$ to 12), *etc.* are useful. A combination of these reactions can give a neutron spectrum in the MeV

3240 region. Indium activation detectors inserted at the center of spherical polyethylene moderators can be
3241 used for neutron spectrometry for the energy range between thermal and 20 MeV (Uwamino and
3242 Nakamura, 1985).

3243

3244 **4.3 Measurement of Residual Radioactivity**

3245

3246 **4.3.1 Introduction**

3247

3248 Residual radioactivity is sometimes significant at locations where the beam losses are high, such as
3249 the beam extraction device, beam dump, energy selection system, components in a passive scattering
3250 treatment port, and delivery nozzle that intercept the beam. Measurement of the radiation intensity at
3251 locations where maintenance work may be done is important in order to avoid any excess personnel
3252 exposure.

3253

3254 Collimators, ridge filters, and range modulators, which are fixed at the treatment port of a passive
3255 irradiation facility, are significantly activated. However, the bolus and the patient collimator for each
3256 patient are irradiated for a short time, and the residual activities last only for a relatively short period
3257 after irradiation because of the short half-lives ($T_{1/2}$) of the induced radioactive isotopes, for example, ^{11}C
3258 ($T_{1/2} = 20.4$ min) in bolus and $^{62\text{m}}\text{Co}$ ($T_{1/2} = 13.9$ min) in collimator (Tujii *et al.*, 2009; Yashima *et al.*,
3259 2003). Thus, the exposure of the treatment staff who handle these patient-specific devices is low (Tujii *et*
3260 *al.*, 2009). However, at most facilities that use passive scattering techniques, these devices are stored for
3261 up to 2 to 3 months before they are shipped out of the facility. At a scanning irradiation facility with a
3262 synchrotron, activation problems are hardly observed at the treatment port.

3263 Compared to the activation at accelerator laboratories for physics research, the activation situation
3264 in particle therapy facilities can be quite different. In patient treatment rooms, the level is usually not
3265 very high. In facilities with a cyclotron, however, the strongest activity is in the degraders and the
3266 following emittance defining collimators, that is, the energy selection system. Usually this system is
3267 located in the beam line directly from the cyclotron and here more than 90 % of the beam intensity is lost
3268 in the degrader and on collimators. This system needs to be accessed for maintenance or repairs only and
3269 can be shielded properly. In the cyclotron itself several hot spots are present due to beam losses. These
3270 can be taken care of by local shielding or removal of the hot components.

3271
3272 Measurement of residual radioactivity is important when the accelerator components, beam
3273 delivery nozzle, and patient-specific irradiation devices are classified as “radioactive” or “not
3274 radioactive” for waste management.

3275

3276 **4.3.2 Ionization Chamber**

3277

3278 Ionization chamber survey meters are the most suitable and reliable detectors for the measurement
3279 of ambient dose rate due to residual radioactivity. Some detectors have removable windows on the
3280 chambers, and they can measure the beta-ray dose that may be important for the estimation of skin dose.

3281

3282 **4.3.3 NaI(Tl) Scintillators**

3283

3284 NaI(Tl) scintillation survey meters with correction circuits for energy dependency give accurate
3285 results of ambient dose rate, similar to an ionization chamber. The lower detection limits are low enough
3286 for background measurements and they can also be used for the measurement of radioactive waste.

3287

3288 Handheld photon spectrometers described in Section 4.2.3.1, which function also as dosimeters,
3289 may be used for nuclide analysis of residual activity. Because of their limited energy resolution,
3290 complicated spectra cannot be resolved. For a precise analysis, high purity germanium (Ge) detectors are
3291 recommended.

3292

3293 **4.3.4 Geiger-Müller Tube**

3294

3295 A Geiger-Müller survey meter with a thin window has almost 100 % sensitivity to the incoming
3296 beta rays, and it is very useful in classifying materials as radioactive or not.

3297

3298 A survey meter having an extendable rod with a small Geiger-Müller counter installed at its tip is
3299 useful for the measurement of high dose rate from a remote position.

3300

3301 **4.3.5 Other Survey Meters for Contamination Measurement**

3302

3303 Detectors such as proportional counters, plastic scintillators, and semiconductor detectors are used
3304 in survey meters for contamination measurements. These survey meters are also useful in classifying
3305 materials as “radioactive” or “not radioactive.” Unlike the Geiger-Müller tube, the properties of these
3306 detectors hardly deteriorate with time.

3307

3308 A hand-foot-clothes monitor is useful equipment for contamination tests of a body. Geiger-Müller
3309 tubes, proportional counters, and plastic scintillators are often used as sensors. Most sensors are sensitive

3310 to beta and gamma rays. Some sensors simultaneously detect alpha-emitter contamination. The monitors
3311 are usually placed at the entrances of controlled areas.

3312

3313 **4.4 Individual Monitoring**

3314

3315 **4.4.1 Introduction**

3316

3317 Individual personnel exposure is classified as external and internal exposures. Internal exposure is
3318 usually important for unsealed-radioisotope handling, and should be considered when highly activated
3319 accelerator devices, such as targets and charge-exchange stripper foils, are handled. If a cyclotron-based
3320 particle therapy facility using passive irradiation systems has many treatment ports and is operated with
3321 high duty factors, this kind of internal exposure may be important. Although internal exposure is usually
3322 not important at particle therapy facilities, one should be cautious with removal of dust from some hot
3323 spots (*e.g.*, degrader region in a cyclotron facility), cooling water which may have been contaminated by
3324 neutron or proton exposure, and activated air in the cyclotron/degrader vault, shortly after switching off
3325 the beam.

3326

3327 Dose equivalents, $H_p(10)$ and $H_p(0.07)$, are measured for the estimation of the individual external
3328 exposure. The former is important for the effective-dose estimation and the latter is used for the
3329 equivalent-dose estimation for skin and eye lenses. Typically, a single personal dosimeter is used, and it
3330 is normally worn on the chest for males or on the abdomen for females. If a strong non-uniform exposure
3331 is expected, supplementary dosimeters are worn on the extremities such as the finger or head.

3332

3333 If accelerator or energy selection devices having high residual activity require hands-on
3334 maintenance, a ring badge worn on a finger is recommended, as the exposure of hands is normally much
3335 higher than that of the torso. Because the exposure of the palm is usually higher than that of the back of
3336 the hand, wearing a ring badge with the sensitive part facing inside is recommended.

3337

3338 **4.4.2 Active Dosimeter**

3339

3340 Many types of active personal dosimeters using semiconductor detectors or small Geiger-Müller
3341 tubes are available. These detectors usually measure and display the accumulated exposure after being
3342 switched on.

3343

3344 Several different types of dosimeters are available. Alarm meters provide an alarm when the
3345 accumulated exposure exceeds a preset value. Small survey meters indicate the dose rate. Others make
3346 audible clicking sounds with a frequency that corresponds to the dose rate. Some record the trend of the
3347 exposure and the data are transmitted to computers for analysis.

3348

3349 Many products are commercially available; for example, DOSICARD,¹⁰ PDM,¹¹ and Thermo
3350 EPD.¹² The last one has all the functions described above. A novel example is PM1208M,¹³ which is a

¹⁰ Canberra Industries, Inc., 800 Research Parkway, Meriden, Connecticut 06450 U.S.A.

¹¹ ALOKA Co., Ltd., 6-22-1, Mure, Mitaka, Tokyo 181-8622 Japan

¹² Thermo Fisher Scientific Inc., Bath Road, Beenham, Reading, Berkshire RG7 5PR, UK

¹³ Polimaster Ltd., 51, Skoriny str., Minsk 220141, Republic of Belarus

3351 wristwatch that includes a gamma-ray dosimeter. NRF30¹⁴ can be connected to the personal access
3352 control system, which records the time of entry and exit and the corresponding exposure.

3353

3354 Though small batteries power these dosimeters, many dosimeters work continuously for a week or
3355 several months. Radio waves of a cellular phone may affect the responses of some of these dosimeters.

3356

3357 **4.4.3 Passive Dosimeter**

3358

3359 Passive dosimeters measure the integrated dose and therefore do not provide any information on
3360 the real-time exposure. However, these dosimeters are small, noise-free, and not susceptible to
3361 mechanical shock. Their measurements are independent of the time structure of a radiation field in
3362 contrast to the active dosimeters, which may give an underestimated value in a strong-pulsed field.

3363

3364 **4.4.3.1 Thermoluminescence Dosimeter (TLD).** An exposed TLD element, such as calcium
3365 sulfate doped with thulium (CaSO₄:Tm), emits light when it is heated. The intensity of the light emission
3366 is a measure of the exposure. The TLD reader can be placed on a desk, and therefore in-house dosimetry
3367 is common. A TLD dosimeter for measuring both photons and beta rays is available. This consists of
3368 several elements having different filters, and both $H_p(10)$ and $H_p(0.07)$ can be measured with one
3369 dosimeter.

3370

3371 Since the size of TLD is small, it can also be used in a ring badge that measures the exposure to the
3372 hands.

3373

¹⁴ Fuji Electric Systems Co. Ltd., 1-11-2, Osaki, Shinagawa, Tokyo 141-0032 Japan

3374 **4.4.3.2 Optically Stimulated Luminescence (OSL) Dosimeter.** An exposed OSL element, such
3375 as carbon-doped aluminum oxide ($\text{Al}_2\text{O}_3:\text{C}$) emits blue light when it is irradiated by a green laser light. A
3376 dosimeter badge consisting of an OSL element and filters, which is used for photons and beta rays, is
3377 commercially available: LUXCEL OSL.¹⁵ A company¹⁶ provides dosimetry service; that is, the company
3378 distributes dosimeter badges consisting of OSL elements, and, after use, it reads and evaluates the
3379 exposure. An OSL reader that can be placed on a desk is also available, and thus in-house dosimetry is
3380 also possible. The dosimeter is applicable for energies between 5 keV and 10 MeV for photons and
3381 between 150 keV and 10 MeV for beta rays. The readable dose ranges between 10 μSv and 10 Sv for
3382 photons and 100 μSv and 10 Sv for beta rays.

3383

3384 **4.4.3.3 Glass Dosimeter.** An exposed chip of silver-doped phosphate glass emits orange light
3385 when it is irradiated with ultraviolet laser light. Several glass elements and filters, assembled as a photon
3386 and beta-ray dosimeter badge, is commercially available.¹⁷ In-house dosimetry and an external-company
3387 service¹⁸ are both available. Reading of the glass element does not reset the dosimeter, and the long-term
3388 accumulated dose can be obtained directly. The dosimeter is reset by annealing at high temperatures.
3389 Performance of the glass dosimeter is almost the same as the OSL dosimeter.

3390

3391 **4.4.3.4 Direct Ion Storage (DIS) Dosimeter.** In a DIS dosimeter, a charge stored in a
3392 semiconductor is discharged by the current of an ionization chamber. The discharge is read as the change

¹⁵ Landauer Inc., 2 Science Road, Glenwood, Illinois 60425-1586 U.S.A.

¹⁶ Landauer Inc., 2 Science Road, Glenwood, Illinois 60425-1586 U.S.A.

¹⁷ Chiyoda Technol Corp., 1-7-12, Yushima, Bunkyo, Tokyo 113-8681 Japan

¹⁸ Chiyoda Technol Corp., 1-7-12, Yushima, Bunkyo, Tokyo 113-8681 Japan

3393 in conductivity. The RADOS DIS-1 dosimeter¹⁹ has a good energy response to photons. The applicable
3394 energy range is between 15 keV and 9 MeV for photons, and 60 keV and 0.8 MeV for beta rays. Photon
3395 doses between 1 μ Sv and 40 Sv, and beta-ray doses between 10 μ Sv and 40 Sv can be read with this
3396 dosimeter. In-house dosimetry is common. It can also be used as an active dosimeter by attaching a small
3397 reader to the detector.

3398

3399 **4.4.3.5 Solid State Nuclear Track Detector.** Recoil protons, which are produced in a
3400 polyethylene radiator by fast neutrons, create small damage tracks on a plastic chip of Allyl Diglycol
3401 Carbonate (ADC or PADC, [Poly]), which is commercially available as CR-39.²⁰ The damage tracks can
3402 be revealed by a suitable etching process (chemical or electrochemical). The tracks can be counted and
3403 the track density can be related to the neutron dose equivalent. A boron converter can be used instead of
3404 the radiator, to detect thermal neutrons through the $^{10}\text{B}(n, \alpha)$ reactions. Commercially available
3405 dosimeters include the Landauer Neutrak 144²¹ which comprises the fast and thermal options with CR-
3406 39. The lower detection limit of the detector is relatively high, which is about 0.1 mSv for thermal
3407 neutrons and 0.2 mSv for fast neutrons. The energy range for fast neutrons is 40 keV to 35 MeV. Use of
3408 external-company²² dosimetry services is usual.

3409

3410 **4.4.3.6 Film Dosimeter.** A film badge dosimeter consists of photographic film and filters. The
3411 film is developed after irradiation, and the photographic density is compared with that of the control film,
3412 which is kept far from radiation sources. A rough estimate of the photon or beta-ray energy can be

¹⁹ RADOS Technology Oy, PO Box 506, FIN-20101 Turku, Finland

²⁰ PPG Industries, One PPG Place, Pittsburgh, Pennsylvania 15272 USA

²¹ Landauer Inc., 2 Science Road, Glenwood, Illinois 60425-1586 U.S.A.

²² Landauer Inc., 2 Science Road, Glenwood, Illinois 60425-1586 U.S.A.

3413 obtained by using a combination of filters. Thermal neutron exposure is measured with a cadmium filter.
3414 Observation of recoil nuclear tracks with a microscope gives the exposure of fast neutrons. External-
3415 company dosimetry services are usually used. In spite of these features, the film badge dosimeter is
3416 disappearing quickly because of the following disadvantages: higher detection limit of about 100 μSv for
3417 photons and beta rays and of several hundreds of μSv for neutrons; and fading phenomenon that makes
3418 the measurement impossible if the dosimeter is left for several months without development after
3419 irradiation.

3420

3421

4.5 Calibration

3422

4.5.1 Introduction

3424

3425 Calibration involves the comparison between the reading of a dosimeter with the dose rate in a
3426 standard radiation field that is traceable to a national standard field, and a description of the relationship
3427 between them. Details of the calibration procedure are precisely explained in the ICRU reports for
3428 photon dosimeters (ICRU, 1992a) and for neutron dosimeters (ICRU, 2001).

3429

3430 The calibration factor, N , is given by:

$$3431 \quad N = H/M \quad (4.1)$$

3432 where H is the dose rate of the standard field, and M is the reading of the detector after necessary
3433 corrections are applied, for example, with atmospheric pressure and with temperature.

3434

3435 There are two kinds of calibration: one is to obtain the detector characteristics of energy, angular
3436 and dose-rate dependencies, and the other is to determine the changes in the detector performance with

3437 time, such as absolute sensitivity. The manufacturer usually does the former calibration with adherence
3438 to national industrial standards. Users do the latter once or twice a year. The latter calibration done by the
3439 user is described below.

3440

3441 **4.5.2 Calibration of Ambient Dose Monitor**

3442

3443 **4.5.2.1 Calibration of Photon Monitor.** A standard field can be achieved by using a standard
3444 gamma-ray source of ^{60}Co or ^{137}Cs . The standard dose rate, H , is obtained with the following formula:

$$3445 \quad H = X \cdot f \quad (4.2)$$

3446 where X is the given exposure rate at a 1 m distance from the standard source, and f is the conversion
3447 factor of exposure to ambient dose equivalent, $H^*(10)$, for the gamma-ray energy of the source. If the
3448 detector is not placed at 1 m distance from the source, then X should be corrected according to the
3449 inverse-square-law of the distance, assuming a point source of radiation.

3450

3451 If a standard exposure dosimeter, which is calibrated in a field having traceability to the national
3452 standard field, is used, then the standard dose rate, H is given by:

$$3453 \quad H = N_s \cdot f \cdot M_s \quad (4.3)$$

3454 where M_s is the reading of the standard dosimeter after necessary corrections are applied, N_s is its
3455 calibration factor, and f is the conversion factor of exposure to ambient dose equivalent, $H^*(10)$.

3456

3457 The photons reaching the calibration point after scattering from the walls, floor, and roof are
3458 ignored in Equation 4.2. In Equation 4.3, the change of photon energy through the scattering is also
3459 ignored. Thus, the detector must not be placed far from the source. On the other hand, if the detector is
3460 placed too close to the source, non-uniform irradiation of the detector is caused and a further

3461 consequence is a larger relative uncertainty in the distance. Therefore, in order to assume a point source
3462 of radiation, the distance should be greater than 5 times the detector diameter, and smaller than 2 m if the
3463 source is not collimated. The detector and the source should be located at least 1.2 m away from the
3464 floor, and 2 m away from the wall and the roof.

3465

3466 **4.5.2.2 Calibration of Neutron Monitor.** ^{252}Cf (average energy = 2.2 MeV) and $^{241}\text{Am-Be}$
3467 (average energy = 4.5 MeV) sources are used for calibration. Since scattering significantly affects the
3468 dose rate for neutrons, it cannot be reduced to negligible levels. The calibration factor, N , for a standard
3469 source with a given neutron emission rate, can be obtained with the following formula:

3470
$$N = \frac{H}{M_F - M_B} \quad (4.4)$$

3471 where H is the dose rate calculated with the product of the source emission rate and the conversion factor
3472 of neutron fluence to dose equivalent, M_F is the reading of the detector irradiated by direct and scattered
3473 neutrons, and M_B is the background reading of the detector irradiated only by scattered neutrons, in
3474 which case the direct neutrons are shielded by a shadow cone placed between the source and the detector.

3475

3476 Shielding of the direct neutrons needs a massive and costly shadow cone. Instead of using
3477 Equation 4.4, the following procedure is also applicable. Since the angular dependence of the neutron
3478 detector sensitivity is usually small, the dose rate, H , including the scattered neutrons at the calibration
3479 point, can be determined with a standard reference dosimeter. A detector to be calibrated is also
3480 irradiated with the direct and scattered neutrons, and the calibration factor, N , is simply obtained with
3481 Equation 4.1 and Equation 4.3, where f is unity if the standard reference dosimeter reads ambient dose
3482 equivalent.

3483

3503 The dose rate at the detector position without the phantom, H , is calculated using Equation 4.2
3504 with the conversion factor of exposure to the $H_P(10)$ dose rate, f . In the case of neutrons, H is calculated
3505 by the product of the given neutron emission rate of the source and the conversion factor of fluence to the
3506 $H_P(10)$ dose rate. The calibration factor, N , is obtained using Equation 4.1 with the standard dose rate, H ,
3507 and the reading of the monitor, M .

3508

3509 The directional personal 10 mm depth dose equivalent is expressed as $H_P(10, \alpha)$, where α is the
3510 angle between the normal direction of the phantom surface and the direction of radiation. The ratio, R , of
3511 $H_P(10, \alpha)$ to $H_P(10, 0^\circ)$ is close to unity ($0.8 < R < 1$ for $\alpha > 75^\circ$) for photons of energies above 0.4 MeV
3512 and for neutrons of energies above 5 MeV. From Fig. 4.3, it can be observed that high-energy particles
3513 are the dominant contributors to the doses, and the angular distribution of the radiation does not seriously
3514 affect the individual exposure. If the angular dependence of the individual monitor is significantly
3515 different from that of $H_P(10, \alpha)$ even at higher energies, the reading of the monitor is not reliable. The
3516 calibration factor, N , for angular incidence should also be considered.

3517

3518 **5. Activation**

3519 *Yoshitomo Uwamino*

3520
3521 **5.1 Introduction**

3522
3523 Induced radioactivity produced in an accelerator and its beam-line components may cause
3524 exposure of maintenance workers, and makes the disposal of activated components difficult. Further,
3525 radioactivity in the vicinity of the treatment port, beam shaping, and delivery systems may result in the
3526 exposure of medical staff. This exposure may not be negligible at a facility that does not use a scanning
3527 irradiation system. At a cyclotron facility, induced radioactivity of the energy selection system (ESS) is
3528 significant.

3529
3530 Accelerated particles exiting the vacuum window interact by nuclear reactions in the air path
3531 upstream of the patient, causing activation. The air is also activated by the secondary neutrons that are
3532 produced by nuclear reactions of charged particles in the equipment and on the patient. These secondary
3533 neutrons also produce radioactivity in equipment cooling water and possibly in groundwater.

3534
3535 Treatment with high-energy charged particles intrinsically activates the diseased part of the
3536 patient. Tujii *et al.* (2009) irradiated a phantom with proton and carbon beams at therapy facilities and
3537 measured the activation. The estimated exposure of medical staffs and family members of the patient was
3538 negligibly small, and the concentration of radioactivity in the excreta of the patient was insignificant
3539 when the dilution at a lavatory was taken into account.

3540

3541 A comprehensive book on induced radioactivity was written by Barbier (1969), and useful data
3542 was published by the International Atomic Energy Agency (IAEA, 1987). Activation-associated safety
3543 aspects of high-energy particle accelerators are discussed in several books (*e.g.*, IAEA, 1988; Sullivan,
3544 1992).

3545

3546 Induced radioactivity and its resulting radiation field can be estimated by using a single Monte
3547 Carlo program starting with the primary accelerated particles (Ferrari, 2005). Several Monte Carlo codes
3548 calculate the production of residual radioactivity, and post-processing programs follow the decay chain
3549 of the radioactivity and calculate the gamma-ray transport and the dose rate. Chapter 6 explains Monte
3550 Carlo methods in detail, while in this chapter, calculation and measurement techniques to determine
3551 activation of equipment, buildings, water, and air are described.

3552

3553 **5.1.1 Activation Reactions**

3554

3555 Since neutrons are not affected by the Coulomb barrier of the nuclei, neutrons of any energy react
3556 with nuclei. Thermal neutrons mostly interact *via* (n, γ) reactions. However, with some nuclides, such as
3557 ${}^6\text{Li}$, they produce ${}^3\text{H}$ through the (n, α) reaction. Neutrons of energy higher than the excited level of the
3558 target nucleus provoke (n, n') reactions. Usually, the excited nucleus immediately transits to its ground
3559 state accompanied by gamma-ray emission. When the neutron energy is sufficiently high enough to
3560 cause particle emission, many types of activation reactions, such as (n, p) , (n, α) , $(n, 2n)$, *etc.* occur.
3561 Relativistic high-energy neutrons cause spallation reactions that emit any type of nuclide lighter than the
3562 target nucleus.

3563

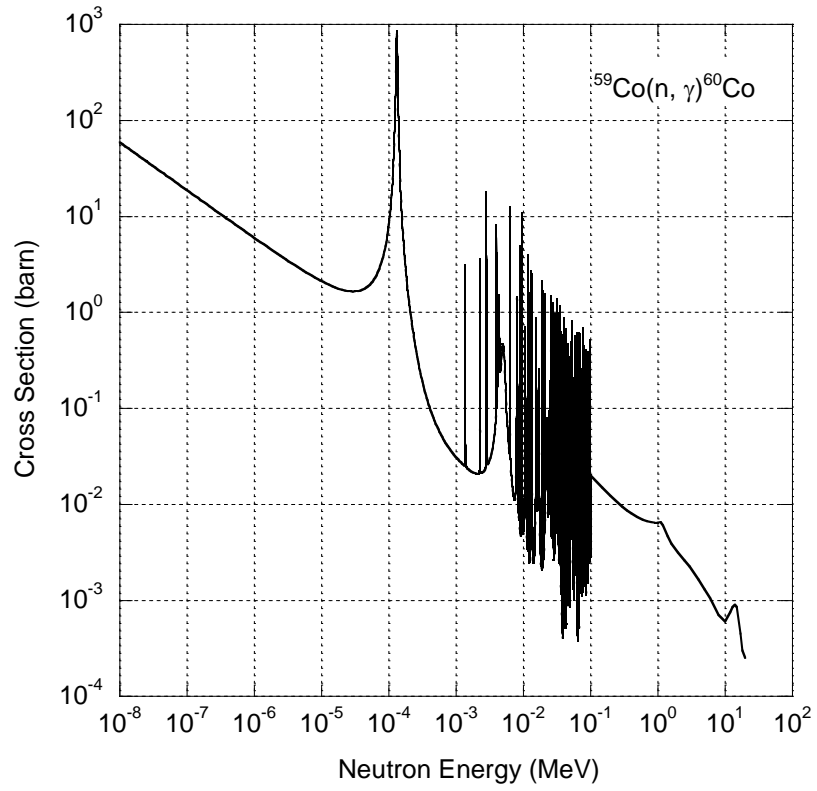
3564 Charged particles with energy lower than the Coulomb barrier do not effectively react with
3565 nuclei. Coulomb excitation causes x-ray emission and fission in special cases, such as in uranium. These
3566 phenomena, however, can be usually ignored because the x-ray energy is low and not penetrative, and
3567 because the fission probability is very small. When the particle energy becomes higher than the Coulomb
3568 barrier, particles produce compound nuclei. Depending upon the excitation energy of the compound
3569 nuclei, (x, γ) reactions (where x is the incident charged particle), and particle-emitting reactions, such as
3570 (x, n) , (x, p) and (x, α) reactions, occur and often result in the production of radioactive nuclides. The
3571 high-energy charged particles can also cause spallation reactions.

3572
3573 Examples of reaction cross sections are shown in Figs. 5.1 and 5.2. Figure 5.1 is the neutron
3574 capture cross section for ^{59}Co . The capture cross sections are generally proportional to $1/v$ (v is the
3575 neutron velocity) or $1/\sqrt{E}$, where E is the energy. They fluctuate at the resonance energy region
3576 according to the characteristics of the nuclide. The $^{59}\text{Co}(n, \gamma)^{60}\text{Co}$ reaction is important for the activation
3577 of stainless steel by thermal neutrons. The cross sections of threshold activation reactions of ^{27}Al are
3578 shown in Fig. 5.2. The threshold energies are 1.9 MeV, 3.2 MeV and 13.5 MeV for the $^{27}\text{Al}(n, p)^{27}\text{Mg}$,
3579 $^{27}\text{Al}(n, \alpha)^{24}\text{Na}$, and $^{27}\text{Al}(n, 2n)^{26}\text{Al}$ reactions, respectively. In general, cross sections for threshold
3580 reactions rapidly increase beyond the threshold energy and have a peak. They decrease beyond the peak
3581 energy, since other reaction channels open with the increase of energy.

3582
3583 Figure 5.3 shows the nuclides produced by various reactions of neutrons and protons. The heavy
3584 ion reactions are more complex and, therefore, it is difficult to show a similar kind of figure.

3585

3586

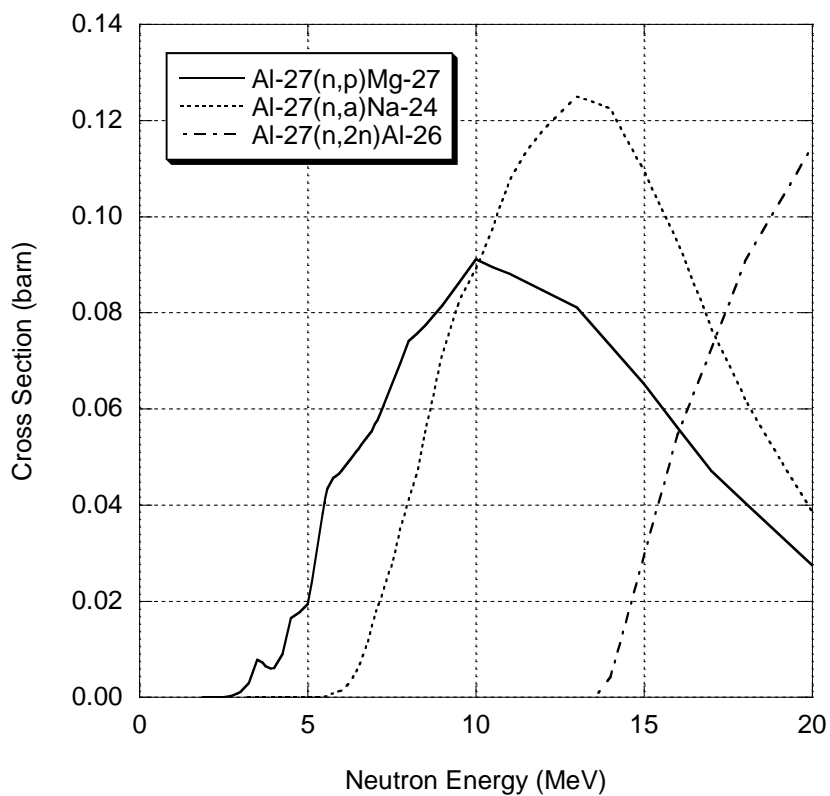


3587

3588 Figure 5.1. Cross section for the $^{59}\text{Co}(n, \gamma)^{60}\text{Co}$ activation reaction as a function of energy (Chadwick *et*
3589 *al.*, 2006).

3590

3591

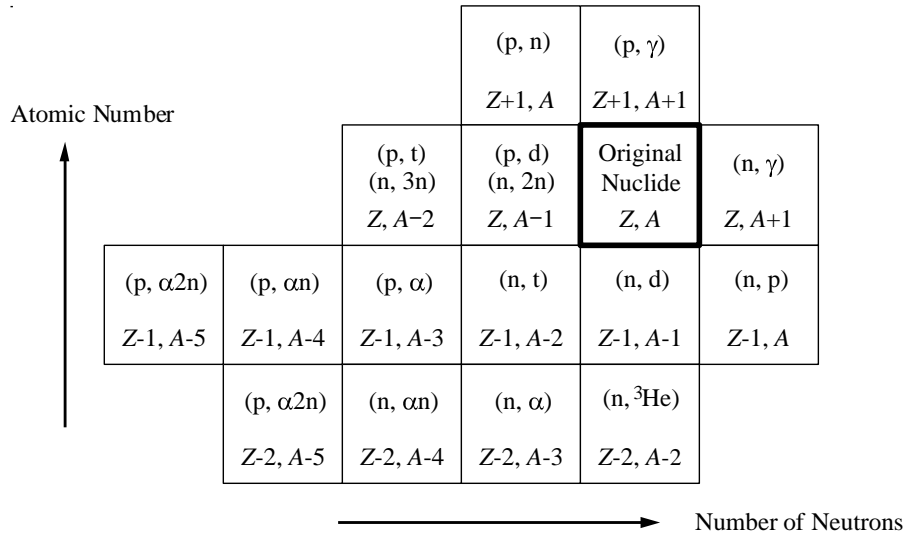


3592

3593 Figure 5.2. Cross sections for the $^{27}\text{Al}(n, p)^{27}\text{Mg}$, $^{27}\text{Al}(n, \alpha)^{24}\text{Na}$, and $^{27}\text{Al}(n, 2n)^{26}\text{Al}$ activation reactions
3594 as a function of energy (Chadwick *et al.*, 2006).

3595

3596



3597

3598 Figure 5.3. Nuclides produced by various nuclear reactions. (n, d) reaction includes (n, pn) reaction, and

3599 (n, t) reaction includes (n, dn) and (n, p2n) reactions, and so on.

3600

3601 **5.1.2 Activation and Decay**

3602

3603 The production rate of a radioactive nuclide, R (s^{-1}), is calculated by the following formula:

3604
$$R = \phi \sigma N_F V \quad (5.1)$$

3605 where ϕ ($cm^{-2} s^{-1}$) is the radiation fluence rate averaged over the irradiation field, σ (cm^2) is the
3606 activation cross section averaged over the radiation energy, N_F (cm^{-3}) is the atomic density of the nuclide
3607 to be activated, and V (cm^3) is the volume of the irradiation field.

3608

3609 The radioactivity, $A(T_R)$ (Bq), immediately after an irradiation time period of T_R (s) is given by
3610 the following formula:

3611
$$A(T_R) = R(1 - e^{-\lambda T_R}) \quad (5.2)$$

3612 where λ (s^{-1}) is the decay constant of the radioactive nuclide. R is the saturation activity. If T_R is much
3613 longer than the half-life, $T_{1/2}$ ($= \ln 2 / \lambda$), $A(T_R)$ becomes equal to R .

3614

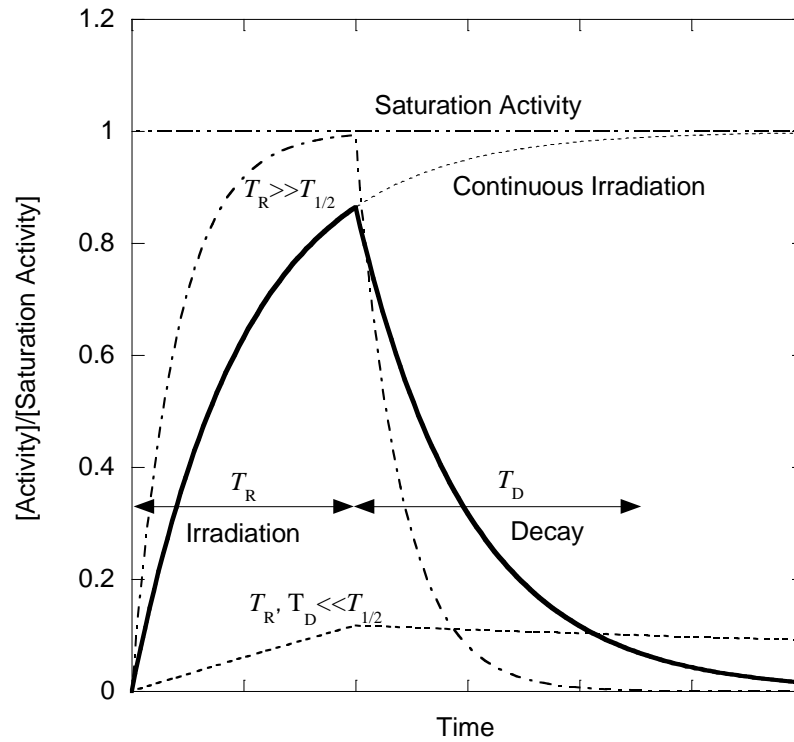
3615 The radioactivity after T_D seconds have elapsed after the irradiation end, $A(T_R + T_D)$ (Bq), is given
3616 by the following formula:

3617
$$A(T_R + T_D) = R(1 - e^{-\lambda T_R})e^{-\lambda T_D} \quad (5.3)$$

3618 Equation 5.3 is shown in Fig. 5.4 with the thick solid line.

3619

3620



3621

3622 Figure 5.4. Change of radioactivity during irradiation and decay. The thick solid line shows the general
3623 case, the dotted and dashed line shows the case of short half-life ($T_R \gg T_{1/2}$), and the dashed line shows
3624 the case of long half-life ($T_R \ll T_{1/2}$ and $T_D \ll T_{1/2}$).

3625

3626 If T_R is much longer than the half-life, $T_R \gg T_{1/2}$, the radioactivity is saturated at the end of
3627 irradiation, and the radioactivity after the irradiation is approximated by the following formula:

$$3628 \quad A(T_R + T_D) \approx R e^{-\lambda T_D} \quad (5.4)$$

3629 The radioactivity reaches a maximum (saturation activity), and decays in a short time after the
3630 irradiation. This is shown by the dotted and dashed line in Fig. 5.4.

3631

3632 If T_R and T_D are much shorter than the half-life, the produced radioactivity accumulates almost
3633 without any disintegration. The amount of radioactivity is much smaller than the saturation value. This is
3634 shown by the dashed line in Fig. 5.4.

$$3635 \quad A(T_R + T_D) \approx \lambda R T_R \quad (5.5)$$

3636

3637 Compared with the high-energy, high-intensity accelerators used for physics research, the beam
3638 intensity of the particle therapy facility is low, and therefore, saturation radioactivity is also low.
3639 Moreover, the irradiation time is short at a therapy facility, and the cumulated radioactivity of long-half-
3640 life nuclides is usually low. Therefore, the exposure of maintenance workers and medical staff is not
3641 usually of major concern at a facility dedicated to charged particle therapy. However, the activation of air
3642 may become significant level in a treatment room and in an enclosure of equipment where high beam
3643 loss occurs.

3644

3645 **5.2 Accelerator Components**

3646

3647 **5.2.1 Residual Activity Induced by Primary Particles**

3648

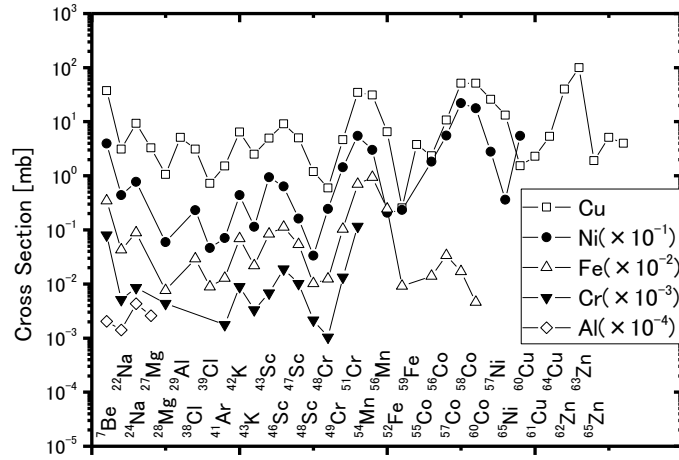
3649 Radioactive nuclides are mostly produced by primary beams in the accelerator and beam-line
3650 components, including beam shaping and delivery devices, and the energy selection system (ESS). The
3651 accelerator and beam-line components are mainly made of aluminum, stainless steel (nickel, chromium
3652 and iron), iron, and copper. Residual activities are induced by spallation reactions occurring between
3653 these materials and the projectile particles.

3654
3655 Because of high melting point and high density, tungsten and tantalum are often used in
3656 accelerators, *e.g.* at an extraction septum of a cyclotron and at beam stoppers. They are not only
3657 activated, but also have a tendency to evaporate and to contaminate the surfaces of the surrounding
3658 materials.

3659
3660 **5.2.1.1 Residual Activities in Al, Cr, Fe, Ni, Cu.** Various radionuclides are produced from
3661 spallation reactions. Reaction cross sections of nuclides produced in Cu, Ni, Fe, Cr, and Al for 400
3662 MeV/nucleon ^{12}C ion irradiation were measured at HIMAC and shown in Fig. 5.5. In Fig. 5.5, a strong
3663 target mass number dependency is not observed, but there is a wider distribution of the produced
3664 nuclides with increasing target mass number.

3665

3666



3667

3668 Figure 5.5. Reaction cross sections of nuclides produced in Cu, Ni, Fe, Cr, and Al for 400MeV/nucleon
3669 ^{12}C ion irradiation (Yashima *et al.*, 2004a).

3670

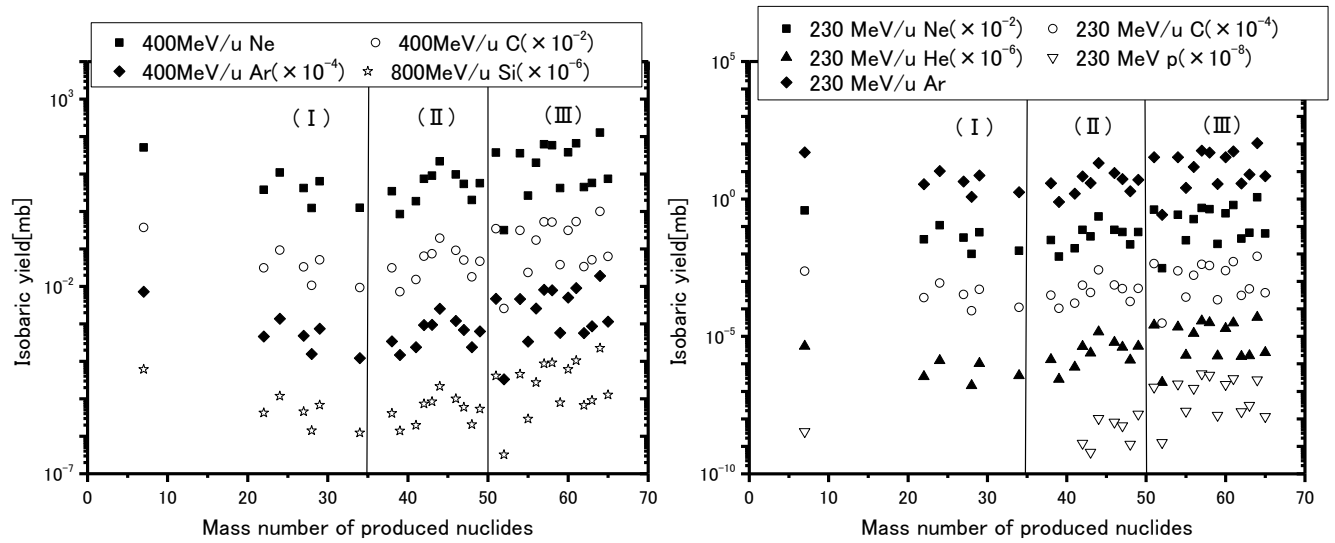
3671 **5.2.1.2 Mass-Yield Distribution of Residual Activities in Cu.** The mass-yield (isobaric-yield)
3672 distributions of nuclides produced in Cu for various projectiles and energies are shown in Fig. 5.6. The
3673 product nuclides can be divided into the three groups of (I) to (III) as shown in Fig. 5.6; (I) target
3674 fragmentation occurring from a reaction of small impact parameter or projectile fragmentation of a heavy
3675 projectile, (III) target fragmentation occurring from a reaction in which the impact parameter is almost
3676 equal to the sum of projectile radius and the target radius, (II) target fragmentation occurring from a
3677 reaction in which the impact parameter lies between (I) and (III).

3678

3679 It is evident from Fig. 5.6 that the cross sections of isobaric yields initially decrease with
3680 increasing mass number difference between Cu and the product nuclide. However, the production cross
3681 sections increase for light nuclides of group (I), since light nuclides like ${}^7\text{Be}$ are produced not only by
3682 heavy disintegrations of the target nuclei through small-impact-parameter reactions, but also as smaller
3683 fragments of light disintegrations. These light nuclides are also produced by projectile fragmentations of
3684 heavy particles.

3685

3686



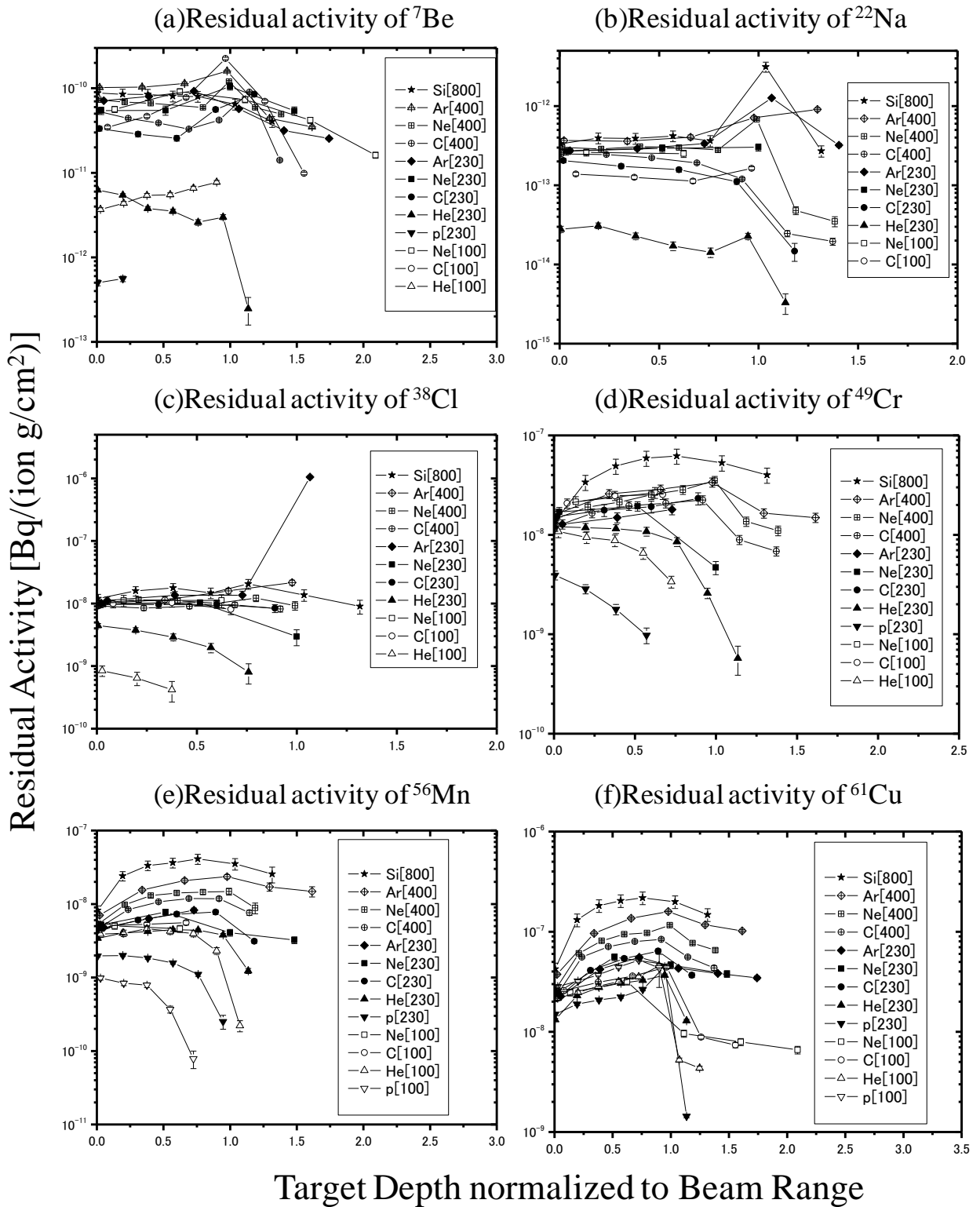
3687

3688 Figure 5.6. Mass-yield (isobaric-yield) distributions of nuclides produced in Cu for various projectile
3689 particles and energies. The distributions are divided into three groups as explained in the text (Yashima
3690 *et al.*, 2002; 2004a).

3691

3692 **5.2.1.3 Spatial Distribution of Residual Activities with Cu Target Depth.** The spatial
3693 distributions of residual activities of ^7Be , ^{22}Na , ^{38}Cl , ^{49}Cr , ^{56}Mn , and ^{61}Cu induced in Cu are shown in
3694 Fig. 5.7(a) to (f) , where the target depth is expressed in units of the projectile range. In this Section and
3695 the following two Sections (5.2.1.4 and 5.2.1.5), the residual activities produced in the vicinity of the
3696 primary ion trajectory are discussed. Whereas the activities are mostly produced by the primary ions,
3697 they include the productions of secondary charged particles and neutrons. Figures 5.7(a) to (f) can be
3698 understood and summarized as follows. When the mass number difference between Cu and the produced
3699 nuclide is large, *i.e.*, the produced nuclide belongs to group (I) in Fig. 5.6, the nuclides are produced
3700 dominantly by the primary projectile reaction. Most of the reaction cross sections therefore slowly
3701 decrease with target depth, according to the attenuation of projectile flux through the target. When the
3702 mass number difference between Cu and the produced nuclide is small, *i.e.*, the nuclides produced
3703 belonging to group (II) or (III) in Fig. 5.6, the fraction of nuclides produced by reactions with secondary
3704 particles is large. With increasing mass number of the produced nuclides and the projectile energy, the
3705 residual activity increases with the depth of the Cu target due to the increasing contribution of secondary
3706 particle reactions. In Fig. 5.7(a), 5.7(b), and 5.7(c), the residual activity increases steeply near the
3707 projectile range in some cases; for example, ^7Be production by 100 MeV/nucleon ^{12}C , ^{22}Na production
3708 by 800 MeV/nucleon ^{28}Si , and ^{38}Cl production by 230 MeV/nucleon ^{40}Ar . This is attributed to the
3709 projectile fragmentation during flight. Since a projectile fragment has the similar velocity and direction
3710 to the projectile ion, the projectile fragment stops at a slightly deeper point than the projectile range.
3711 Similar phenomenon are expected in ^{11}C production by ^{12}C irradiation.

3712



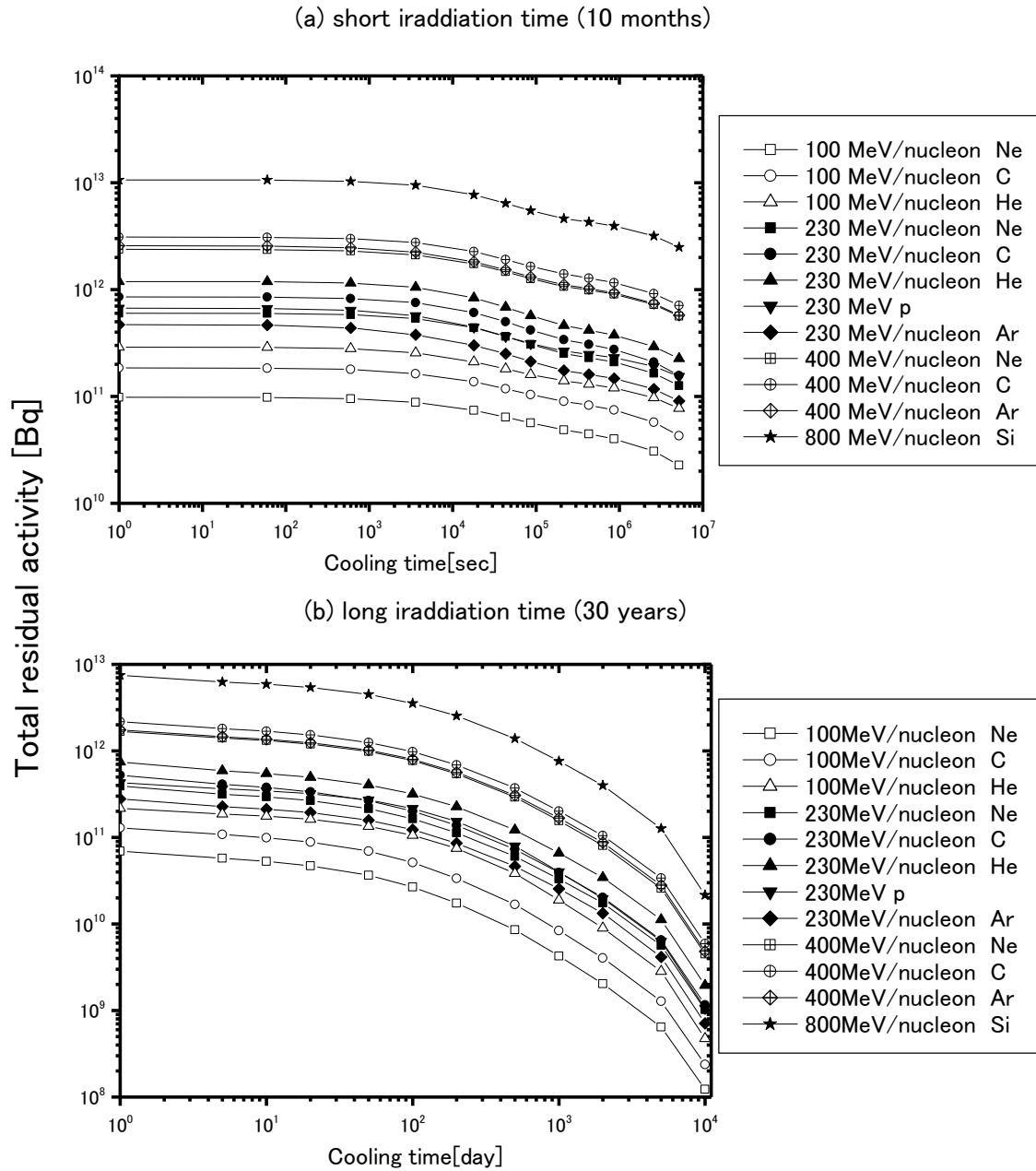
3713

3714 Figure 5.7. Spatial distribution of residual activities with Cu target depth for various projectile types and
 3715 energies (Yashima *et al.*, 2004b).

3716

3717 **5.2.1.4 Total Residual Activity Estimation Induced in Cu Target.** Cooling down of the total
3718 residual activity induced in Cu target, which was estimated from the above-mentioned measured spatial
3719 distribution, is shown in Fig. 5.8 (a) and 5.8(b) for a short irradiation time and a long irradiation time (10
3720 months and 30 years, respectively) under the condition of 6.2×10^{12} particles/sec, *i.e.*, 1 particle μA (1
3721 μA) beam intensity. Notice that the x-axis unit is second for Fig. 5.8(a), and day for Fig. 5.8(b).
3722

3723



3724

3725 Figure 5.8. Total residual activity induced in Cu target irradiated by 1- μ A ions (Yashima *et al.*, 2004b).

3726

3727 The total residual activity produced in a thick target at the end of irradiation is shown as a
3728 function of the total projectile energy in Fig. 5.9(a). The projectile particles are same as those of Fig. 5.8.
3729 The total activity for the same projectile energy per nucleon decreases with increasing projectile mass
3730 number except for 230 MeV proton irradiation. This can be explained as follows. Because the production
3731 cross sections of these nuclides do not depend strongly on the projectile mass number having the same
3732 energy per nucleon (Yashima *et al.*, 2002; 2004a), the residual activities are larger with lighter
3733 projectiles, which have longer ranges. 230 MeV protons have the same range as 230 MeV/nucleon He
3734 and have smaller cross sections as shown in Fig. 5.6. Therefore, the total activity produced by protons is
3735 smaller than that by He. When the total activity produced by a specific particle is compared, it increases
3736 with increasing projectile energy per nucleon.

3737

3738 The majority of the residual activities is dominated by $^{61,64}\text{Cu}$, $^{57,58}\text{Co}$, ^{52}Mn , ^{51}Cr , and ^7Be at the
3739 end of irradiation; ^{65}Zn , $^{56,57,58}\text{Co}$, ^{54}Mn , and ^{51}Cr at a cooling time of two months; and ^{60}Co and ^{44}Ti
3740 after 30 years of cooling, respectively. The fraction of these nuclides produced by reactions with
3741 secondary particles is also large. The residual activities are therefore larger with higher energy
3742 projectiles, which produce more secondary particles. The specific residual activity per unit mass of Cu
3743 target is shown as a function of total projectile energy in Fig. 5.9(b). The target is a Cu cylinder having a
3744 cross section of 1 cm^2 and a length equal to the projectile range. In Fig. 5.9(b), the specific residual
3745 activity increases with increasing the total projectile energy.

3746

3747

(a) residual activity

3748

3749

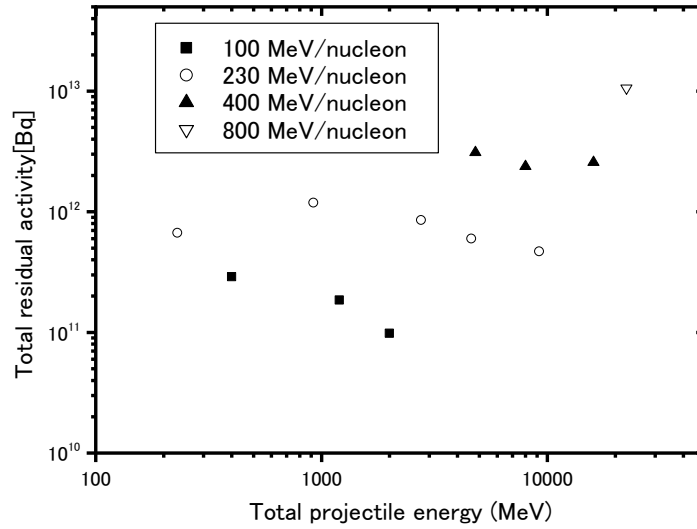
3750

3751

3752

3753

3754



3755

(b) specific activity

3756

3757

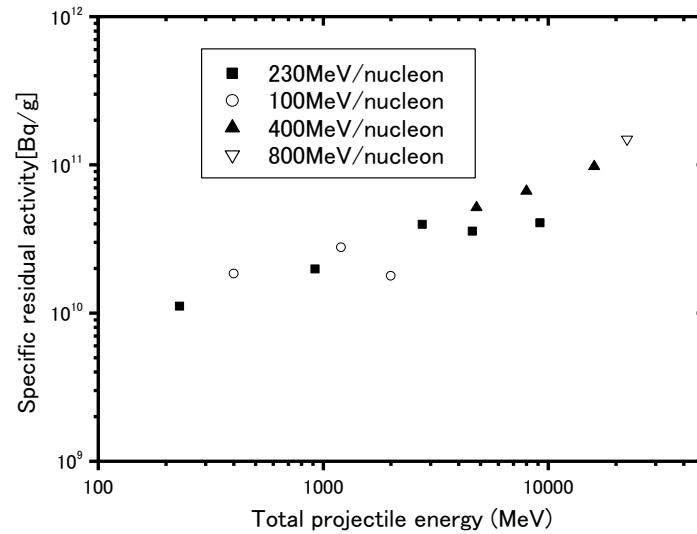
3758

3759

3760

3761

3762



3763

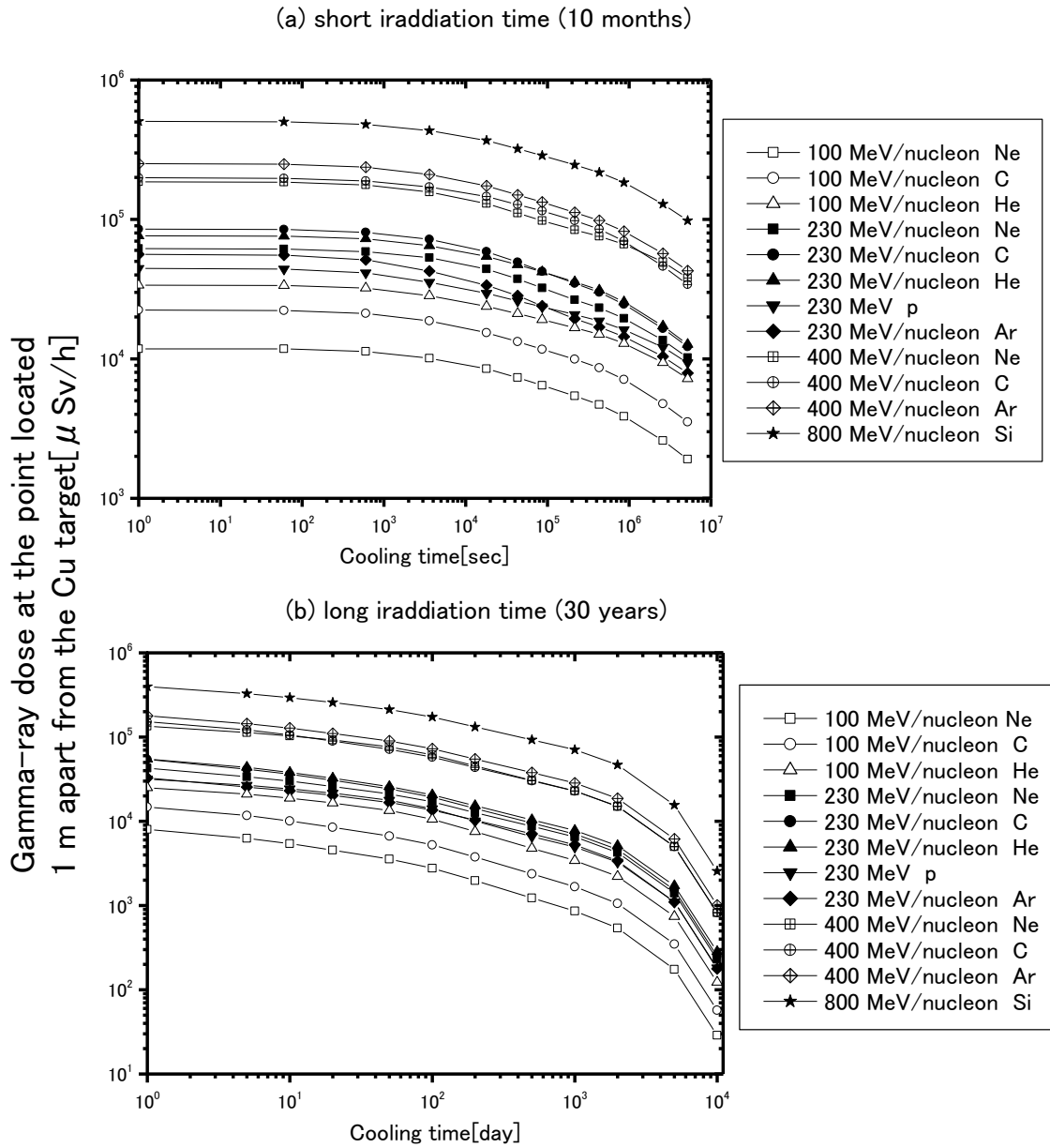
Figure 5.9. Projectile energy dependence of total residual activity and specific residual activity induced

3764

in Cu target immediately after the 10 month $1\text{-}\mu\text{A}$ irradiation (Yashima *et al.*, 2004b).

3765

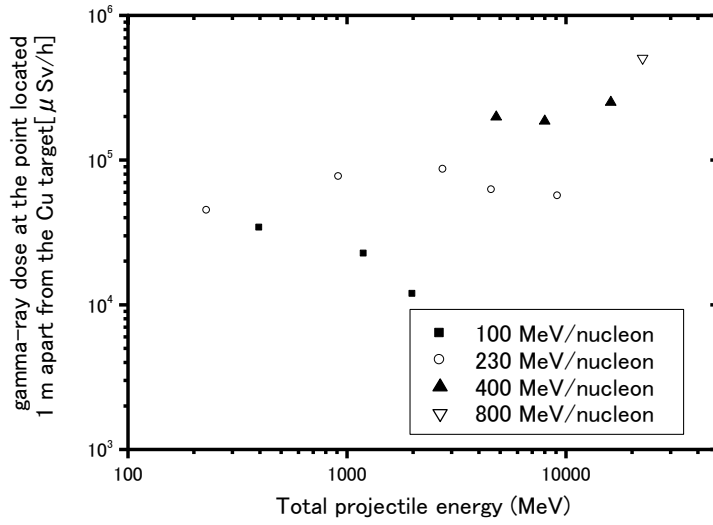
3766 **5.2.1.5 Gamma-Ray Dose Estimation from Residual Activity in Cu Target.** The decay of the
3767 gamma-ray effective-dose rate at the point located 1 m distant from the Cu target is shown in Fig. 5.10(a)
3768 and (b) for a short irradiation time and a long irradiation time (10 months and 30 years, respectively).
3769 The contribution of annihilation photons is included in the dose rate. The dose rate at the end of
3770 irradiation is shown as a function of total projectile energy in Fig. 5.11. The energy and projectile
3771 dependence of gamma-ray dose is similar to that of residual activity.
3772



3773

3774 Figure 5.10. Gamma-ray dose from total residual activities induced in Cu target irradiated by 1- μ A ions
 3775 (Yashima *et al.*, 2004b).

3776



3777

3778 Figure 5.11. Projectile dependence of gamma-ray effective dose from total residual activity induced in
3779 Cu target immediately after the 10 month $1\text{-}\mu\text{A}$ irradiation (Yashima *et al.*, 2004b).

3780

3781 **5.2.2 Residual Activities Induced by Secondary Neutrons**

3782

3783 Radioactive nuclides are also induced by secondary neutrons, the energies of which extend up to
3784 the primary proton energy, and in the case of heavy ions, up to about double the primary particle energy
3785 per nucleon.

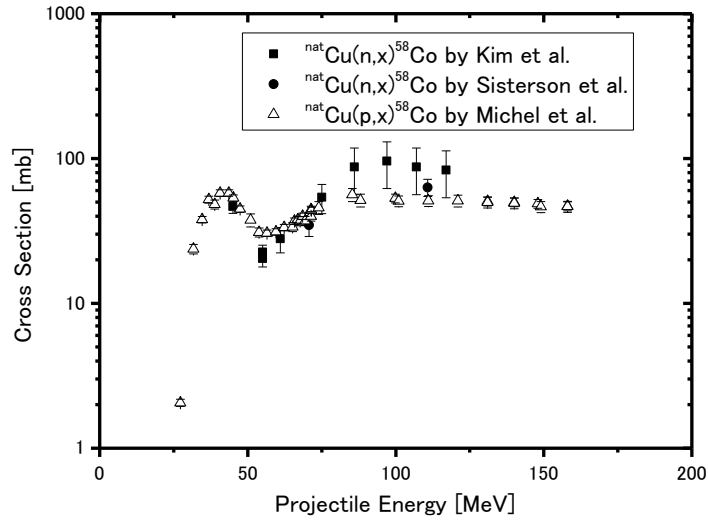
3786

3787 Because of high permeability, neutron activation is widely distributed, while the activation by
3788 charged particles is limited to within the particle range. The intensity of secondary high-energy neutrons
3789 is strongly forward-peaked along the primary-particle direction, and decreases with the inverse square of
3790 the distance from the effective source.

3791

3792 Neutron-induced reaction cross section data are very scarce above 20 MeV. It is often assumed
3793 that the cross sections have the same value as proton-induced cross sections above 100 MeV. As an
3794 example, a comparison of cross sections of $^{nat}\text{Cu}(n, x)^{58}\text{Co}$ and $^{nat}\text{Cu}(p, x)^{58}\text{Co}$ reactions is shown in Fig.
3795 5.12. In Fig. 5.12, neutron-induced reaction cross sections are slightly larger than proton-induced
3796 reaction cross sections above 80 MeV.

3797



3798

3799 Figure 5.12. Cross sections of the $^{nat}\text{Cu}(n, x)^{58}\text{Co}$ and the $^{nat}\text{Cu}(p, x)^{58}\text{Co}$ reactions (Kim *et al.*, 1999;
3800 Michel *et al.*, 1997; Sisterson *et al.*, 2005).

3801

3802 Thermal neutrons are almost uniformly distributed inside an accelerator enclosure. The fluence ϕ_{th}
3803 at places further than 2 m from the neutron production point can be estimated by the following simple
3804 formula (Ishikawa, 1991):

3805
$$\phi_{th} = \frac{CQ}{S} \quad (5.6)$$

3806 where C is a constant estimated to be 4, Q is the number of total produced neutrons, and S is the total
3807 inside surface area of an enclosure, including the walls, the floor, and the roof.

3808

3809 Table 5.1 shows the characteristic radionuclides produced in metals by thermal neutrons. Mn and
3810 Co are impurities in iron and stainless steel. ^{56}Mn is also produced by fast neutrons in the $^{56}\text{Fe}(n, p)$
3811 reaction. Brass is an alloy of Cu and Zn. Lead bricks sometimes contain Sb to improve the mechanical
3812 characteristics.

3813

3814 Table 5.1 Characteristic radionuclides produced in metals by thermal-neutron capture. Gamma rays of
3815 which emission probabilities are larger than 1 % are listed (Firestone, 1999; Sullivan 1992).

Radionuclide	Half-life	Decay mode	γ -ray (emission)	Fertile nuclide, abundance, and capture cross section	
⁵⁶ Mn	2.58 hour	β^- : 100%	847 keV (98.9%)	⁵⁵ Mn, 100%, 13.3b	
			1811 keV (27.2%)		
			2113 keV (14.3%)		
⁶⁰ Co	5.27 year	β^- : 100%	1173 keV (100%)	⁵⁹ Co, 100%, 37.2b	
			1332 keV (100%)		
⁶⁴ Cu	12.7 hour	EC: 43.6%	511 keV (β^+)	⁶³ Cu, 69.2%, 4.5b	
		β^+ : 17.4%			
		β^- : 39.0%			
⁶⁵ Zn	244.3 day	EC: 98.6%	1116 keV (50.6%)	⁶⁴ Zn, 48.6%, 0.76b	
		β^+ : 1.4%	511 keV (β^+)		
^{69m} Zn	13.8 hour	IT: 100%	439 keV (94.8%)	⁶⁸ Zn, 18.8%, 0.07b	
¹²² Sb	2.72 day	β^- : 97.6%	564 keV (70.7%)	¹²¹ Sb, 57.4%, 5.9b	
			EC: 2.4%		693 keV (3.9%)
					603 keV (98.0%)
					646 keV (7.3%)
¹²⁴ Sb	60.2 day	β^- : 100%	723 keV (11.3%)	¹²³ Sb, 42.6%, 4.1b	
			1691 keV (48.5%)		
			2091 keV (5.7%)		
<i>etc.</i>					

3816

3817

3818 **5.3 Concrete**

3819

3820 The amount of induced radioactivity and activity concentration in concrete used for shielding is
3821 smaller than that in the accelerator components that are directly irradiated by the primary accelerator
3822 beams. After accelerator operation has ceased, workers inside the shielded room are exposed by gamma
3823 rays from ^{24}Na (half-life = 15 hours) in the concrete. After accelerator decommissioning, the shielding
3824 barriers are also dismantled. In this case, special care must be taken because of long-lived residual
3825 radioactivity.

3826

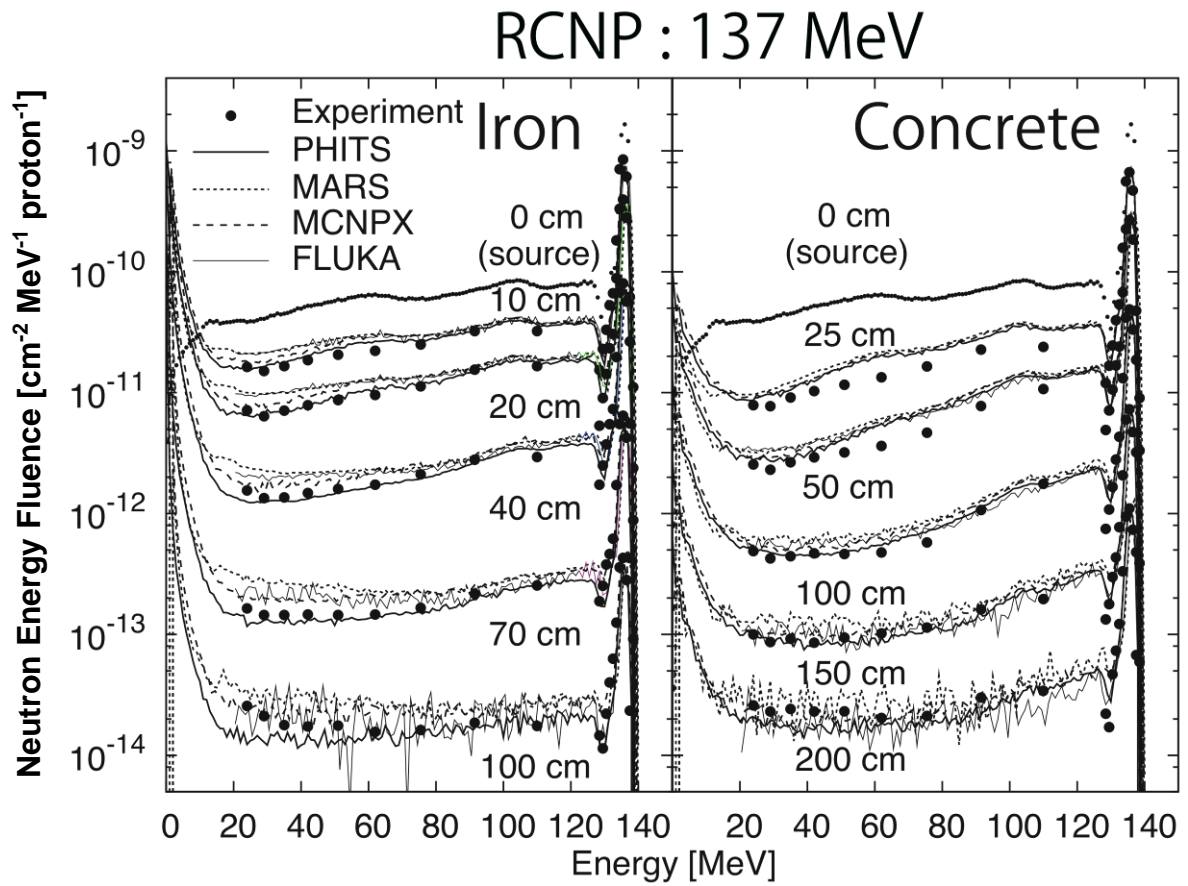
3827 Measured and calculated secondary neutron spectra in thick shields are shown in Fig. 5.13.
3828 Neutron spectra do not change much, and high-energy reactions are still important at locations deep
3829 within the shields. Radioactivity decreases exponentially with concrete depth.

3830

3831

3832

3833



3834

3835 Figure 5.13. Measured and calculated secondary neutron spectra in thick concrete or iron shields
3836 irradiated by 140 MeV p-Li neutron source at RCNP (Kiriwara *et al.*, 2008).

3837

3838 Several measurements were made in 4 m thick concrete shields of a neutron irradiation facility
3839 using a 500 MeV proton synchrotron (Oishi *et al.*, 2005), in 0.5 m thick shields of several proton
3840 cyclotrons (Masumoto *et al.*, 2008; Wang *et al.*, 2004), and in 6 m thick 12 GeV proton synchrotron
3841 shields (Kinoshita *et al.*, 2008). Typical radionuclides present in concrete are ^{22}Na , ^7Be , ^3H , ^{46}Sc , ^{54}Mn ,
3842 ^{60}Co , ^{134}Cs , and ^{152}Eu . When concrete comes into contact with groundwater, ^{22}Na and ^3H are dissolved in
3843 the water, though the amount of radioactivity in the water is usually very small.

3844

3845 The most important long-lived radioactive nuclides of concern in decommissioning are ^{22}Na ,
3846 ^{60}Co , and ^{152}Eu . ^{60}Co and ^{152}Eu are produced by thermal neutron capture reactions with Co and Eu
3847 impurities in the concrete. The amounts of these impurities are small, but the $^{59}\text{Co}(n, \gamma)$ and $^{151}\text{Eu}(n, \gamma)$
3848 cross sections are large. However, ^{22}Na is produced by nuclear spallation reactions of high-energy
3849 neutrons. Exemption concentration levels (IAEA, 1996) are 10 Bq g^{-1} for these nuclides. ^{60}Co activities
3850 in iron reinforcing rods in concrete are important because ^{59}Co impurities are large in iron.

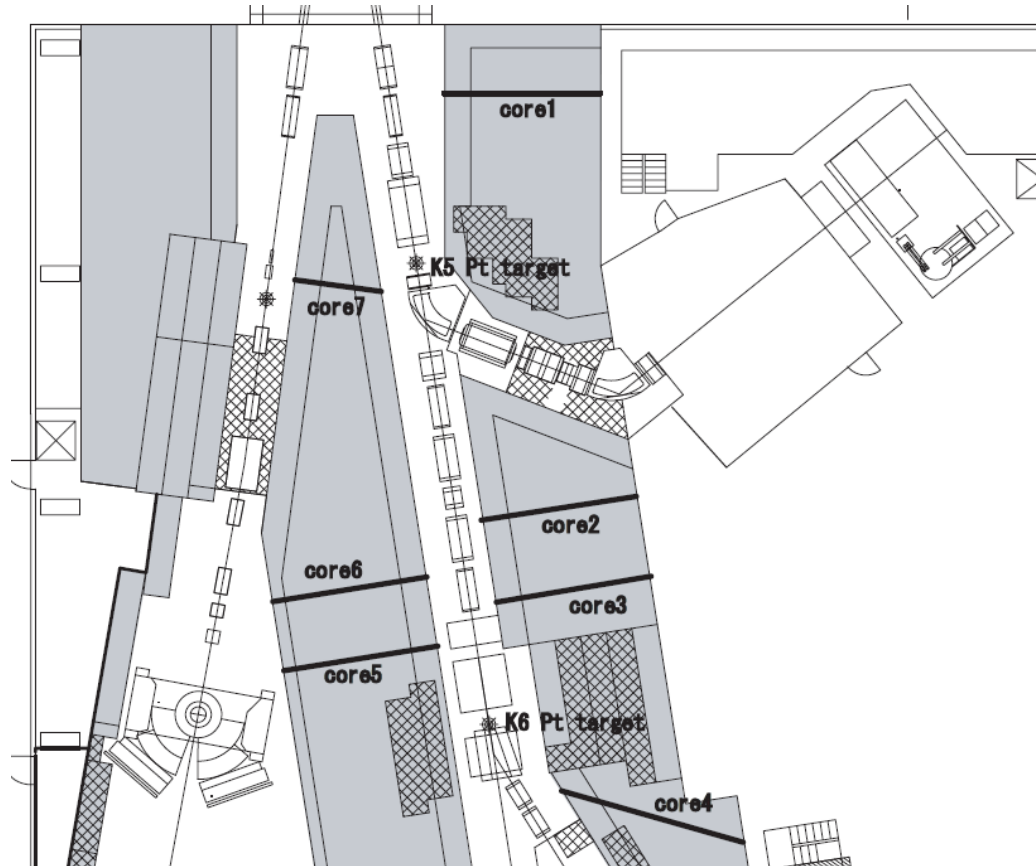
3851

3852 Because the amounts of impurities of ^{59}Co and ^{151}Eu depend upon the concrete composition, it is
3853 difficult to estimate the activities. Typically, the activity of ^3H is about ten times higher than that of ^{60}Co
3854 and ^{152}Eu (Masumoto *et al.*, 2008), although the exemption level for ^3H is much larger, 10^6 Bq g^{-1} . ^3H are
3855 produced by both nuclear spallation reactions and thermal-neutron capture.

3856

3857 The depth profile of activity in the concrete shields of a 12 GeV proton synchrotron facility (Fig.
3858 5.14) were measured. Samples of concrete cores were obtained by boring holes up to depths of 4 m to 6
3859 m in the walls. Gamma activity was measured using germanium detectors, and ^{22}Na , ^{54}Mn , ^{60}Co , and
3860 ^{152}Eu γ -rays were identified. The concrete sample was heated, and tritium was collected in a cold trap.
3861 Beta activity was measured using liquid scintillation counters. The results are shown in Fig. 5.15. The

3862 radioactivity of nuclides produced by high-energy reactions, such as ^{22}Na , decrease exponentially as the
3863 penetration depth in the shield increases. The activity of radionuclides produced by neutron capture
3864 reactions, such as ^{60}Co and ^{152}Eu , increase from the inner surface up to the depth of about 20 cm, then
3865 decrease with increasing the depth (Kinoshita *et al.*, 2008).
3866

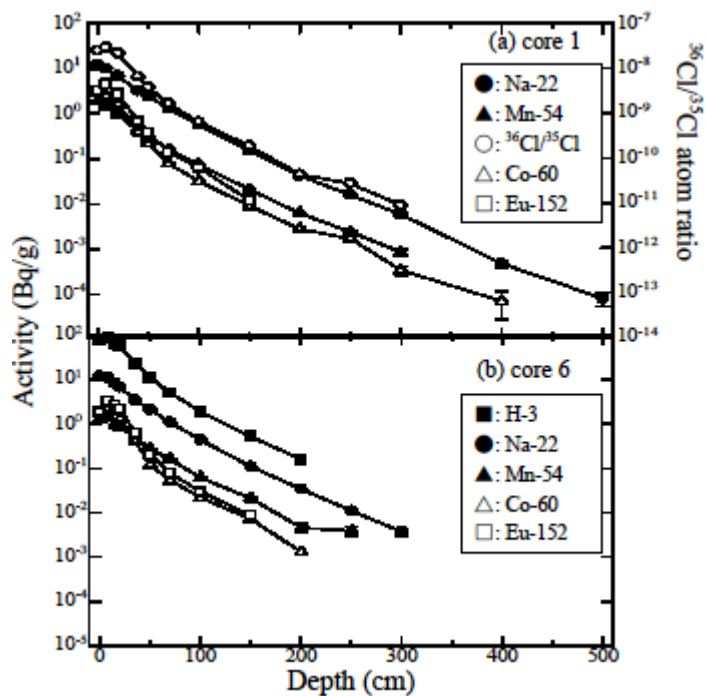


3867

3868 Figure 5.14. Plan view of concrete shields near the Pt targets in a 12 GeV proton synchrotron facility

3869 (Kinoshita *et al.*, 2008). Sampling locations of radioactivity are shown at core 1 to 7.

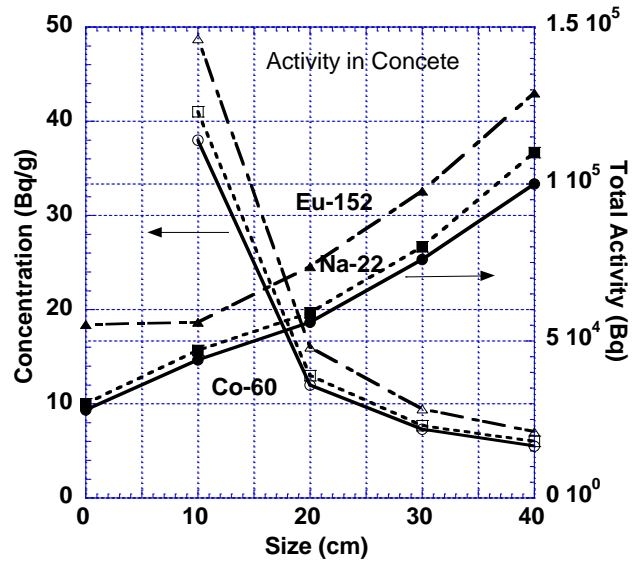
3870



3871
3872 Figure 5.15. Depth profile of radioactivity in 6 m thick concrete shields near the platinum targets
3873 irradiated in a 12 GeV proton synchrotron facility shown in Fig. 5.14 (Kinoshita *et al.*, 2008).
3874

3875 It is easier if the concentration of radioactivity can be estimated from the measured surface dose
3876 rates. Dose rates from concrete were calculated with an assumption that the activity is uniformly
3877 distributed in several sizes of rectangular parallelepipeds. With a dose rate of 1 $\mu\text{Sv/h}$ at 10 cm distance
3878 from the surface, the total amount and concentration of radioactivity were calculated and the results are
3879 shown in Fig. 5.16 (Ban *et al.*, 2004). Both the concentration and total quantity of activity do not exceed
3880 IAEA exemption levels (IAEA, 1996) at the same time. The activity concentration and the total activity
3881 of the exemption levels are 10 Bq/g and 1×10^6 Bq for ^{22}Na , 10 Bq/g and 1×10^5 Bq for ^{60}Co , and 10
3882 Bq/g and 1×10^6 Bq for ^{152}Eu .
3883

3884



3885

3886 Figure 5.16. Total activity and concentration in 5 cm thick rectangular parallelepiped made of concrete
3887 when the ambient dose equivalent $H^*(10 \text{ mm})$ rate at 10 cm distant is $1 \mu\text{Sv/h}$. Activity is uniformly
3888 distributed in concrete (Ban *et al.*, 2004).

3889

3890 Usually it is difficult to calculate radioactivity in concrete shields because irradiation conditions
3891 and the composition of the concrete are not well known. Benchmark calculations were done at the KENS
3892 spallation neutron source facility (Oishi *et al.*, 2005). Source neutrons from a tungsten target bombarded
3893 by 500 MeV protons were calculated using the NMTC/JAM code (Niita, 2001). Neutron-induced
3894 activities in 4 m thick concrete were calculated using the NMTC/JAM code at neutron energies above 20
3895 MeV, and using the MCNP5 code below 20 MeV. Good agreement to within factors of 2 to 5 were
3896 obtained for the nuclides that were not produced mainly by the spallation reactions, though there were
3897 large differences for ^{28}Mg , ^{52}Mn , ^7Be , and ^{56}Co .

3898

3899 **5.4 Cooling and Groundwater**

3900

3901 **5.4.1 Activation Cross Sections**

3902

3903 Cooling water for magnets, slits and stoppers in the beam transport line, and the energy selection
3904 system (ESS), *etc.* is activated by secondary neutrons produced by beam losses of the accelerated
3905 particles. However, at slits and stoppers and at the extraction deflector of a cyclotron, the accelerated
3906 particles may directly hit and activate the cooling water. High-energy secondary neutrons produced by
3907 beam losses and treatment irradiations may penetrate the shielding and activate the groundwater.

3908

3909 High-energy neutrons produce ^{14}O , ^{15}O , ^{13}N , ^{11}C , ^7Be , and ^3H through spallation reactions of
3910 oxygen. These production cross sections are shown in Table 5.2 (Sullivan, 1992). The cross sections
3911 shown are for neutrons above 20 MeV.

3912

3913 The activation cross sections of protons that pass through the cooling water are thought to be equal
3914 to those of neutrons, and Table 5.2 is applicable to the proton reactions. Natural oxygen contains 0.205
3915 % of ^{18}O . If protons hit water, positron-emitting ^{18}F , with a half-life of 1.83 hours, is produced by the
3916 $^{18}\text{O}(\text{p}, \text{n})$ reaction. These reaction cross sections are shown in Fig. 5.17.

3917

3918 On the other hand, since the mass number of ^{12}C is large, the reaction cross sections of ^{12}C are
3919 also large. If the geometrical cross section is considered, the cross section of the $^{16}\text{O}+^{12}\text{C}$ reaction is
3920 assumed to be 1.87 times larger than that of $^{16}\text{O}+\text{p}$ reaction. The ^{12}C cross sections thus obtained are also
3921 shown in Table 5.2.

3922

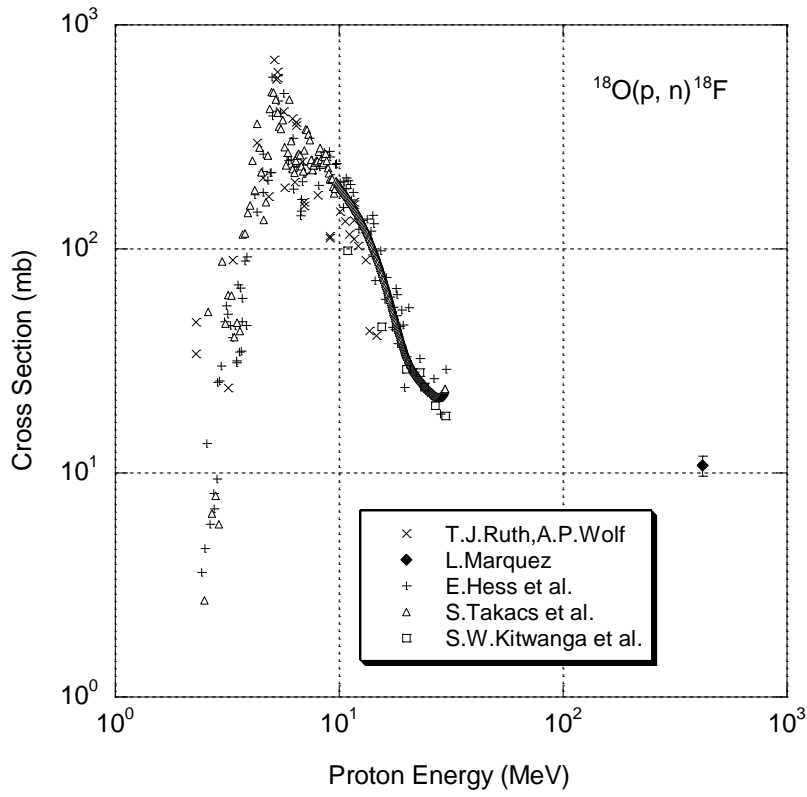
3923 Table 5.2. Water activation cross sections for neutrons and protons. The parenthesized values are for ^{12}C
3924 ions. (Firestone, 1999; Sullivan, 1992)

Nuclide	Half-life	Decay Mode, γ -ray Energy and Emission Probability	Cross Section	
			Oxygen (mb ^a)	Water (cm ⁻¹) ^b
^3H	12.3 year	β^-	30 (56)	1.0×10^{-3} (1.9×10^{-3})
^7Be	53.3 day	EC, 0.478 MeV γ 10.5%	5 (9)	1.7×10^{-4} (3.1×10^{-4})
^{11}C	20.4 min	β^+	5 (9)	1.7×10^{-4} (3.1×10^{-4})
^{13}N	9.97 min	β^+	9 (17)	3.0×10^{-4} (5.6×10^{-4})
^{14}O	1.18 min	β^+ , 2.3 MeV γ 99.4%	1 (2)	3.3×10^{-5} (6.2×10^{-5})
^{15}O	2.04 min	β^+	40 (75)	1.3×10^{-3} (2.5×10^{-3})

3925 ^a 1 mb = 1×10^{-3} b = 1×10^{-27} cm²

3926 ^b Atomic densities are H: 6.67×10^{22} cm⁻³, O: 3.34×10^{22} cm⁻³.

3927



3928

3929 Figure 5.17. Cross sections of $^{18}\text{O}(p, n)^{18}\text{F}$ activation reaction (Hess *et al.*, 2001; Kitwanga *et al.*, 1990;

3930 Marquez, 1952; Ruth and Wolf, 1979; Takacs *et al.*, 2003).

3931

3932 **5.4.2 Effects of Water Activation**

3933

3934 The radioactivity of ^{14}O , ^{15}O , ^{13}N , and ^{11}C , all of which have short half-lives, reaches saturation in
3935 a short irradiation time. The annihilation photons produced by these positron-emitting nuclides increase
3936 the dose rate around cooling-water pipes and ion-exchange resin tanks. The dose rate around a cooling-
3937 water pipe of infinite length is given by the following formula, when the self-absorption of photons by
3938 the water and the pipe wall is ignored:

3939
$$E = \frac{\pi^2 \gamma_E r^2 c}{d} \quad (\mu\text{Sv/h}) \quad (5.7)$$

3940 where

3941 E is the effective dose rate ($\mu\text{Sv/h}$);

3942 γ_E is the effective dose rate factor ($0.00144 \mu\text{Sv/h Bq}^{-1} \text{cm}^{-2}$ for positron-emitting nuclide);

3943 r is the radius of the cooling-water pipe (cm);

3944 c is the concentration of positron-emitting nuclides in water (Bq cm^{-3}); and

3945 d is the distance between the cooling-water pipe and the point of interest (cm).

3946

3947 The radioactivity of ^{14}O , ^{15}O , ^{13}N , and ^{11}C rapidly decreases after the end of irradiation, and the
3948 dose rate also decreases. However, the accumulated ^{18}F and ^7Be in the ion-exchange resin result in
3949 measurable dose rates. If the proton beam directly penetrates the water, the dose rate due to ^{18}F may be
3950 significant for about a day. ^7Be should be taken care of when the ion-exchange resin is replaced. Its half-
3951 life, however, is 53 days, and ^7Be disappears after 2 or 3 years. ^3H (T) stays in water in the form of HTO,
3952 and accumulates because of its long half-life (12.3 years). The concentration should be measured
3953 periodically. However, the beam intensity at a particle therapy facility is low, and the concentration is
3954 usually much lower than the limit for disposal into the sewer system.

3979 Activation of air is caused by the secondary neutrons at a particle therapy facility; however, it is
3980 also caused by the primary particles in the air path between the accelerator vacuum system and the
3981 patient position.

3982

3983 A detailed estimation of the air activation can be done with Monte Carlo codes as shown in
3984 Chapter 6. At most particle therapy facilities, however, the air activation is much lower than the
3985 regulation levels, and a rough estimation is usually enough, as is explained in the following text. If the
3986 estimated value is close to the regulation level, a detailed estimation should be done.

3987

3988 The airborne radionuclides produced by high-energy neutrons are mainly ^3H , ^7Be , ^{11}C , ^{13}N , ^{14}O ,
3989 and ^{15}O . Thermal neutrons produce ^{41}Ar . The production cross sections of these nuclides are listed in
3990 Table 5.3 (Sullivan, 1992). Cross sections shown for N and O are for neutrons above 20 MeV.

3991

3992 The cross sections of N and O for protons can be considered equal to those for neutrons, and
3993 Table 5.3 is applicable to protons. The geometrical cross section of $^{14}\text{N}+^{12}\text{C}$ is 1.90 times larger than that
3994 of $^{14}\text{N}+\text{p}$, and that of $^{16}\text{O}+^{12}\text{C}$ is 1.87 times larger than that of $^{16}\text{O}+\text{p}$. The cross sections for ^{12}C ions
3995 obtained using the previously mentioned ratios are also shown in Table 5.3 in parentheses.

3996

3997 Table 5.3. Air activation cross sections for neutrons and protons. The parenthesized values are for ¹²C
3998 ions. (Firestone, 1999; Sullivan, 1992)

Nuclide	Half-life	Emission of beta, gamma	Cross Section		
			Nitrogen (mb ^a)	Oxygen (mb ^a)	Air (cm ⁻¹) ^b
³ H	12.3 year	β ⁻	30 (57)	30 (56)	1.5x10 ⁻⁶ (2.8x10 ⁻⁶)
⁷ Be	53.3 day	EC, 0.478MeV γ 10.5%	10 (19)	5 (9)	4.4x10 ⁻⁷ (8.4x10 ⁻⁷)
¹¹ C	20.4 min	β ⁺	10 (19)	5 (9)	4.4x10 ⁻⁷ (8.4x10 ⁻⁷)
¹³ N	9.97 min	β ⁺	10 (19)	9 (17)	4.9x10 ⁻⁷ (9.2x10 ⁻⁷)
¹⁴ O	1.18 min	β ⁺ , 2.3MeV γ 99.4%	0 (0)	1 (2)	1.1x10 ⁻⁸ (2.0x10 ⁻⁸)
¹⁵ O	2.04 min	β ⁺	0 (0)	40 (75)	4.2x10 ⁻⁷ (7.8x10 ⁻⁷)
⁴¹ Ar	1.82 hour	β ⁻ , 1.3MeV γ 99.1%	610 (for ⁴⁰ Ar)		1.42x10 ⁻⁷

3999 ^a 1 mb = 1×10⁻³ ^b = 1×10⁻²⁷ cm²

4000 ^b Atomic densities are N: 3.91x10¹⁹ cm⁻³; O: 1.05x10¹⁹ cm⁻³; ⁴⁰Ar:2.32x10¹⁷ cm⁻³.

4001

4002 **5.5.2 Estimation of Concentration of Air Activation**

4003

4004 Several formulae for the estimation of radionuclide concentration in the air are shown below

4005 (RIBF, 2005). The air in a room is assumed to be uniformly mixed.

4006 Explanatory notes for the symbols are as follows:

4007 A_0 : saturated activity (Bq) produced in a room, which is equal to R of Eq. (5.1)

4008 λ : decay constant (s^{-1})

4009 V : volume of the room (cm^3)

4010 v : ventilation speed of the room ($cm^3 s^{-1}$)

4011 v_A : ventilation speed at the stack of the facility ($cm^3 s^{-1}$)

4012 ε : penetration rate of the filter if a purification system is installed (1.0 except for 7Be)

4013 T_R : irradiation time (s)

4014 T_D : decay time between the end of irradiation and the start of ventilation (s)

4015 T_E : working time of persons in the room (s)

4016 T_W : time between the end of irradiation and the start of the next irradiation (s)

4017 The air concentrations in the room and at the stack should be estimated at the planning stage of
4018 the facility and compared with the regulatory limits. Then the required ventilation can be determined.

4019

4020 **5.5.2.1 Radionuclide Concentrations of Exhaust Air.** Case 1: Average concentration at the
4021 stack during one irradiation cycle, *i.e.*, between the start of the first and second irradiations, under the
4022 condition of continuous ventilation; C_1

4023
$$C_1 = \frac{\varepsilon v \lambda A_0}{v_A V (\lambda + \frac{v}{V}) (T_R + T_W)} \left[T_R - \frac{1}{\lambda + \frac{v}{V}} \left\{ 1 - e^{-(\lambda + \frac{v}{V}) T_R} \right\} e^{-(\lambda + \frac{v}{V}) T_W} \right] \quad (5.9)$$

4024

4025 Case 2: Average concentration at the stack during one irradiation cycle under the condition that
4026 the ventilation is stopped during the irradiation and started at time T_D after the irradiation is stopped; C_2
4027 (Average value during the ventilating time of $T_W - T_D$)

$$4028 \quad C_2 = \frac{\varepsilon v A_0}{v_A V (\lambda + \frac{v}{V}) (T_W - T_D)} (1 - e^{-\lambda T_R}) e^{-\lambda T_D} \{1 - e^{-(\lambda + \frac{v}{V})(T_W - T_D)}\} \quad (5.10)$$

4029 **5.5.2.2. Radionuclide Concentrations of Room Air.** Case 3: Air concentration of the
4030 continuously ventilated treatment room at the time the irradiation is stopped; C_3

$$4031 \quad C_3 = \frac{\lambda A_0}{V (\lambda + \frac{v}{V})} \{1 - e^{-(\lambda + \frac{v}{V}) T_R}\} \quad (5.11)$$

4032
4033 Case 4: Average air concentration in a room during the working time of T_E under the condition
4034 that work and the ventilation are started simultaneously at a time T_D after the irradiation was stopped; C_4

$$4035 \quad C_4 = \frac{A_0}{V (\lambda + \frac{v}{V}) T_E} (1 - e^{-\lambda T_R}) e^{-\lambda T_D} \{1 - e^{-(\lambda + \frac{v}{V}) T_E}\} \quad (5.12)$$

4036
4037 This condition can be applied to an accelerator enclosure, for example, where persons enter only
4038 at maintenance time.

4039

4040

6. Monte Carlo Codes for Particle Therapy

4041

Stefan Roesler

4042

4043

6.1 General-Purpose Codes

4044

4045 Nowadays the use of general-purpose particle interaction and transport Monte Carlo codes is
4046 often the most accurate and efficient choice to design particle therapy facilities. Due to the widespread
4047 use of such codes in all areas of particle physics and the associated extensive benchmarking with
4048 experimental data, the modeling has reached an unprecedented level of accuracy. Furthermore, most
4049 codes allow the user to simulate all aspects of a high-energy particle cascade in one and the same run:
4050 from the first interaction of a TeV nucleus over the transport and re-interactions (hadronic and
4051 electromagnetic) of the secondaries produced, to detailed nuclear fragmentation, the calculation of
4052 radioactive decays, and even of the electromagnetic shower caused by the radiation from such decays.
4053 Consequently, there is no longer any need for time-consuming multi-step calculations employing
4054 different Monte Carlo codes that significantly increases the consistency of the results and greatly reduces
4055 the uncertainties related to the subsequent use of different codes.

4056

4057 At the same time, computing power has increased exponentially, allowing one to perform
4058 complex simulations with low statistical uncertainty in a few hours or days. Often the time spent to set
4059 up a simulation and to post-process its results significantly exceeds the actual computation time, despite
4060 the fact that many general-purpose codes now come with user-friendly graphical interfaces that have
4061 significantly reduced the preparation and post-processing phases as well. It follows that it is often more
4062 economical to invest resources in a careful study optimizing the facility shielding than in conservative
4063 shielding and infrastructure that compensate for less accurate estimates.

4064

4065 The following general-purpose Monte Carlo codes are commonly used for radiation transport
4066 simulations and will be described further below: FLUKA (Ferrari, 2005; Battistoni *et al.*, 2007),
4067 GEANT4 (Agostinelli *et al.*, 2003; Allison *et al.*, 2006), MARS15 (Mokhov, 1995; Mokhov and
4068 Striganov, 2007; Mokhov, 2009), MCNPX (Pelowitz, 2005; McKinney *et al.*, 2006), PHITS (Iwase,
4069 2002; Niita, 2006), and SHIELD/SHIELD-HIT (Geithner *et al.*, 2006; Gudowska *et al.*, 2004).

4070

4071

6.2 Areas of Application

4072

6.2.1 Shielding Studies and Secondary Doses to the Patient

4074

4075 The areas of application of Monte Carlo codes include all radiation protection aspects of the
4076 facility design. The most prominent application is shielding design where only Monte Carlo codes allow
4077 a careful optimization of complex access mazes, ducts, wall materials, and wall thicknesses that would
4078 be impossible to describe with analytical methods. The risks to personnel and patients due to secondary
4079 whole-body irradiation are typically calculated by folding fluence spectra with energy-dependent
4080 conversion coefficients that have also been obtained with detailed Monte Carlo simulations, *e.g.*,
4081 employing complex voxel phantoms of the human body (Pelliccioni, 2000). Numerous shielding studies
4082 done especially for particle research accelerators and, more recently, for therapy facilities have used
4083 Monte Carlo codes. Examples can be found in Agosteo *et al.* (1996b; 1996c), Brandl *et al.* (2005), Fan *et al.*
4084 *et al.* (2007), Newhauser *et al.* (2005a), Polf *et al.* (2005), Popova (2005), Schneider *et al.* (2002), Titt *et al.*
4085 (2005), and Zheng *et al.* (2008). Some aspects of secondary radiation production in the beam-line
4086 elements are discussed in Chapter 7.

4087

4088 Monte Carlo simulations can also assess secondary doses to the patient, directly through the
4089 calculation of energy deposition in individual organs by using phantoms of the human body (see Chapter
4090 7).

4091

4092 **6.2.2 Activation Studies**

4093

4094 The Monte Carlo simulation of all aspects of activation has grown significantly over the past
4095 years due to the availability and increasing quality of both microscopic models for the production of
4096 individual nuclides and experimental benchmark data. While an uncertainty factor of 2 to 5 in such
4097 predictions was considered reasonable in the past, modern codes are now able to predict individual
4098 isotopes often with a 30 % or better accuracy (Brugger *et al.*, 2006). In addition to the production of
4099 radionuclides, some codes also allow (in the same simulation) the computation of radioactive decay and
4100 the transport of the decay radiation and, thus, of residual doses (Brugger *et al.*, 2005). Consequently, the
4101 material choice and design of shielding and accelerator components can be optimized in this regard
4102 during the design stage, thus reducing costs at a later stage that result from precautionary measures such
4103 as unnecessary accelerator down-times to allow for “cool-down” of components or temporary protection.

4104

4105 The capability of accurately predicting radioactive nuclide production and distributions with
4106 Monte Carlo methods has now even entered the field of particle therapy quality assurance (*e.g.*, positron
4107 emission tomography, PET; see, for example, Parodi *et al.*, 2007 and Pshenichnov *et al.*, 2007). This
4108 field is, however, outside of the scope of this review. Air and water activation are also typically
4109 estimated with Monte Carlo simulations, although in this case the direct calculation of nuclide
4110 production is usually replaced by off-line folding of particle fluence spectra with evaluated cross section

4111 data due to the low density of the media and the associated inefficient nuclide production during a
4112 simulation.

4113

4114 **6.3 Requirements**

4115

4116 The requirements can be subdivided into two categories: those related to physics modeling and
4117 those associated with the user-friendliness of the code. While details on different Monte Carlo codes are
4118 given further below, this Chapter provides some guidance as to which code might best fulfill the various
4119 requirements.

4120

4121 **6.3.1 Shielding Studies**

4122

4123 A code to be used for shielding design at a particle therapy facility should be able to describe
4124 interactions of hadrons and nuclei with energies up to a few hundred MeV/u in arbitrary materials.
4125 Because exposures behind shielding are typically caused by neutrons, an accurate description of double
4126 differential distributions of neutrons and light fragments emitted in an interaction, as well as their
4127 transport through the shield down to thermal energies, is vital. For ion beams and shielding in the
4128 forward (beam) direction, a detailed treatment of projectile fragmentation by the respective code is of
4129 equal importance. A folding with energy-dependent dose equivalent conversion coefficients (for
4130 example, those summarized in Pelliccioni, 2000) and direct scoring of the latter quantity is usually most
4131 convenient for the user, and the code should offer this option. The contribution to the total dose behind
4132 shielding due to electromagnetic cascades is usually small ($\sim 20\%$) as compared to the contribution by
4133 neutrons. Still, a coupled simulation of both hadronic and electromagnetic showers through the shield is

4134 necessary for benchmarking the calculations with measurements (the radiation monitors may have an
4135 enhanced response to electromagnetic particles), and for establishing so-called field calibration factors.

4136

4137 The availability of variance reduction (biasing) techniques is a ‘must’ in order for a Monte Carlo
4138 code to be used for the design of thick shielding (one meter or more) and complex access mazes. In
4139 contrast to an analog Monte Carlo simulation, in which physics processes are sampled from actual phase
4140 space distributions, a biased simulation samples from artificial distributions with the aim of achieving a
4141 faster convergence of the calculated quantities to the true values (*i.e.*, a faster reduction of the variance)
4142 in the phase space regions of interest, *e.g.*, behind thick layers of shielding. Note that a biased simulation
4143 predicts average quantities but not their higher moments and can, therefore, not reproduce correlations
4144 and fluctuations. A rigorous mathematical treatment of variance reduction techniques can be found in
4145 several textbooks; see for instance Lux and Koblinger (1991) and Carter and Cashwell (1975).

4146

4147 There exist several variance reduction methods. The choice of the most appropriate method
4148 depends on the actual problem, with a combination of different techniques often being the most effective
4149 approach. The so-called “region importance biasing” is the easiest method to apply and safest to use. The
4150 shield is split into layers that are assigned importance factors. The values of the factors increase towards
4151 the outside of the shield, with the relative value of the factors of two adjacent layers equal to the inverse
4152 of the dose attenuation in that layer.

4153

4154 FLUKA (Ferrari, 2005; Battistoni *et al.*, 2007) and MCNPX (Pelowitz, 2005; McKinney *et al.*,
4155 2006) are two general-purpose codes that include powerful variance reduction techniques and have
4156 therefore been used widely in shielding studies.

4157

4158 **6.3.2 Activation Studies**

4159

4160 A reliable description of inelastic interactions by microscopic models is indispensable for
4161 activation studies of beam-line and shielding components. Only activation by low-energy neutrons
4162 constitutes an exception where evaluated experimental data on nuclide production are typically available
4163 in the respective neutron transport library. Activation of accelerator components is often dominated by
4164 spallation reactions. An accurate simulation of these reactions requires a generalized intra-nuclear
4165 cascade model with pre-equilibrium emission, as well as models for evaporation, fission, and
4166 fragmentation. The description of the break-up of a highly excited heavy residual (so-called multi-
4167 fragmentation), which can be very complex and too time-consuming during a shower simulation, is often
4168 approximated by a generalized evaporation of nuclides with mass numbers of up to 20 or more.
4169 Predictions for the production of individual nuclides are non-trivial and depend on the quality of many
4170 different physics models, not only for the inelastic interaction and nuclear break-up but also for particle
4171 transport and shower propagation. Thus, detailed benchmark exercises to assess the reliability of the
4172 results are of utmost importance. Typically, the longer the cooling time, the less nuclides contribute to
4173 the total activation, and therefore, details of the production of individual nuclides become more
4174 important. At short cooling times (up to a few days) over- and underestimations of the nuclide
4175 production tend to cancel each other so that integral quantities such as total activity or residual doses are
4176 much less affected by model uncertainties. Both MARS15 and MCNPX can use the Cascade-Exciton
4177 Model (CEM) and Los Alamos Quark Gluon String Model (LAQGSM) for hadronic interactions that
4178 have been shown in extensive benchmark experiments to provide reliable predictions for nuclide
4179 production (Mashnik, 2009). The FLUKA code also includes detailed microscopic models for nuclide
4180 productions which have been proven to give very accurate results (Brugger *et al.*, 2006). In this case, the

4181 models are fully integrated into the code, providing a high level of quality assurance that is often needed
4182 in safety-related applications.

4183

4184 In the past, residual dose rates were often estimated by means of so-called omega factors that
4185 relate the density of inelastic interactions in a solid material to contact dose-equivalent rates caused by
4186 radioactive nuclides in the material. At present, more and more codes include a description of radioactive
4187 decay and the transport of decay radiation, and allow one to avoid approximations inherent to omega
4188 factors. A code capable of a direct simulation of radioactive decay should be preferred for this type of
4189 study because handling of activated components is an important cost factor due to decreasing dose limits
4190 and also due to the increasing importance of the optimization principle during the design stage. At
4191 present, the FLUKA Monte Carlo code gives the most consistent and reliable single-step prediction of
4192 residual dose rates (Ferrari, 2005; Battistoni *et al.*, 2007; Brugger *et al.*, 2005). Other general purpose
4193 codes make use of omega factors (MARS15) or require a separate calculation of the radioactive decay
4194 with a different code (MCNPX).

4195

4196 **6.3.3 Secondary Doses to Patients**

4197

4198 Monte Carlo simulations have been used extensively to study secondary doses in patients (see
4199 Chapter 7). Such simulations obviously require an accurate modeling of the transport, interaction, and
4200 fragmentation (for ion beams) of the primary beam in tissue-equivalent material, as well as a fully
4201 coupled hadronic and electromagnetic shower simulation. The capability of the transport code to use
4202 voxel phantoms usually increases the reliability of the predictions due to the great detail in which the
4203 human body can be modeled with such phantoms. GEANT4 (Agostinelli *et al.*, 2003; Allison *et al.*,

4204 2006; Rogers *et al.*, 2007) and FLUKA (Ferrari, 2005; Battistoni *et al.*, 2007; Battistoni *et al.*, 2008) are
4205 two examples of codes that support voxel geometries.

4206

4207 **6.3.4 User-Friendliness**

4208

4209 In addition to physics modeling, the user-friendliness of a code can be of significant importance.
4210 As mentioned earlier, increasing computing power greatly reduces the time actually spent for the
4211 calculation such that, in many cases, the time necessary to set up a simulation and process its results
4212 becomes a dominating factor. To address this problem, graphical user interfaces that also take over a
4213 basic check of input options exist for many codes. A few examples can be found in Vlachoudis, 2009;
4214 Theis *et al.*, 2006; and Schwarz, 2008. The check of input options is vital as increasing user-friendliness
4215 is associated with increasing usage of the code as a “black-box,” and one risks having simulation
4216 artefacts being taken into account undetected. Furthermore, it is observed that the acceptance of the
4217 results, *e.g.*, by authorities, can depend a great deal on the way the results are presented. In this regard,
4218 three-dimensional geometry visualization, the overlay of results onto the geometry, and the use of color
4219 contour plots can be of importance. Finally, it should be noted that despite the enormous advantages of
4220 graphical user interfaces, a minimum knowledge on the available physical models is indispensable in
4221 order to judge on the accuracy of the obtained results.

4222

4223 **6.4 Overview of the Most Commonly Used Codes**

4224

4225 **6.4.1 FLUKA**

4226

4227 FLUKA is a general-purpose particle interaction and transport code with roots in radiation
4228 protection studies at high energy accelerators (Ferrari, 2005; Battistoni *et al.*, 2007). It therefore
4229 comprises all features needed in this area of application, such as detailed hadronic and nuclear interaction
4230 models, full coupling between hadronic and electromagnetic processes, and numerous variance reduction
4231 options.

4232

4233 The module for hadronic interactions is called PEANUT and consists of a phenomenological
4234 description (Dual Parton Model-based Glauber Gribov cascade) of high-energy interactions (up to 20
4235 TeV), a generalized intra-nuclear cascade, and pre-equilibrium emission models, as well as models for
4236 evaporation, fragmentation, fission, and de-excitation by gamma emission. Interactions of ions are
4237 simulated through interfaces with different codes based on models applicable in certain ranges of energy
4238 (DPMJET3 above 5 GeV/nucleon, rQMD-2.4 between 0.1 and 5 GeV/nucleon, Boltzmann Master
4239 Equation below 0.1 GeV/nucleon; see Battistoni, 2007 and references therein).

4240

4241 The transport of neutrons with energies below 20 MeV is performed by a multi-group algorithm
4242 based on evaluated cross section data (ENDF/B, JEF, JENDL, *etc.*) binned into 260 energy groups, 31 of
4243 which are in the thermal energy region. For a few isotopes (^1H , ^6Li , ^{10}B , ^{14}N), pointwise cross sections
4244 can be optionally used during transport. The detailed implementation of electromagnetic processes in the
4245 energy range between 1 keV and 1 PeV is fully coupled with the models for hadronic interactions.

4246

4247 Many variance reduction techniques are available in FLUKA, including weight windows, region
4248 importance biasing, and leading particle, interaction, and decay length biasing (among others). The
4249 capabilities of FLUKA are unique for studies of induced radioactivity, especially with regard to nuclide
4250 production, decay, and transport of residual radiation. In particular, particle cascades by prompt and

4251 residual radiation are simulated in parallel based on the microscopic models for nuclide production and a
4252 solution of the Bateman equations for activity built-up and decay.

4253

4254 FLUKA is written in Fortran77 and runs on most Linux and Unix platforms on which the
4255 compiler g77 is installed. The code is distributed in binary form, with the addition of the source code for
4256 user routines and common blocks (<http://www.fluka.org>). The complete FLUKA source code is available
4257 by request after an additional registration procedure (see <http://www.fluka.org/fluka.php> for details). No
4258 programming experience is required unless user routines are needed for specific applications.

4259

4260 **6.4.2 GEANT4**

4261

4262 GEANT4 is an object-oriented toolkit originally designed to simulate detector responses of
4263 modern particle and nuclear physics experiments (Agostinelli *et al.*, 2003; Allison *et al.*, 2006). It
4264 consists of a kernel that provides the framework for particle transport, including tracking, geometry
4265 description, material specifications, management of events, and interfaces to external graphics systems.

4266

4267 The kernel also provides interfaces to physics processes. In this regard, the flexibility of
4268 GEANT4 is unique as it allows the user to freely select the physics models that best serve the particular
4269 application needs. Implementations of interaction models exist over an extended range of energies, from
4270 optical photons and thermal neutrons to high-energy interactions required for the simulation of
4271 accelerator and cosmic ray experiments. In many cases, complementary or alternative modeling
4272 approaches are offered from which the user can choose.

4273

4274 Descriptions of intra-nuclear cascades include implementations of the Binary and the Bertini
4275 cascade models. Both are valid for interactions of nucleons and charged mesons, the former for energies
4276 below 3 GeV, and the latter for energies below 10 GeV. At higher energies (up to 10 TeV), three models
4277 are available: a high-energy parameterized model (using fits to experimental data), a quark-gluon string
4278 model, and the Fritiof fragmentation model, with both the quark-gluon string model and the Fritiof
4279 fragmentation model based on string excitations and decay into hadrons. Nuclear de-excitation models
4280 include abrasion-ablation and Fermi-breakup models. Furthermore, heavy-ion interactions can also be
4281 simulated if the appropriate packages are linked.

4282

4283 The package for electromagnetic physics comprises the standard physics processes as well as
4284 extensions to energies below 1 keV, including emissions of x rays, optical photon transport, *etc.*

4285

4286 To facilitate the use of variance reduction techniques, general-purpose biasing methods such as
4287 importance biasing, weight windows, and a weight cut-off method have been introduced directly into the
4288 toolkit. Other variance reduction methods, such as leading particle biasing for hadronic processes, come
4289 with the respective physics packages,.

4290

4291 GEANT4 is written in C++ and runs on most Linux and Unix platforms as well as under
4292 Windows with CygWin Tools. The code and documentation can be downloaded from the GEANT4
4293 website at <http://cern.ch/geant4>. Experience in C++ programming is indispensable for using the code.

4294

4295 **6.4.3 MARS15**

4296

4297 The MARS15 code system (Mokhov, 1995; Mokhov and Striganov, 2007; Mokhov, 2009) is a
4298 set of Monte Carlo programs for the simulation of hadronic and electromagnetic cascades that is used for
4299 shielding, accelerator design, and detector studies. Correspondingly, it covers a wide energy range: 1
4300 keV to 100 TeV for muons, charged hadrons, heavy ions and electromagnetic showers; and 0.00215 eV to
4301 100 TeV for neutrons.

4302
4303 Hadronic interactions above 5 GeV can be simulated with either an inclusive or an exclusive
4304 event generator. While the former is CPU-efficient (especially at high energy) and based on a wealth of
4305 experimental data on inclusive interaction spectra, the latter provides final states on a single interaction
4306 level and preserves correlations. In the exclusive mode, the cascade-exciton model CEM03.03 describes
4307 hadron-nucleus and photo-nucleus interactions below 5 GeV, the Quark-Gluon String Model code
4308 LAQGSM03.03 simulates nuclear interactions of hadrons and photons up to 800 GeV and of heavy ions
4309 up to 800 GeV/nucleon, and the DPMJET3 code treats the interactions at higher energies. The exclusive
4310 mode also includes models for a detailed calculation of nuclide production *via* evaporation, fission, and
4311 fragmentation processes.

4312
4313 MARS15 is also coupled to the MCNP4C code that handles all interactions of neutrons with
4314 energies below 14 MeV. Produced secondaries other than neutrons are directed back to the MARS15
4315 modules for further transport.

4316
4317 Different variance reduction techniques, such as inclusive particle production, weight windows,
4318 particle splitting, and Russian roulette, are available in MARS15. A tagging module allows one to tag the
4319 origin of a given signal for source term or sensitivity analyses. Further features of MARS15 include a
4320 MAD-MARS Beam-Line Builder for a convenient creation of accelerator models.

4321

4322 MARS15 modules are written in Fortran77 and C. The code runs on any Linux or Unix platform
4323 in both single- and multi-processor modes. A powerful user-friendly graphical user interface provides
4324 various visualization capabilities. The code must be installed by the author on request (for details see
4325 Mokhov, 2009).

4326

4327 **6.4.4 MCNPX**

4328

4329 MCNPX originates from the Monte Carlo N-Particle transport (MCNP) family of neutron
4330 interaction and transport codes and, therefore, features one of the most comprehensive and detailed
4331 descriptions of the related physical processes (Pelowitz, 2005; McKinney *et al.*, 2006). Later it was
4332 extended to other particle types, including ions and electromagnetic particles. This allowed an expansion
4333 of the areas of application from those purely neutronics-related to accelerator shielding design, medical
4334 physics, and space radiation, among others.

4335

4336 The neutron interaction and transport modules use standard evaluated data libraries mixed with
4337 physics models where such libraries are not available. The transport is continuous in energy and includes
4338 all features necessary for reactor simulations, including burn-up, depletion, and transmutation. Different
4339 generalized intra-nuclear cascade codes can be linked to explore different physics implementations, such
4340 as CEM2K, INCL4 and ISABEL (see McKinney *et al.*, 2006 and references therein). They either contain
4341 fission-evaporation models or can be coupled to such models (*i.e.*, ABLA), allowing detailed predictions
4342 for radionuclide production. While the intra-nuclear cascade codes are limited to interaction energies
4343 below a few GeV, a link to the Quark-Gluon String Model code LAQGSM03 extends this energy range

4344 to about 800 GeV. The latter code also allows the simulation of ion interactions. Electromagnetic
4345 interactions are simulated in MCNPX by the ITS 3.0 code.

4346

4347 MCNPX contains one of the most powerful implementations of variance reduction techniques.
4348 Spherical mesh weight windows can be created by a generator in order to focus the simulation time on
4349 certain spatial regions of interest. In addition, a more generalized phase space biasing is also possible
4350 through energy- and time-dependent weight windows. Other biasing options include pulse-height tallies
4351 with variance reduction and criticality source convergence acceleration.

4352

4353 MCNPX is written in Fortran90 and runs on PC Windows, Linux, and Unix platforms. The code
4354 (source code, executables, data) is available to nearly everyone (subject to export controls on sensitive
4355 countries) from the Radiation Safety Information Computational Center (<http://www-rsicc.ornl.gov>) in
4356 Oak Ridge, TN, U.S.A. Experience in programming is not required for many applications.

4357

4358 **6.4.5 PHITS**

4359

4360 The Particle and Heavy-Ion Transport code System PHITS (see Iwase, 2002; Niita, 2006 and
4361 references therein) was among the first general-purpose codes to simulate the transport and interactions
4362 of heavy ions in a wide energy range, from 10 MeV/nucleon to 100 GeV/nucleon. It is based on the high-
4363 energy hadron transport code NMTC/JAM that was extended to heavy ions by incorporating the JAERI
4364 Quantum Molecular Dynamics code JQMD.

4365

4366 Below energies of a few GeV, hadron-nucleus interactions in PHITS are described through the
4367 production and decay of resonances, while at higher energies (up to 200 GeV) inelastic hadron-nucleus

4368 collisions proceed *via* the formation and decay of so-called strings that eventually hadronize through the
4369 creation of (di)quark-anti(di)quark pairs. Both are embedded into an intra-nuclear cascade calculation.
4370 Nucleus-nucleus interactions are simulated within a molecular dynamics framework based on effective
4371 interactions between nucleons.

4372

4373 The generalized evaporation model GEM treats the fragmentation and de-excitation of the
4374 spectator nuclei and includes 66 different ejectiles (up to Mg) and fission processes. The production of
4375 radioactive nuclides, both from projectile and target nuclei, thus follows directly from the mentioned
4376 microscopic interaction models.

4377

4378 The transport of low-energy neutrons employs cross sections from evaluated nuclear data
4379 libraries such as ENDF and JENDL below 20 MeV and LA150 up to 150 MeV. Electromagnetic
4380 interactions are simulated based on the ITS code in the energy range between 1 keV and 1 GeV. Several
4381 variance reduction techniques, including weight windows and region importance biasing, are available
4382 in PHITS.

4383

4384 Due to its capability to transport nuclei, PHITS is frequently applied in ion-therapy and space
4385 radiation studies. The code is also used for general radiation transport simulations, such as in the design
4386 of spallation neutron sources.

4387

4388 The PHITS code is available for download from its Web site, <http://phits.jaea.go.jp/>

4389

4390 **6.4.6 SHIELD/SHIELD-HIT**

4391

4392 The SHIELD Monte Carlo code (Sobolevsky, 2008; Dementyev and Sobolevsky, 1999) simulates
4393 the interactions of hadrons and atomic nuclei of arbitrary charge and mass number with complex
4394 extended targets in the energy range from 1 MeV/nucleon to 1 TeV/nucleon, and down to thermal
4395 energies for neutrons.

4396

4397 Inelastic nuclear interactions are described by the so-called multi-stage dynamical model
4398 (MSDM). The name refers to the different stages through which a hadronic interaction proceeds in
4399 SHIELD: fast cascade stage, pre-equilibrium emission of nucleons and light nuclei, and a nuclear
4400 fragmentation and de-excitation stage. Interactions above 1 GeV are simulated by the quark-gluon string
4401 model (QGSM), while the Dubna Cascade Model (DCM) handles intra-nuclear cascades at lower
4402 energies. The models implemented for the equilibrium de-excitation of a residual nucleus cover all
4403 aspects of this stage, such as evaporation, fission, Fermi break-up of light nuclei, and multi-
4404 fragmentation. In the latter case, the disintegration of highly excited nuclei into several excited fragments
4405 is described according to the statistical models of multi-fragmentation (SMM). Neutron transport below
4406 14.5 MeV is simulated by the LOENT (Low Energy Neutron Transport) code based on 28 energy groups
4407 and using the data system ABBN.

4408

4409 The code SHIELD-HIT (Gudowska *et al.*, 2004; Geithner *et al.*, 2006), a spin-off of SHIELD,
4410 specializes in the precision simulation of interaction of therapeutic beams with biological tissue and
4411 tissue-like materials. Improvements in SHIELD-HIT, relevant for light-ion therapy, comprise ionization
4412 energy-loss straggling and multiple Coulomb scattering effects of heavy charged particles. Further
4413 aspects of particle transport that were modified when compared to SHIELD include updated stopping
4414 power tables, an improved Fermi break-up model, and an improved calculation of hadronic cross
4415 sections.

4416

4417 The code can be obtained from the authors by request (for further information, see

4418 <http://www.inr.ru/shield>).

4419

7. Patient Dose from Secondary Radiation

Harald Paganetti and Irena Gudowska

4420
4421
4422
4423
4424
4425
4426
4427
4428
4429
4430
4431
4432
4433
4434
4435
4436
4437
4438
4439
4440
4441
4442
4443

When charged particles such as protons and carbon ions are used in cancer therapy, secondary particles such as neutrons, protons, pions, and heavy charged ions are produced through nuclear inelastic reactions of the primary ions with the beam-line components and the patients themselves. These particles may possess very high energies (up to several hundred MeV) and undergo a variety of cascade events during their transport through the patient, which generate new series of secondary particles. An extensive part of the patient body may be exposed to the complex radiation field. Secondary radiation produced in the beam-line components and that reaches the patient can be regarded as external radiation. On the other hand, secondary particles produced in the patient represent an internal radiation source.

The number of review articles in the literature shows the increased awareness regarding health risks due to secondary radiation for patients undergoing radiation therapy (Palm and Johansson, 2007; Suit *et al.*, 2007; Xu *et al.*, 2008). Numerous experimental and theoretical studies have been done and many results have been published. There are quite a few uncertainties leading to controversies among experts in the field (Brenner and Hall, 2008b; Chung *et al.*, 2008; Gottschalk, 2006; Hall, 2006; Paganetti *et al.*, 2006). In this chapter, the secondary doses (both absorbed doses and equivalent doses delivered to the tissue) produced in proton and carbon ion beams of different energies are discussed. Concepts of equivalent dose or dose equivalent applied to secondary radiation in ion therapy are explained. We summarize the main issues with regard to cancer risk due to secondary radiation (*i.e.*, neutrons) in heavy charged particle radiation therapy. Given the amount of material published by several groups, this chapter cannot be comprehensive and we discuss only a subset of the available data.

4444

4445

7.1 Sources of Secondary Radiation

4446

7.1.1 Secondary Particles Produced in the Beam-Line Elements

4448

4449 Secondary particles like neutrons, protons, and light charged ions (^2H , ^3H , ^3He , ^4He , *etc.*) are
4450 produced when primary ion beams interact through nuclear reactions with beam-line components or in
4451 patients. As far as the dose outside the main radiation field is concerned, proton beams deposit secondary
4452 dose mostly *via* secondary neutrons. For light-ion radiation therapy, heavier by-products might occur.
4453 However, such contributions are likely to be stopped in the multiple collimators or scatterers. The
4454 production of neutrons outside the patient depends on the material (type and dimensions) in the beam
4455 path and, hence, depends on the design of the beam line.

4456

4457 For protons and carbon-ion beams delivered by cyclotrons with a fixed energy, a significant
4458 amount of secondary radiation is produced in the energy selection systems, which include energy
4459 degraders of variable thickness and energy-defining slits. These degraders are usually outside the
4460 treatment room (in the accelerator vault) and thus do not cause secondary dose exposure of the patient.
4461 However, special care must be taken where the degradation is done, at least partially, directly upstream
4462 of the patient position. This is the case, for example, in beam lines devoted to ophthalmic applications,
4463 using small fields (*e.g.*, < 3 cm diameter) and low energies (< 70 MeV) but with high dose rates (*e.g.*, 15
4464 to 20 Gy/min).

4465

4466 Neutrons and protons produced in the nozzle can undergo tertiary interactions in the beam-line
4467 elements, which result in the cascade of high-energy secondaries. Depending on the beam focusing and

4468 scattering components, certain fractions of these high-energy secondaries, mainly neutrons, reach the
4469 patient. High-energy neutrons (of energies greater than 10 MeV) and high-energy protons produced by
4470 an intra-nuclear cascade process, are mainly forward-peaked. Neutrons of energies below 10 MeV are
4471 produced by an evaporation process and are emitted fairly isotropically around each source in the
4472 treatment head. In general, high-Z materials generate more neutrons per incoming proton than low-Z
4473 materials. However, it is not practical to manufacture most treatment head devices with, for example,
4474 low-Z and high-density plastic materials. Some of the materials typically used in treatment heads are
4475 brass, steel, carbon, or nickel.

4476

4477 Design of proton therapy beam delivery systems and treatment heads can have considerable
4478 variations when comparing different facilities. In addition, the beam and treatment-head configuration is
4479 dependent on the treatment field size. Broad-beam, energy-modulated (or passively scattered) proton
4480 therapy needs various scatterers, beam-flattening devices, collimators, and energy-modulation devices to
4481 produce the spread-out Bragg peaks. Additionally, for each treatment field, individual apertures and
4482 range compensators are generally used. Consequently, the neutron fluence and energy spectrum
4483 produced in the treatment head of a proton therapy machine used for broad-beam energy-modulated
4484 treatments depends on several factors. These include the characteristics of the beam entering the
4485 treatment head (energy, angular spread); the material in the double-scattering system and range
4486 modulator; and the field size upstream of the final patient-specific aperture (Mesoloras *et al.*, 2006).
4487 Depending on the field size incident on the aperture, the latter can cause neutron dose variations up to
4488 one order of magnitude. The complexity of field delivery, specifically for passive-scattering techniques,
4489 causes considerable variations in neutron doses and prevents us from defining a ‘typical’ neutron
4490 background representing proton therapy in general (Gottschalk, 2006; Hall, 2006; Paganetti *et al.*, 2006;
4491 Zacharatou Jarlskog and Paganetti, 2008b).

4492

4493 In proton therapy, generally only neutrons and protons of high energies, especially those
4494 produced in the final target-shaped collimators located close to the patient, are of concern for undesired
4495 exposures in the patient. In addition, most proton therapy delivery systems allow the delivery of only a
4496 few fixed-field sizes impinging on the final patient specific aperture. Consequently, the efficiency of
4497 most proton therapy treatment heads is quite low (below 30% and even as low as 10% for typical field
4498 sizes). This implies that the neutron yield from such treatment heads typically increases with decreasing
4499 field size for passive-scattering proton beam treatments, as has been demonstrated in experiments
4500 (Mesoloras *et al.*, 2006) and Monte Carlo simulations (Zacharatou Jarlskog *et al.*, 2008).

4501

4502 For beam scanning, a proton pencil beam is magnetically scanned throughout the target volume
4503 without the need for scattering, flattening, or compensating devices. Therefore, for scanned beams the
4504 intensity of secondary radiation is much lower than for passive systems because there is little material in
4505 the beam path (typically only monitor ionization chambers or beam position monitors).

4506

4507 In passive-scattering systems where patient-specific collimators are routinely used, the patient is
4508 also exposed to out-scattered primary particles from the edges of the collimator. This process is
4509 especially important in proton therapy beams, where the edge-scattered protons influence the lateral out-
4510 of-field dose distribution in a patient. Note that this radiation is referred to as scattered radiation as
4511 compared to secondary radiation consisting of secondary particles and is not discussed in this chapter.

4512

4513 **7.1.2 Secondary Particles Produced in the Patient**

4514

4515 Secondary radiation is also produced in the patient. In proton therapy, the most significant (in
4516 terms of dose) secondary particles from nuclear interactions are either protons or neutrons. Those protons
4517 that originate from a primary proton have a lower energy than the primary proton and typically
4518 contribute to the dose in the main radiation field, *e.g.*, in the entrance region of the Bragg curve
4519 (Paganetti, 2002). Secondary neutrons, however, can deposit dose at large distances from the target in the
4520 patient. They deposit most of their dose *via* protons generated in neutron-nucleus interactions. Thus,
4521 these protons can be produced anywhere in the human body.

4522

4523 The difference in neutron dose between scanned beams and passively scattered beams is mainly
4524 determined by the ratio of internal (generated in the patients) and external (generated in the treatment
4525 head) neutrons. This ratio depends heavily on the organ and its distance to the treatment target volume
4526 (Jiang *et al.*, 2005). It was concluded that the ratio of neutron dose generated by treatment-head neutrons
4527 to patient-generated neutrons could be as much as one order of magnitude, which depends mainly on the
4528 design of the treatment head and on the field size (Jiang *et al.*, 2005). Typically, neutron absorbed dose
4529 generated by neutrons from the treatment head dominates, which implies that proton beam scanning
4530 substantially reduces neutron dose to patients.

4531

4532 The neutron yield and the neutron dose due to neutrons generated in the patient depends on the
4533 range of the beam (Zheng *et al.*, 2007). The greater the penetration of the beam, the greater is the overall
4534 likelihood of a nuclear interaction producing neutrons. In addition, the neutron yield depends on the
4535 irradiated volume simply because a bigger volume requires more primary protons in order to deposit the
4536 prescribed dose in the target. Thus, in contrast to external neutrons, internal neutron yields typically
4537 increase with increasing treatment volume.

4538

4539 The situation is far more complex in light-ion therapy than it is in proton therapy. With light-ion
4540 beams, the primary ions are fragmented due to nuclear inelastic collisions with the atomic nuclei in the
4541 tissue. This process results in beam-produced secondary ions and attenuation of the primary beam
4542 intensity. Also the target nuclei can undergo nuclear fragmentation that results in the production of
4543 secondary ions that are generally of low energies and a deposit local energy close to the ion track.
4544 Neutrons and secondary ions with atomic masses lower than that of the primary ions are produced, *e.g.*,
4545 hydrogen, helium, lithium, beryllium, boron, carbon. These lighter fragments can have longer ranges and
4546 wider energy distributions than the primary ions and give rise to a characteristic undesirable dose tail
4547 beyond the Bragg peak and broadening of the transverse dose profiles along the beam path.

4548

4549 In the same way as the incident particle, the beam-produced fragments will undergo elastic
4550 scattering with the target nuclei. Heavier beam fragments with atomic number $Z > 2$ generally scatter
4551 through small angles, whereas the scattering of lighter beam fragments of $Z \leq 2$ results in larger angle
4552 scattering which broadens the beam and contributes to the dose outside the treatment field. Fast beam-
4553 produced secondaries are focused mainly in the forward direction, but can also have a noticeable angular
4554 spread. Target-produced secondaries on the other hand, have a much wider angular distribution, but as
4555 they generally have low energies they are transported only short distances. Beam-produced fragments,
4556 especially neutrons and secondary protons, may possess high energies (Gudowska and Sobolevsky,
4557 2005; Gunzert-Marx *et al.*, 2008; Porta *et al.*, 2008), causing dose deposition at larger distances outside
4558 the treated volume. Simultaneously, as they traverse the patient they undergo nuclear interactions with
4559 the tissue elements that result in the generation of high-energy secondaries, produced in the cascade of
4560 events.

4561

7.2 Out of Treatment Field Absorbed Dose to Patients (Secondary Dose)

4562

4563

7.2.1 Experimental Methods

4565

4566 A variety of theoretical and experimental studies have been conducted to determine the
4567 distributions of secondary particles produced in water and tissue-equivalent materials when irradiated
4568 with ion beams at energies of therapeutic interest. These studies concern both the depth dependence and
4569 spatial distributions of the charged secondaries produced in the water, carbon, PMMA, and different
4570 tissue-equivalent phantoms, as well as the energy spectra of particles leaving the irradiated phantoms or
4571 the patient. A large fraction of the published data addresses the production of fast neutrons, neutron
4572 energy spectra, and neutron angular distributions by stopping ion beams of different energies in thick
4573 tissue-equivalent targets.

4574

4575 In addition, various groups from radiation therapy facilities have performed experiments to assess
4576 secondary doses. In proton therapy, measurements have been primarily concentrated on the use of
4577 Bonner spheres (Mesoloras *et al.*, 2006; Schneider *et al.*, 2002; Yan *et al.*, 2002). Thermoluminescence
4578 dosimetry has been applied as well (Francois *et al.*, 1988a; Reft *et al.*, 2006). CR-39 plastic nuclear track
4579 detectors were used in the studies by Schneider *et al.* (2002) and Moyers *et al.* (2008), whereas a bubble
4580 detector was used by Mesoloras *et al.* (2006). An improved neutron rem-counter, WENDI, was applied
4581 for neutron dose measurement in carbon beams in the energy range 100 to 250 MeV/u (Iwase *et al.*,
4582 2007). Microdosimetric detector systems are very promising in terms of providing reliable dose
4583 estimates. Microdosimetric distributions of secondary neutrons produced by 290 MeV/nucleon carbon
4584 beams have been measured by using a tissue-equivalent proportional counter (Endo *et al.*, 2007). Silicon-
4585 based microdosimetry provided information on the depth and lateral distance dependence of the dose

4586 equivalent for a passively scattered proton beam (Wroe *et al.*, 2007; Wroe *et al.*, 2009). In other areas of
4587 radiation protection and radiation therapy, microdosimetric concepts have been shown to be powerful
4588 tools for relative comparisons of treatment field characteristics in terms of lineal energy (Hall *et al.*,
4589 1978; Loncol *et al.*, 1994; Morstin and Olko, 1994; Paganetti *et al.*, 1997).

4590

4591 **7.2.2 Calculation Methods (Monte Carlo Techniques)**

4592

4593 Secondary doses, in particular neutron doses, are difficult to measure. Neutrons are indirectly
4594 ionizing and interact sparsely causing only low absorbed doses. Although this makes Monte Carlo
4595 methods very valuable, even Monte Carlo codes have considerable uncertainties when it comes to
4596 simulating secondary particle production because the underlying physics is not known with sufficient
4597 accuracy. Firstly, there is insufficient experimental data of inelastic nuclear cross sections in the energy
4598 region of interest in heavy charged particle radiation therapy. Secondly, neutron and secondary charged
4599 particle emissions from nuclear interactions can be the result of very complex interactions. There are
4600 uncertainties in the physics of pre-equilibrium and fragmentation as well as the intra-nuclear cascade
4601 mechanisms, the latter being based in parameterized models for Monte Carlo transport calculations.
4602 Several codes have been used to study low doses in radiation therapy, in particular neutron doses
4603 generated in proton and ion therapy. The Monte Carlo code MCNPX (Pelowitz, 2005) was used to assess
4604 neutron and photon doses in proton beams (Fontenot *et al.*, 2008; Moyers *et al.*, 2008; Perez-Andujar *et*
4605 *al.*, 2009; Polf and Newhauser, 2005; Taddei *et al.*, 2008; Zheng *et al.*, 2007; Zheng *et al.*, 2008).
4606 Further, FLUKA (Battistoni *et al.*, 2007; Ferrari *et al.*, 2005) and GEANT4 (Agostinelli *et al.*, 2003;
4607 Allison *et al.*, 2006) were applied to assess secondary doses in proton beams (in Agosteo *et al.*, (1998)
4608 and Jiang *et al.*, (2005), and Zacharatou Jarlskog *et al.*, (2008), respectively). Other codes used for ions
4609 are SHIELD-HIT (Dementyev and Sobolevsky, 1999; Gudowska *et al.*, 2004) and PHITS (Iwase *et al.*,

4610 2002; Niita *et al.*, 2006). For light ion beams, studies of secondary neutron doses were done with
4611 FLUKA (Porta *et al.*, 2008), PHITS (Gunzert-Marx *et al.*, 2008; Iwase *et al.*, 2007), GEANT4
4612 (Pshenichnov *et al.*, 2005), and SHIELD-HIT (Gudowska *et al.*, 2002; Gudowska *et al.*, 2004;
4613 Gudowska *et al.*, 2007; Gudowska and Sobolevsky, 2005; Iwase *et al.*, 2007). A review of Monte Carlo
4614 codes used in radiation protection is presented in Chapter 6 of this report.

4615

4616 In order to describe the radiation field incident on the patient, the treatment head needs to be
4617 simulated. Monte Carlo simulations of treatment heads have been extensively reported for protons
4618 (Newhauser *et al.*, 2005b; Paganetti, 1998; 2006; Paganetti *et al.*, 2004). The characterization of the
4619 beam entering the treatment head is typically based on parameterizations obtained from measurements
4620 (Cho *et al.*, 2005; Fix *et al.*, 2005; Janssen *et al.*, 2001; Keall *et al.*, 2003; Paganetti *et al.*, 2004).

4621

4622 Simulating secondary dose in the patient geometry can, in principle, be done in a similar fashion
4623 as calculating primary dose using Monte Carlo simulations (Paganetti *et al.*, 2008). The difference is that
4624 the quantity of interest is not the absorbed dose but the equivalent dose, which is a parameterization of
4625 radiation effects. Thus, calculations of the secondary equivalent doses to patients require particle and
4626 particle energy-dependent radiation weighting factors in order to consider the biological effectiveness
4627 (see section on equivalent dose below). There are different ways to determine equivalent doses using
4628 Monte Carlo simulations, as discussed by the ICRU (1998). One possible strategy is to calculate the
4629 average absorbed dose for the organ under consideration and scale the dose with an average radiation
4630 weighting factor. Another approach frequently used (Polf and Newhauser, 2005; Zheng *et al.*, 2007) is to
4631 calculate the particle fluences at the surface of a region of interest (organ) and then use energy dependent
4632 fluence-to-equivalent dose conversion coefficients (Alghamdi *et al.*, 2005; Boag, 1975; Bozkurt *et al.*,
4633 2000; 2001; Chao *et al.*, 2001a; 2001b; Chen, 2006; NCRP, 1971). In this case, dose deposition events

4634 are not explicitly simulated. Using this method, Sato *et al.* (2009) have calculated organ-dose-equivalent
4635 conversion coefficients for neutron and proton monoenergetic beams in adult male and adult female
4636 reference phantoms using the PHITS code.

4637

4638 When dealing with neutrons, Monte Carlo simulations are typically quite time consuming (in
4639 order to achieve a reasonable statistical accuracy) when based on the dose actually deposited *via*
4640 neutrons. However, it is presumably more accurate to score each energy deposition event (*i.e.*, without
4641 using fluence-to-dose conversion). Fast neutrons lose most of their kinetic energy in the initial relatively
4642 small number of interactions. In the low/thermal energy region, there is a decreasing probability for
4643 neutrons to slow down and cause a large number of elastic scatterings in soft tissues, causing the neutron
4644 energy distributions in the patient to be dominated by low-energy neutrons (Jiang *et al.*, 2005).

4645

4646 An explicit simulation applying radiation weighting factors on a step-by-step basis considering
4647 particle type, particle history, and particle energy has been done to assess organ-specific neutron
4648 equivalent doses in proton-beam therapy (Zacharatou Jarlskog *et al.*, 2008). If a neutron was in the
4649 interaction history of the dose depositing particle, the dose deposition was considered to be due to a
4650 neutron and a neutron radiation weighting factor was then assigned. Similarly, if a proton from a proton
4651 chain deposited the absorbed dose, the dose depositions would be classified as proton induced. For each
4652 interaction chain history. a division into different groups was done depending on particle energy in order
4653 to apply energy-dependent quality factors.

4654

4655 Different dose-scoring methods were compared by Zacharatou Jarlskog and Paganetti (2008a).
4656 For neutron equivalent doses in proton beam therapy, it was found that using average weighting factors

4657 can underestimate the neutron equivalent dose in comparison to those calculated on a step-by-step basis.
4658 The difference was found to be around 25% depending on organ and field specifications.

4659

4660 In the approach applied by Pshenichnov *et al.* (2005) and Gudowska *et al.* (2007) the neutron
4661 absorbed doses delivered to tissue-equivalent phantoms by proton and carbon-ion beams were
4662 determined by two sets of calculations. First, Monte Carlo simulation was performed with the full
4663 hadronic cascade and transport of all secondary particles, whereas in the second simulation the secondary
4664 neutrons were produced at the point of interaction but excluded from further transport through the
4665 phantom. By comparison of the energy deposited in the phantom in these two calculations, the absorbed
4666 dose due to secondary neutrons was determined.

4667

4668 **7.2.3 Human Phantoms**

4669

4670 Measurements or simulations of secondary doses in simple geometries are useful in
4671 understanding the relative differences between treatment modalities or beam conditions. However, a
4672 more meaningful assessment has to be based on actual patient geometries. Because of the concern of
4673 excessive radiation with most imaging techniques, whole-body scans are rarely available. In order to
4674 perform Monte Carlo simulations considering organs not imaged for treatment planning, the use of
4675 computational phantoms is a valuable option.

4676

4677 Interestingly, these kinds of simulations could potentially provide dosimetric information to
4678 improve risk models based on long-term follow up of radiation therapy patients and the knowledge of the
4679 organ doses they received during the course of their treatment for the primary cancer.

4680

4681 The simpler the geometry, the faster a Monte Carlo simulation typically is. Consequently,
4682 simulations were based initially on stylized phantoms (Snyder *et al.*, 1969), including male and female
4683 adult versions (Kramer *et al.*, 1982; Stabin *et al.*, 1995). Cristy and Eckerman (1987) introduced a series
4684 of stylized pediatric and adult phantoms based on anthropological reference data (ICRP, 1975). Such
4685 phantoms are based on simple geometrical shapes, *e.g.*, an elliptical cylinder representing the arm, torso,
4686 and hips, a truncated elliptical cone representing the legs and feet, and an elliptical cylinder representing
4687 the head and neck. In terms of media, a distinction is drawn only between bone, soft tissue, and lung.
4688 Stylized models have been used for a variety of simulations for radiation protection, nuclear medicine,
4689 and medical imaging (ICRP, 1975; 1991; 1998; ICRU, 1992a; 1992b; NCRP, 1996). Work has been
4690 done on organ doses from medical exposures using stylized models (Stovall *et al.*, 1989; Stovall *et al.*,
4691 2004) and to derive dose-response relationships for patients in epidemiological studies. Because human
4692 anatomy is much more complex than that modeled with stylized models, results based on such model
4693 calculations are controversial and uncertainties may be significant (Lim *et al.*, 1997; Ron, 1997).
4694 Simulated organ and marrow doses based on stylized models have not produced strong correlations with
4695 radiotoxicity (Lim *et al.*, 1997).

4696

4697 A more realistic representation of the human body can be achieved using voxel phantoms. Each
4698 voxel is identified in terms of tissue type (soft tissue, hard bone, *etc.*) and organ identification (lungs,
4699 skin, *etc.*) (Zaidi and Xu, 2007). Lee *et al.* (2006a) analyzed the differences between the use of stylized
4700 phantoms and the use of voxel phantoms and found dosimetric differences of up to 150% in some
4701 organs. Other similar studies showed differences in organ doses as high as 100% (Chao *et al.*, 2001a;
4702 Jones, 1998; Lee *et al.*, 2006a; Petoussi-Henss *et al.*, 2002). The discrepancies were explained by the
4703 geometrical considerations in the stylized phantom, *i.e.*, relative positions of organs and organ shapes.

4704

4705 Many different voxel phantoms have been created. One of the first was used to compute dose
4706 from dental radiography (Gibbs *et al.*, 1984). This was followed by developments of Zubal and Harell
4707 (1992) of a head-torso phantom used to estimate absorbed doses using Monte Carlo simulations (Stabin
4708 *et al.*, 1999). Kramer *et al.* (2003; 2006) developed male and female adult voxel models. Recently, a
4709 voxel-based adult male phantom was introduced with the aim of using it for Monte Carlo modeling of
4710 radiological dosimetry (Zhang *et al.*, 2008). Models of pregnant patients have been introduced (Shi and
4711 Xu, 2004; Shi *et al.*, 2004; Xu *et al.*, 2007). Realistic models of the pregnant patient representing three-,
4712 six-, and nine-month gestational stages were constructed by Bednarz and Xu (2008). The many different
4713 types and properties of voxel phantoms have been reviewed by Zaidi and Xu (2007).

4714

4715 A popular voxel phantom is the adult male model, VIP-Man (Xu *et al.*, 2000; 2005), developed
4716 from anatomical color images of the Visible Man from the Visible Human Project by the National
4717 Library of Medicine (Spitzer and Whitlock, 1998). Part of it is shown in Figure 7.1 and distinguishes
4718 adrenal glands, bladder, esophagus, gall bladder, stomach mucosa, heart muscle, kidneys, large intestine,
4719 liver, lungs, pancreas, prostate, skeletal components, skin, small intestine, spleen, stomach, testes,
4720 thymus, thyroid, gray matter, white matter, teeth, skull CSF, male breast, eye lenses, and red bone
4721 marrow (Spitzer and Whitlock, 1998; Xu *et al.*, 2000). It has a resolution of $0.33 \times 0.33 \times 1 \text{ mm}^3$. The
4722 composition of VIP-Man tissues/materials was done according to ICRU specifications (ICRU, 1989).

4723

4724

4725

4726

4727

4728

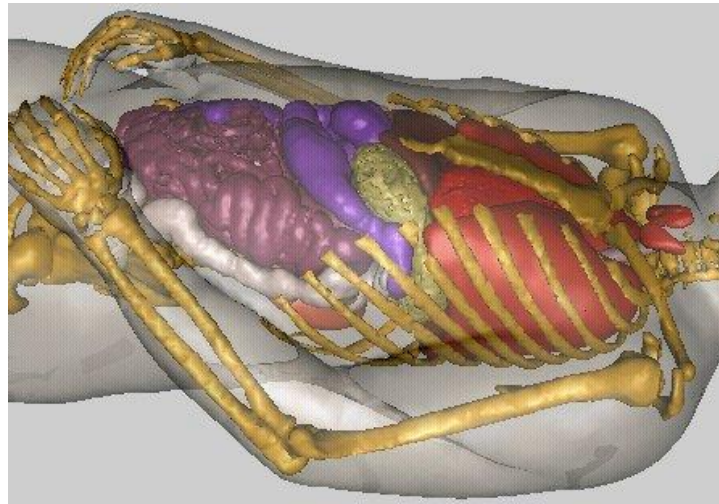
4729

4730

4731

4732

4733



4734 Figure 7.1. Torso of the whole-body adult male model, VIP-Man (Xu *et al.*, 2000), developed from
4735 anatomical color images of the Visible Man from the Visible Human Project by the National Library of
4736 Medicine (Spitzer and Whitlock, 1998).

4737

4738

4739 It has been recognized that secondary doses in radiology and radiation therapy are of particular
4740 concern for pediatric patients. Thus, there was a need for pediatric studies (Francois *et al.*, 1988b). Quite
4741 a few pediatric phantoms have been designed (Caon *et al.*, 1999; Lee and Bolch, 2003; Nipper *et al.*,
4742 2002; Staton *et al.*, 2003; Zankl *et al.*, 1988). Such phantoms cannot be generated by scaling an adult
4743 phantom because of the differences in relative organ position, relative organ sizes, and even organ
4744 composition as a function of a person's age. A series of five computational phantoms of different ages
4745 were constructed from CT images of live patients for use in medical dosimetry (Lee and Bolch, 2003;
4746 Lee *et al.*, 2005; Lee *et al.*, 2006b; Lee *et al.*, 2007a; Lee *et al.*, 2007b; Lee *et al.*, 2008). The phantoms
4747 approximate the bodies of a 9-month-old, 4-year-old, 8-year-old, 11-year-old, and 14-year-old child with
4748 resolutions between $0.43 \times 0.43 \times 3.0 \text{ mm}^3$ and $0.625 \times 0.625 \times 6.0 \text{ mm}^3$. Age-interpolated reference
4749 body masses, body heights, sitting heights, and internal organ masses as well as changes in geometry and
4750 material composition as a function of age and gender were assigned according to ICRP references
4751 (2003a). For the lungs, effective densities were assigned so that the total lung mass would match its
4752 interpolated reference mass (inclusive of pulmonary blood). Later, a newborn phantom was added to this
4753 series (Nipper *et al.*, 2002). Initially these phantoms did not have arms and legs. Extremities are relevant
4754 when computing doses for risk estimations because of their active bone marrow. Thus, a set of truly
4755 whole-body voxel phantoms of pediatric patients were developed through the attachment of arms and
4756 legs (Lee *et al.*, 2006b).

4757

4758 Comparative organ dosimetry between stylized and tomographic pediatric phantoms proved that
4759 stylized phantoms are inadequate for secondary dose estimations (Lee *et al.*, 2005). Here, a series of
4760 photon beams were used to 'irradiate' a stylized 10-year-old child phantom, a stylized 15-year-old child
4761 phantom, and a more realistic 11-year-old male child phantom within MCNPX. For example, dose

4762 coefficients for the thyroid were significantly lower in the UF 11-year-old child phantom, particularly
4763 under the lateral irradiation geometries, than seen in the stylized model.

4764
4765 Voxel phantoms are largely based on CT images and manually segmented organ contours.

4766 Uncertainties are introduced because of image noise and because some representations of mobile organs
4767 may be blurred. Further, in order to match a particular patient as closely as possible, one might have to
4768 interpolate between two different phantoms of a specific age. Organ dimensions can only be modified by
4769 changing the voxel resolution, which generally limits the modification to uniform scaling. Creating a
4770 non-50th percentile individual from a reference 50th-percentile cannot be done realistically for a number
4771 of reasons (for example, because of the difference in the distribution of subcutaneous fat).

4772
4773 To overcome these limitations, voxel data can be combined with surface equations to design
4774 hybrid models. In these phantoms, the boundary of each organ can be adjusted to the desired shape and
4775 volume using patient-specific images and deformable image registration. A series of reference (*i.e.*, 50th
4776 height/weight percentile) pediatric hybrid phantoms based on NURBS (non-uniform B-spline fits; see
4777 Piegl, 1991) surfaces has been developed (Lee *et al.*, 2007a). A similar hybrid approach to phantom
4778 construction has been made in nuclear imaging (Tsui *et al.*, 1994). Segars *et al.* (Garrity *et al.*, 2003;
4779 Segars *et al.*, 1999; Segars, 2001) developed the 4D NURBS-based Cardiac-Torso model that is used as
4780 a deformable model to simulate SPECT images and respiratory motion (Segars and Tsui, 2002).
4781 Initially, phantoms have been used in combination with analytical dose models. Diallo *et al.* (1996)
4782 estimated the dose to areas volumes outside the target volume using a whole-body phantom. However,
4783 Monte Carlo methods are typically the method of choice. In order to use whole-body computational
4784 voxel phantoms with Monte Carlo codes, these either have to be able to handle voxelized geometries,
4785 *i.e.*, a large amount of individual voxels, or to incorporate contoured organ shapes *via* surface equations.

4786 For dose calculations involving real patient data, the information stored for each CT voxel is a
4787 Hounsfield number, which reflects the attenuation coefficient of tissues to diagnostic x rays. In contrast,
4788 for phantom simulations each voxel is usually tagged with a specific material composition and density.
4789 Many of the phantoms listed above have been implemented in Monte Carlo codes. Using Monte Carlo
4790 simulations, two mathematical models of a patient were used to assess the clinical relevance of
4791 computational phantoms (Rijkee *et al.*, 2006). The VIP-Man was implemented in four Monte Carlo
4792 codes: EGS4 (Chao *et al.*, 2001a; 2001b; Chao and Xu, 2001), MCNP (Bozkurt *et al.*, 2000), MCNPX
4793 (Bozkurt *et al.*, 2001), and GEANT4 (Jiang *et al.*, 2005; Zacharatou Jarlskog *et al.*, 2008), to calculate
4794 organ doses for internal electrons (Chao and Xu, 2001), external photons (Chao *et al.*, 2001a), external
4795 electrons (Chao *et al.*, 2001b), external neutrons (Bozkurt *et al.*, 2000; 2001), and external protons (Jiang
4796 *et al.*, 2005; Zacharatou Jarlskog *et al.*, 2008). Pediatric voxel models have been used within GEANT4 to
4797 assess organ-specific doses in proton therapy (Zacharatou Jarlskog *et al.*, 2008). Xu *et al.* (2007)
4798 implemented a pregnant female model based on voxelization of a boundary representation in the Monte
4799 Carlo codes EGS4 and MCNPX. The same group then implemented anatomically realistic models of the
4800 pregnant patient representing three-, six-, and nine-month gestational stages into MCNPX (Bednarz and
4801 Xu, 2008). Further, studies involving parts of a patient's geometry have been done using phantoms, *e.g.*,
4802 with a high-resolution eye model (Alghamdi *et al.*, 2007).

4803

4804 **7.3 Results of Measurements of Secondary Doses in Particle Therapy**

4805

4806 Secondary radiation from therapeutic proton beams has been measured by several groups (see
4807 *e.g.*, Agosteo *et al.*, 1998; Binns and Hough, 1997; Mesoloras *et al.*, 2006; Newhauser *et al.*, 2005b; Polf
4808 and Newhauser, 2005; Roy and Sandison, 2004; Schneider *et al.*, 2002; Tayama *et al.*, 2006; Wroe *et al.*,
4809 2007; Yan *et al.*, 2002). The secondary dose due to neutrons, protons, and photons was studied by

4810 Agosteo *et al.* (1998). The dose due to secondary and scattered photons and neutrons varied from 0.07 to
4811 0.15 milligray per treatment gray (mGy/Gy) at different depths and distances to the field edge. Secondary
4812 doses for proton beam delivery using passive scattered beams of 160 MeV and 200 MeV were measured
4813 by Yan *et al.* (2002) and Binns and Hough (1997), respectively. Neutron equivalent doses of up to 15
4814 millisievert per treatment gray (mSv/Gy) were deduced. Polf and Newhauser (2005) studied the neutron
4815 dose in a passive-scattering delivery system. The neutron dose decreased from 6.3 to 0.6 mSv/Gy with
4816 increasing distance to isocenter and increased as the range modulation increased. Tayama *et al.* (2006)
4817 measured neutron equivalent doses up to 2 mSv/Gy outside of the field in a 200 MeV proton beam.

4818
4819 Measurements were also done using anthropomorphic phantoms and microdosimetric detectors
4820 (Wroe *et al.*, 2007). Equivalent doses from 3.9 to 0.18 mSv/Gy were measured when moving from 2.5
4821 cm to 60 cm distance from the field edge. The dose and dose equivalent delivered to a large phantom
4822 patient outside a primary proton field were determined experimentally using silver halide film, ionization
4823 chambers, rem meters, and CR-39 plastic nuclear track detectors by Moyers *et al.* (2008). The purpose of
4824 another investigation using etch-track detectors was to measure the impact of Ti-alloy prostheses on the
4825 neutron dose during proton and photon radiotherapy (Schneider *et al.*, 2004). Roy and Sandison (2004)
4826 irradiated an anthropomorphic phantom and found secondary neutron doses between 0.1 and 0.26
4827 mSv/Gy for a passive-scattering system with a beam energy of 198 MeV. Secondary neutron dose
4828 equivalent decreased rapidly with lateral distance from the field edge. Subsequently, a systematic study
4829 on secondary neutron dose equivalent using anthropomorphic phantoms was done (Mesoloras *et al.*,
4830 2006). The neutron dose decreased with increasing aperture size and air gap, implying that the brass
4831 collimator contributes significantly to the neutron dose. The contribution by neutrons generated in the
4832 patient increased with field size. Due to the reduced area available for interaction with the patient

4833 collimator, as aperture size increases, externally generated neutrons decrease with field size. The neutron
4834 dose varied from 0.03 to 0.87 mSv/Gy for large fields.

4835

4836 The results from all these studies vary significantly with details of the beam-delivery system and
4837 because the neutron doses decrease rapidly with lateral distance from the proton field, making them
4838 heavily dependent on the precise point of measurement. For a scanning system, measurements of the
4839 secondary neutron dose were performed using a Bonner sphere and CR39 etch detectors by Schneider *et*
4840 *al.* (2002). The measured neutron equivalent doses varied between 2 and 5 mSv/Gy for target volumes
4841 of 211 cm³ (sacral chordoma) and 1253 cm³ (rhabdomyosarcoma), respectively, and 0.002 to 8 mSv/Gy
4842 for lateral distances of 100 cm to 7 cm from the isocenter. In the region of the Bragg peak, the neutron
4843 equivalent dose for a medium-sized target volume reached ~ 1 % of the treatment dose. They concluded
4844 that a beam line using the passive-scattering technique shows at least a ten-fold secondary neutron dose
4845 disadvantage as compared with the spot-scanning technique.

4846

4847 Using Bonner spheres for measurements in carbon as well as in proton beams, it was found that
4848 the neutron ambient dose equivalent in passive-particle radiotherapy is equal to or less than that in
4849 photon radiotherapy with 6 MV beams (Yonai *et al.*, 2008). Microdosimetric data have been obtained in
4850 carbon beams as well (Endo *et al.*, 2007). Downstream of the Bragg peak, the ratio of the neutron dose to
4851 the carbon dose at the Bragg peak was found to be $< 1.4 \times 10^{-4}$ and the ratio of neutron dose to the carbon
4852 dose was $< 3.0 \times 10^{-7}$ on a lateral face of a phantom. The neutron contamination in therapeutic ¹²C beams
4853 has been studied experimentally (Gunzert-Marx *et al.*, 2004; Gunzert-Marx *et al.*, 2008; Iwase *et al.*,
4854 2007; Schardt *et al.*, 2006). The yield, energy spectra, and angular distribution of fast neutrons and
4855 secondary charged particles were measured for 200 MeV/u carbon ions impinging on a water-equivalent
4856 phantom (Gunzert-Marx *et al.*, 2004; Gunzert-Marx *et al.*, 2008). It was found that the neutrons were

4857 mainly emitted in the forward direction. The reported neutron dose of 8 mGy per treatment Gy was less
4858 than 1 % of the treatment dose, whereas the absorbed dose due to secondary charged particles was about
4859 94 mGy per treatment Gy. From the resulting yield of 0.54 neutrons with energies above 20 MeV per
4860 primary ion, a neutron dose of 5.4 mSv per treatment gray equivalent (GyE) delivered to the target was
4861 estimated. Schardt *et al.* (2006) compared neutron doses in proton and carbon-ion therapy using beam
4862 scanning techniques. The secondary neutron absorbed doses per treatment dose were found to be similar.
4863 Although the cross sections for neutron production are much higher for therapeutic carbon- ion beams
4864 compared to proton beams, the neutron absorbed dose is expected to be similar (albeit with a different
4865 neutron energy distribution). Due to the higher LET of carbon ions, fewer particles are needed to deliver
4866 the same target dose compared to protons, approximately compensating for the higher neutron
4867 production per primary particle.

4868

4869 Other than in proton therapy, the depth-dose curves of light-ion beams show a fragmentation tail
4870 beyond the Bragg peak (Matsufuji *et al.*, 2003; Schimmerling *et al.*, 1989). Neutron production by
4871 fragmentation of light ions in water and graphite was investigated by Cecil *et al.* (1980) and by
4872 Kurosawa *et al.* (1999), respectively. Using ^{12}C beams of 200 and 400 MeV/u kinetic energy, the
4873 production of secondary fragments from nuclear reactions in water was investigated at GSI, Darmstadt,
4874 Germany (Gunzert-Marx *et al.*, 2004; Gunzert-Marx *et al.*, 2008; Haettner *et al.*, 2006). Fast neutrons
4875 and energetic charged particles (p-, d-, t-, α -particles) emitted in forward direction were detected by a
4876 BaF2/plastic scintillation-detector telescope and neutron energy spectra were recorded using time-of-
4877 flight techniques.

4878

4879

7.4 Results for Calculated Secondary Doses to Patients

4880

4881 Monte Carlo simulations have been used in several studies of secondary doses. Agosteo *et al.*
4882 (1998) analyzed the neutron dose for a passive-beam delivery system with a beam energy of 65 MeV.
4883 The absorbed dose due to neutrons varied between 3.7×10^{-7} and 1.1×10^{-4} Gy per treatment Gy
4884 depending on the distance from the field. For a high-energy proton beam, the secondary dose due to
4885 photons and neutrons varied from 0.146 to 7.1×10^{-2} mGy per treatment Gy for depths ranging from 1 to
4886 8 cm and distances to the field edge ranging from 9 to 15 cm. Polf and Newhauser (2005) found in their
4887 MCNPX calculations that the neutron dose decreased from 6.3 to 0.63 mSv/Gy as the distance from the
4888 field center was increased from 50 to 150 cm. In a subsequent study this group has reported equivalent
4889 doses up to 20 mSv/Gy (Zheng *et al.*, 2007). The dose increased as the modulation extent was increased.
4890 The neutron dose equivalent per therapeutic proton absorbed dose was estimated for passively spread
4891 treatment fields using Monte Carlo simulations by Polf *et al.* (2005). For a beam with 16 cm range and a
4892 5×5 cm² field size, the results show an equivalent dose of 0.35 mSv/Gy at 100 cm from the isocenter.
4893 Further, Monte Carlo calculations for a passive-scattering proton therapy treatment nozzle were done for
4894 various settings of the range modulator wheel (Polf and Newhauser, 2005). Zheng *et al.* (2007) also
4895 analyzed secondary radiation for a passive-scattering proton therapy system using Monte Carlo
4896 simulations. The whole-body effective dose from secondary radiation was estimated for a passively
4897 scattered proton treatment beam incident on an anthropomorphic phantom (Taddei *et al.*, 2008). The
4898 results show a dose equivalent of 567 mSv, of which 320 mSv was attributed to leakage from the
4899 treatment head. Using the MCNPX code it was shown that the range modulation wheel is the most
4900 intense neutron source of any of the beam-modifying devices within the treatment head (Perez-Andujar
4901 *et al.*, 2009). Simulations by Moyers *et al.* (2008) illustrated that most of the neutrons entering the
4902 patient are produced in the final patient-specific aperture and pre-collimator just upstream of the
4903 aperture, not in the scattering system. Additionally, Monte Carlo simulations were performed using the
4904 FLUKA code for a 177 MeV scanned proton beam by Schneider *et al.* (2002). For the proton-beam

4905 scanning system, neutron equivalent doses between 2 and 5 mSv/Gy were measured for target volumes
4906 of 211 cm³ (sacral chordoma) and 1253 cm³ (rhabdomyosarcoma), respectively, and 0.002 to 8 mSv/Gy
4907 for lateral distances of 100 cm to 7 cm from the isocenter (Schneider *et al.*, 2002).

4908

4909 Secondary particle production in tissue-like and shielding materials for light and heavy ions was
4910 done using the Monte Carlo code SHIELD-HIT (Gudowska *et al.*, 2002; Gudowska *et al.*, 2004). For ion
4911 beams, simulations of secondary particle production and absorbed dose to tissue were done by
4912 Gudowska and Sobolevsky (Gudowska *et al.*, 2007; Gudowska and Sobolevsky, 2005). For a 200 MeV
4913 proton beam, these authors reported the neutron absorbed dose delivered to the water and A-150
4914 phantoms of about 0.6 % and 0.65 % of the total dose, respectively. The calculated absorbed dose due to
4915 secondary neutrons produced by a 390 MeV/u ¹²C beam in the water and A-150 phantoms were 1.0%
4916 and 1.2% of the total dose, respectively.

4917

4918 Further, simulations using a Monte Carlo model for light-ion therapy (MCHIT) based on the
4919 GEANT4 toolkit were done by Pchenichnov *et al.* (2005). The energy deposition due to secondary
4920 neutrons produced by ¹²C beams in water was estimated to be 1 % to 2 % of the total dose, *i.e.*, slightly
4921 above the neutron contribution (~ 1 %) induced by a 200 MeV proton beam. Morone *et al.* (2008)
4922 studied the neutron contamination in an energy modulated carbon-ion beam using the FLUKA Monte
4923 Carlo.

4924

4925 The mathematical anthropomorphic phantoms EVA-HIT and ADAM-HIT have been used in the
4926 Monte Carlo code SHIELD-HIT07 for simulations of lung and prostate tumors irradiated with light ions
4927 (Hultqvist and Gudowska, 2008). Calculations were performed for ¹H, ⁷Li, and ¹²C beams in the energy
4928 range 80 to 330 MeV/u. The secondary doses to organs due to scattered primary ions and secondary

4929 particles produced in the phantoms were studied, taking into account the contribution from secondary
4930 neutrons, secondary protons, pions, and heavier fragments from helium to calcium. The calculated doses
4931 to organs per dose to target (tumor) were of the order of 10^{-6} to 10^{-1} mGy/Gy and generally decrease with
4932 increasing distance from the target.

4933

4934 Figure 7.2 summarizes some of the experimental and theoretical results of neutron doses as a
4935 function of lateral distance from the field edge for various proton-beam facilities and beam parameters.
4936 These data share a very similar trend although the values show significant variations associated with
4937 different beams and field parameters.

4938

4939
4940
4941
4942
4943
4944
4945
4946
4947
4948
4949
4950
4951
4952
4953
4954
4955
4956
4957
4958

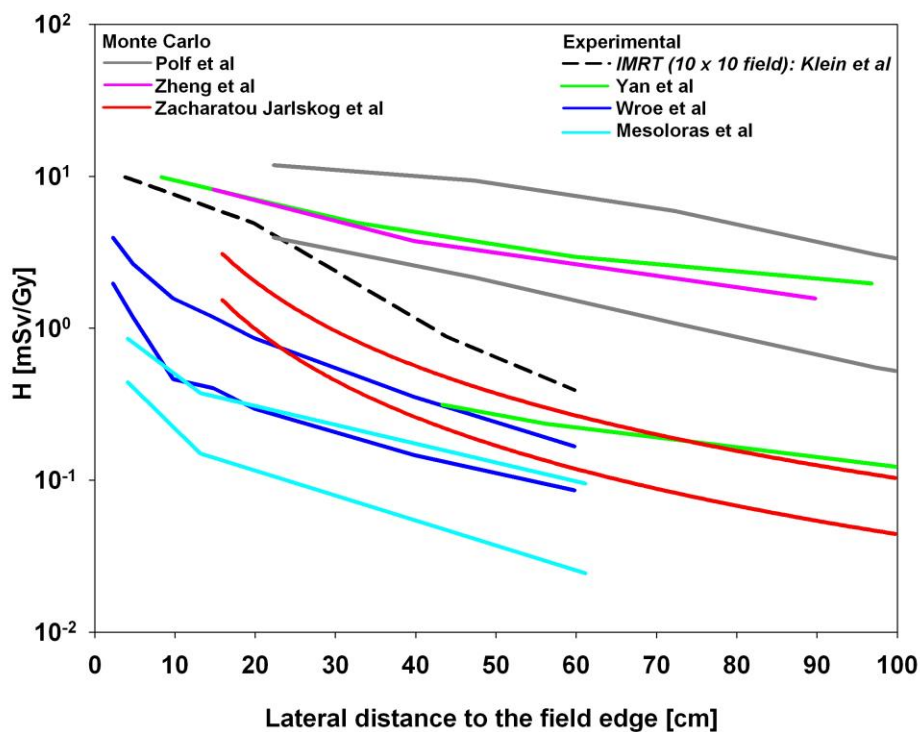


Figure 7.2. Equivalent doses as a function of distance to the field edge for therapeutic proton beams using passive-scattering techniques. Shown are data from experiments (Mesoloras *et al.*, 2006; Wroe *et al.*, 2007; Yan *et al.*, 2002) and calculations (Polf and Newhauser, 2005; Zacharatou Jarlskog and Paganetti, 2008a; Zheng *et al.*, 2007). In most cases, several beam parameters were considered and we plot two curves, the maximum and minimum findings. Also shown is the scattered photon dose for an intensity-modulated x-radiation therapy (IMRT) case assuming a 10 cm × 10 cm field (Klein *et al.*, 2006).

4959 While the data shown in Figure 7.2 help to understand differences among different beam-delivery
4960 conditions, epidemiological studies require the use of organ-specific doses for proper risk analysis. To
4961 this end, a number of recent studies have used whole-body patient phantoms and Monte Carlo
4962 simulations to calculate organ doses for different proton treatment conditions.

4963

4964 Organ doses out of the target (tumor) volume in the whole-body VIP-Man model for proton
4965 therapy treatments have been studied by Jiang *et al.* (2005) assuming treatments of a tumor in the head
4966 and neck region and a tumor in the lung. The simulations were based on the GEANT4 Monte Carlo code.
4967 The treatment head simulation incorporated the different settings (combinations of scatterers, variable
4968 jaws, *etc.*) necessary to simulate hardware configurations for each treatment field. The average neutron
4969 dose equivalent for organs of the abdomen region was 1.9 and 0.2 mSv/Gy for a lung tumor and
4970 paranasal sinus treatment plans, respectively. The dose in the red bone marrow was found to be 3 to 4
4971 orders of magnitude lower than the prescribed dose to the tumor volume. However, the dose distribution
4972 is highly non-uniform. The yield, the quality factors, and the absorbed doses from neutrons produced
4973 internally in the patient's body and externally in the treatment nozzle were analyzed for each organ.
4974 Internal neutrons include the neutrons produced in the patient *via* interactions of primary protons and the
4975 later generation of neutrons originating from them. In contrast, external neutrons are those generated in
4976 the treatment nozzle and also the next generation of neutrons generated by them in the patient. Jiang *et*
4977 *al.* (2005) reported, for internal and external neutrons, the equivalent doses for individual organs. The
4978 simulations confirmed that the externally produced neutrons dominate the secondary neutron dose.

4979

4980 Using a Monte Carlo model of a proton therapy treatment head and a computerized
4981 anthropomorphic phantom, Fontenot *et al.* (2008) determined that the effective dose from secondary
4982 radiation per therapeutic dose for a typical prostate patient was ~ 5.5 mSv/Gy. The secondary dose

4983 decreased with distance from the isocenter, with a maximum of 12 mSv/Gy for the bladder. The specific
4984 aim of the study by Taddei *et al.* (2009) was to simulate secondary doses to organs following cranio-
4985 spinal irradiation with proton therapy. A passive-scattering proton treatment unit was simulated using
4986 Monte Carlo simulations methods and a voxelized phantom to represent the pediatric patient. For a
4987 treatment using delivering 30.6 Gy to the target plus a boost of 23.4 Gy, the predicted effective dose
4988 from secondary radiation was 418 mSv, of which 344 mSv were from neutrons originating outside the
4989 patient. Monte Carlo simulations of secondary radiation for passively scattered and scanned-beam proton
4990 irradiation of cranio-spinal lesions were also done using a male phantom (Newhauser *et al.*, 2009).
4991 Zacharatou Jarlskog *et al.* (2008) simulated proton beam therapy for pediatric patients and considered
4992 several proton fields of varying field size, beam range and modulation width for the treatment of tumors
4993 in the intracranial region. To simulate age- and organ-specific equivalent doses, one adult phantom and
4994 five pediatric phantoms (a 9-month old, a 4-year old, an 8-year old, an 11-year old, and a 14-year old)
4995 were considered. Organ doses were presented as a function of organ index for up to 48 different organs
4996 and structures. The organ-specific neutron equivalent doses varied as a function of field parameters.
4997 Further, variations in dose between different organs was caused by differences in volume, in their
4998 distance to the target, and in their elemental composition. For example, a greater range in tissue requires
4999 a higher beam energy and thus more material (tissue) is needed to reduce the penetration of the proton
5000 beam. Consequently, simulations based on the voxel phantom of a 4-year-old resulted in neutron
5001 equivalent doses of about 1.3 mSv/Gy in the lungs for short-range fields and about 2.7 mSv/Gy for long-
5002 range fields. Neutron equivalent doses to organs increased with treatment volume because the number of
5003 protons necessary to deposit the prescription dose in the target had to increase. The neutron equivalent
5004 dose due to external neutrons typically increases with decreasing field size (Gottschalk, 2006; Paganetti
5005 *et al.*, 2006). It was found that for a small target volume, the contribution of neutrons from the treatment
5006 head can be close to 99 % of the total neutron contribution, while for a large target volume it can go

5007 down to ~ 60 %. The neutron equivalent dose was as high as 10 mSv/Gy in organs located near the target
5008 but decreased rapidly with distance (Zacharatou Jarlskog *et al.*, 2008). Figure 7.3 shows how the thyroid,
5009 esophagus and liver equivalent doses vary significantly with patient age (Zacharatou Jarlskog *et al.*,
5010 2008). Younger patients are exposed to a higher neutron contribution from the treatment head because of
5011 their smaller bodies. With increasing distance from the target, doses vary more significantly with patient
5012 age. For example, simulation based on the phantom of a 9-month old showed ~ 50 % higher dose to the
5013 thyroid compared to simulations based on an adult phantom. In the case of esophagus, the ratio of the
5014 dose to the phantoms of the adult to the 9-month old child was roughly a factor of 4. Simulations showed
5015 that the maximum neutron equivalent dose delivered to an organ was ~ 10 mSv/Gy (Zacharatou Jarlskog
5016 *et al.*, 2008). Organs at larger distances from the target will show higher dependency on the patient age;
5017 *e.g.*, for the same field, the factor of dose increase for liver is approximately 20.
5018

5019
5020
5021
5022
5023
5024
5025
5026
5027
5028
5029
5030
5031
5032
5033
5034

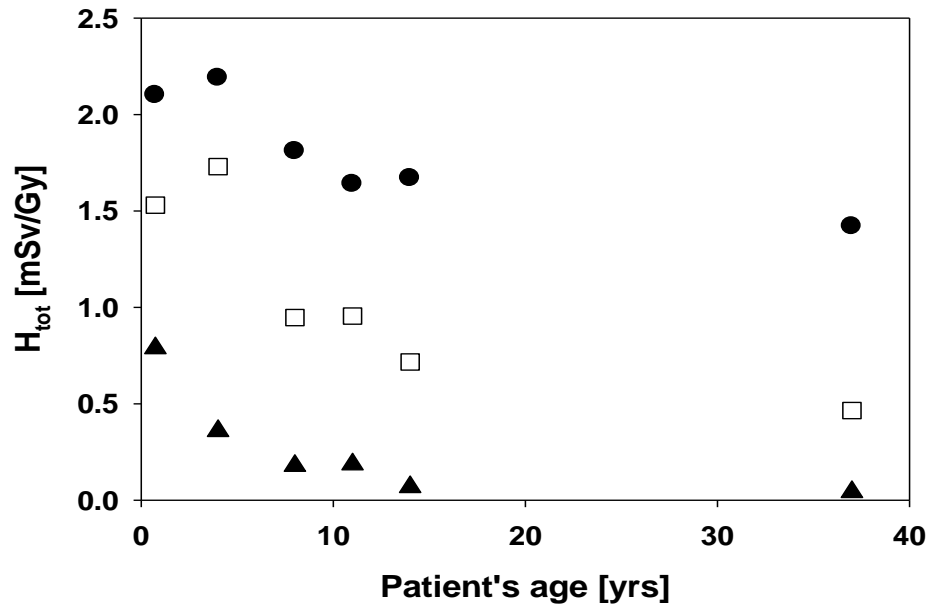


Figure 7.3. Organ equivalent dose in the thyroid (circles), esophagus (squares) and liver (triangles) as a function of patient age averaged over six different cranial treatment fields. (Zacharatou Jarlskog *et al.*, 2008)

5035 Table 7.1 shows, averaged over eight proton therapy fields used in the head and neck region
5036 (Zacharatou Jarlskog *et al.*, 2008), how the equivalent doses compare with doses from chest CT scans.
5037 Apparently, for young patients it could correspond to on average of about 25 additional CT scans for the
5038 fields considered. A similar analysis was done by Moyers *et al.* (2008). In their study, the total dose
5039 equivalent outside of the field was similar to that received by patients undergoing IMRT. At the center of
5040 a patient, the dose equivalent for a full course of treatment was comparable to that delivered by a single
5041 whole-body CT scan.
5042

5043

5044

5045 Table 7.1. Equivalent doses (in mSv) for thyroid and lung due to secondary neutron radiation for a 70 Gy
5046 treatment of a brain lesion (averaged over eight treatment fields). The values are compared to the
5047 radiation to be expected from a chest CT scan as a function of patient's age. (Zacharatou Jarlskog *et al.*,
5048 2008)

5049

5050

	4-year old	11-year old	14-year old	Average
H to thyroid from proton therapy	195.4	166.0	155.1	
H to thyroid from chest CT scan	9.0	5.2	6.9	
Therapy / CT scan (thyroid)	21.6	31.8	22.4	25.3
H to lung from proton therapy	128.2	54.7	34.7	
H to lung from chest CT scan	13.9	12.0	12.6	
Therapy / CT scan (lung)	9.3	4.5	2.8	5.5

5051

5052

5053

5054

5055

5056

5057 In order to apply the appropriate energy-dependent radiation weighting factor for neutrons, the
5058 energy of the neutrons causing dose deposition in organs needs to be determined. Figure 7.4 shows the
5059 energy distribution of neutrons at the surface of several organs (Jiang *et al.*, 2005). Fast neutrons lose
5060 most of their kinetic energy in the initial relatively small number of scatterings. In the low/thermal
5061 energy region, there is a decreasing probability for neutrons to slow down, causing a large number of
5062 elastic scatterings in soft tissues with a prevailing field of low-energy neutrons in the patient. However,
5063 the dose deposition events (and thus the determination of the radiation weighting factor) are mainly due
5064 to higher energy neutrons (> 10 MeV). Zheng *et al.* (2008) calculated the neutron spectral fluence using
5065 Monte Carlo simulations
5066

5067

5068

5069

5070

5071

5072

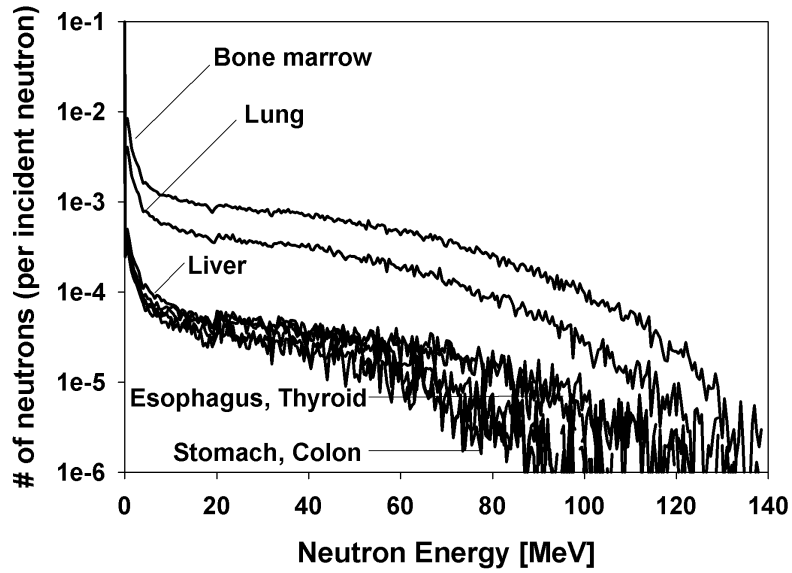
5073

5074

5075

5076

5077



5078 Figure 7.4. Energy distribution of external neutrons (per incident neutron entering the patient) arriving at
5079 the outer surface of some major organs lateral to the field edge under a head and neck tumor plan. (Jiang
5080 *et al.*, 2005)

5081

5082 **7.5 Biological Effects of Secondary Particles (Low- and High-LET Particles, Low Doses)**

5083

5084 The radiation quality of particles is often classified by their linear energy transfer (LET).

5085 Although there is not a direct relationship between LET and biological effect, higher linear energy

5086 transfer radiations in most situations cause more severe damage to tissue. The parameter often used to

5087 compare the biological effect of different radiations in radiation therapy is the relative biological

5088 effectiveness (RBE). The RBE is defined as the ratio of the doses required by two different types of

5089 radiation to cause the same level of effect for a specified end point. The RBE depends on dose, dose rate,

5090 overall treatment time, fractionation, tissue, and endpoint. It is only defined with respect to a reference

5091 radiation. To understand the effect of scattered or secondary radiation in ion therapy one has to examine

5092 low-dose radiation effects. Because the RBE is defined for a given level of effect and increases with

5093 decreasing dose (neglecting the potential effect of low-dose hypersensitivity and threshold effects), one

5094 has to consider RBE_{max} , *i.e.*, the RBE extrapolated to the zero dose level on the survival curves for a

5095 specified radiation such as neutrons and the reference radiation.

5096

5097 The dose deposited by secondary neutron radiation is typically quite low. While it may be

5098 straightforward with simple laboratory cell systems to extrapolate high- or medium-level dose-response

5099 data to low doses, it is very difficult to extrapolate to low doses with complex systems. This is due to

5100 competing effects influencing in particular the low dose region. The biological effectiveness of radiation

5101 depends on many different physical factors (*e.g.*, dose, dose rate, track structure) and biological factors

5102 (*e.g.*, tissue type, endpoint, repair capacity, and intrinsic radiosensitivity).

5103

5104 The biological effect of neutrons is a complex matter because neutrons are indirectly ionizing. At

5105 very low energies (below 1 MeV) neutrons contribute to absorbed dose by elastic scattering processes

5106 (protons); by protons produced in neutron capture in nitrogen; by recoil of carbon, oxygen, nitrogen
5107 atoms; and partly by γ -rays from thermal neutron capture processes in hydrogen. For higher energy
5108 neutrons (around 1 to 20 MeV) a substantial amount of dose is deposited *via* recoil protons.

5109

5110 To assess the risk of developing a second tumor from radiation therapy, the parameter of interest
5111 is fractionated low-dose delivery leading to carcinogenesis. Such data are sparse, in particular at doses
5112 below 0.1 Gy. Furthermore, the data on carcinogenesis in animal models based on fission neutrons reveal
5113 that the dose-response relationship is non-linear (except for the initial portion), making extrapolation to
5114 low doses very difficult and unreliable. As discussed by Edwards (1999), it is very difficult, and
5115 associated with big uncertainties, to fit the correct initial slopes to neutron and reference radiations
5116 because of the significant experimental uncertainties.

5117

5118 The vast majority of data on neutron RBE has been obtained using fission neutrons. Fission
5119 neutrons typically have energies between (on average) 1 and 1.5 MeV. It has been shown (Shellabarger
5120 *et al.*, 1980) that even single doses of 1 mGy of 0.43 MeV neutrons have the potential to increase the
5121 tumor induction rate for fibroadenomas in rats. Broerse *et al.* (1986) have shown for the incidence of
5122 benign mammary tumors in rats that 0.5 MeV neutrons are significantly more effective than 15 MeV
5123 neutrons. Others have studied this as well (Fry, 1981). Because of the lack of high-energy neutron
5124 carcinogenesis data, extrapolations have been made of the energy dependence of the measured neutron
5125 (RBE_{max}) values up to much higher neutron energies (ICRP, 1991; 2003b; 2008; ICRU, 1986; NCRP,
5126 1990; 1991).

5127

5128 Based on the human data from neutron dose estimates to Japanese atomic bomb survivors (Egbert
5129 *et al.*, 2007; Nolte *et al.*, 2006), two independent groups have estimated the most likely RBE_{max} for

5130 neutron-induced carcinogenesis in humans to be 100 for solid-cancer mortality (Kellerer *et al.*, 2006) and
5131 63 for overall cancer incidence (Little, 1997), respectively. The radiation field to which the atomic bomb
5132 survivors were exposed is of course much different from the conditions in radiation therapy.

5133

5134 As has been discussed, for example, in the review by Kocher *et al.* (2005) and by Brenner and
5135 Hall (2008b), considerable uncertainties exist for neutron RBE values because of the paucity of data on
5136 RBEs at energies outside the range of about 0.1 to 2 MeV; *i.e.*, the energies of most fission neutrons.
5137 Reviews by the NCRP (1990) and Edwards (1999) did not include data for neutrons above 20 MeV.

5138

5139 **7.6 Concept of Equivalent Dose to Patient Due to Secondary Particles**

5140

5141 **7.6.1 Radiation Weighting Factors**

5142

5143 In the low-dose region of secondary radiation, the use of the term “radiation weighting factor”
5144 instead of RBE emphasizes the fact that the quality or weighting factor is typically not endpoint- or dose-
5145 dependent. The radiation weighting factor superseded the quantity “quality factor” (ICRP, 1991). The
5146 conservative radiation weighting factors (w_R) as defined, for example, by the ICRP (2003b; 2008), can be
5147 associated with RBE_{max} . Thus, for radiation protection involving relatively low dose levels, the radiation
5148 weighting factor is defined as a conservative and simplified measure of the RBE. For radiation protection
5149 purposes one is interested in defining a parameter that is largely independent of dose and biological
5150 endpoint (*e.g.*, a maximum RBE). There are three main reasons for this: first, dose levels of interest in
5151 radiation protection are typically low; second, recommendations for the general public should be easy to
5152 understand; and third, a radiation protection recommendation does not aim at accuracy but provides a
5153 conservative guideline.

5154

5155 For γ rays, fast electrons, and x rays, a radiation weighting factor of 1 can be assumed (ICRP,
5156 1991) (although there is evidence based on chromosomal aberration data and on biophysical
5157 considerations that, at low doses, the biological effectiveness per unit absorbed dose of standard x rays
5158 may be about twice that of high-energy photons). The ICRP recommends for photons and electrons a
5159 radiation weighting factor of 1, for protons a weighting factor of 2, and for alpha particles a weighting
5160 factor of 20 (ICRP, 2008).

5161

5162 For neutrons, the ICRP defines an energy dependent bell-shaped curve with a maximum
5163 weighting factor of 20 at around 1 MeV (ICRP, 1991; 2003b; 2008). Ambiguities in weighting factor
5164 assignments exist for uncharged particles. For example, fast neutrons deposit their energy mostly *via*
5165 secondary protons. Nevertheless, the maximum radiation weighting factor recommendation for neutrons
5166 is 20, while the factor for protons has a constant value of 2.

5167

5168 One has to keep in mind that radiation weighting was recommended for radioprotection purposes
5169 and the applicability to secondary radiation produced in the patient is questionable. The weighting factors
5170 are given for external radiation and could be applied to the secondary radiation produced in the beam-
5171 line components. However, the secondary radiation produced in the patient can be regarded as an internal
5172 radiation source and the use of weighting factors in this case is problematic. The quality factor is defined
5173 as a function of the unrestricted linear energy transfer, whereas the radiation weighting factor is defined
5174 as a function of particle and particle energy. Both concepts should result in similar outcomes. However,
5175 in particular for indirectly ionizing radiation like neutrons, some inconsistencies exist with these
5176 concepts as was discussed in section 7.2.2.

5177

5178 **7.6.2 Equivalent Dose**

5179

5180 The ICRP also defines a radiation protection quantity, equivalent dose, as the average absorbed
5181 dose in an organ or tissue multiplied by the radiation weighting factor for the type, and sometimes the
5182 energy, of the radiation (ICRP, 2003b). The radiation weighting factor converts the absorbed dose in
5183 gray (Gy) to sievert (Sv). Another radiation protection quantity is “effective dose” which normalizes
5184 partial-body exposures in terms of whole-body stochastic risk (ICRP, 2003b). The ICRP developed the
5185 concept of effective dose in order to recommend an occupational dose limit for radiation protection.
5186 However, effective dose is not measurable or additive, and it depends on the so-called tissue weighting
5187 factors that are subject to revision. The ICRP has stated that, for situations involving high doses, doses
5188 should be evaluated in terms of absorbed dose and, where high-LET radiations (*e.g.*, neutrons or alpha
5189 particles) are involved, an absorbed dose weighted with an appropriate RBE should be used. Further, the
5190 ICRP (1991) states that the effective dose concept should not be used to indicate risk for specific
5191 individuals.

5192

5193 When estimating equivalent doses under various conditions, *e.g.*, in the case of a patient treated
5194 with radiation therapy, the dose rate (fractionation) has to be taken into account. Radiation therapy is
5195 typically delivered in multiple fractions, *e.g.*, on 30 consecutive days (typically excluding weekends).
5196 Most risk models are valid for a single irradiation. The difference in effect between a single fraction and
5197 a multiple fraction irradiation with the same dose is due to the difference in repair capacity of the tissues.
5198 In order to account for this effect, a dose and dose-rate effectiveness factor (DDREF) has to be applied.
5199 DDREF is 1 for neutrons due to their high LET nature (Kocher *et al.*, 2005). DDREF is applied for doses
5200 below 0.2 Gy and for chronic exposure. The Biological Effects of Ionizing Radiation (BEIR) committee
5201 (BEIR, 2006) recommends the use of an average correction factor of 1.5 to take into account

5202 fractionation when using dosimetric data for risk analysis for solid tumors and linear dose-response
5203 relationships. While this is appropriate for photon radiation, equivalent doses from high-LET radiation,
5204 like neutrons, should not be scaled using DDREF when dealing with low dose exposure because of the
5205 different biological mechanisms with which neutrons interact with tissues (Kocher *et al.*, 2005). There
5206 can even be an inverse dose-rate effect describing a situation where the biological effectiveness of high-
5207 LET radiation increases with decreasing dose rate. However, this effect is typically not seen at lower
5208 doses.

5209

5210 **7.7 Early and Late Effects**

5211

5212 Volumes in the patient receiving dose can be separated into three regions: 1) the target (tumor),
5213 characterized by the planning target volume (PTV) treated with the therapeutic dose; 2) organs at risk
5214 typically defined in the tumor vicinity (these may intersect with the beam path and are allowed to receive
5215 low to intermediate doses); and 3) the rest of the patient body, which may receive low doses.

5216

5217 Dose delivered to healthy tissues can lead to severe side effects, *e.g.*, affecting the functionality of
5218 organs (see *e.g.*, Nishimura *et al.*, 2003) or even causing a second cancer. In the tumor and along the path
5219 of the therapeutic radiation beam, one may have to accept a risk for developing even significant side
5220 effects because of the therapeutic benefit. A significant number of second tumors is found in the margins
5221 of the target volume (Dorr and Herrmann, 2002). Such effects are not necessarily proportional to dose.
5222 For example, if the dose is prescribed with the aim of killing tumor cells without leaving behind cells
5223 with the potential for mutation, the risk of radiation-induced cancer within the target volume might be
5224 smaller than the risk in the surrounding tissues receiving intermediate doses.

5225

5226 Organs that are part of the patient volume imaged for treatment planning are considered in the
5227 treatment planning process by using dose constraints. They typically receive medium doses ($> 1\%$ of the
5228 prescribed target dose). The dose is due to scattering of the particle beam and due to the fact that these
5229 organs lie within the primary beam path. The total dose delivered is termed integral dose. Other organs
5230 are further away from the target volume and receive low doses ($< 1\%$ of the prescribed target dose).
5231 These organs are typically not imaged or outlined for treatment planning. The dose is a result of radiation
5232 being scattered at large angles in the treatment head, radiation leakage through the treatment head, and
5233 secondary radiation, *i.e.*, radiation generated by interactions of the primary radiation with material in the
5234 treatment head or the patient. Some treatment techniques, while aiming at highly conformal dose to the
5235 target, do not necessarily deliver lower doses to areas distant from the target. Several authors have
5236 cautioned that compared with conventional radiotherapy, the use of IMRT or proton therapy could result
5237 in a higher incidence of radiation-induced second cancers (Hall, 2006; Hall and Wu, 2003; Kry *et al.*,
5238 2005; Paganetti *et al.*, 2006). Because doses are low, the main concerns are late effects and, in particular,
5239 second cancers.

5240

5241 Treatment-related cancers are a well-recognized side effect in radiation oncology (Schottenfeld
5242 and Beebe-Dimmer, 2006; Tubiana, 2009; van Leeuwen and Travis, 2005). The likelihood of developing
5243 a second cancer depends on both the entire irradiated volume and on the volume of the high-dose region.
5244 With respect to radiation-induced sarcoma, the main concern is not primarily the dose far away from the
5245 beam edge, but the dose delivered directly in the beam path. The second malignancy rates in children
5246 from incidental normal tissue dose are of the order of 2 to 10 % 15 to 20 years after radiotherapy
5247 (Broniscer *et al.*, 2004; Jenkinson *et al.*, 2004; Kuttesch Jr. *et al.*, 1996). Others have estimated the
5248 cumulative risk for the development of second cancers over a 25-year follow-up interval as ranging from
5249 5 to 12 % (de Vathaire *et al.*, 1989; Hawkins *et al.*, 1987; Olsen *et al.*, 1993; Tucker *et al.*, 1984) with

5250 conventional radiation therapy as a predisposing factor (de Vathaire *et al.*, 1989; Potish *et al.*, 1985;
5251 Strong *et al.*, 1979; Tucker *et al.*, 1987). Radiation can cause intracranial tumors after therapeutic cranial
5252 irradiation for leukemia (Neglia *et al.*, 1991), tinea capitis (Ron *et al.*, 1988; Sadetzki *et al.*, 2002), and
5253 intracranial tumors (Kaschten *et al.*, 1995; Liwnicz *et al.*, 1985; Simmons and Laws, 1998). The median
5254 latency of second cancers has been reported as 7.6 years in one group of patients (Kuttesch Jr. *et al.*,
5255 1996). In patients with pituitary adenoma a cumulative risk of secondary brain tumors of 1.9 to 2.4 % at
5256 ~ 20 years after radiotherapy and a latency period for tumor occurrence of 6 to 21 years was reported
5257 (Brada *et al.*, 1992; Minniti *et al.*, 2005). Brenner *et al.* (2000) examined second cancers from prostate
5258 radiotherapy and found that the absolute risk was 1.4 % for patients surviving longer than 10 years. The
5259 relative risk of developing a second cancer is less in patients with smaller treatment volumes (Kaido *et*
5260 *al.*, 2001; Loeffler *et al.*, 2003; Shamisa *et al.*, 2001; Shin *et al.*, 2002; Yu *et al.*, 2000). Data on
5261 radiation-induced cancer and mortality after exposure to low doses data have been summarized in the
5262 BEIR VII (Biological Effects of Ionizing Radiation) report for various organs (BEIR, 2006).

5263

5264 The relative risk of irradiated versus non-irradiated population for fatal solid cancer for persons
5265 30 years of age for 1 Sv of whole-body irradiation was estimated to be 1.42 (Preston *et al.*, 2004). Pierce
5266 *et al.* (1996) estimated lifetime excess risks of radiation-associated solid cancer death rates and lifetime
5267 excess risks for leukemia as a function of age, gender, and dose. The risk was higher for those exposed at
5268 younger ages (Imaizumi *et al.*, 2006). High rates of late (50 years after exposure) second cancers are
5269 pertinent to risk estimates based on patient follow-up data extending to only 10 to 20 years. Thus,
5270 estimates of radiation-induced cancer risk in radiation treated patients must be considered to be less than
5271 the actual lifetime risk.

5272

5273 Often the highest incidence of radiation-associated second tumors occurs at field peripheries and
5274 not at the field center (Epstein *et al.*, 1997; Foss Abrahamsen *et al.*, 2002). However, even doses
5275 delivered far outside the main field have been associated with second tumors. Decades ago, the scalps of
5276 children in Israel were irradiated to induce alopecia for the purpose of aiding the topical treatment of
5277 tinea capitis (Ron *et al.*, 1988). Mean doses to the neural tissue were ~ 1.5 Gy. The relative risk of tumor
5278 formation at 30 years compared with the general population was 18.8 for schwannomas, 9.5 for
5279 meningiomas, and 2.6 for gliomas with a mean interval for tumor occurrence of 15, 21, and 14 years,
5280 respectively. Sadetzki *et al.* (2002) report on the development of meningiomas after radiation for tinea
5281 capitis with a time from exposure to meningioma diagnosis of 36 years. A recent study has concluded
5282 that, even 40 years after initial radiation treatment of cervical cancer, survivors remain at an increased
5283 risk of second cancers (Chaturvedi *et al.*, 2007).

5284

5285 Second cancers are late effects and thus of particular importance in the treatment of childhood
5286 cancers. For childhood cancers, the relative five-year survival rate has risen from 56 % for children
5287 diagnosed between 1974 to 1976 to 79 % for those diagnosed in the period 1995 to 2001 (Jemal *et al.*,
5288 2006); the current ten-year survival rate is ~ 75 % (Ries *et al.*, 2006). Although the majority of children
5289 with cancer can expect a long life post-treatment, a second cancer will occur in some pediatric cancer
5290 patients following successful treatment of the original disease (Ron, 2006). Most published data are
5291 based on the Childhood Cancer Survivor Study, an ongoing multi-institutional retrospective study of
5292 over 14,000 cases (Bassal *et al.*, 2006; Kenney *et al.*, 2004; Neglia *et al.*, 2001; Sigurdson *et al.*, 2005).

5293

5294

7.8 Models

5295

5296 **7.8.1 Model Concepts**

5297

5298 Cancer risk is specified as either the risk for incidence or the risk for mortality. Dose-response
5299 relationships are typically defined as a function of age, gender, and site. The cancer incidence rate at a
5300 given point in time is defined as the ratio of number of diagnosed individuals in a time interval divided
5301 by the interval duration and the total number of unaffected individuals at the beginning of this interval.
5302 Cancer risk, on the other hand, is defined as the probability for disease occurrence in the population
5303 under observation, *i.e.*, risk equals the ratio of number of diagnosed to total number of individuals in the
5304 given time interval. The baseline risk refers to the incidence of cancer observed in a group without a
5305 specific risk factor (*e.g.*, the un-irradiated reference population). In order to obtain a measure of the
5306 relation between the incidence rate in the exposed population and the incidence rate in the unexposed
5307 population, one can use either their difference or their ratio.

5308

5309 Quite often, risk estimates are performed using whole-body effective doses and organ weighting
5310 factors (EPA, 1994; 1999; ICRP, 1991; 2003b; NCRP, 1993). The NCRP defines probabilities of fatal
5311 cancer for bladder, bone marrow, bone surface, breast, esophagus, colon, liver, lung, ovary, skin,
5312 stomach, thyroid, and remainder of the body (NCRP, 1993). The ICRP defines a whole-body effective
5313 dose with organ-specific weighting factors (ICRP, 2003b). The methodology was originally designed for
5314 setting radiation protection limits by making sure the radiation exposures to workers are controlled to a
5315 level that is considered to be safe (ICRP, 1991; 2003b). Tissue weighting factors employed by the NCRP
5316 and ICRP for the effective dose are gender- and age-averaged values applying a radiation independent
5317 dose-rate correction. Thus, these models are rough approximations which yield a nominal risk value of 5
5318 $\times 10^{-2}/\text{Sv}$. Effective doses are suited for radiation protection studies but it has to be stated clearly that
5319 they are not suited for risk models for secondary cancer, which are site specific. The ICRP has advised

5320 against the use of effective dose for the risk of a single patient and of a site-specific tumor.
5321 Epidemiological risk assessments should be based on organ-specific equivalent doses. The BEIR report
5322 (2006) provides formalisms to calculate organ-specific risks of cancer incidence and mortality. Dose-
5323 response relationships are typically defined as a function of age, gender, and site.

5324

5325 Relative risk (RR) is the rate of disease among groups with a specific risk factor (*e.g.*, having
5326 received some radiation) divided by the rate among a group without that specific risk factor. Excess
5327 relative risk (ERR) is defined as the rate of an effect (*e.g.*, cancer incidence or mortality) in an exposed
5328 population divided by the rate of the effect in an unexposed population minus 1, or $RR-1$. In risk models
5329 using ERR, the excess risk is expressed relative to the background risk. Absolute risk is the rate of a
5330 disease among a population, *e.g.*, cancer cases per capita per year. Excess absolute risk (EAR) is the rate
5331 of an effect (*e.g.*, cancer incidence or mortality) in an exposed population minus the rate of the effect in
5332 an unexposed population. Thus, in risk models using EAR, the excess risk is expressed as the difference
5333 in the total risk and the background risk. The latter depends on the area in which the person lives, their
5334 age, sex, and date of birth (Ries *et al.*, 2003). When modeling a dose-response relationship for a specific
5335 disease, one can either use the concept of ERR or the concept of EAR. In general, estimates based on
5336 ERR can have less statistical uncertainties and thus are more meaningful for small risks. On the other
5337 hand, EAR is often used to describe the impact of a disease on the population. The excess risk can be
5338 calculated as a function of attained age of the individual, age at exposure, dose received, sex index, and
5339 an index denoting population characteristics. The lifetime attributable risk (LAR) is the probability that
5340 an irradiated individual will develop a radiation-induced cancer in their lifetime (Kellerer *et al.*, 2001). It
5341 includes cancers that would develop without exposure but which occur sooner in life due to radiation.
5342 The LAR can be estimated as an integral of excess risk over all attained ages using either ERR or EAR
5343 (BEIR, 2006).

5344

5345 The models presented in BEIR report (2006) define the relation between the incidence rate in the
5346 exposed population and the incidence rate in the unexposed population. The excess risk can be calculated
5347 as a function of attained age of the individual: a , age at exposure, e ; dose received, D ; sex index, s ; and
5348 time since exposure, t . One assumes a linear (solid cancers) or quadratic (leukemia) function of dose. The
5349 BEIR committee suggests that ERR for solid cancers (except for breast and thyroid) depend on age only
5350 for exposures under age 30. Specific parameterizations are given for estimation of breast cancer risk,
5351 thyroid cancer risk, and leukemia.

5352

5353 Schneider and Kaser-Hotz (2005) proposed the concept of “organ equivalent dose” (OED), in
5354 which any dose distribution in an organ is equivalent and corresponds to the same OED if it causes the
5355 same radiation-induced cancer incidence. For low doses, the OED is simply the average organ dose. At
5356 high doses the OED is different, because cell killing becomes important. The basis for the OED model is
5357 the dose-response relationship for radiation-induced cancer for different organs. The model is a linear-
5358 exponential dose-response model that takes into account cell-killing effects by an exponential function
5359 that depends on the dose and the organ-specific cell sterilization factor that is determined by Hodgkin’s
5360 disease data. The dose distributions used to determine the organ-specific cell sterilization factor were
5361 calculated in individual organs for which cancer incidence data were available. Kry *et al.* (2005) pointed
5362 out that developing concepts like the OED model suffers from major deficiencies, such as single specific
5363 irradiated populations. However, the OED approach has the advantage compared to the BEIR model that
5364 it is able also to estimate cancer risk from medium to high dose exposures, *i.e.*, in the vicinity of the
5365 target (Schneider *et al.*, 2006; Schneider *et al.*, 2007).

5366

5367 By developing models based on the atomic bomb data, differences in the radiation exposure
5368 compared to radiation treatments need to be considered. Even though most bomb survivors were exposed
5369 to low doses (< 0.1 Gy), some were exposed to doses exceeding 0.5 Gy, thus influencing the risk
5370 estimation. The risk is also dose-rate dependent. Grahn *et al.* (1972) observed reduction in leukemia
5371 incidence by a factor of ~ 5 with reduction of dose to 0.2 to 0.3 Gy/day. Ullrich *et al.* (Ullrich, 1980;
5372 Ullrich *et al.*, 1987) reported on dose-rate dependencies for the incidence of lung adenocarcinoma in
5373 mice. Maisin *et al.* (1991) found that ten fractions of 0.6 Gy yielded more cancers than a dose of 6 Gy in
5374 mice following whole-body irradiation. Brenner and Hall (1992) discussed this inverse effect of dose
5375 protraction for cancer induction. Dose rate effects are well understood for therapeutic dose levels with
5376 low-LET radiation (Paganetti, 2005). Most risk models account for dose rate effects by introducing
5377 scaling factors. However, the effect of dose protraction may be different in low dose regions in particular
5378 for neutron irradiation. While a positive “dose and dose-rate effect factor” (DDREF) is established for
5379 scattered photon doses, there is evidence for no dose-rate effect or even a reverse dose-rate effect for low
5380 doses of neutron radiation. This effect is a well-known phenomenon for high-LET radiation (Kocher *et*
5381 *al.*, 2005).

5382

5383 To establish a more precise dose-response relationship for second cancers as a function of
5384 modality, treatment site, beam characteristics, and patient population, progressively larger
5385 epidemiological studies are required to quantify the risk to a useful degree of precision in the low dose
5386 regions (Brenner *et al.*, 2003). In order to facilitate the evaluation of dose-response relationships as
5387 defined in epidemiological models, organ-specific dosimetry is needed. In fact, one of the reasons for
5388 considerable uncertainties in the current risk models is that actual second cancer incidences from
5389 radiation therapy patients are difficult to interpret due to the lack of accurate organ-specific dosimetric

5390 information. Further, simple dose-response relationships can be misleading. Dose-rate effects certainly
5391 play a role (Gregoire and Cleland, 2006).

5392

5393 **7.8.2 Dose-Response Relationships**

5394

5395 Various low-dose response relationships for second cancer induction have been discussed
5396 (Brenner *et al.*, 2003). Studies on leukemia suggest that the carcinogenic effect of radiation decreases at
5397 high doses because cell killing starts to dominate mutation (Upton, 2001). Patients treated with radiation
5398 for cervical cancer showed an increased risk of developing leukemia with doses up to ~ 4 Gy, which
5399 decreased at higher doses (Blettner and Boice, 1991; Boice *et al.*, 1987). Sigurdson *et al.* (2005) found
5400 that the risk for developing a second thyroid cancer after childhood cancer increased with doses up to ~
5401 29 Gy and then decreased. There is other evidence that the risk of solid tumors might level off at 4 to 8
5402 Gy (Curtis *et al.*, 1997; Tucker *et al.*, 1987). For pediatric patients, Ron *et al.* (1995) showed that a linear
5403 dose-response relationship best described the radiation response down to 0.1 Gy. In general, a linear
5404 dose-response curve is assumed for solid cancers (Little, 2000; 2001; Little and Muirhead, 2000).

5405

5406 It has been shown that even a single particle can cause mutations in a single-cell irradiation
5407 process. This is an indication of a linear dose-response relationship (Barcellos-Hoff, 2001), at least down
5408 to about 0.1 Gy (Frankenberg *et al.*, 2002; Han and Elkind, 1979; Heyes and Mill, 2004; NCRP, 2001).
5409 For even lower doses a small decrease in transformation has been reported (Ko *et al.*, 2004) while some
5410 data suggest a non-linear dose-response curve (Sasaki and Fukuda, 1999). Others have suggested a
5411 protective effect (Calabrese and Baldwin, 2000; 2003; Feinendegen, 2005; Hall, 2004; Upton, 2001).
5412 Results of whole-body irradiation (WBI) of primates with a follow-up of 24 years show no increase in
5413 cancer for 0.25 to 2.8 Gy (Wood, 1991).

5414

5415 Most currently used risk models are based on these data. Both the BEIR VII Committee (2006)
5416 and the ICRP (1991) recommend, for doses below 0.1 Gy, a “linear no-threshold” (LNT) model. This
5417 concept has been challenged by recent data (Tubiana *et al.*, 2009).

5418

5419 Assumptions about dose-response relationships for tumor induction are largely based on the
5420 atomic bomb survivor data. These are consistent with linearity up to ~ 2.5 Sv with a risk of ~ 10 %/Sv
5421 (Pierce *et al.*, 1996; Preston *et al.*, 2003). However, some analyses show a linear dose response for
5422 cancer incidence between 0.005 and 0.1 Sv (Pierce and Preston, 2000), some indicate a deviation from
5423 linearity (Preston *et al.*, 2004), and some find no increased cancer rate at doses less than 0.2 Sv
5424 (Heidenreich *et al.*, 1997). There is even some evidence for a decreasing slope for cancer mortality and
5425 incidence. This may be caused by the existence of small subpopulations of individuals showing
5426 hypersensitivity (ICRP, 1999). There might also be reduced radioresistance in which a small dose
5427 decreases the radiosensitivity, as has been reported for carcinogenesis (Bhattacharjee and Ito, 2001),
5428 cellular inactivation (Joiner *et al.*, 2001), mutation induction (Ueno *et al.*, 1996), chromosome aberration
5429 formation (Wolff, 1998), and *in vitro* oncogenic transformation (Azzam *et al.*, 1994). Further, linearity
5430 would not necessarily hold if multiple radiation-damaged cells influenced each other (Ballarini *et al.*,
5431 2002; Little, 2000; Little and Muirhead, 2000; Nasagawa and Little, 1999; Ullrich and Davis, 1999). An
5432 increasing slope seems to fit dose-effect relations for radiation-induced leukemia (Preston *et al.*, 2003),
5433 while a threshold in dose seems to be present for radiation-induced sarcoma (White *et al.*, 1993). Also,
5434 animal data have not shown significant cancer excess for doses below 100 mSv (Tubiana, 2005). The
5435 lack of evidence of a carcinogenic effect for low doses could be because the carcinogenic effect is too
5436 small to be detected by statistical analysis or because there is a threshold.

5437

7.9 Risks of Radiation-Induced Secondary Cancers in Particle Therapy

5438

5439

5440 Second malignancies are a major source of morbidity and mortality in pediatric cancer survivors.
5441 Although IMRT provides highly conformal dose to the target volume at high doses, due to the increased
5442 volume of tissue receiving lower doses it may nearly double the risk of second malignancy compared
5443 with 3D conformal techniques (Hall and Wu, 2003). Protons reduce the integral dose by a factor of 2 to
5444 3 compared to photon techniques and can thus be expected to decrease second cancer risk.

5445

5446 Recently, the comparative risk for developing second malignancies from scattered photon dose in
5447 IMRT and secondary neutron dose in proton therapy has been assessed by analyzing clinical data (Chung
5448 *et al.*, 2008). The study matched 503 patients treated with proton radiation therapy from 1974 to 2001 at
5449 the Harvard Cyclotron Laboratory and 1591 photon patients from the Surveillance, Epidemiology, and
5450 End Results (SEER) cancer registry. Patients were matched by age at radiation treatment, year of
5451 treatment, cancer histology, and site of treatment. The median age in both groups was comparable. It was
5452 found that 6.4 % of proton patients developed a second malignancy as compared to 12.8 % of photon
5453 patients. The median follow-up was 7.7 years in the proton cohort and 6.1 years in the photon cohort.
5454 After adjusting for gender and the age at treatment, the results indicated that the use of proton radiation
5455 therapy is associated with a lower risk of a second malignancy compared to photon radiation therapy.

5456

5457 Because we can assume (for passive-scattering techniques) that the majority of the neutrons in the
5458 patient are generated in the treatment head, we can infer that proton beam scanning reduces the neutron
5459 dose exposure significantly, in particular for small treatment fields (*i.e.*, small apertures in scattering
5460 systems). In fact, it has been demonstrated that scanned proton beams result in a lower second cancer risk
5461 than passive-scattered protons or photons (Miralbell *et al.*, 2002; Schneider *et al.*, 2002). Miralbell *et al.*

5462 (2002) assessed the potential influence of improved dose distribution with proton beams compared to
5463 photon beams on the incidence of treatment-induced second cancers in pediatric oncology. Two children,
5464 one with a parameningeal rhabdomyosarcoma (RMS) and a second with a medulloblastoma, were
5465 considered. They showed that proton beams have the potential to reduce the incidence of radiation-
5466 induced second cancers for the RMS patient by a factor of > 2 and for the medulloblastoma case by a
5467 factor of 15 when compared with IMRT (Table 7.2). These data for scanned proton beams do not include
5468 any secondary neutron component. Thus the improvement is simply due to a smaller irradiated high-dose
5469 volume.

5470

5471

5472

5473 Table 7.2. Estimated absolute yearly rate of second cancer incidence after treating a medulloblastoma
5474 case with either conventional x ray, IMRT, or scanned proton beams. (Miralbell *et al.*, 2002)

5475

5476

5477

5478

5479

5480

5481

5482

5483

5484

Tumor site	X-rays (%)	IM X-rays (%)	Protons (%)
Stomach and esophagus	0.15	0.11	0.00
Colon	0.15	0.07	0.00
Breast	0.00	0.00	0.00
Lung	0.07	0.07	0.01
Thyroid	0.18	0.06	0.00
Bone and connective tissue	0.03	0.02	0.01
Leukemia	0.07	0.05	0.03
All secondary cancers	0.75	0.43	0.05
Relative risk compared to standard X-ray plan	1	0.6	0.07

5485 The magnitude of second cancer risk in patients treated with passive and scanned proton radiation
5486 has also been estimated utilizing computer simulations of organ doses using computational phantoms
5487 (Brenner and Hall, 2008b; Jiang *et al.*, 2005; Newhauser *et al.*, 2009; Taddei *et al.*, 2009; Zacharatou
5488 Jarlskog and Paganetti, 2008b). Based on dosimetric data on organ doses given by Jiang *et al.* (2005),
5489 Brenner and Hall (2008a) estimated second cancer risks for various organs assuming a neutron RBE
5490 value of 25. They reported that lifetime cancer risk due to external neutrons in passive-scattered proton
5491 therapy is 4.7 % and 11.1 % for a cured 15-year-old male and female, respectively. The estimations were
5492 based on a proton treatment for lung cancer. The risk decreased to 2 % and 3 %, respectively, for an adult
5493 patient.

5494

5495 Based on Monte Carlo simulations using a treatment head model and a voxelized phantom,
5496 Taddei *et al.* (2009) estimated the second cancer risk from secondary radiation following cranio-spinal
5497 irradiation with proton therapy. An effective dose corresponding to an attributable lifetime risk of a fatal
5498 second cancer of 3.4 % was determined. The equivalent doses that predominated the effective dose from
5499 secondary radiation were in the lungs, stomach, and colon. Further, cranio-spinal irradiation of a male
5500 phantom was calculated for passively scattered and scanned-beam proton treatment units (Newhauser *et*
5501 *al.*, 2009). The total lifetime risk of second cancer due exclusively to secondary radiation was 1.5 % for
5502 the passively scattered treatment versus 0.8 % for the scanned proton-beam treatment.

5503

5504 Based on the data on organ neutron equivalent doses using five pediatric computational
5505 phantoms, risk estimations based on BEIR risk models have been done (Zacharatou Jarlskog and
5506 Paganetti, 2008b). For eight proton fields to treat brain tumors, the risk for developing second cancer in
5507 various organs was calculated. Figure 7.5 shows the lifetime attributable risk (LAR) for some of the
5508 organs. It was found that young patients are subject to significantly higher risks than adult patients due to

5509 geometric differences and age-dependency of risk models. In particular, a comparison of the lifetime
5510 risks showed that breast cancer should be the main concern for females, whereas for males, risks for lung
5511 cancer, leukemia, and thyroid cancer were more significant. Other than for pediatric patients, leukemia
5512 was the leading risk for an adult. Most of the calculated lifetime risks were below 1 % for the 70 Gy
5513 treatment considered. The only exceptions were breast, thyroid, and lung for females. For female thyroid
5514 cancer the treatment risk can exceed the baseline risk. The patient's age at the time of treatment plays a
5515 major role (Zacharatou Jarlskog and Paganetti, 2008b).
5516

5517
 5518
 5519
 5520
 5521
 5522
 5523
 5524
 5525
 5526
 5527
 5528
 5529
 5530
 5531
 5532
 5533
 5534
 5535

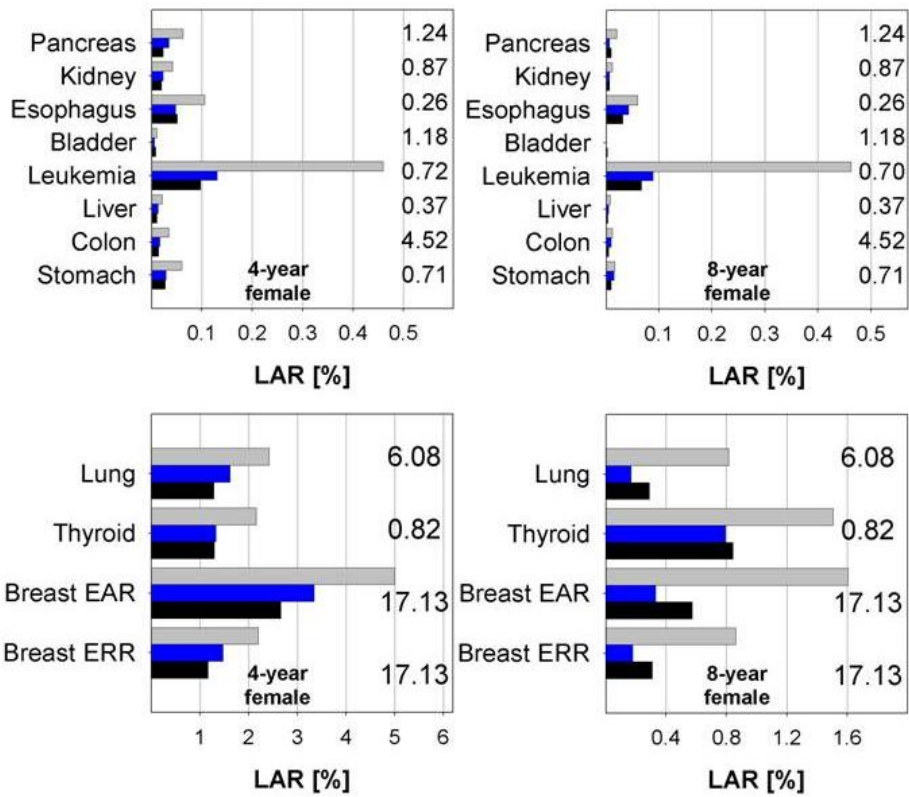


Figure 7.5. Lifetime attributable risk [%] based on a 70 Gy treatment for various second cancers for 4-year-old and 8-year-old brain tumor patients. The three colors refer to three different treatment fields. The numbers on the right represent the baseline risks for these cancers. (Zacharatou Jarlskog and Paganetti, 2008b)

5560 higher neutron RBE values have been found for various endpoints both *in vivo* and *in vitro* (Dennis,
5561 1987; Edwards, 1999; NCRP, 1990). The NCRP has shown neutron radiation weighting factors of more
5562 than 80 for fission neutrons considering several radiation endpoints in the energy range of 1 to 2 MeV,
5563 where the ICRP recommendation assumes a weighting factor of 20 (NCRP, 1990). Dennis (1987) has
5564 reviewed experimental neutron RBE data and found maximum *in vivo* values at low doses of up to 71.
5565

5566 There are insufficient data to define the radiation effectiveness of neutrons for epidemiological
5567 endpoints. The radiation weighting factor recommendation by the ICRP may not reflect reality as it does
5568 focus on radiation protection rather than radiation epidemiology. The ICRP explicitly states that the term
5569 effective dose is a quantity for use in radiation protection and not in epidemiology. These limitations
5570 have to be considered when analyzing secondary doses.

5571
5572 There are many different contributions that provide uncertainties in absolute risk estimates that
5573 have been given in the literature. Kry *et al.* (2007) examined the uncertainty in absolute risk estimates
5574 and in the ratio of risk estimates between different treatment modalities using the NCRP/ICRP risk
5575 model and a risk model suggested by the U.S. Environmental Protection Agency (EPA, 1994; 1999).
5576 They found that the absolute risk estimates of fatal second cancers were associated with very large
5577 uncertainties, thus making it difficult to distinguish between risks associated with the different treatment
5578 modalities considered.

5579
5580 Several risk models have been proposed and used to estimate the risk of second malignancies
5581 induced by radiation treatment. The models in use today are largely based on the atomic bomb survival
5582 data. Both the BEIR VII Committee (2006) and the ICRP (1991) recommend, for doses below 0.1 Gy, a
5583 linear dose-response relationship without a low-dose threshold based on the epidemiological data

5607 Although dosimetric data, experimental as well as theoretical, are known by now to a sufficient
5608 degree of accuracy, the actual cancer risk associated with the absorbed doses is not well known at all.
5609 This is due to huge uncertainties in the biological effectiveness of neutrons at low doses and due to huge
5610 uncertainties in current epidemiological risk models.

5611

5612 Clinical data are difficult to interpret because of inter-patient variability and lack of dosimetric
5613 information in the low dose region. However, improved dosimetric data in combination with long-term
5614 patient follow-up might eventually lead to improved risk models.

5615

8. Safety Systems and Interlocks

Jacobus Maarten Schippers

8.1 Introduction

The purpose of safety systems and interlocks (particle-beam interruption systems) in a particle therapy facility is threefold:

1. to protect personnel, patients, and visitors from inadvertent exposure to overly excessive radiation doses;
2. to protect patients from receiving an incorrect dose or a dose in an incorrect volume; and
3. to protect equipment and environment against heat, radiation damage, or activation.

How these goals are implemented depends strongly on the local radiation protection legislation, the specific requirements and traditions of the institute concerned, and the standards to which the company delivering the equipment adheres. In this chapter several methods and relevant parts of either planned or actually installed safety systems are discussed, with the sole purpose of showing the underlying philosophy and how one could implement such systems in practice. Therefore, the description of the systems is by no means complete and is sometimes simplified. Most examples of the systems discussed in this chapter refer to the situation at the Center for Proton Therapy at the Paul Scherrer Institute (PSI) in Switzerland as they existed or were planned at the time of writing this chapter. Other methods will be applicable to other treatment facilities or when other irradiation techniques are applied. Due to the differences and continuing developments in legislation, it is up to the reader to decide which ideas or systems could be of use in one's own country or facility. The purpose of this chapter is to inform the

5640 reader about the different aspects of safety systems that need to be addressed; to give a potential user
5641 enough background information and some suggestions to define one's own list of criteria for a safety
5642 system in order to have relevant and thorough discussions with the vendors; and to provide information
5643 to help users understand, judge, and eventually criticize a vendor's proposal and to check compliance
5644 with local requirements and regulations.

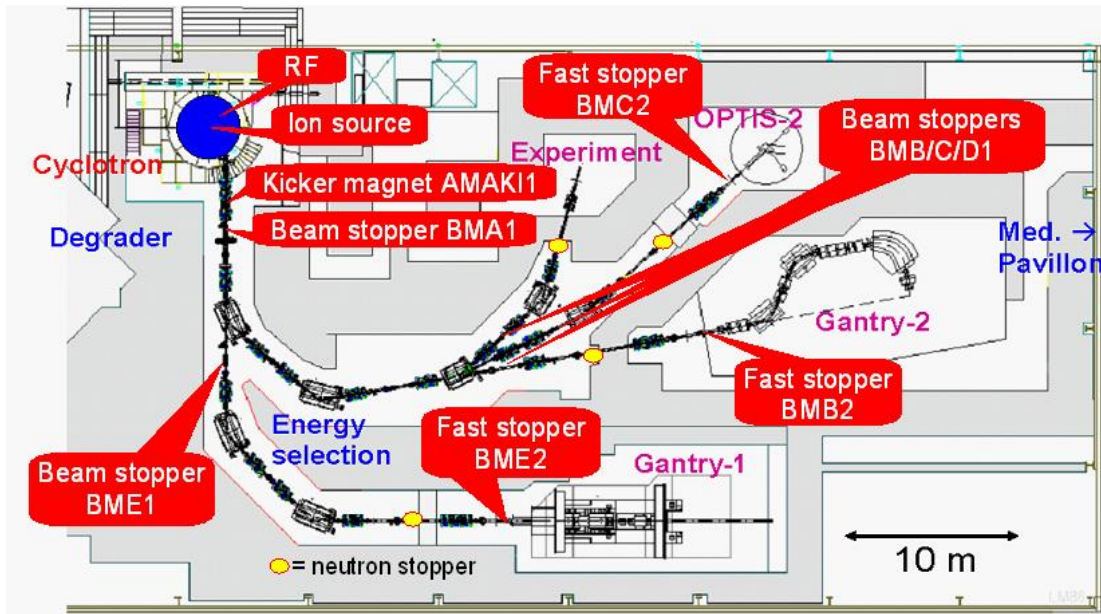
5645

5646 Figure 8.1 shows the facility at PSI, which has been built and designed in-house. Within a
5647 research collaboration with the supplier of the cyclotron, PSI has contributed to the development of the
5648 accelerator, its interfaces, and control system. The experience obtained since the start of particle therapy
5649 at PSI in 1980 has evolved in the current design of the control and safety systems. Until 2005, the
5650 therapy program ran parallel with the physics program at PSI by using a fraction of the high intensity
5651 proton beam (Pedroni *et al.*, 1995). This type of operation imposed special constraints on the design of
5652 the safety systems, such as the rigorous separation of patient safety functions from the machine control
5653 system. This philosophy has been used again in the newly built stand-alone proton therapy facility that
5654 has been in use since 2007. This therapy facility (Schippers *et al.*, 2007) consists of a cyclotron, energy
5655 degrader and beam analysis system, two rotating gantries (Gantry 1 and Gantry 2, the latter of which is
5656 not yet operational at the time of writing), an eye treatment room (OPTIS2), and a room for experimental
5657 measurements.

5658

5659

5660



5661

5662

5663

5664 Figure 8.1. Floor plan of the proton therapy facility at PSI, indicating the actuators that can be used to
5665 stop or intercept the beam. (Courtesy of PSI)

5666

5667

5668 At PSI the three safety functions mentioned above are controlled by three separate systems: a
5669 Personnel Safety System (PSS); a Patient Safety System (PaSS); and a Run Permit System (RPS). The
5670 PSS and PaSS operate separately from the control system of the machine (cyclotron and beam lines). The
5671 separation of functions reduces the risks and complexity that might occur in the case of a system in
5672 which the design is based on one combined operation and safety system in which “everything is
5673 connected to everything else.” Of course, well-designed systems with a global function approach to the
5674 facility can be conceived without this separation, but the separated function approach leaves more
5675 freedom for further technical developments. The control system architecture at PSI allows explicit
5676 visibility of these functions in the system architecture.

5677

5678 In the case of an undesired input signal or status, each of the three safety systems has the
5679 capability to “trip”: it sends a signal that switches the beam off or prevents the beam from being switched
5680 on. The event of changing into a state which is not “OK” is usually referred to as “a trip” or “an interlock
5681 trip.” Each safety system has its own sensor systems, actuators, switches, and computer systems.
5682 Although actuators that can switch off the beam (Fig. 8.1) can be activated by more than one safety
5683 system, they have separate inputs/outputs for the signals from/to each of these safety systems. In many
5684 cases, dedicated diagnostic signals are also used to determine if the actuator is working properly. Apart
5685 from the statuses “OK” and “not OK,” the other possible states of an actuator might be “NC” (not
5686 connected) and “err” (short circuit). This defines the fail-safe nature of the signals.

5687

5688 The displays in the control room indicate which system causes the interception or interruption of
5689 the beam and allow a detailed in-depth analysis in order to find out the cause of such an error status. All
5690 events are logged with time reference stamps.

5691

5692 In this chapter, these three safety systems and their implementation will be described. Although
5693 some issues are specific to PSI (*e.g.*, the spot scanning technique; see Pedroni *et al.*, 1995) or to the use
5694 of a cyclotron, the concepts are applicable to any facility. The most important aspect of the safety
5695 concept used at PSI is the complete and rigorous separation of the three systems. By this, a very flexible
5696 arrangement has been created. Some general issues on safety systems are discussed in Sec. 8.1, followed
5697 by information on the beam-intercepting devices in Sec. 8.2, with Sec. 8.3 describing the relevant aspects
5698 of the control system at PSI, and Sec. 8.4, 8.5, and 8.6 providing a detailed description of the three safety
5699 systems.

5700

5701 **8.1.1 Safety Requirements**

5702

5703 The risk limitation and reduction required by various authorities depends upon local laws and
5704 administration rules, and is in steady development. An FDA approval (U.S.A.), CE conformity procedure
5705 (E.U.), or similar authorization by equivalent bodies in other countries of the facility could be required.
5706 When the research and development of the equipment and software was started a long time ago, or when
5707 it is not thought that the system will be put on the market, an adaptation of the project into a more
5708 regulated form is generally not possible without substantial effort. For these special cases, special
5709 regulations might exist.

5710

5711 However, for proton/ion therapy, the practical implementation of existing regulations might
5712 sometimes not be evident or applicable. Then one has to negotiate with the appropriate authorities, *e.g.*,
5713 regarding how the documentation and test procedures should be designed in order to obtain approval for
5714 treatments. In any case, a state-of-the-art approach would at least consist of a report with a thorough
5715 description of the safety systems, a risk analysis, operating instructions, and a list of tests to be done with

5716 a specified frequency of these tests. In general, the results of initial and periodic tests must be available
5717 for the appropriate authorities.

5718

5719 **8.1.2 Safety Standards**

5720

5721 To the best of the author's knowledge, there are no existing specific norms or widely applicable
5722 safety guidelines specifically for proton and ion therapy facilities at this time. However, in some
5723 countries authorities follow or adapt applicable existing recommendations or guidelines for linear
5724 accelerators for photon or electron therapy, and regulations for particle therapy facilities are being
5725 developed. The current recommendations and guidelines present generally accepted safety standards for
5726 radiation therapy, many of which are also applicable to proton and ion therapy. One could, for instance,
5727 use the applicable parts of the standards for medical electron linear accelerators, as given in the
5728 International Electrotechnical Commission's Publication 60601-2-1 (1998). As an example, in proton or
5729 ion therapy, it would then also require two dose monitors in the treatment nozzle, one giving a stop
5730 signal at 100 % and the second monitor giving a stop signal at approximately 110 % of the prescribed
5731 dose. Also, useful guidelines can be found in the recently issued new IEC Publication 62304 (2006),
5732 which deals with software for medical applications.

5733

5734 Criteria for accidental exposures in radiotherapy are listed in ICRP Publication 86 (2000). An
5735 overdose due to a failure in procedure or in equipment is classified as a "Class I hazard," when the extra
5736 dose could cause death or serious injury. Within this class, two types of hazards are distinguished: type
5737 A, which can likely be responsible for life-threatening complications (25 % overdose or more of the total
5738 prescribed treatment dose); and type B (5 to 25 % dose excess over the total treatment dose), which
5739 increases the probability of an unacceptable treatment outcome (complications or lack of tumor control).

5740

5741 One of the goals of a patient safety system could thus be defined as preventing an excess dose
5742 that is due to an error in dose delivery and exceeds 5 % of the treatment dose, which is typically ~ 3 Gy.

5743

5744 **8.1.3 Risk Analysis**

5745

5746 The requirements for and extent of a risk analysis for medical devices differ from country to
5747 country and are in steady development, so a general rule cannot be given. Furthermore, there is no
5748 unique way of performing a risk analysis, but one can obtain good working structures from existing
5749 norms and recommendations on medical devices. Note, however, that whether and under which
5750 conditions proton or ion therapy equipment and its accessories fall under the definition of “a medical
5751 device” can differ from country to country (although, in the EU it is the same for all members).

5752

5753 In ISO 14971 (2007), the general process of how risk management could be applied to medical
5754 devices is given. On the ISO Web site mentioned in the above standard, a list of member countries that
5755 have recognized ISO 14971 is given. This ISO norm presents an organizational structure of activities
5756 related to risk management. One can typically distinguish the following steps in a risk management
5757 process:

- 5758 • *Risk analysis*: identification of hazardous situations and risk quantification, *e.g.*, by
5759 analyzing fault trees;
- 5760 • *Risk evaluation*: decide upon need for risk reduction;
- 5761 • *Risk control*: describe measures (definition, implementation, and verification) to reduce
5762 risk;
- 5763 • *Residual risk evaluation*: what is the risk after implementing the measures;

- 5764 • *(Post) production information*: review the actual implementation and observe how these
5765 implementations perform in real practice. This gives the process the capability to update
5766 the risk analysis and to react to observed problems after production.

5767

5768 For an estimation of the amount of needed safety measures, one could use a process in analogy to
5769 the one given in IEC Publication 61508 (2005) as a guideline. In Part 5 of this international standard for
5770 the functional safety of electrical, electronic, and programmable electronic equipment, many examples
5771 are given to categorize hazardous events in a “hazard severity matrix” by means of their impact and their
5772 probability of occurrence. When the combination of severity and occurrence (*i.e.*, the risk) exceeds a
5773 certain threshold, a measure must be taken. The robustness of such a measure (the Safety Integrity Level,
5774 or SIL) must increase with the risk. One way to increase the robustness of a measure is to add
5775 redundancy, *i.e.*, to increase the number of independent safety related systems that comprise the measure
5776 taken. Specialized companies have developed software tools as an aid to make such a risk analysis.

5777

5778 **8.1.4 Interlock Analysis and Reset**

5779

5780 An interlock trip occurs when a device, component, measurement, or signal under the control of a
5781 specific safety system is found in an undesirable state with respect to specified tolerances. It is important
5782 to reset the interlock signals and restore the machine setting to their normal operating states as soon as
5783 possible after the machine state is “OK” again. This is necessary in order to limit waiting time, but also
5784 to prevent loss of extra time for retuning of the machine to its normal operating state due, *e.g.*, to
5785 temperature drifts. This applies especially to interlock trips that were caused by a condition that was not
5786 met for only a short time interval, but which was not caused by a malfunctioning device. For example,
5787 one could think of an interlock trip caused by a transient state in which not all components are in an

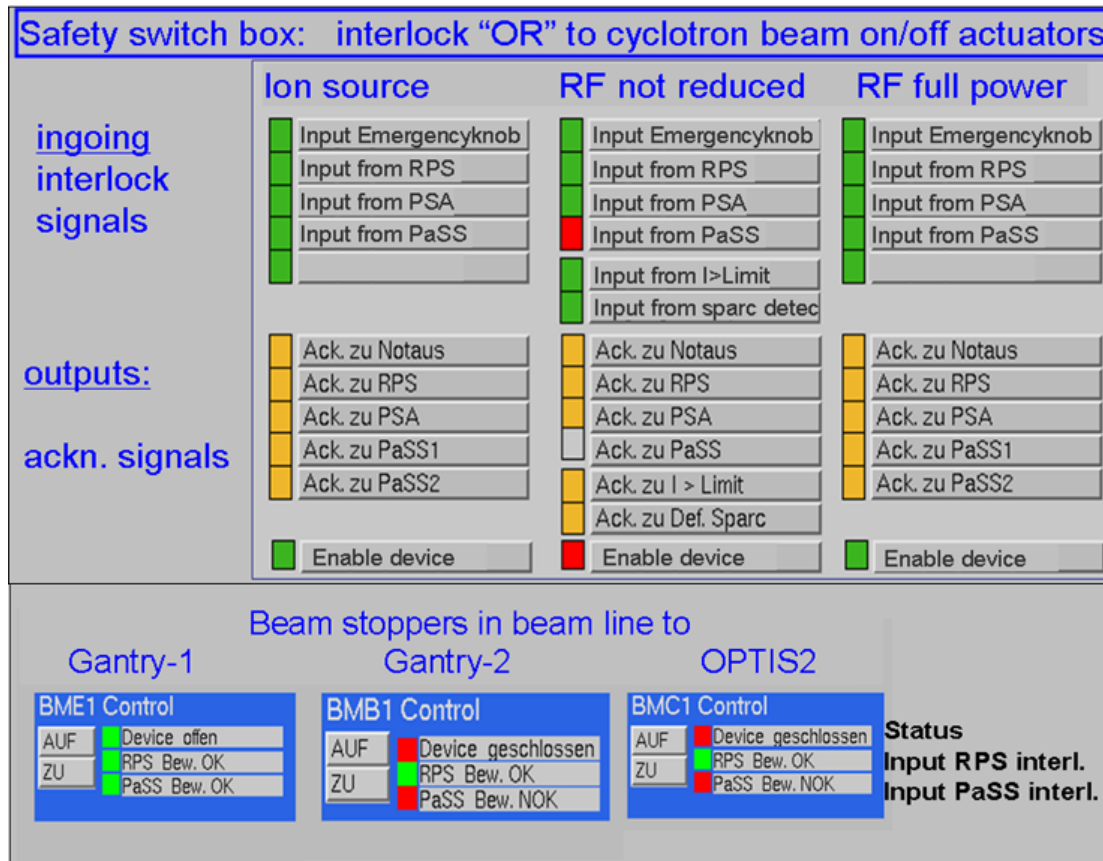
5788 “OK” status. It could also occur due to a short occurrence of a too high beam current, which might
5789 happen when the intensity (signal) is noisy.

5790

5791 In order to recognize the cause of an interlock trip, a clear indication of the signals and an error
5792 logging with time stamps of the underlying process and relevant events are essential tools for the
5793 diagnosis and repair of problems. Figure 8.2 shows the PSI user interface in the control room as an
5794 example.

5795

5796



5797

5798

5799 Figure 8.2. The user interface of PSI’s control system showing the status of beam-intercepting actuators
 5800 in the cyclotron (controlled *via* a Safety Switch Box) and area-specific beam stoppers “BMx1.” (“Offen”
 5801 means “open”; “geschlossen” means “closed.”) (Courtesy of PSI)

5802

5803

5804 The programs displaying the interlock status and bypasses (“bridges”) must be capable of giving
5805 easy and quick access to such data. Data from deeper levels that cannot be displayed on the main screen,
5806 or more detailed information on the status of specific beam-line sections or devices, can be found by
5807 clicking on the components of interest or on a details field in the main screen. Depending on the failure
5808 scenario, the continuation of the therapy has to be forbidden or disabled and a comprehensive evaluation
5809 of the machine status and the dose already delivered to the patient must be carried out. An easily
5810 interpreted interlock analysis program to inform the (therapy) operator can save a lot of time.

5811

5812 After resetting an interlock, the beam should not be automatically switched on again. For safety
5813 reasons, a dedicated manual action should be required to switch the beam on again.

5814

5815 **8.1.5 Quality Assurance**

5816

5817 Although rigorous tests of interlock systems must be done in theory, in practice it is impossible to
5818 test all conceivable situations (control system configurations). However, a set of tests can be done to
5819 verify that the entire system is working properly. For this purpose one can design tests during the
5820 commissioning of the system (which could be part of the acceptance tests) as well as tests during the
5821 operational phase of the facility. The combination of such tests should then exclude (or reveal) all errors
5822 that one could think of. When a commercial therapy system is obtained, the possibilities for end user
5823 testing are limited; however, a vendor should be able to state what type of tests have been done.

5824

5825 During the commissioning of any proton or ion therapy facility, certified or not, several quality
5826 assurance tests can be done by generating specific fault conditions. Sometimes the system needs to be
5827 “fooled” in order to reach a faulty state for the test. Some possible testing scenarios include a sudden

5828 increase of beam current; detuning of magnets; setting the energy degrader or collimator in the wrong
5829 position; placing a radioactive source in front of a dosimeter; pressing emergency buttons; or bypassing
5830 the limit switches on mechanical beam stoppers. Some of these tests are also incorporated in a quality
5831 control program of periodic tests.

5832

5833 All modifications or substantial repairs of the therapy equipment or control systems need to be
5834 documented and followed by an “end-to-end test,” described in the quality control program of the
5835 facility. Similar to standard radiation therapy, in a partial simulation of a treatment, a dose distribution is
5836 delivered to a phantom in a treatment room. Measurements are made of the dose and proton range within
5837 the phantom, and specified functions of the Patient Safety System are tested.

5838

5839 **8.2 Methods of Turning off the Beam**

5840

5841 In a particle accelerator and beam transport system there are many mechanisms for turning the
5842 beam off. The action of each actuator (method or device) has its own specific reaction time, varying from
5843 a few microseconds to fractions of a second. Also the time and effort to switch the beam on again
5844 depends on the actuator. In case of severe risk (determined by a risk analysis; see Sec. 8.1.3), several
5845 actuators must switch the beam off at the same time (redundancy). In case of low risk or routine switch-
5846 off, only one actuator will work, but if the beam does not stop in time, the action of more actuators will
5847 follow. When a cyclotron is used as the accelerator, one might consider keeping the beam on, but only
5848 allow the beam to be transported to a certain element in the beam line, *e.g.*, by using an inserted
5849 mechanical beam stopper. In case of a synchrotron, one might decide to stop the slow extraction and
5850 store the beam in the synchrotron. In this case, an additional fast kicker magnet in the beam line to the
5851 treatment areas can be used to suppress protons that “leak out” of the synchrotron. For cyclotrons, one

5852 should limit the duration of this type of interruption to avoid unnecessary accumulation of radioactivity
5853 in and around the beam stopper. In case of a synchrotron, one might completely decelerate the beam in
5854 the synchrotron and, in some cases, dump the low-energy beam on a beam dump when the waiting time
5855 would be so long that beam losses would start to activate the machine.

5856

5857 Most of the beam interrupting components can receive a “beam off” command from different
5858 systems. At PSI these systems are the machine control system (see Sec. 8.3) and the safety systems PSS,
5859 RPS and PaSS.

5860

5861 Beam interrupting components implemented at PSI as well as those used in commercial facilities
5862 are devices typical for cyclotron/synchrotron laboratories. When using external ion sources (*e.g.*, ECR
5863 electron cyclotron resonance ion source) in ion therapy facilities, or staged accelerator systems (*e.g.*, an
5864 injector followed by a synchrotron), beam interruption can be done with similar methods. With a
5865 synchrotron, however, one should realize that an interruption in the injection line or at the ion source is
5866 decoupled from the beam to the treatment room. In this section an overview of components that turn off
5867 the beam will be given. This is followed by a discussion of their use and the implications for the time and
5868 actions that are needed after an interruption to get the beam back in the treatment room again.

5869

5870 **8.2.1 Beam Interrupting Components**

5871

5872 When a synchrotron is used, there are different options to stop the beam before it enters the beam
5873 transport system. One could stop the radio frequency (RF) kicker that performs the slow extraction
5874 process, and thus reduce the extracted intensity. One could also use a fast kicker magnet in the ring to
5875 dump the stored particles on a beam dump. This can be done immediately in case of a severe emergency,

5876 or after deceleration to reduce the amount of radioactivity in the beam dump. The method (or methods)
5877 used depends on the type of synchrotron and the manufacturer. In addition, one can shut off the ion
5878 source. In general, more than one of these actions can be used to achieve safety redundancy.

5879

5880 In a cyclotron facility, the devices that can turn the beam off include fast and normal mechanical
5881 beam stoppers, and fast deflection magnets in the beam line. In addition, one can switch off the RF
5882 acceleration voltage of the cyclotron or the ion source arc current, or use a fast electrostatic deflector in
5883 the center of the cyclotron. Below, some details of the beam interrupting devices used at PSI are listed as
5884 examples, starting from the center of the cyclotron.

5885

5886 As in all proton cyclotrons, the ion source is located at the center of the cyclotron and at PSI it is
5887 of the “cold cathode” type (Forringer *et al.*, 2001). The performance of such a source is compromised
5888 when it undergoes a fast switch-off (within < 1 min). Moreover, because the beam intensity decay is
5889 slow when the source is switched off, taking several fractions of a second, the source should only be
5890 switched off in severe cases. In general, some instability after switching on again might be expected in
5891 any type of ion source.

5892

5893 The next beam interruption device is a set of parallel plates, mounted near the center of the
5894 cyclotron. Between these plates an electric field in the vertical direction can be generated. This field
5895 deflects the protons, which still have low energy, in the vertical direction, so that they are stopped on a
5896 collimator that limits the vertical aperture. This very fast (40 μ s) system stops the protons before they are
5897 accelerated to energies at which they can produce radioactivity.

5898

5899 The RF of the cyclotron offers two options to switch the beam off: a reduced power mode (in
5900 which a fraction of the nominal RF-power is applied), or switching the RF completely off. The reduced
5901 mode also prevents the beam from being accelerated. This mode is used for non-severe reasons to switch
5902 off the beam, thus allowing a fast return of the beam. The reaction time is less than 50 μ s.

5903

5904 After extraction from the cyclotron, the first beam-intercepting device is a fast kicker magnet,
5905 AMAKI. When the current in this magnet is switched on, it deflects the beam within 50 μ s onto a beam
5906 dump next to the beam axis. This kicker magnet is the main “beam on-off switch” used during therapy. It
5907 plays an essential role in the spot-scanning technique used at PSI. The magnet is equipped with an
5908 independent magnet current verification device as well as with magnetic field switches to measure
5909 whether the magnet has reacted within an appropriate time.

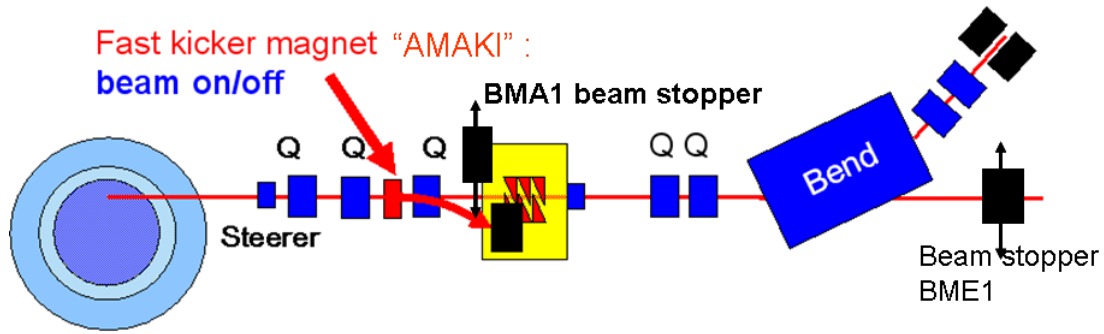
5910

5911 The mechanical beam stopper, BMA1 (reaction time < 1 s), is located downstream of AMAKI.
5912 This stopper is only opened when beam is allowed downstream. When closed, the cyclotron can be
5913 ramped up and the extracted beam can be measured and prepared independently of the status of the other
5914 beam lines or treatment rooms (see Fig. 8.3).

5915

5916

5917



5918

5919

5920 Figure 8.3. The first beam line section with a fast kicker magnet serving as main beam "on/off" switch.

5921 (Courtesy of PSI)

5922

5923

5924 A mechanical stopper, BMx1, is located at the start of each beam line section specific for a
5925 treatment room (“x” indicates beam line/treatment room B, C, D or E). This stopper must be closed in
5926 order to allow persons to enter a treatment room. Only one of the BMx1s can be open at a time to prevent
5927 the beam from entering the wrong room due to a magnet failure.

5928

5929 In the beam line leading to each treatment room an additional fast mechanical stopper, BMx2
5930 (reaction time < 60 ms), is inserted for longer beam interruptions and when a PaSS interlock trip occurs.
5931 The beam stoppers are also used to stop the beam in normal operation and to measure the beam current.
5932 Furthermore, a moveable neutron stopper (a block of iron) is mounted just upstream of the hole in the
5933 wall through which the beam line enters the treatment room. The neutron stoppers are not allowed to be
5934 struck directly by the proton beam and can therefore only be inserted when the preceding BMx1 stopper
5935 is closed. Otherwise an interlock trip will be generated.

5936

5937 **8.2.2 Use of the Different Beam Interrupting Components**

5938

5939 When the beam is stopped for normal operation reasons, the appropriate actuator is selected to
5940 minimize the activation and radiation load as well as to minimize the time to get back to stable operation.
5941 For beam interruptions up to a few minutes, the fast kicker magnet AMAKI is used. For longer
5942 interruptions, the goal is to stop the beam at low proton energy in the cyclotron with the vertical
5943 deflector.

5944

5945 In case of a detected error state, the beam is switched off by one of the safety systems. Table 8.1
5946 lists the various beam-intercepting actuators and when they are used by the three safety systems. The
5947 major factor that determines which device is to be used is the reaction time. The combination of reaction

5948 time and dose rate determines the extra dose received by the patient when the beam is shut down during
5949 treatment due to an error condition. The goal of the Patient Safety System is to limit the extra dose in
5950 such cases. This goal is discussed more specifically in Sec. 8.5.1, where two types of errors are
5951 described. The first is an extra dose due to an error in the dose application, but dealt with by, for
5952 example, the dual monitor system. The extra unintended dose must be lower than 10 % of the fraction
5953 dose (IEC, 1998). At PSI, we aim for less than 2 % of the fraction dose, *i.e.*, typically 4 cGy for Gantry-
5954 1. The second dose error is more serious and falls under the “radiation incident” category. In case of a
5955 radiation incident, the goal of the Patient Safety System is to prevent an unintended extra dose larger
5956 than 3 Gy (see Sec. 8.1.2 and 8.5.1).
5957

5958 Table 8.1. Beam-Intercepting Actuators and their Use In PSS, PaSS, and RPS. (Courtesy of PSI)
5959

Beam turn-off method used ^a	Personnel Safety System PSS	Patient Safety System PaSS	Run Permit System RPS
kicker magn.AMAKI		ALOK ^b	ILK ^d from beam line
Fast stopper BMx2		ALOK	
RF cyclotron “reduced”		ATOT ^c	ILK from beam line
RF cyclotron “off”	alarm	ETOT: Emergency off	ILK from cyclotron
Ion source off	alarm	ETOT: Emergency off	ILK from cyclotron
Beam stopper BMA1		ATOT	ILK from beam line
Beam stopper BMx1	when alarm in x, otherwise status check only	ATOT	
Neutron stopper x	when alarm in x, otherwise status check only		when BMx1 closes

5960

5961 ^a The first column indicates which of the Beam-off switches is used when one of the three safety
5962 systems (PSS, PaSS and RPS) generates a signal listed in column 2, 3 and 4 respectively.

5963 ^b “ALOK” indicates a local PaSS alarm, caused by a device within a treatment room.

5964 ^c A more serious alarm, “ATOT” indicates a global alarm from the PaSS, which requires general beam
5965 off.

5966 ^d “ILK” means “interlock signal,” and “x” represents a given beam line toward a specific treatment room
5967 (B,C,D, etc.).

5968

5969

5970 Table 8.2 shows the list of switching devices with the response times of the actuators and the
5971 approximate response time of the beam detectors and processing electronics. The calculated extra dose
5972 deposition includes the complete system response time. With the regular beam setting for Gantry-1,
5973 which has 100 nA extracted from the cyclotron, the dose rate of the pencil beam in the Bragg peak (*i.e.*, a
5974 volume of $< 1 \text{ cm}^3$) is approximately 6 Gy/s. When the Patient Safety System detects an error, *e.g.*, the
5975 beam has not been switched off on time, it will switch off the RF. The extra dose is then 0.09 cGy, which
5976 is far below the maximum error of 4 cGy.
5977

5978 Table 8.2. Response times for beam interruption by the different beam stop methods and estimated extra
5979 dose deposition at Gantry 1 at PSI for two cases with different extracted beam intensities I_p .^a (Courtesy
5980 of PSI)

Device	Response time Device, sensor & electronics	Dose with 6 Gy/s ($I_p=100$ nA) nominal case	Dose with max. intensity ($I_p=1000$ nA) worst case
Kicker magn. AMAKI	50 μ s 100 μ s	0.09 cGy	0.9 cGy
RF cyclotron "off" RF cyclotron "reduced"	50 μ s 100 μ s	0.09 cGy	0.9 cGy
Ion source	20 ms 100 μ s	12 cGy	120 cGy
Fast Beam stop. BME2	60 ms 100 μ s	36 cGy	360 cGy
Beam stopper BME1	< 1 s	<6 Gy	<60 Gy
Beam stopper BMA1	< 1 s	<6 Gy	<60 Gy

5981

5982 ^a Note that the maximum possible current extracted from the cyclotron in normal operation conditions is
5983 only a factor 10 larger than the normal current during Gantry-1 operation.

5984

5985

5986 When using a cyclotron, an unintended increase of the beam intensity can occur. In a synchrotron
5987 this might also happen due to extraction instabilities; however, the number of protons is limited to those
5988 stored in the ring. In a cyclotron an unintended increase of the beam intensity might happen due to, for
5989 example, a sudden crack in the aperture of the ion source. To limit the beam intensity, fixed collimators
5990 in the central region of the cyclotron are provided. These are designed such that they intercept most of
5991 the unwanted additional intensity because protons originating from such an event are not well-focused.
5992 When the intensity becomes higher than allowed (this limit depends on the application; for eye
5993 treatments at PSI, it is a few times higher than for treatments at the gantry), it will be detected by the
5994 permanently installed beam-intensity monitors at the exit of the cyclotron. These monitors will cause an
5995 alarm signal and the two fast-switching devices (AMAKI and RF) will stop the beam. Even though there
5996 will be a time delay in the signaling and the operation of the devices, the extra dose will stay below 3 Gy,
5997 as specified in Sec. 8.1.2 and 8.5.1. To prevent the extremely unlikely event that these fast and redundant
5998 systems fail, mechanical beam stoppers are also inserted into the beam line to stop the beam. Due to their
5999 longer reaction time a higher excess dose will be given to the patient, but only in case both fast systems
6000 fail (see Table 8.2).

6001

6002 **8.3 Control Systems, Mastership, and Facility Mode**

6003

6004 The operation of the accelerator and beam lines (*e.g.*, setting the current of a power supply,
6005 inserting a beam monitor, measuring the beam intensity) is done by means of a control system. The
6006 safety systems must work independently of the control system. The only interactions between the safety
6007 systems and the control system are receiving and sending status information. Because the concept of the
6008 control system architecture is related to the goals and the design of the safety systems, some essential
6009 aspects are discussed in this section. Questions such as who is in control in case of having multiple

6010 treatment rooms (mastership), who can do what (machine access control) and when (facility mode), and
6011 how is a separation of (safety) systems guaranteed, need to be considered in any design. In this section
6012 these aspects will be elucidated by discussing the concepts used at PSI.

6013

6014 **8.3.1 Control Concept**

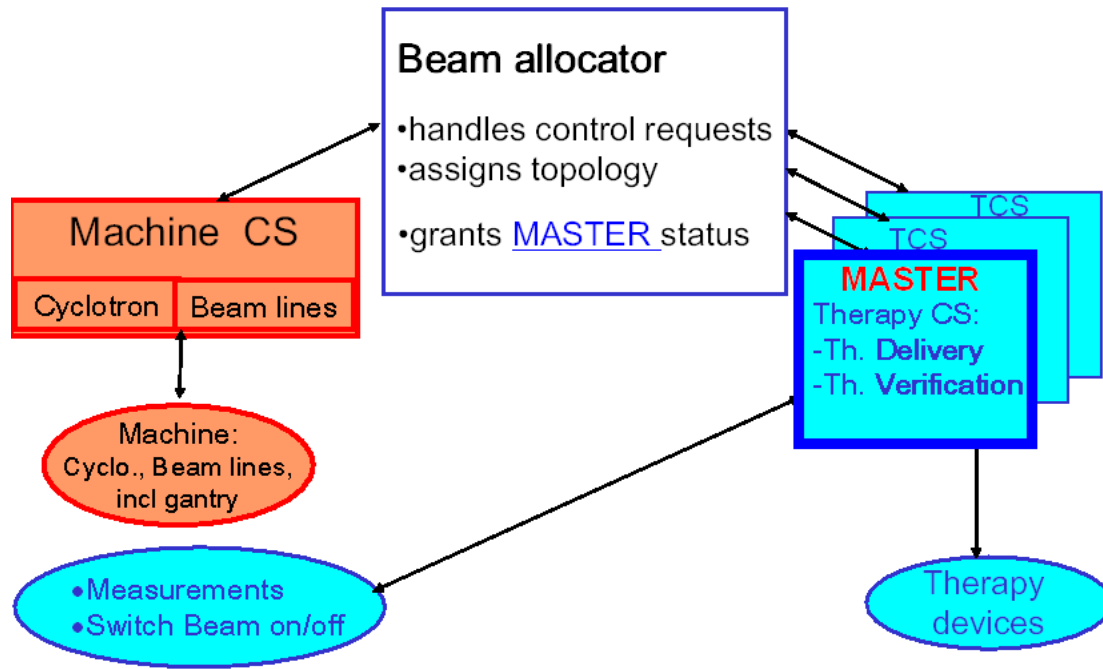
6015

6016 At PSI, a rigorous separation has been achieved between the responsibilities of cyclotron and
6017 beam transport lines and those related to the treatment equipment. This decouples the tasks and
6018 responsibilities of the machine as a beam delivery system and a user who decides whether the beam is
6019 accepted or not for a treatment.

6020

6021 This separation is reflected in the control system architecture (see Fig. 8.4). A Machine Control
6022 System (MCS) controls the accelerator and beam lines and it only controls the machine performance
6023 itself. Each treatment area has its own Therapy Control System (TCS). Each TCS communicates with the
6024 MCS *via* a Beam Allocator (BAL), a software package that grants the TCS of the requesting area
6025 exclusive access (the Master status) to the corresponding beam line up to the accelerator. Also, it grants
6026 the Master TCS a selected set of actions. This includes control of the degrader, beam line magnets and
6027 kicker, and the right to give beam on/off commands. The Master TCS will ask the MCS *via* the BAL to
6028 set the beam line according a predefined setting list. Independently of the MCS, the Master TCS will
6029 start, verify, use, and stop the beam.

6030



6031

6032

6033 Figure 8.4. Concept of the different control systems. Only one of the Therapy Control Systems (TCS,
6034 right side) has mastership over the facility and can set beam line components *via* the Beam Allocator

6035 (BAL). Necessary measurements and beam on/off is done directly by the Master TCS. (Courtesy of PSI)

6036

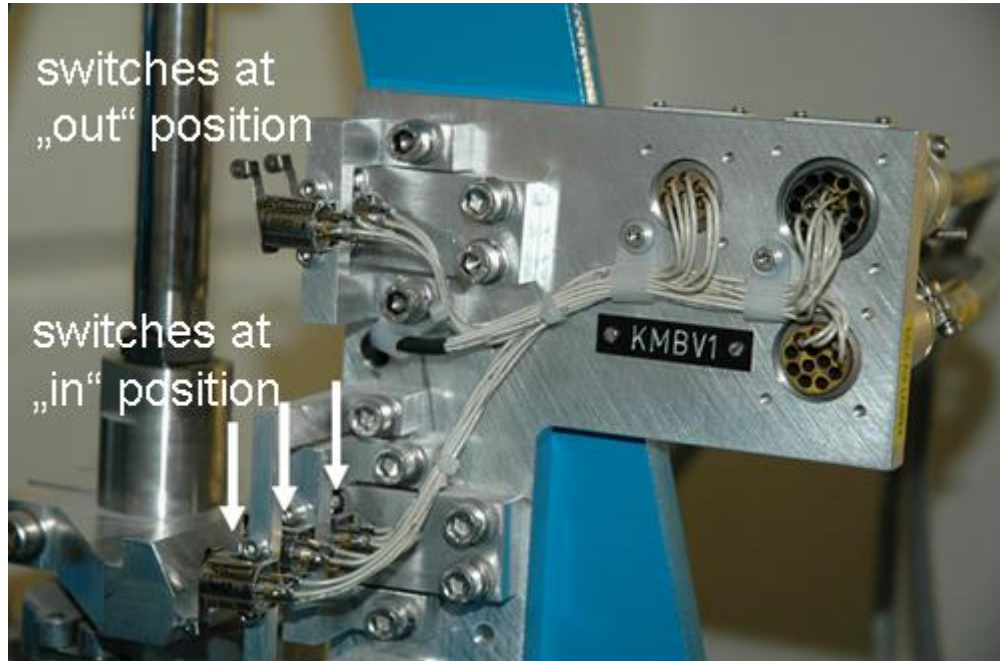
6037

6038 **8.3.2 Separation of Systems**

6039

6040 The separation of the safety systems as well as the control systems extends to the cabling of the
6041 hardware, and if possible to the hardware itself (*e.g.*, ion chambers). Each system has its own signal
6042 cables and limit switches. As can be seen in Figure 8.5, the closed (“in”) position of a mechanical beam
6043 blocker is equipped with three limit switches, one for each safety system.

6044



6045

6046

6047 Figure 8.5. Partial view of a mechanical actuator of a stopper. Each safety system (for machine,

6048 personnel, and patients) has its own signal, resulting in three limit switches on this stopper. (Courtesy of

6049 PSI)

6050

6051

6052 **8.3.3 Facility Modes**

6053

6054 In order to organize when certain operator actions are allowed, three different facility modes have
6055 been defined. The Therapy Mode is used for patient treatment. The Diagnostic Mode is used for tuning a
6056 beam line which is allocated to an area with Master status. Normally no patient treatment is allowed.
6057 However, in case of a minor problem (*e.g.*, bridging a RPS interlock signal due to a problem with a
6058 vacuum pump), this mode can be used to finish a treatment. Special rules apply in this case (see Sec.
6059 8.6.1). The facility can only be in Therapy Mode or Diagnostic Mode when requested by the control
6060 system of a treatment room. The Machine Mode is used for the daily setup of the machine and allows
6061 beam tests to be made with the accelerator and the energy degrader. In Machine Mode, the facility safety
6062 system is set to a virtual user area “accelerator”; opening of all the beam stoppers BMx1 is disabled and
6063 beam cannot be directed to the user areas.

6064

6065 Only the operator of the treatment area that has obtained mastership is able to set the facility
6066 mode to Therapy Mode or Diagnostic Mode and use the beam. Switching from an area which is in
6067 Diagnostic Mode to an area in Therapy Mode requires a procedure which first forces the beam line and
6068 current setting into a safe state.

6069

6070 **8.3.4 Treatment Procedure and Typical Operator Actions**

6071

6072 The way a facility is operated is strongly site dependent. At PSI there is an operator crew in a
6073 main control room (24hrs/day, 7 days/week) and there are local radiation therapists (or therapy operators)
6074 at every treatment room. The task of the operator in the main control room is to prepare and check the
6075 accelerator and beam lines early in the morning and to store specific machine parameters for several

6076 standard beam intensities for the day. When these activities have been completed, the mastership is
6077 handed over to the first treatment area, where QA checks are to be performed. This QA comprises the
6078 set-up and check of the scanning parameters, dose delivery, and interlock system.

6079

6080 During the day, until the last patient has been treated, the radiation therapists are responsible for
6081 setting the machine and safety systems in the mode that allows patient treatment or switching of
6082 treatment areas. Changing facility mode is done *via* a well defined procedure that validates the integrity
6083 of the system.

6084

6085 When a particular room is ready to receive beam for a patient treatment, the radiation therapist in
6086 that treatment room requests mastership from the Beam Allocator application (BAL; see Sec. 8.3.1) to
6087 be able to start therapy operation. Mastership is granted when not possessed by another treatment room.
6088 For efficient use of the beam time, the radiation therapist of each treatment room needs to be informed of
6089 the status and progress of the treatments in the other rooms. Although not yet implemented at PSI, one
6090 could imagine a screen showing the expected time left until mastership is released by the current Master
6091 treatment room. In most commercial systems, the control system has an application which provides
6092 information about the treatment status and patient flow in each treatment room and proposes or alerts the
6093 next treatment room in the queue to get mastership.

6094

6095 When mastership has been obtained and the patient is ready for treatment, the radiation therapist
6096 selects the steering file and presses the “GO” button. This starts the computer program on the Therapy
6097 Control System (TCS) that executes the treatment. The TCS executes the sequence of commands listed
6098 in the steering file for this treatment that was generated by the treatment planning system. This file
6099 contains all necessary parameters and the appropriate order of actions to perform the treatment. After the

6100 treatment has reached a normal end, the kicker magnet AMAKI deflects the beam automatically to stop
6101 the beam and, in addition, beam stopper BMx2 is inserted automatically. When mastership is released
6102 (treatment is completed) or the room is to be entered by the therapist, beam stoppers BMA1 and BMx1
6103 are also inserted as well as the neutron stopper.

6104

6105 In case of an interlock trip during treatment, the radiation therapist who has mastership
6106 determines the cause by checking the displays of the interlock system and the error log. When the
6107 problem is transient or can be solved, the system is reset by the radiation therapist and the spot scanning
6108 continues where it had stopped. If the treatment cannot be resumed within a few minutes (depending on
6109 the patient), the partial treatment is logged and documented and the patient is taken from the gantry to the
6110 preparation room. On the other hand, when an interlock occurs, the mastership can be given to the main
6111 control room so that the problem can be solved by a machine operator. When the problem has been
6112 solved, the patient will be brought back to the gantry and repositioned. After getting back the mastership,
6113 the procedure for restarting an interrupted treatment is performed and then the treatment will continue at
6114 the spot number (and its corresponding position) where the treatment had stopped. The TCS always
6115 keeps track of the spot number and the monitor units applied using a power fail safe procedure.

6116

6117 **8.3.5 Hardware**

6118

6119 In the sections dealing with the respective safety systems, details of the hardware are given. In
6120 general, one should try to use well-proven components and systems. Aspects to consider when selecting
6121 hardware are: robustness; fail-safe design; which transient states are possible; what if the device is
6122 switched off or cables not connected; robustness and signaling of overflow or signal saturation; time
6123 response (speed as well as reproducibility); possible SIL level; and certification by manufacturer.

6124 Programmable Logic Controllers (PLCs) can be used for user interface applications and general control
6125 functions. In general, however, PLCs are not allowed to be used in safety systems. Therefore, some
6126 companies have developed dedicated and certified safety PLCs. To reach the required level of safety,
6127 special concepts (*e.g.*, redundancy) have been integrated into the PLC design. One part of these concepts
6128 is a rigorous test program that is to be performed after any small change in a program of the PLC.

6129

6130 When speed or a reproducible time response is an issue (*e.g.*, in switch-off systems) advanced
6131 logic components and/or Digital Signal Processors (DSPs) are preferred.

6132

6133 **8.4 Personnel Safety System**

6134

6135 A Personnel Safety System (PSS) needs to be robust to prevent irradiation of staff or other
6136 persons; however, it needs a certain flexibility to ensure reliable beam operation and both fast and easy
6137 access to areas where patients are treated. Considerable experience exists with such systems in
6138 accelerator laboratories and radiation therapy departments, although there are different constraints in
6139 these applications. In a proton or ion therapy facility, the philosophies of an accelerator laboratory and a
6140 radiation therapy department must be combined. The PSS used at PSI is based on the philosophy of an
6141 accelerator laboratory, but for the application in the treatment rooms it has implemented an extension
6142 dedicated to patient treatment. The accelerator laboratory type of system that is normally installed at the
6143 PSI accelerator complex is applied to the access control of the room for experimental measurements and
6144 to the cyclotron/beam-line vaults. Access to these areas is controlled (*via* PSS) by the operators in the
6145 permanently manned control room for all accelerators at PSI. The necessary communication with these
6146 operators when entering these areas is usually organized differently in a hospital-based facility. On the

6147 other hand, the system used for the therapy rooms at PSI is not much different from the system used in a
6148 hospital-based proton or ion therapy facility.

6149

6150 **8.4.1 Purpose**

6151

6152 The purpose of a PSS is to prevent people from reaching areas where beam can be delivered,
6153 which can eventually result in an accidental exposure due to particle or photon irradiation. Specifically, a
6154 PSS has to ensure that no beam can be transferred into an area accessible to personnel. On the other
6155 hand, personnel access has to be inhibited if beam operation is possible in that area. Furthermore, PSS
6156 signals can be used to monitor radiation levels in accessible controlled areas for which the beam is
6157 blocked. The radiation dose in an accessible area could be too high due to uncontrolled beam losses in a
6158 neighboring area. A PSS must generate an interlock trip when an event occurs (*e.g.*, a limit switch opens)
6159 or when a critical situation develops that does not concur with the actual PSS access conditions, *i.e.*, an
6160 excessive dose rate in an accessible controlled area.

6161

6162 The designation of different areas according to their radiological risk and the associated
6163 accessibility concepts are applied in different way in different countries. For example, areas can be
6164 designated as “forbidden,” “locked,” “controlled,” “surveyed,” “public,” “staff only,” *etc.* Sometimes
6165 one uses indications of radioactivity levels (“red,” “yellow,” “green”), or lamps indicating “beam on” or
6166 “beam off.” These assignments should be associated with a risk evaluation that determines the area
6167 classification and the access rules. Apart from the goal to protect persons, it is also of utmost importance
6168 that the access rules are easy to understand and maintain. When access is “forbidden,” it should not be
6169 possible to enter accidentally.

6170

6171 In most countries, areas with an enhanced radiological risk must be designated as “controlled
6172 areas” or the equivalent. For such areas, access restrictions must exist as prescribed by local rules. The
6173 most common requirement is the wearing of individual dose meters applicable to the potential type of
6174 radiation occurring (*i.e.*, neutron radiation or γ radiation) in order to detect the radiation exposure of
6175 people. Frequently, a level classification is assigned to the controlled areas. This level classification is
6176 related to the level of contamination risk (leading to an adapted dress code), possible dose rate
6177 (potentially resulting in restricted occupation time), or possible presence of the proton beam. The
6178 accessibility depends on the area type (level) and status of the PSS, and can be designated “free” or
6179 “limited” access areas for authorized personnel.

6180

6181 **8.4.2 Modes of Operation**

6182

6183 At PSI the access status of an area is set by the PSS and is displayed at a panel near the entrance
6184 of the area (see Sec. 8.4.5.1).

6185

6186 It can have the following modes:

- 6187 • “free”: doors can be open.
- 6188 • “limited”: the door is unlocked remotely by the control room operator and each person
6189 must take a key from the key bank at the door.
- 6190 • “locked”: the door is locked. It is possible that there is beam present in the area or that the
6191 dose rate in the area is above a specified limit.
- 6192 • “alarm”: Beam is switched off and the door of the area is released.

6193

6194 Treatment rooms can only be “free” or “locked.” When the area has the status “locked,” either a
6195 door is locked or a light barrier will detect a person entering the room and initiate an alarm; see below.

6196

6197 When a treatment room “x” is accessible, one must ensure that no beam can be sent into the
6198 room. This is guaranteed by inserting the beam stopper BMx1 and a neutron stopper just upstream of the
6199 hole in the wall where the beam line enters this room. When the accessible area is a beam-line vault or
6200 the cyclotron vault, the cyclotron RF as well as the ion source must be switched off.

6201

6202 Table 8.3 summarizes the different conditions and actions related to the PSS access control. In
6203 order to switch the mode of an area from “free” to “limited” or “locked,” a search for persons in the room
6204 is mandatory. The search is made by the last person leaving the area, who must push several buttons at
6205 different locations in the area, to ensure the complete search has been made. Also, an audio signal warns
6206 people to leave the area (except in treatment rooms). When a person wants to enter the cyclotron/beam-
6207 line vaults or the experimental vault again, this can be done in “limited” access mode. In this mode, each
6208 person entering the area must take a key from the key bank near the door. In order to switch the access
6209 mode of an area from “limited” to “locked,” no search is needed, but all keys must be in the key bank at
6210 the entrance door of the area before that vault’s status can be switched back to “locked.” Only when the
6211 area is “locked” can BMx1 and its neutron stopper can be removed from the beam line, or the cyclotron
6212 RF and ion source can be switched on again.

6213 Table 8.3. Status and actions of beam intercepting components for area access.

Reason for beam off by Personnel Safety System	Beam interrupting components				Other constraints
	RF	Ion source	BMx1	Neutron stopper x	
allowed access to user area x			must be in	must be in	Area dose monitor being checked (prevents access or evokes alarm signal when dose rate too high)
allowed access in cyclotron/beam-line vault, when the area is (limited) accessible	must be off	must be off			Lead shield must be at degrader Area dose monitor being checked (prevents access or evokes alarm signal when dose rate too high)
Emergency off request / Alarm signal in cyclotron/beam-line vault e.g: -emergency button pressed -failure in safety relevant element -local dose monitor above limit	Switch off	Switch off			
Emergency off request / Alarm signal in user area x e.g: -emergency button pressed -failure in safety relevant element -local dose monitor above limit	Switch off	Switch off	insert	insert	

6214

6215

6216 The entry of all vaults and rooms is through a maze. A polyethylene door is mounted at the exit
6217 of the mazes to the patient treatment rooms. It is not closed during patient treatment in order to allow fast
6218 access to a patient by the therapist. In the maze, a light barrier that detects a person who enters the
6219 corridor is used in Therapy Mode. The light barrier will trigger an alarm that stops the RF and the ion
6220 source, and inserts BMx1 and corresponding neutron stopper x. The polyethylene door must be closed
6221 for non-therapy operation in a treatment room (*e.g.*, QA, calibrations, *etc.*).

6222
6223 At PSI, the access status of the cyclotron vault and experimental room can only be changed
6224 remotely by an operator in the control room. The treatment rooms, however, have a local control panel
6225 near the door by which the medical staff can set the access status themselves (“free” or “locked”).

6226
6227 Emergency-off buttons are mounted in each area and in each vault to initiate an alarm by a person
6228 who is still in the room. This alarm switches the RF and ion source off, inserts BMx1, and unlocks the
6229 area entrance doors.

6230

6231 **8.4.3 Rules of Beam Turn-Off**

6232

6233 Because the PSS basically only gives permission to turn the RF and ion source on after checking
6234 if all conditions are met, it is, in effect, passive with respect to beam control. During beam operation, if
6235 one of the conditions is not met anymore, permission will be removed and the beam (RF and ion source)
6236 turned off. It is important that the beam does not automatically switch on after it has been switched off
6237 due to an interlock trip and reset again. Beam must always be turned on deliberately by the operator.

6238

6239 **8.4.4 Functional Implementation**

6240

6241 The PSS system runs on a dedicated safety PLC that is certified for safety functions. It is
6242 constructed of fail-safe components and is completely separated from other systems. This system has its
6243 own dedicated actuator supervision sensors (*e.g.*, limit switches or end switches) to register the status of
6244 connected actuators such as beam stoppers. When the PSS causes an interlock trip, beam and neutron
6245 stoppers will “fall” into their closed position. At PSI, the motion of mechanical stoppers is controlled by
6246 compressed air in addition to gravity (fail-safe). In the event of such a trip, several devices (mechanical
6247 stoppers but also RF) will act at the same time to intercept the beam.

6248

6249 A separate PSS input is present in the control boxes of the RF and ion source. A fail-safe signal
6250 must be present to allow “RF on” or “ion source on.” If a cable is disconnected the signal is absent.

6251

6252 **8.4.5 Components**

6253

6254 The PSS is only one part of a system ensuring personnel safety. Several devices, with different
6255 functions, are connected to this system; some of them will be discussed here.

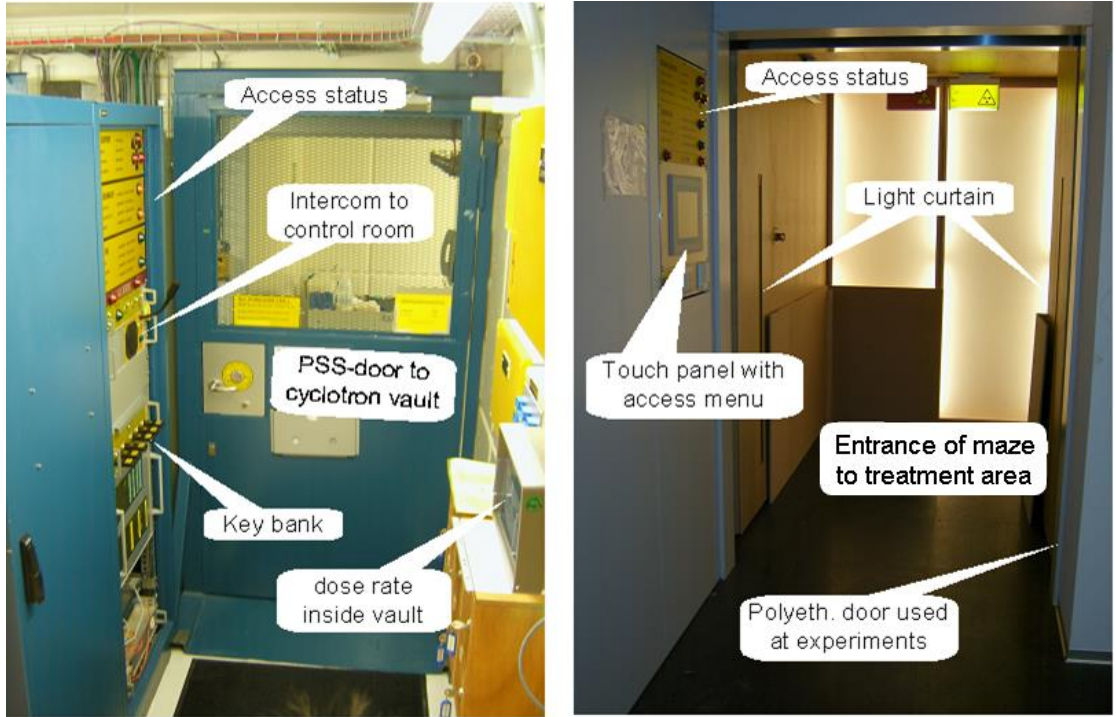
6256

6257 **8.4.5.1 Area Access Control.** The implementation of access control in a hospital-based proton
6258 or ion therapy facility can be organized quite similarly to a conventional radiation therapy facility. The
6259 way it is implemented might also depend on the distance and visual contact situation between the control
6260 desk of the radiation therapist and the door to the treatment room.

6261

6262 At PSI, dedicated cabinets for area access control are installed near the entrance door of each area
6263 (Fig. 8.6). The cabinets at the therapy areas are equipped with touch panels that guide the user through a

6264 menu of required sequential actions to allow access or to allow beam into the area. The panels and key
6265 banks at the beam-line vault are installed next to a dedicated PSS door. The access status is visible on the
6266 panel and a direct intercom connection to the control room is used if one wants to change the access
6267 status or enter the vault in “limited” access mode. At PSI, no “beam on” type of signal is displayed at the
6268 door. The access status only forbids or permits beam in the area, but whether beam is actually sent to the
6269 area is up to the user.
6270



6271

6272

6273 Figure 8.6. Personnel Safety System units at vault entrance and treatment room entrance (Courtesy of

6274 PSI)

6275

6276 For radiation shielding purposes, the cyclotron vault has an additional concrete door at the maze
6277 entrance from the vault. Inside the vaults, warning lights and audio signals provide warning before the
6278 access mode is changed to “locked.” In order to prevent patient confusion, this is not done inside the
6279 patient treatment rooms at PSI. However, local regulations might impose that beam on/off warning lights
6280 must also be installed or used in the treatment rooms.

6281

6282 **8.4.5.2 Detectors.** Monitors are mounted in the vaults, controlled areas, and patient treatment
6283 rooms to protect personnel against radiation. The extension for proton or ion therapy is that monitors
6284 must be installed for gamma rays as well as for neutrons (see Chapter 4). They must trigger an alarm that
6285 leads to an interlock trip when the area is in “free” or in “limited” access mode and a dose rate above a
6286 preset threshold is detected. At the exits of the cyclotron/beam-line vault and the experimental area at
6287 PSI, hand/foot monitors are installed. These are not connected to the interlocks.

6288

6289 **8.5 Patient Safety System**

6290

6291 The purpose of the Patient Safety System (PaSS) is to guarantee a safe treatment of the patient.
6292 This has led to the rigorous separation of the functionality and safety systems, and it enabled PSI to build
6293 a dedicated patient safety system that can be understood by all users and is well documented. The design
6294 of the PSI system is based on general safety concepts and safety functions, which can in principle be
6295 applied in any particle therapy system. In this section, the concepts of the system will be discussed first,
6296 followed by a more detailed description of the components with the purpose of illustrating how the
6297 concepts can be realized in practice. As a consequence, a simplified description is given, which is by no
6298 means complete. Finally, the PSI-specific situation with respect to spot scanning will be addressed,

6299 followed by the rules applied by the Patient Safety System to turn the beam off, and some remarks on
6300 quality assurance.

6301

6302 **8.5.1 Purpose**

6303

6304 The task of any Patient Safety System (PaSS) is to comply with established requirements in order
6305 to reach the essential safety goals for patient protection. These goals can be formulated as such:

6306

6307 *Goal 1: No serious radiation accidents can occur.*

6308 The most serious accident is the delivery of an unintended high dose to the patient. The first and
6309 most important safety aim is to prevent an unintentional additional dose delivery greater than 3 Gy
6310 (5 % of the total treatment dose) in case of a serious radiation accident. This is in correspondence
6311 with the claim to prevent all Class I hazards of type A and B, following the classification for
6312 accidental exposures published in ICRP Publication 86 (2000). The main concerns here are the
6313 monitoring and beam switch-off systems.

6314

6315 *Goal 2: To apply the correct and known radiation dose.*

6316 Any error in the total treatment dose delivered can adversely increase the probability of an
6317 unacceptable treatment outcome (lack of tumor control or increased complications). Therefore, the
6318 second safety goal is to prevent the occurrence of such errors during therapy, *e.g.*, by using a
6319 redundant dose monitoring system in the nozzle of the beam delivery system, and to limit the
6320 unintended extra dose due to such errors (IEC, 1998). This extra unintended dose must be lower
6321 than 10 % of the fraction dose (IEC, 1998). At PSI, we aim for less than 2 % of the fraction dose,
6322 *i.e.*, 4 cGy for Gantry 1.

6323

6324 *Goal 3: To apply the dose to the correct position in the patient.*

6325 The main concerns here are the control of the position (checked by means of a position sensitive
6326 ionization chamber in the nozzle of the beam delivery system) and energy of the beam (checked by
6327 means of a dedicated position signal from the degrader and dedicated reading of bending magnet
6328 settings), and the position of the patient (by prior CT scout views, x rays, cameras).

6329

6330 *Goal 4: Applied dose and dose position must be known at all times.*

6331 If the irradiation is interrupted at any time, the dose already given and the beam position of the last
6332 irradiated spot must be known.

6333

6334 **8.5.2 Functional Requirements**

6335

6336 The amount of the dose and the position of applied dose are monitored by the therapy control and
6337 therapy monitoring systems (see Sec. 8.5.4.4). The major requirement of the Patient Safety System is to
6338 cause an interlock trip when the tolerance limits in this monitoring system or in other devices that
6339 monitor the status of crucial beam line and accelerator components are exceeded. In general, this is in
6340 analogy with the usual practice in radiation therapy to record and verify all the parameters being used
6341 during the treatment and interrupting treatment in case of lack of agreement between planned and real
6342 values. This could be done, *e.g.*, by using commercially available “Record and Verify” systems. Due to
6343 the high degree of complexity of a proton or ion therapy system, the number of available parameters is
6344 too large to deal with for this purpose. Furthermore, many parameters have no relevance for the safety of
6345 the patient. Therefore, in every proton or ion therapy facility, a selection of the relevant parameters or
6346 components must be made. The most important components selected for this purpose at PSI are

6347 described in 8.5.4.4. Further, to avoid severe radiation accidents and to switch off the beam with high
6348 reliability after each interlock trip, a redundant system is needed with multiple independent systems to
6349 switch the beam off.

6350

6351 In a system with multiple treatment areas, a secure patient treatment in a pre-selected area must
6352 be guaranteed, and interferences from other parts of the treatment facility are not allowed. It is usually
6353 required to be able to sequentially treat patients in different areas with a switching time of less than one
6354 minute.

6355

6356 An important specification is the independence of the treatment delivery and patient safety
6357 system from the rest of the facility, including the control systems. Signals from beam-line devices that
6358 are crucial for safe operation are directly sent to the PaSS and the PaSS also has direct access to selected
6359 components to switch off the beam. It has no other control functionality than switching off the beam (or
6360 preventing the switching on of the beam) through these devices when an anomaly has been detected.

6361

6362 When a patient is being treated, all parameter values, patient-specific or field-specific devices,
6363 and machine settings must be read from the steering file generated by the treatment planning system. One
6364 important task of a Patient Safety System is to ensure that the correct devices are installed and that
6365 parameters are set appropriately.

6366

6367 At PSI, the irradiation of the patient is fully automated, which minimizes human errors. Before
6368 the treatment starts, the TCS reads all instructions, all settings of the machine, and dose limits from the
6369 steering file. The PaSS also obtains the steering file information and makes an independent check of the
6370 settings of selected critical devices, and watches relevant measurements. When the treatment is started,

6371 the TCS starts the actions listed in the steering file and the PaSS verifies online if the treatment proceeds
6372 as it should.

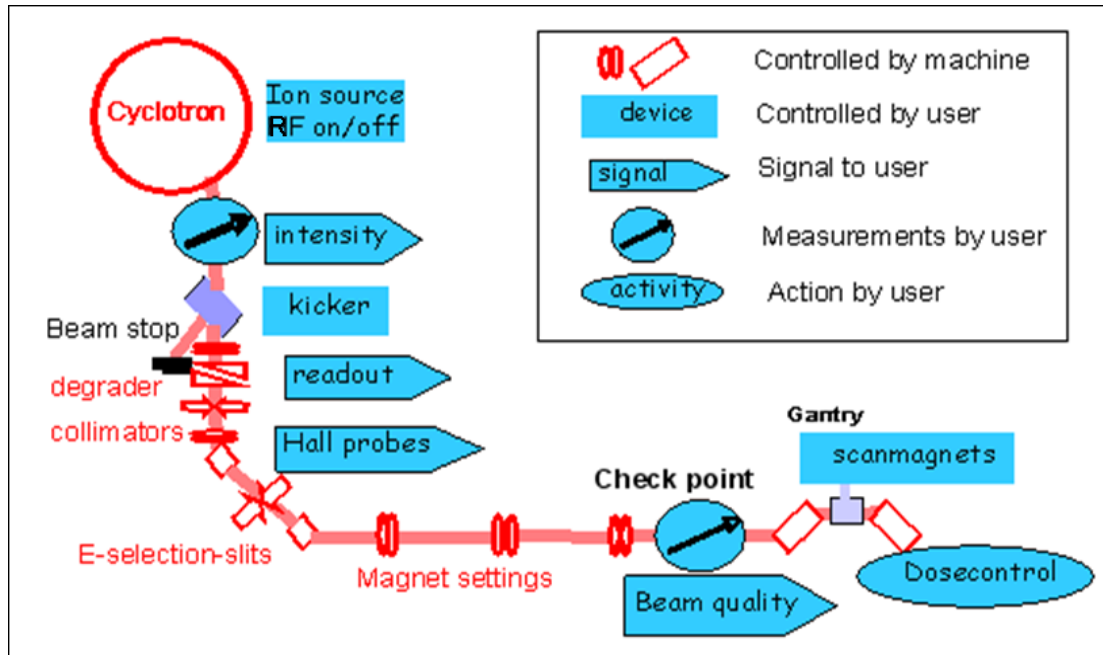
6373

6374 **8.5.3 Description of System**

6375

6376 During a treatment the (Master) TCS sends instructions to the machine control system (MCS; see
6377 Sec. 8.3). In the scanning technique employed at PSI, the beam-line settings vary during the treatment
6378 because the energy is also a beam-line parameter. For each beam energy the MCS will use a predefined
6379 setting of the beam line (a “tune”). During treatment, a sequence of tunes is used as given in the steering
6380 file. For every tune to be set, the TCS sends the tune information to the MCS, which sets the degrader
6381 and the magnets, *etc.* accordingly. The TCS automatically verifies whether the beam characteristics
6382 satisfy the user’s needs by means of dedicated beam diagnostics at the checkpoints, and dedicated signals
6383 from energy-defining elements. The Patient Safety System automatically checks the results of these
6384 verifications (Jirousek *et al.*, 2003). Note that all these readout systems are exclusively used by PaSS (the
6385 blue boxes in Figure 8.7).

6386



6387

6388

6389 Figure 8.7. Signals to the Therapy Control System (TCS) of Gantry-1 are indicated with arrow-boxes.

6390 Components controlled by TCS or PaSS are in rectangular boxes and the oval boxes indicate actions by

6391 TCS or PaSS. (Courtesy of PSI)

6392

6393

6394 **8.5.4 Components of the Patient Safety System (PaSS)**

6395

6396 The main components of the PaSS are:

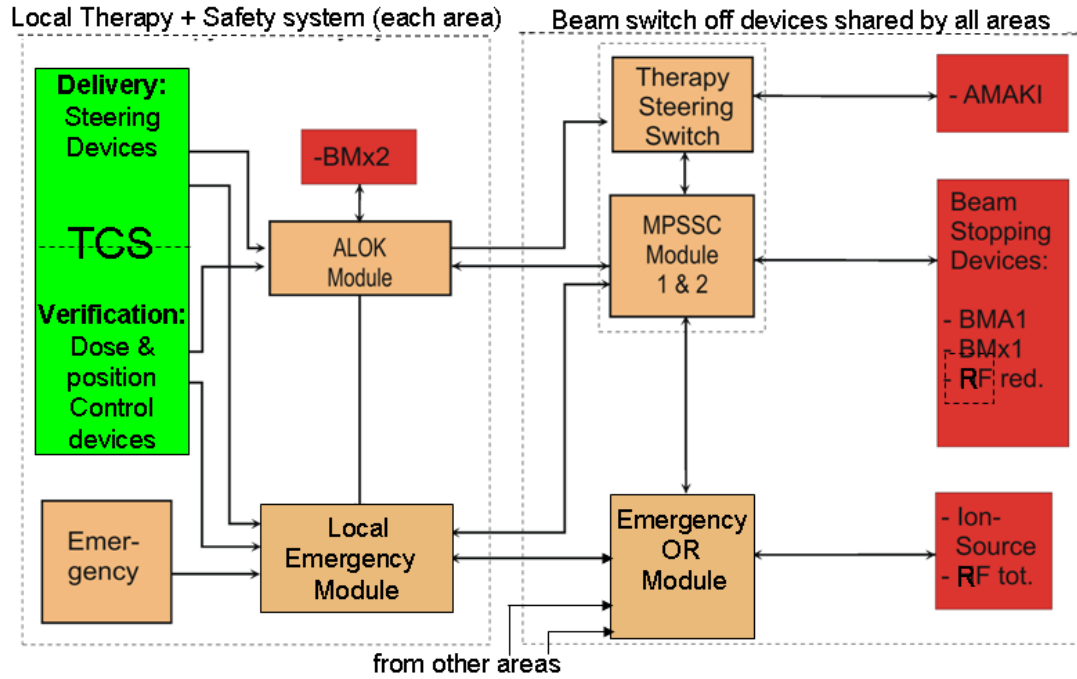
- 6397 • *Main Patient Safety Switch and Controller (MPSSC)*: a central system that controls and
6398 supervises a unique beam line and area allocation to only one user or treatment room (the
6399 Master treatment room) at a time and transfers or triggers interlock signals.
- 6400 • *Local PaSS*: the local patient safety system of a treatment room. It monitors all the signals
6401 (interlocks, warnings, and “beam ready”) connected to the Therapy Control System of this
6402 room and can generate and send interlock to the local and remote actuators.
- 6403 • *Emergency OR module*: a logic unit that generates a global emergency beam switch-off
6404 signal when either one of the input signals (permanent hardwired connections to each
6405 room) is not OK. Being an independent device, it also acts as a redundant safety switch-
6406 off for the MPSSC.
- 6407 • *Detectors and sensors*: these devices are wired to the PaSS.
- 6408 • *Beam-interrupting devices*: The actuators are activated by the local PaSS or the MPSSC.
6409 For details, see Sec. 8.2.

6410

6411 In addition, there are modules that read out, digitize, process, and distribute the signals observed
6412 by the PaSS. These modules perform simple tasks that are implemented in the low-level software or
6413 firmware and they operate independently of the control system (except for being informed of the
6414 currently requested beam tune).

6415

6416 In the following subsections, the function of the main components will be described in more
6417 detail. The organization of these components and the interlock signals are schematically displayed in
6418 Figure 8.8.
6419



6420

6421

6422 Figure 8.8. The connection between the Local Patient Safety System (Local PaSS) of each area, MPSSC

6423 (Main Patient Safety Switch and Controller), Emergency OR module, and the major beam on/off

6424 actuators. The Emergency OR can generate a redundant switch-off signal, hard wired to the RF and ion

6425 source. (Courtesy of PSI)

6426

6427 **8.5.4.1 Main Patient Safety Switch and Controller (MPSSC).** A topology control must be
6428 implemented because there are multiple areas for treatments or experiments in the facility. Therefore an
6429 important part of the PaSS is a central system that controls and supervises a unique beam line and area
6430 allocation to only one user or treatment room (the Master treatment room) at a time. This system, the
6431 Main Patient Safety Switch and Controller (MPSSC) monitors the interlocks and status of all areas. It
6432 controls and supervises a unique beam line and area allocation, then sets its operation mode according to
6433 a defined sequence including the following steps: disable the beam stoppers in all areas, and enable the
6434 beam stopper BMx1 in the Master area. The exclusivity of the granting of the Master status will be
6435 checked. It enables the Master user to switch on the beam with the fast kicker magnet AMAKI and
6436 monitors its interlock status. Further, it monitors the operation of the beam interrupting elements and
6437 verifies the consistency of the ready signal returned from the RPS and the reservation signal from the
6438 Master area's TCS.

6439
6440 The MPSSC will generate an interlock trip when one of the above mentioned supervising
6441 functions indicates an error or an inconsistency. In case of a failure within the MPSSC and its beam
6442 actuators, the MPSSC will generate a emergency interlock (ETOT). The MPSSC has been built in a
6443 redundant configuration.

6444
6445 **8.5.4.2 Local PaSS.** Each area has a local PaSS that is embedded in the TCS of that area and that
6446 monitors all the signals connected to that TCS (interlocks, warnings, and "beam ready"). It generates and
6447 monitors the pre-programmed AMAKI on/off signals for the spot scanning and monitors the remaining
6448 beam intensity in case of a local interlock ("ALOK"). The local PaSS can stop the beam independently
6449 of the MPSSC status. In that case, it uses BMx2, a beam blocker controlled solely by the local PaSS.

6450

6451 **8.5.4.3 Emergency OR Module.** The Emergency OR module is a logic unit with permanent
6452 hardwired input signals from each area. It generates a global emergency switch-off signal “ETOT” when
6453 there is an alarm signal on one of the input signals. The electronic module has no processors and acts as a
6454 simple logic “OR” function to pass the alarm signal on to the RF and ion source. As can be seen in Fig.
6455 8.8, the system is independent of the MPSSC and user status. The independence guarantees that the beam
6456 can be turned off by two redundant systems, each using a separate set of beam stopping actuators.

6457

6458 **8.5.4.4 Detectors and Safety-Relevant Signals from Various Components.** The signals from
6459 the beam line leading to an interlock trip from the Patient Safety System come from:

- 6460 • dedicated beam-intensity monitors (ionization chambers and a measurement of the
6461 secondary electron emission from a foil, which does not saturate at high intensities);
- 6462 • dedicated reading of the degrader position to verify the set beam energy;
- 6463 • dedicated magnetic switch in the AMAKI kicker magnet, to verify the action of the
6464 kicker;
- 6465 • dedicated Hall probes in each dipole magnet to verify the set beam energy;
- 6466 • beam-intensity monitors at the check points (specific locations along the beam line); and
- 6467 • monitors in the beam nozzle upstream of the patient, which encompass, *e.g.*, the plane
6468 parallel-plate ionization chambers “Monitor 1” and “Monitor 2” in Gantry 1 (the latter of
6469 which has a larger gap to provide diversity in sensor design; see Sec. 8.5.5). “Monitor 3”
6470 is an ionization chamber to measure dose as well, but equipped with a grid to have a faster
6471 response. In addition, multi-strip ion chambers are used to measure the position of the
6472 pencil beam during the delivery of each spot.

6473

6474 **8.5.4.5 Electronics, Hardware, and Firmware.** The hardware platform used in the PaSS is an
6475 Industry Pack (IP) carrier board with a Digital Signal Processor (DSP). The logic to switch the beam off
6476 is embedded in IP modules mounted on the carrier boards.

6477
6478 Several methods are used to enhance reliability. Redundant paths were implemented between the
6479 subsystems to avoid single points of failure. Further , diagnostic coverage in the system has been
6480 increased. At the same time, care has been taken to use diversity, such as the use of different types of
6481 sensors, but also the supervision of actuators as well as the direct detection of the beam status.

6482

6483 **8.5.5 Implementation of the PaSS for Dose Application and Spot Scanning**

6484

6485 The use of the spot-scanning technique at PSI has specific implications for the design details of
6486 the patient safety system. In Gantry-1 of PSI, the dose is applied by discrete spot scanning. The eye
6487 treatment in OPTIS2 is performed with a scattered beam that is applied as a sequence of single spots
6488 from the control system point of view. The application of the spot sequence is the most critical phase in
6489 terms of patient safety. The dose is delivered as a sequence of static dose deliveries (“discrete spot
6490 scanning”). The dose of each spot is checked online during the spot application. The dose delivery is
6491 based on the signal of Monitor 1 in the treatment nozzle. For the dose verification, two other monitors,
6492 Monitor 2 and Monitor 3, are used.

6493

6494 The radiation beam is switched off by the fast kicker magnet AMAKI between each spot
6495 delivery. The Monitor 2 preset value is always programmed with a built-in safety margin added to the
6496 prescribed dose. If Monitor 1 fails, then the beam is switched off by the Monitor 2 preset counter. The
6497 spot overdose resulting from this delay is estimated to be at maximum 0.04 Gy, which is 2 % of the

6498 fraction dose (PaSS Safety Goal 2). This corresponds to a fault situation and therefore an interlock signal
6499 will be generated (beam switch-off with interruption of the treatment). If no interlock signals were
6500 generated and if all the measuring systems show that the spot deposition has been carried out correctly,
6501 the TCS sets the actuators, verifies actuators, and applies the next dose spot. The maximum dose per spot
6502 that can be planned or given is limited by the maximum value that is allowed to be stored in the register
6503 of the preset counter.

6504

6505 A fixed upper limit for the maximum dose and dwell time of a spot is defined within the
6506 hardware. These limits are checked by watchdogs (also called backup timers) in the PaSS. These are
6507 separate electronic counters measuring the spot dose and the spot dwell time. If a defined value is
6508 exceeded (counter overflow), then an error signal will be produced automatically. Each watchdog is set
6509 back to zero at the end of the irradiation and approval of the spot dose. If the beam remains switched on
6510 unintentionally, the watchdogs will prevent a patient overdose greater than the maximum defined spot
6511 dose.

6512

6513 **8.5.6 Rules for Turning the Beam Off**

6514

6515 The layout of the safety system for beam switch-off with the interconnections between local
6516 interlock modules and the shared beam switch devices is drawn schematically in Fig. 8.8. Here one can
6517 see the central role of the MPSSC. It checks the interlock status of all areas, enables the main user to
6518 switch the kicker AMAKI, and controls its interlock status. It controls the commands of the Master user
6519 and the operation of specific beam-interrupting elements (reduced RF and the mechanical beam stoppers
6520 BMA1 and BMx1).

6521

6522 The PaSS can generate beam-off signals with different consequences and for different reasons.
6523 The signals and their causes are listed in Table 8.4. Their interlock level (hierarchy) and the switch-off
6524 action are listed in Table 8.5.
6525

6526 Table 8.4. The interlock signals of the Patient Safety System and examples of their causes.

6527

PaSS interlock signal	General cause	Examples of specific causes
ALOK	error detected within the local therapy control system	<ul style="list-style-type: none"> • Functional errors in a local device of TCS • Crossing of dose or position limits checked in the steering software.
ATOT	severe error detected in the allocated user safety system or error in the shared safety system that might lead to an uncontrolled deposition of dose or injury of a person	<ul style="list-style-type: none"> • Error in the allocated user safety system • AMAKI error, area reservation error • Watchdog error in any TCS which is in Therapy Mode • Error in any of the beam switch-off devices BMA1, BME1, RF red. • Error in MPSSC boards and firmware
ETOT	emergency signal generated in any user safety system or error detected in ATOT generation	<ul style="list-style-type: none"> • Emergency button pushed in any user safety system • Beam detected and ATOT interlock present • Error in the beam switch-off devices, RF off, or ion source • Error in the local supervision of emergency status.

6528

6529

6530 Table 8.5. The hierarchy of the interlock signals from the Patient Safety System and the components that
 6531 will switch off the beam.

6532

Interlock Level / Beam Switch-Off Control Function			Measures for Beam-Off
ETOT	ATOT	AOK	Beam Off command
			Send current through kicker magnet AMAKI
			Close local beam stopper BMx2
			Close beam stopper BMx1
			Close beam stopper BMA1
			Reduce RF power to 80%
			Switch off RF power
		Switch off ion-source power supply	

6533

6534

6535 During treatment, all relevant safety checks are performed for each spot. If there is any
6536 discrepancy between the prescribed and measured values of dose (Monitor 1, 2) or spot position (multi-
6537 strip monitor in the nozzle of the gantry, or a segmented ion chamber in the nozzle of OPTIS2), or in the
6538 case of a technical fault, the result is always an immediate interruption of the treatment and the
6539 generation of a local interlock trip “ALOK.”

6540

6541 The watchdogs that check fixed upper limits for the maximum dose and dwell time of a spot will
6542 automatically produce a global interlock “ATOT” if a defined value is exceeded (counter overflow).
6543 Figure 8.8 also shows that, through the separate connection to the Emergency OR module, the local
6544 system has the redundant capability of generating a global switch-off signal (“ETOT”), independent of
6545 the beam-line Master. The ETOT controls the switch-off of the ion source and the RF system.

6546

6547 **8.5.7 Quality Assurance**

6548

6549 As described in Sec. 8.1.5, frequent checks are performed of the Patient Safety System and each
6550 treatment area. The checks are described in a QA manual, which also prescribes the frequency of the
6551 tests (daily, weekly, monthly, yearly, *etc.*).

6552

6553 During the building phase of the facility, a rigorous quality test program has been undertaken.
6554 Not all possible configurations of a complete system can be checked; therefore, a procedure has been
6555 developed for performing separate bench tests during the production phase of the electronic components
6556 that are used in the Patient Safety System. With a simulation program that generates many initial
6557 conditions for the electronic circuit boards under test, the boards have been tested and automatic test
6558 reports have been generated.

8.6 Machine Safety: Run Permit System

6559

6560

6561 A machine safety interlock system should be used in every accelerator system. The tasks of this
6562 interlock system are protection of the machine and its subsystems from damage due to wrong actions or
6563 faulty devices, and to prevent unwanted high beam intensities. In the following sections, the system will
6564 be described in more detail.

6565

8.6.1 Purpose

6567

6568 The machine interlock system at PSI is called the Run Permit System (RPS). It checks the status
6569 of signals from all beam lines and cyclotron devices and compares these signals with the requested
6570 topology (beam-line sections that will be used). The beam can only be switched on when the RPS allows
6571 this; *i.e.*, when its “beam-off” signal is “false.” This is done when a topology has been reserved and when
6572 all devices in this topology have been set to their values and return an “OK” status. After the beam-off
6573 status has been set to false, it sends a “machine ready” signal to the (Master) TCS, which then can
6574 actually switch on the beam (with the kicker magnet AMAKI).

6575

6576 The task of the RPS is to prevent the machine from being damaged, to prevent unnecessary
6577 activation, and to prevent higher beam intensities than those allowed by the authorities. It does not check
6578 beam optics, or whether the calculated settings of magnets are correct. However, from beam diagnostics,
6579 several signals are observed online and bending magnet currents should be within intervals
6580 corresponding with the used beam lines. Furthermore, the RPS will switch the beam-off to “true” when
6581 fatal device faults are registered, such as an excessive temperature in a power supply or excessive
6582 pressure in the vacuum system.

6583

6584 A bridge can be set to ignore these signals in the case of non-severe failure signals. In Therapy
6585 Mode, however, no bridge is allowed. A protocol, signed by designated persons, must be used for cases
6586 when one has to run with a bridged signal (“degraded mode”). Running in Therapy Mode with a bridged
6587 signal is only allowed when an approval procedure by qualified persons is carried out, and only for a
6588 limited time (*e.g.*, one day).

6589

6590 Some functions of the RPS are redundantly implemented in the PaSS for therapy purposes (*e.g.*, a
6591 limit on the maximum allowed beam intensity). The “responsibilities” of RPS and PaSS, however, are
6592 strictly separated and the systems do not rely on each other.

6593

6594 **8.6.2 Functional Requirements**

6595

6596 The RPS is not intended to be used for personnel or patient safety; therefore, the requirements
6597 with respect to redundancy and “fail-safe” are less critical. However, for the RPS, general design rules
6598 (*e.g.*, cabling, where a failed connection invokes a safe state) apply that result in a high safety standard.
6599 An important requirement that applies specially for a proton therapy facility is that the RPS must be able
6600 to quickly change its settings, as the operational requirements change quickly. Because an important
6601 requirement for a proton therapy facility is a high uptime and high availability for the treatments, this
6602 requires special precautions against false alarms and the implementation of a user interface with clear
6603 data logging, failure recognition, and easy retrieval of the sequences that can lead to an interlock trip.

6604

6605 Most of the auxiliary devices possess their own device-safety system that checks the proper
6606 working of the devices. From these devices only status signals and, when available, detailed error

6607 information are sent to the RPS inputs. These are sent over fail-safe connections. Connections to the
6608 actuators as well as the end switches of beam stopping devices are separate from the ones of PaSS and
6609 PSS.

6610

6611 **8.6.3 Description of System**

6612

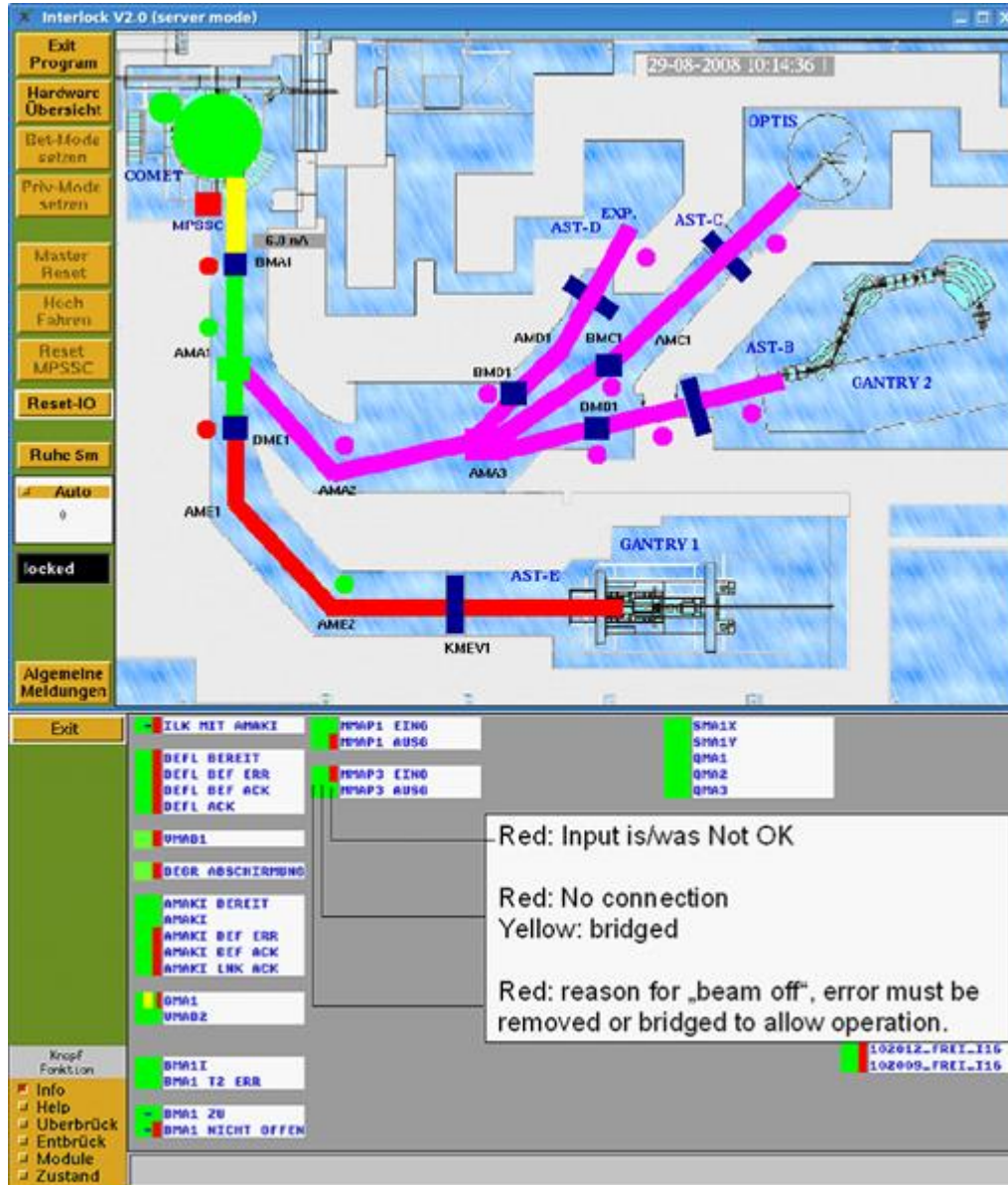
6613 Before turning the beam on, the topology and operation mode (Therapy, Diagnostic or Machine)
6614 are sent to a computer program that generates the unique logic configurations and defines the beam
6615 switch-off chain. Unlike the switch-off chain, which is hardwired to the various components that can
6616 switch off the beam; the data acquisition and element control are performed by software in VME
6617 computers.

6618

6619 The user interface (Fig. 8.9) indicates the RPS status by coloring the cyclotron and beam line
6620 sections. Green indicates that the section is ready for beam; red that it is not ready for beam; and yellow
6621 that it is ready, but with “bridges” applied. When an interlock trip from the RPS occurs, the cause of the
6622 sequences is logged and listed with time stamps in a message window. When clicking with the mouse on
6623 a beam line section, a screen with the status of all its components will show up for further analysis.

6624

6625



6626

6627

6628 Figure 8.9. Overview of the machine interlock (RPS) status. In the top figure, the beam line colors

6629 indicate the status of the corresponding beam line section. The bottom figure shows the status of

6630 individual components in the “bridged” first beam line section. (Courtesy of PSI)

6631

6632

6633

6634 **8.6.4 Components and Conditions That Are Checked**

6635

6636 Inputs that cause the logic to generate a switched-off signal are deduced from the status of the
6637 following component groups:

6638

6639 a) Active devices: power supplies of bending magnets, quadrupole magnets, and steering
6640 magnets belonging to the selected topology. The status signals yield information on the
6641 cooling, the ready signal (actual current = requested current), and a few general signals of
6642 the power supply.

6643 b) Devices with a verification/guarding role: beam current monitors (also ratios between
6644 monitors), slit and collimator currents, beam currents from beam stoppers, temperature
6645 measurements, water flow controls, *etc.*

6646 c) Configuration (topology) dependent parameters: magnet current intervals, positions of the
6647 neutron stoppers, beam stoppers, vacuum valves in the beam line, *etc.*

6648

6649 Many of the interlock trips will be caused by a device error, sent by a device that is part of the
6650 active topology. When an error occurs, it usually has an effect on the beam characteristics and beam
6651 losses. Some changes in beam losses can also lead to interlock trips. This intrinsic redundancy is very
6652 useful and, with the aid of proper logging with time stamps, helps in a quick diagnosis of a problem
6653 consisting of a chain of events.

6654

6655 **8.6.5 High-Reliability Components and Fail-Safe Design**

6656

6657 The Run Permit System is built of dedicated modules (Run Permit System module, RPSM), each
6658 having multiple I/O channels. Up to 4 RPSMs are mounted on a VME Basis plate. The direction of the
6659 signal flow is programmed in firmware (XILINX). The logic that determines whether to switch off or not
6660 is part of this program. Therefore, this logic is independent of the machine control system. The control
6661 system communicates with the RPSMs *via* I/O-Computers (IOCs) to obtain the switch-off diagnostics
6662 and information for the visualization programs, or to perform periodic tests.

6663

6664 The following security measures are incorporated in each RPSM:

6665

- 6666 a) The inputs and outputs are equipped with three-wire connections, so that disconnections
6667 or shorts are recognized and the module changes its state into “NC” (not connected) or
6668 “err” (short).
- 6669 b) Every RPSM is characterized by an individual ID number.
- 6670 c) The consistency of the internal firmware program is checkable by means of Check Sums.
- 6671 d) The Machine Control System must use an encrypted communication procedure to write
6672 into the control register or the bypass/bridging register. The new content of these registers
6673 must be identified with the ID number of the RPSM in which has been written.
- 6674 e) The data read from an RPSM must be signed with its ID number.
- 6675 f) The RPSMs have a dedicated input which can be used by the Machine Control System to
6676 enforce a beam-off command for test purposes. The time interval between this command
6677 and the actual beam off is logged and can be read by the Machine Control System.

6678

6679 **8.6.6 Rules for Turning the Beam Off**

6680

6681 Beam turn-off is implemented by the Run Permit System with a three-fold redundancy:

6682

6683 a) fast kicker magnet AMAKI;

6684 b) RF at reduced power so that particles are not accelerated. This is done if the fast kicker

6685 magnet does not react within 50 to 100 μ sec, or when the integrated charge on BMA1

6686 increases by a certain value within a preset time. This last error condition has been

6687 implemented to avoid unnecessary activation;

6688 c) Switch-off the ion source when the RF does not react in time.

6689

6690 **8.6.7 Tests and Quality Assurance (QA)**

6691

6692 The frequency of component periodic tests depends on their relative importance in terms of
6693 machine security.

6694

6695 Several tests are performed online: cross checks with PaSS signals; checks of cable connections
6696 between RPS modules and those of the input signals; and check-sum verification of the XILINX
6697 contents.

6698

6699 In the Machine Control System, several test procedures are built-in and are typically run every week:

6700

6701 a) test switch-off *via* primary switch-off channels and analysis of switch-off times;

6702 b) checks of contacts of limit switches of moveable components (*e.g.*, beam stoppers);

6703 c) checks of interlocks on the allowed topology-dependent current interval of magnet

6704 currents.

6705

6706 Additional tests are done after maintenance or repair. These tests are of course related to the components

6707 involved in the maintenance or repair.

6708

Glossary

6709

6710

6711 **absorbed dose (D):** The quotient of $D = \frac{d\bar{\varepsilon}}{dm}$ where $d\bar{\varepsilon}$ is the mean energy imparted by ionizing

6712 radiation to matter of mass dm . The unit is J kg^{-1} . The special name for the unit of absorbed dose
6713 is the gray (Gy).

6714 **activation:** The process of inducing radioactivity by irradiation.

6715 **ALOK:** Local interlock signal from PaSS

6716 **AMAKI:** Fast magnetic kicker used at PSI

6717 **ambient dose equivalent ($H^*(d)$):** The dose equivalent at a point in a radiation field that would be
6718 produced by the corresponding expanded and aligned field in the ICRU sphere (diameter = 30
6719 cm, 76.2 % O, 10.1 % H, 11.1 % C, and 2.6 % N) at a depth, d , on the radius opposing the
6720 direction of the aligned field (ICRU, 1993). The ambient dose equivalent is measured in Sv.

6721 **attenuation length (λ):** The penetration distance in which the intensity of the radiation is attenuated by
6722 a factor of e.

6723 **BAL:** Beam allocation system

6724 **BMxi:** Mechanical beam stopper number i, in beam line x at PSI

6725 **bridge:** The bypass of a system, irrespective its status.

6726 **compound nucleus:** A metastable nucleus that exists during the time between the fusion of a target
6727 nucleus X and a impinging particle p and the separation into a residual nucleus Y and a outgoing
6728 particle q . Niels Bohr introduced this concept in 1936.

6729 **computational human phantom:** Computer representation of the human body

6730 **conversion coefficients:** The quotient of the dose equivalent under specified conditions and the
6731 associated field quantity (for example, fluence).

- 6732 **Coulomb barrier:** The repulsive Coulomb force between the target nucleus and the charged particle
6733 that an impinging charged particle does not have enough velocity to overcome ; hence, the
6734 collision does not take place. The Coulomb barrier lowers the probability of nuclear reactions of
6735 charged particles.
- 6736 **degrader:** A system to slow down the particles to a chosen energy.
- 6737 **directional dose equivalent $H'(d, \Omega)$:** The dose equivalent at a point in a radiation field that would be
6738 produced by the corresponding expanded field in the ICRU sphere at a depth, d , on the radius in a
6739 specified direction, Ω (ICRU, 1993). The directional dose equivalent is measured in Sv.
- 6740 **dose equivalent (H):** The product of Q and D at a point in tissue, where D is the absorbed dose and Q is
6741 the quality factor at that point. Thus, $H = Q D$. The unit of dose equivalent in the SI system of
6742 units is joules per kilogram (J kg^{-1}) and its special name is the sievert (Sv).
- 6743 **DSP:** Digital Signal Processor
- 6744 **ECR source:** An ion source often used for heavy ions, applying ionization by electron cyclotron
6745 resonance.
- 6746 **effective dose:** Weighted sum of various organ or tissue doses using organ weighting factors
- 6747 **Emergency OR module:** A logic “OR” unit used for an emergency-off.
- 6748 **equivalent dose (H_T):** A quantity in a tissue or organ that is used for radiation protection purposes and
6749 takes into account the different probability of effects which occur with the same absorbed dose
6750 delivered by radiation with different radiation weighting factors (w_R). It is given by
- 6751
$$H_T = \sum_R w_R D_{T,R},$$
 where $D_{T,R}$ is the mean absorbed dose in the tissue or organ, T, due to radiation
6752 R, and w_R is the corresponding radiation weighting factor. The unit of equivalent dose is the
6753 sievert (Sv).
- 6754 **ETOT:** Global emergency switch-off signal from PaSS

- 6755 **excess absolute risk (EAR):** Rate of an effect in an exposed population minus the rate of the effect in an
6756 unexposed population
- 6757 **excess relative risk (ERR):** Rate of an effect in an exposed population divided by the rate of the effect
6758 in an unexposed population minus 1
- 6759 **exemption:** The determination by a regulatory body that a radioactive source need not be subject to
6760 regulatory control on the basis that the exposure due to the source is too small.
- 6761 **external radiation:** Secondary radiation produced in the treatment head
- 6762 **fluence (Φ):** The quotient of dN by dA where dN is the number of particles incident on a sphere of cross-
6763 sectional area dA . The unit is m^{-2} or cm^{-2} .
- 6764 **generalized intra-nuclear cascade:** Description of nuclear interactions at energies up to a few GeV
6765 which is based on a cascade of elastic and inelastic collisions between hadrons and nucleons
6766 inside the nuclei involved in the interaction. Nuclear potentials, Fermi motion, and relativistic
6767 effects are taken into account.
- 6768 **general-purpose particle interaction and transport Monte Carlo codes:** Monte Carlo codes which
6769 allow the simulation of hadronic and electromagnetic cascades in matter in a wide energy range.
6770 They can therefore be used in a large variety of studies and is not restricted to certain
6771 applications.
- 6772 **impact parameter:** In a nuclear collision between a target nucleus X and an impinging particle p , the
6773 distance between the locus of p and the straight line of the same direction that passes the center of
6774 X . The impact parameter is measured at a position far from X , where any force does not affect the
6775 locus of p .
- 6776 **interlock system:** Interruption system of the particle beam
- 6777 **internal radiation:** Secondary radiation produced in the patient
- 6778 **IOC:** Computer dedicated communication (Input/Output)

- 6779 **isobar:** A nucleus having the same mass number but having a different atomic number.
- 6780 **isobaric yield:** The isobaric yield is the production probability of nuclei having a specific mass number
6781 after a nuclear collision.
- 6782 **Local PaSS:** The local patient safety system of an area
- 6783 **MCS:** Machine Control System
- 6784 **microscopic model:** Description of nuclear interactions based on models for interactions between the
6785 constituents of the colliding hadrons and nuclei (*e.g.*, nucleons, quarks, and gluons).
- 6786 **MPSSC:** Main Patient Safety Switch and Controller
- 6787 **nuclear fragmentation:** The break-up of a nucleus as a consequence of an inelastic interaction.
- 6788 **operational quantity:** A quantity with which, by means of its measurement, compliance with dose limits
6789 may be demonstrated. Examples of operational quantities are ambient dose equivalent, directional
6790 dose equivalent, and personal dose equivalent.
- 6791 **OPTIS:** A proton therapy beam line dedicated for eye treatments.
- 6792 **out-of-field dose:** Dose outside the area penetrated by the primary beam
- 6793 **PaSS:** Patient Safety System
- 6794 **personal dose equivalent ($H_p(d)$):** The dose equivalent in soft tissue at an appropriate depth, d , below a
6795 specified point on the body. The personal dose equivalent is measured in Sv.
- 6796 **PLC:** Programmable Logic Controller
- 6797 **prompt radiation:** Radiations that are immediately emitted by nuclear reactions of primary accelerated
6798 particles.
- 6799 **protection quantity:** Dosimetric quantities specified in the human body by the ICRP. Examples of
6800 protection quantities are effective dose and equivalent dose.
- 6801 **PSI:** Paul Scherrer Institute, Switzerland
- 6802 **PSS:** Personnel Safety System

- 6803 **quality factor:** Conservatively defined weighting factor to indicate the biological effectiveness as a
6804 function of linear energy transfer
- 6805 **radiation weighting factor:** Conservatively defined weighting factor to indicate the biological
6806 effectiveness as a function of particle type and energy for external whole body exposure
- 6807 **relative biological effectiveness (RBE):** Ratio of the doses required by two different types of radiation
6808 to cause the same level of effect for a specified end point
- 6809 **relative risk (RR):** Rate of disease among groups with a specific risk factor divided by the rate among a
6810 group without that specific risk factor
- 6811 **residual radiation:** Primary accelerated particles and their secondary radiations of neutrons and charged
6812 particles produce radionuclides. Radiations, such as photons and beta rays, which are emitted by
6813 disintegrations of these induced radionuclides are called residual radiations.
- 6814 **resonance:** A phenomenon that occurs when the projectile particle energy coincides with the energy
6815 level of the target nucleus, and a large peak appears in the reaction cross section.
- 6816 **RF:** Radiofrequency; the accelerating voltage of an accelerator
- 6817 **RPS:** Run Permit System, also called accelerator/machine interlock system
- 6818 **RPSM:** Dedicated modules in RPS having multiple I/O channels
- 6819 **saturation activity:** The maximum radioactivity induced by irradiation. Saturation activity is reached
6820 when the irradiation time becomes longer than several times the half-life.
- 6821 **scattered radiation:** Radiation caused by scattering of the primary beam
- 6822 **secondary radiation:** Radiation by secondary particles produced when the primary beam interacts with
6823 beam-line components or within patients
- 6824 **SIL:** Safety Integrity Level; the robustness of such a measure or a device

- 6825 **spallation:** The process in which a heavy nucleus emits a large number of particles as a result of the
6826 collision. between the target nucleus and a high-energy heavy projectile nucleus. Any kind of
6827 nucleus lighter than the disintegrating heavy nucleus can be produced in a spallation reaction.
- 6828 **stylized phantoms:** Computer representation of the human body using simple geometrical shapes
- 6829 **TCS:** Treatment Control System
- 6830 **Thick Target Yield (TTY):** Secondary radiation emission from a target, of which the thickness is
6831 slightly larger than the range of the irradiating charged particles. Examples of TTY quantities are
6832 the total neutron yield and the neutron energy angular distribution.
- 6833 **trip:** A signal that switches the beam off.
- 6834 **tune:** Predefined setting of the beam line
- 6835 **variance reduction techniques:** One of several procedures used to increase the precision of the
6836 estimates that can be obtained for a given number of iterations.
- 6837 **voxelized phantom:** Computer representation of the human body using a grid geometry
- 6838 **watchdog:** Backup timer; electronic counters measuring the duration of dose application
- 6839

References

- 6840
- 6841
- 6842 AESJ (2004). Atomic Energy Society of Japan, *Radiation Dose Conversion Coefficients for Radiation*
6843 *Shielding Calculations*, AESJ-SC-R002:2004 (Atomic Energy Society of Japan, Tokyo).
- 6844 Agosteo, S. (2001). "Radiation Protection at Medical Accelerators," *Radiat. Prot. Dosim.* **96**, 393-406.
- 6845 Agosteo, S., Fasso, A., Ferrari, A., Sala, P., R., Silari, M. and Tabarelli de Fatis, P. (1995). "Double
6846 differential distributions attenuation lengths and source terms for proton accelerator shielding,"
6847 in *Proc. Shielding Aspects of Accelerators, Targets and Irradiation Facilities (SATIF-2)*, 12-13
6848 October 1995, Geneva (Nuclear Energy Agency, Organization for Economic Co-operation and
6849 Development, Paris).
- 6850 Agosteo, S., Fasso, A., Ferrari, A., Sala, P., R., Silari, M., and Tabarelli de Fatis, P., (1996a). "Double
6851 differential distributions and attenuation in concrete for neutrons produced by 100-400 MeV
6852 protons on iron and tissue targets." *NIM Phys. Res.* **B114**, 70-80.
- 6853 Agosteo, S. *et al.* (1996b). "Shielding Calculations for a 250 MeV Hospital-based Proton Accelerator,"
6854 *NIM Phys. Res.* **A 374**, 254-268.
- 6855 Agosteo, S., Birattari, C., Corrado, M., G., and Silari, M., (1996c). "Maze design of a gantry room for
6856 proton therapy," *NIM Phys. Res. A* **382**, 573-582.
- 6857 Agosteo, S., Birattari, C., Caravaggio, M., Silari, M., and Tosi, G. (1998). "Secondary neutron and
6858 photon dose in proton therapy," *Radiother. Oncol.* **48**, 293-305.
- 6859 Agosteo S., Nakamura, T., Silari, M., and Zajacova, Z. (2004a). "Attenuation curves in concrete of
6860 neutrons from 100 to 400 MeV per nucleon He, C, Ne, Ar, Fe and Xe ions on various targets,"
6861 *NIM Phys. Res.* **B217**, 221-236.

- 6862 Agosteo, S., Magistris, M., Mereghetti, A., Silari, M., and Zajacova, Z. (2004b). "Shielding data for 100
6863 to 250 MeV proton accelerators: double differential neutron distributions and attenuation in
6864 concrete," *NIM Phys. Res.* **B265**, 581-589.
- 6865 Agostinelli, S., *et al.* (2003). "GEANT4 - A simulation toolkit," *NIM Phys. Res. A* **506**, 250-303.
- 6866 Ahmed, S.N. (2007). *Physics and Engineering of Radiation Detection*, (Academic Press, San Diego,
6867 CA).
- 6868 Alberts, W.G., Dietze, E., Guldbakke, S., Kluge, H., and Schuhmacher, H. (1989). "International
6869 intercomparison of TEPC systems used for radiation protection," *Radiat. Prot. Dosim.* **29**, 47-53.
- 6870 Alghamdi, A.A., Ma, A., Tzortzis, M., and Spyrou, N.M. (2005). "Neutron-fluence-to-dose conversion
6871 coefficients in an anthropomorphic phantom," *Radiat. Prot. Dosim.* **115**, 606-611.
- 6872 Alghamdi, A.A., Ma, A., Marouli, M., Albarakati, Y., Kacperek, A., and Spyrou, N.M. (2007). "A high-
6873 resolution anthropomorphic voxel-based tomographic phantom for proton therapy of the eye,"
6874 *Phys. Med. Biol.* **52**, N51-59.
- 6875 Allison, J., *et al.* (2006). "GEANT4 Developments and Applications," *IEEE Transactions on Nuclear
6876 Science* **53**, 270-278.
- 6877 Amaldi, U. and Silari, M. (Eds.) (1995). *The TERA Project and the Centre for Oncological
6878 Hadrontherapy*, The TERA Foundation, (INFN, Frascati. II ed).
- 6879 Amaldi, U. and Kraft, G. (2005). "Recent applications of Synchrotrons in cancer therapy with Carbon
6880 Ions," *Europhysics News* **36**, 114-118.
- 6881 ASTM (2003). ASTM International, *Cement Standards and Concrete Standards*, ASTM Standard C657
6882 (ASTM International, West Conshohocken, PA).

- 6883 ASTM (2007) . ASTM International, *Standard Test Methods for Instrumental Determination of Carbon,*
6884 *Hydrogen, and Nitrogen in Petroleum Products and Lubricants*, ASTM Standard D5291 (ASTM
6885 International, West Conshohocken, PA).
- 6886 Avery, S., Ainsley, C., Maughan, R., and McDonough, J. (2008). "Analytical Shielding Calculations for
6887 a Proton Therapy Facility," *Radiat. Prot. Dosim.* **131** (2), 167-179.
- 6888 Awschalom, M. (1987). *Radiation Shielding for 250 MeV Protons*, (Fermi National Accelerator
6889 Laboratory, USA).
- 6890 Awschalom, M. and Sanna, R.S. (1985). "Applications of Bonner sphere detectors in neutron field
6891 dosimetry," *Radiat. Prot. Dosim.* **10**, 89-101.
- 6892 Azzam, E.I., Raaphorst, G.P., and Mitchel, R.E. (1994). "Radiation-induced adaptive response for
6893 protection against micronucleus formation and neoplastic transformation in C3H 10T1/2 mouse
6894 embryo cells," *Radiat. Res.* **138**, S28-31.
- 6895 Ballarini, F., Biaggi, M., Ottolenghi, A., and Sabora, O. (2002). "Cellular communication and bystander
6896 effects: a critical review for modelling low-dose radiation action," *Mutat. Res.* **501**, 1-12.
- 6897 Ban, S., Nakamura, H., and Hirayama, H. (2004). "Estimation of amount of residual radioactivity in
6898 high-energy electron accelerator component by measuring the gamma-ray dose rate," *J. Nucl. Sci.*
6899 *Tech.*, Suppl. **4**, 168-171.
- 6900 Barbier, M. (1969). *Induced Radioactivity*, (North Holland Publ. Co., Amsterdam).
- 6901 Barcellos-Hoff, M.H. (2001). "It takes a tissue to make a tumor: epigenetics, cancer and the
6902 microenvironment," *J. Mammary Gland Biol. Neoplasia* **6**, 213-221.
- 6903 Bassal, M., Mertens, A.C., Taylor, L., Neglia, J.P., Greffe, B.S., Hammond, S., Ronckers, C.M.,
6904 Friedman, D.L., Stovall, M., Yasui, Y.Y., Robison L.L., Meadows, A.T., and Kadan-Lottick,
6905 N.S. (2006). "Risk of selected subsequent carcinomas in survivors of childhood cancer: a report
6906 from the Childhood Cancer Survivor Study," *J. Clin. Oncol.* **24**, 476-483.

- 6907 Battistoni, G., Muraro, S., Sala, P., R., Cerutti, F., Ferrari, A., Roesler, S., Fasso, A., and Ranft, J., (2007).
6908 "The FLUKA code: Description and benchmarking," in *Proc. of the Hadronic Shower Simulation*
6909 *Workshop 2006, Fermilab*, 6-8 September 2006, M., Albrow, R., Raja Eds., *AIP Conference*
6910 *Proceeding* **896**, 31-49.
- 6911 Battistoni, G., *et al.* (2008). "The FLUKA code and its use in hadron therapy," *Nuovo Cimento C* **31**, 69-
6912 75.
- 6913 Bednarz, B. and Xu, X.G. (2008). "A feasibility study to calculate unshielded fetal doses to pregnant
6914 patients in 6-MV photon treatments using Monte Carlo methods and anatomically realistic
6915 phantoms," *Med. Phys.* **35** (7).
- 6916 BEIR (2006). *Health risks from exposure to low levels of ionizing radiation, BEIR VII, Phase 2*, National
6917 Research Council of the National Academy of Science (National Academies Press, Washington,
6918 DC).
- 6919 BfG (2004). Bundesamt für Gesundheit, Abteilung Strahlenschutz, Sektion Aufsicht und
6920 Bewilligung, *Richtwerte für Ortsdosisleistungen in nuklearmedizinischen Betrieben*,
6921 (Eidgenössisches Departement des Innern EDI, Switzerland).
- 6922 Bhattacharjee, D. and Ito, A. (2001). "Deceleration of carcinogenic potential by adaptation with low dose
6923 gamma irradiation," *In Vivo* **15**, 87-92.
- 6924 Binns, P.J. and Hough, J.H. (1997). "Secondary dose exposures during 200 MeV proton therapy,"
6925 *Radiat. Prot. Dosim.* **70**, 441-444.
- 6926 Birattari, C., Ferrari, A., Nuccetelli, C., Pelliccioni, M., and Silari, M. (1990). "An extended range
6927 neutron rem counter," *Nucl. Instr. and Meth.*, **A297**, 250-257.
- 6928 Blettner, M. and Boice, J.D., Jr. (1991). "Radiation dose and leukaemia risk: general relative risk
6929 techniques for dose-response models in a matched case-control study," *Stat. Med.* **10** 1511-1526.

- 6930 Boag, J.W. (1975). "The statistical treatment of cell survival data," pp. 40-53 in *Proc. of the Sixth, L.H.*
6931 *Gray Conference: Cell survival after low doses of radiation*, Alper, T., Ed.
- 6932 Boice, J.D., Jr., Blettner, M., Kleinerman, R.A., Stovall, M., Moloney, W.C., Engholm, G., Austin, D.F.,
6933 Bosch, A., Cookfair, D.L., Krementz, E.T., and *et al.* (1987). "Radiation dose and leukemia risk
6934 in patients treated for cancer of the cervix," *J. Natl. Cancer Inst.* **79**, 1295-1311.
- 6935 Bozkurt, A., Chao, T.C., and Xu, X.G. (2000). "Fluence-to-dose conversion coefficients from
6936 monoenergetic neutrons below 20 MeV based on the VIP-man anatomical model," *Phys. Med.*
6937 *Biol.* **45**, 3059-79.
- 6938 Bozkurt, A., Chao, T.C., and Xu, X.G. (2001). "Fluence-to-dose conversion coefficients based on the
6939 VIP-man anatomical model and MCNPX code for monoenergetic neutrons above 20 MeV,"
6940 *Health Phys.* **81**, 184-202.
- 6941 Brada, M., Ford, D., Ashley, S., Bliss, J.M., Crowley, S., Mason, M., Rajan, B., and Traish, D. (1992).
6942 "Risk of second brain tumour after conservative surgery and radiotherapy for pituitary adenoma,"
6943 *BMJ* **304**, 1343-1346.
- 6944 Brandl, A., Hranitzky, C., and Rollet, S., (2005). "Shielding variation effects for 250 MeV protons on
6945 tissue targets," *Radiat. Prot. Dosim.* **115**, 195–199.
- 6946 Brenner, D.J. and Hall, E.J. (1992). "Commentary 2 to Cox and Little: radiation-induced oncogenic
6947 transformation: the interplay between dose, dose protraction, and radiation quality," *Adv. Radiat.*
6948 *Biol.* **16**, 167-179.
- 6949 Brenner, D.J. and Hall, E.J. (2008) "Secondary neutrons in clinical proton radiotherapy:, A.charged
6950 issue," *Radiother. Oncol.* **86** (2), 165-170.
- 6951 Brenner, D.J., Curtis, R.E., Hall, E.J., and Ron, E. (2000). "Second malignancies in prostate carcinoma
6952 patients after radiotherapy compared with surgery," *Cancer* **88**, 398-406.

- 6953 Brenner, D.J., Doll, R., Goodhead, D.T., Hall, E.J., Land, C.E., Little, J.B., Lubin, J.H., Preston, D.L.,
6954 Preston, R.J., Puskin, J.S., Ron, E., Sachs, R.K., Samet, J.M., Setlow, R.B., and Zaider, M.
6955 (2003). "Cancer risks attributable to low doses of ionizing radiation: assessing what we really
6956 know," *Proc. Natl. Acad. Sci. U.S.A.* **100**, 13761-13766.
- 6957 Broerse, J.J., Hennen, L.A., and Solleveld, H.A. (1986). "Actuarial analysis of the hazard for mammary
6958 carcinogenesis in different rat strains after X- and neutron irradiation," *Leukemia Research* **10**,
6959 749-754.
- 6960 Broniscer, A., Ke, W., Fuller, C.E., Wu, J., Gajjar, A. and Kun, L.E. (2004). "Second neoplasms in
6961 pediatric patients with primary central nervous system tumors: the St. Jude Children's Research
6962 Hospital experience," *Cancer* **100**, 2246-2252.
- 6963 Brugger, M., Khater, H., Mayer, S., Prinz, A., Roesler, S., Ulrici, L., and Vincke, H., (2005).
6964 "Benchmark studies of induced radioactivity produced in LHC materials, Part II: remanent dose
6965 rates," *Radiat. Prot. Dosim.* **116**, 12-15.
- 6966 Brugger, M., Ferrari, A., Roesler, S., and Ulrici, L., (2006). "Validation of the FLUKA Monte Carlo
6967 code for predicting induced radioactivity at high-energy accelerators," *NIM Phys. Res. A* **562**,
6968 814-818.
- 6969 Calabrese, E.J. and Baldwin, L.A. (2000). "The effects of gamma rays on longevity," *Biogerontology* **1**,
6970 309-319.
- 6971 Calabrese, E.J. and Baldwin, L.A. (2003). "The hormetic dose-response model is more common than the
6972 threshold model in toxicology," *Toxicol. Sci.* **71**, 246-250.
- 6973 Caon, M., Bibbo, G. and Pattison, J. (1999). "An EGS4-ready tomographic computational model of a 14-
6974 year-old female torso for calculating organ doses from CT examinations," *Phys. Med. Biol.* **44**,
6975 2213-2225.

- 6976 Caporaso, G. (2009). "High Gradient Induction Linacs for Hadron Therapy," *1st International Workshop*
6977 *on Hadron Therapy for Cancer* 24 April – 1 May 2009, Erice, Sicily.
6978 <http://erice2009.na.infn.it/TalkContributions/Caporoso.pdf>, accessed May 15, 2009.
- 6979 Carter, L.,L., and Cashwell, E.,D. (1975). "Particle-transport simulation with the Monte Carlo method,"
6980 *ERDA Crit. Rev. Ser.*, (National Technical Information Service, Springfield, VA).
- 6981 CFR (2007). Code of Federal Regulations, Title 10, Part 835, *Occupational Radiation Protection*, (U.S.
6982 Department of Energy, Washington, DC).
- 6983 Chadwick, M.B., Oblozinsky, P., Herman, M., *et al.* (2006). "ENDF/B-VII.0: Next generation evaluated
6984 nuclear data library for nuclear science and technology," *Nuclear Data Sheets* **107**, 2931-3060.
- 6985 Chao, T.C. and Xu, X.G. (2001). "Specific absorbed fractions from the image-based VIP-Man body
6986 model and EGS4-VLSI Monte Carlo code: Internal electron emitters," *Phys. Med. Biol.* **46**, 901-
6987 927.
- 6988 Chao, T.C., Bozkurt, A. and Xu, X.G. (2001a). "Conversion coefficients based on the VIP-Man
6989 anatomical model and GS4-VLSI code for external monoenergetic photons from 10 keV to 10
6990 MeV," *Health Phys.* **81**, 163-183.
- 6991 Chao, T.C., Bozkurt, A. and Xu, X.G. (2001b) "Organ dose conversion coefficients for 0.1-10 MeV
6992 external electrons calculated for the VIP-Man anatomical model," *Health Phys.* **81**, 203-214.
- 6993 Chaturvedi, A.K., Engels, E.A., Gilbert, E.S., Chen, B.E., Storm, H., Lynch, C.F., Hall, P., Langmark, F.,
6994 Pukkala, E., Kaijser, M., Andersson, M., Fossa, S.D., Joensuu, H., Boice, J.D., Kleinerman, R.A
6995 and Travis, L.B (2007). "Second cancers among 104,760 survivors of cervical cancer: evaluation
6996 of long-term risk," *J. Natl. Cancer Inst.* **99**, 1634-1643.
- 6997 Chen, J. (2006). "Fluence-to-absorbed dose conversion coefficients for use in radiological protection of
6998 embryo and foetus against external exposure to protons from 100 MeV to 100 GeV," *Radiat.*
6999 *Prot. Dosim.* **118**, 378-383.

- 7000 Chilton, A.B., Shultis, J.K., and Faw, R.E. (1984). *Principles of Radiation Shielding*, (Prentice-Hall Inc,
7001 Englewood Cliffs, NJ).
- 7002 Cho, S.H., Vassiliev, O.N., Lee, S., Liu, H.H., Ibbott, G.S., and Mohan, R. (2005). "Reference photon
7003 dosimetry data and reference phase space data for the 6 MV photon beam from varian clinac
7004 2100 series linear accelerators," *Med. Phys.* **32**, 137-148.
- 7005 Chung, C.S., Keating, N., Yock, T. and Tarbell, N. (2008). "Comparative Analysis of Second
7006 Malignancy Risk in Patients Treated with Proton Therapy versus Conventional Photon Therapy,"
7007 *Int. J. Radiat. Oncol. Biol. Phys.* **72** S8.
- 7008 Cloth, P. *et al.* (1983). "The KFA-Version of the High-Energy Transport Code HETC and the
7009 generalized Evaluation Code SIMPLE," *Kernforschungsanlage Jülich, Jül-Spez* **196**.
- 7010 Coutrakon, G..B. (2007). "Accelerators for heavy-charged particle radiation therapy," *Technology in*
7011 *Cancer Research and Treatment*, **6(4)** Supplement.
- 7012 Coutrakon, G., Bauman, M., Lesyna, D., Miller, D., Nusbaum, J., Slater, J., Johannig, J., Miranda, J.,
7013 DeLuca, P.M., Siebers, J., and Ludewigt, B. (1990). "A prototype beam delivery system for the
7014 proton medical accelerator at Loma Linda," *Med. Phys.* **18 (6)**, 1093-1099.
- 7015 Cristy, M. and Eckerman, K.F. (1987). "Specific absorbed fractions of energy at various ages from
7016 internal photon sources," Report ORNL/TM-8381/I-VII (Oak Ridge National Laboratory,
7017 Battelle, TN, USA).
- 7018 Curtis, R.E., Rowlings, P.A., Deeg, H.J., Shriner, D.A., Socie, G., Travis, L.B., Horowitz, M.M.,
7019 Witherspoon, R.P., Hoover, R.N., Sobocinski, K.A., Fraumeni, J.F. Jr. and Boice, J.D., Jr. (1997).
7020 "Solid cancers after bone marrow transplantation," *N. Engl. J. Med.* **336**, 897-904.
- 7021 de Vathaire, F., Francois, P., Hill, C., Schweisguth, O., Rodary, C., Sarrazin, D., Oberlin, O., Beurtheret,
7022 C., Dutreix, A. and Flamant, R. (1989). "Role of radiotherapy and chemotherapy in the risk of
7023 second malignant neoplasms after cancer in childhood," *Br. J. Cancer* **59**, 792-796.

- 7024 Debus, J. (1998). *Proposal for a dedicated Ion Beam Facility for Cancer Theray*, Groß, K.D., Pavlovic,
7025 M., Eds. (GSI, Darmstadt, Germany).
- 7026 Dementyev, A.,V., and Sobolevsky, N.,M. (1990). "SHIELD-universal Monte Carlo hadron transport
7027 code: scope and applications," *Radiation Measurements* **30**, 553-557.
- 7028 Dennis, J.A. (1987). "The relative biological effectiveness of neutron radiation and its implications for
7029 quality factor and dose limitation," *Progress in Nuclear Energy* **20**, 133-149.
- 7030 Diallo, I., Lamon, A., Shamsaldin, A., Grimaud, E., de Vathaire, F. and Chavaudra, J. (1996).
7031 "Estimation of the radiation dose delivered to any point outside the target volume per patient
7032 treated with external beam radiotherapy," *Radiother. Oncol.* **38**, 269-271.
- 7033 DIN (2003). Deutsches Institut für Normung, e.V., *Medical Electron Accelerators – Part 2: Radiation*
7034 *Protection Rules for Installation*, German Technical Standards 6847 (Deutsches Institut für
7035 Normung, e.V., Berlin).
- 7036 Dinter, H., Dworak, D., Tesch, K. (1993). "Attenuation of the neutron dose equivalent in labyrinths
7037 through an accelerator shield," *NIM Phys. Res. A* **330**, 507-512.
- 7038 Dittrich, W. and Hansmann, T. (2006). "Radiation Measurements at the RPTC in Munich for
7039 Verification of Shielding Measures around the Cyclotron Area," in *Proc. Shielding Aspects of*
7040 *Accelerators, Targets and Irradiation Facilities (SATIF 8)*, 22-24 May 2006, Gyongbuk,
7041 Republic of Korea (Nuclear Energy Agency, Organization for Economic Co-operation and
7042 Development, Paris).
- 7043 Dorr, W. and Herrmann, T. (2002). "Second primary tumors after radiotherapy for malignancies.
7044 Treatment-related parameters," *Strahlenther Onkol* **178**, 357-362.
- 7045 Edwards, A.A. (1999). "Neutron RBE values and their relationship to judgements in radiological
7046 protection," *J. Radiol. Prot.* **19**, 93-105.

- 7047 Egbert, S.D., Kerr, G.D. and Cullings, H.M. (2007). "DS02 fluence spectra for neutrons and gamma rays
7048 at Hiroshima and Nagasaki with fluence-to-kerma coefficients and transmission factors for
7049 sample measurements," *Radiat. Environ. Biophys.* **46**, 311-325.
- 7050 Eickhoff, H., Haberer, T., Schlitt, B., and Weinrich, U. (2003). "HICAT – The German Hospital- based
7051 light Ion Cancer Therapy Project," in *Proc. of the Particle Accelerator Conference (PAC03)*, 12-
7052 16 May 2003, Portland, Oregon.
- 7053 Endo, S., Tanaka, K., Takada, M., Onizuka, Y., Miyahara, N., Sato, T., Ishikawa, M., Maeda, N.,
7054 Hayabuchi, N., Shizuma, K. and Hoshi, M. (2007). "Microdosimetric study for secondary
7055 neutrons in phantom produced by, a.290 MeV/nucleon carbon beam," *Med. Phys.* **34**, 3571-3578.
- 7056 Engle, W.A. Jr. (1967). "A User's Manual for ANISN, A one-dimensional discrete Ordinates Transport
7057 Code with anisotropic Scattering," *USAEC Report K-1963*.
- 7058 EPA (1994). Environmental Protection Agency, *Estimating radiogenic cancer risks*, EPA 402-R-93-076
7059 (Environmental Protection Agency, Washington, DC).
- 7060 EPA (1999). Environmental Protection Agency, *Estimating radiogenic cancer risks. Addendum:*
7061 *Uncertainty analysis*, EPA 402-R-99-003 (Environmental Protection Agency, Washington, DC).
- 7062 Epstein, R., Hanham, I. and Dale, R. (1997). "Radiotherapy-induced second cancers: are we doing
7063 enough to protect young patients?" *Eur. J. Cancer* **33**, 526-530.
- 7064 EURATOM (1996). "Council Directive 96/29/Euratom, Laying down basic safety standards for the
7065 Protection of the Health of Workers and the General Public against the Dangers arising from
7066 ionizing Radiation," *Official Journal L* **159**, 29.6.1996, 1–114.
- 7067 Fan, J., Luo, , W., Fourkal, E., Lin, T., Li, J., Veltchev, I. and Ma, C-M. (2007). "Shielding design
7068 for a laser-accelerated proton therapy system," *Phys. Med. Biol.* **52**, 3913–3930.

- 7069 Fasso, A. *et al.* (1997). "FLUKA: New Developments in FLUKA, Modelling Hadronic and EM
7070 Interactions," in *Proc. of the 3rd Workshop on Simulating Accelerator Radiation Environments*,
7071 May 1997, Ed., H. Hirayama, KEK Proc. 97-5. 32-43 (KEK, Tsukuba, Japan).
- 7072 Fasso, A., Ferrari, A., Ranft, J., and Sala, P.R. (2001). "FLUKA: status and prospective for hadronic
7073 applications," p.955 in *Proc. of the Monte Carlo 2000 Conference*, Lisbon, 23-26 October 2000
7074 (Springer-Verlag, Berlin).
- 7075 Fasso, A., Ferrari, A., Ranft, J., and Sala, P.R. (2005). "FLUKA: A Multi-Particle Transport Code,"
7076 CERN-2005-10, INFN/TC_05/11, SLAC-R-773.
- 7077 Fehrenbacher, G., Gutermuth, F., and Radon, T. (2001). "Neutron Dose Assessments for the Shielding of
7078 the planned heavy Ion Cancer Therapy Facility in Heidelberg," GSI Report 2001-05 (GSI,
7079 Darmstadt, Germany).
- 7080 Fehrenbacher, G., Gutermuth, F., and Radon, T. (2002a). "Calculation of Dose Rates near the Horizontal
7081 Treatment Places of the heavy Ion Therapy Clinic in Heidelberg by means of Monte-Carlo-
7082 Methods," *unpublished internal note at GSI* (GSI, Darmstadt, Germany).
- 7083 Fehrenbacher, G., Gutermuth, F., and Radon, T. (2002b), "Estimation of Carbon-Ion caused Radiation
7084 Levels by Calculating the Transport of the produced Neutrons through Shielding Layers," *GSI
7085 Scientific Report 2001*, **205**.
- 7086 Fehrenbacher, G., Gutermuth, F., and Radon, T. (2007a). "Shielding Calculations for the Ion Therapy
7087 Facility HIT," pp. 33-36 in *Ion Beams in Biology and Medicine, 39, Annual Conference of the
7088 German-Swiss Association for Radiation Protection and 11th Workshop of Heavy Charged
7089 Particles in Biology and Medicine* (IRPA Fachverband für Strahlenschutz, Switzerland and
7090 Germany).
- 7091 Fehrenbacher, G., Gutermuth, F., Kozlova, E., Radon, T., Aumann, T., Beceiro, S., Bleis, T. Le,
7092 Boretzky, K., Emling, H., Johansson, H., Kiselev, O., Simon, H., and Typel, S. (2007b).

- 7093 “Measurement of the fluence response of the GSI neutron ball in high-energy neutron fields
7094 produced by 500 AMeV and 800 AMeV deuterons,” *Radiat. Prot. Dosim.* **126**, 497-500.
- 7095 Fehrenbacher, G., Kozlova, E., Gutermuth, F., Radon, T., Schülz, R., Nolte, R., and Böttger, R. (2007c).
7096 “Measurement of the fluence response of the GSI neutron ball dosimeter in the energy range from
7097 thermal to 19 MeV,” *Radiat. Prot. Dosim.* **126**, 546-548.
- 7098 Fehrenbacher, G., Festag, J.G., Grosam, S., Vogt, K., and Becker, F. (2008). “Measurements of the
7099 ambient dose equivalent of produced X-rays at the linear accelerator UNILAC of GSI,” in *Proc.*
7100 *of the 12th Congress of the International Radiation Protection Association, IRPA12* (Buenos
7101 Aires).
- 7102 Feinendegen, L.E. (2005). "Evidence for beneficial low level radiation effects and radiation hormesis,"
7103 *Br. J. Radiol.* **78**, 3-7.
- 7104 Ferrari, A., Pelliccioni, M., and Pillon, M. (1996). “Fluence to effective dose and effective dose
7105 equivalent conversion coefficients for photons from 50 keV to 10 GeV,” *Radiat. Prot. Dosim.*,
7106 **67**, 245-251.
- 7107 Ferrari, A., Pelliccioni, M., and Pillon, M. (1997). “Fluence to effective dose conversion coefficients for
7108 neutrons up to 10 TeV,” *Radiat. Prot. Dosim.*, **71**, 165-173.
- 7109 Ferrari, A., Sala, P.R., Fasso, A. and Ranft, J. (2005). "FLUKA: a multi-particle transport code," *CERN*
7110 *Yellow Report CERN 2005-10; INFN/TC 05/11, SLAC-R-773* (CERN, Geneva, Switzerland).
- 7111 Ferrarini, M. (2007). personal communication, Politecnico di Milano, Dipartimento di Ingegneria
7112 Nucleare, Via Ponzio 34/3, 20133, Milano.
- 7113 Firestone, R.B. (1999). *Table of Isotopes: 1999 Update*, 8th ed. CD-ROM (Wiley Interscience, Malden,
7114 MA).
- 7115 Fix, M.K., Keall, P.J. and Siebers, J.V. (2005). "Photon-beam subsource sensitivity to the initial electron-
7116 beam parameters," *Med. Phys.* **32**, 1164-1175.

- 7117 Flanz, J., Durlacher, S., Goitein, M., Levine, A., Reardon, P., and Smith, A. (1995) "Overview of the
7118 MGH-Northeast Proton Therapy Center plans and progress," *NIM Phys. Res. B* **99**, 830-834.
- 7119 Flanz, J., DeLaney, T.F., and Kooy, H.M. (2008). "Particle Accelerators 27-32," *Proton and Charged*
7120 *Particle Radiotherapy* (Lippincott Williams & Wilkins, Philadelphia, USA).
- 7121 Followill, D., Geis, P. and Boyer, A. (1997). "Estimates of whole-body dose equivalent produced by
7122 beam intensity modulated conformal therapy," *Int. J. Radiat. Oncol. Biol. Phys.* **38**, 667-672.
- 7123 Fontenot, J., Taddei, P., Zheng, Y., Mirkovic, D., Jordan, T. and Newhauser, W. (2008). "Equivalent
7124 dose and effective dose from stray radiation during passively scattered proton radiotherapy for
7125 prostate cancer," *Phys. Med. Biol.* **53**, 1677-1688.
- 7126 Forringer, E. and Blosser, H.G. (2001). "Emittance measurements of a cold cathode internal ion source
7127 for cyclotrons," in *Proc. of the 16th International Conference on Cyclotrons and their*
7128 *Applications*, Marti, F., Ed., *AIP Conference Proceedings*, **600**, 277-279.
- 7129 Foss Abrahamsen, A., Andersen, A., Nome, O., Jacobsen, A.B., Holte, H., Foss Abrahamsen, J., and
7130 Kvaloy, S. (2002). "Long-term risk of second malignancy after treatment of Hodgkin's disease:
7131 the influence of treatment, age and follow-up time," *Ann. Oncol.* **13**, 1786-1791.
- 7132 Francois, P., Beurtheret, C., and Dutreix, A. (1988a). "Calculation of the dose delivered to organs outside
7133 the radiation beams," *Med. Phys.* **15**, 879-883.
- 7134 Francois, P., Beurtheret, C., Dutreix, A., and De Vathaire, F. (1988b) "A mathematical child phantom for
7135 the calculation of dose to the organs at risk," *Med. Phys.* **15**, 328-333.
- 7136 Frankenberg, D., Kelnhofer, K., Baer, K., and Frankenberg-Schwager, M. (2002). "Enhanced Neoplastic
7137 Transformation by Mammography, X.Rays Relative to 200 kVp X Rays: Indication for a Strong
7138 Dependence on Photon Energy of the RBE(M) for various End Points," *Radiat. Res.* **157**, 99-105.
- 7139 Freytag, E. (1972). "Strahlenschutz an Hochenergiebeschleunigern" *Reihe Wissenschaft und Technik:*
7140 *Nukleare Elektronik und Messtechnik*, Karlsruhe. **3** (G.Braun: Karlsruhe, Germany).

- 7141 Fry, R.J. (1981). "Experimental radiation carcinogenesis: what have we learned?" *Radiat. Res.* **87**, 224-
7142 239.
- 7143 Furukawa, T. *et al.* (2006). "Design of Synchrotron and Transport Line for Carbon Therapy Facility and
7144 related Machine Study at HIMAC," *NIM Phys. Res. A* **562**, 1050-1053.
- 7145 Garrity, J.M., Segars, W.P., Knisley, S.B., and Tsui, B.M.W. (2003). "Development of, a dynamic model
7146 for the lung lobes and airway tree in the NCAT phantom," *IEEE Transactions in Nuclear Science*
7147 **50**, 378-383.
- 7148 Geisler, A.E., Hottenbacher, J., Klein, H.-U., Krischel, D., Röcken, H., Schillo, M., Stephani, T.,
7149 Timmer, J.H. (2007). "Commissioning of the ACCEL 250 MeV Proton Cyclotron," *Cyclotrons*
7150 *and Their Applications* **18** (Accel Instruments GmbH, Bergich Gladbach, Germany).
- 7151 Geithner, O., Andreo, P., Sobolevsky, N.,M., Hartmann, G., and Jäkel, O., (2006). "Calculation of
7152 stopping power ratios for carbon ion dosimetry," *Phys. Med. Biol.* **51**, 2279-2292.
- 7153 Gibbs, S.J., Pujol, A., Chen, T.S. and *et al.* (1984). "Computer-simulation of patient dose from dental
7154 radiography." *Journal of Dental Research* **63**, 209.
- 7155 Gilbert, W.S., *et al.* (1968). "Shielding Experiment at the CERN Proton Synchrotron," *CERN-LBL-*
7156 *RHEL, Rep. UCRL-17941* (Lawrence Berkeley Lab., Berkeley, CA, USA).
- 7157 Goebel, K., Stevenson, G.R., Routti, J.T., and Vogt, H.G. (1975). "Evaluating dose rates due to neutron
7158 leakage through the access tunnels of the SPS," CERN Internal Report LABII-RA/Note/75-10.
- 7159 Gottschalk, B. (2006). "Neutron dose in scattered and scanned proton beams: in regard to Eric, J. Hall
7160 (Int., J. Radiat. Oncol. Biol. Phys. 2006;65:1-7)," *Int. J. Radiat. Oncol. Biol. Phys.* **66**, 1594;
7161 author reply 5.
- 7162 Grahn, D., Fry, R.J., and Lea, R.A. (1972). "Analysis of survival and cause of death statistics for mice
7163 under single and duration-of-life gamma irradiation," *Life. Sci. Space. Res.* **10**, 175-186.

- 7164 Gregoire, O. and Cleland, M.R. (2006). "Novel approach to analyzing the carcinogenic effect of ionizing
7165 radiations," *Int. J. Radiat. Biol.* **82**, 13-19.
- 7166 GRPO (2005). German Radiation Protection Ordinance, *Veordnung über den Schutz vor Schäden durch*
7167 *ionisierende Strahlen (Strahlenschutzverordnung – StrlSchV)*. (Bundesministerium der Justis,
7168 Germany).
- 7169 Gudowska, I. and Sobolevsky, N. (2005). "Simulation of secondary particle production and absorbed
7170 dose to tissue in light ion beams," *Radiat. Prot. Dosim.* **116**, 301-306.
- 7171 Gudowska, I., Andreo, P., and Sobolevsky, N. (2002). "Secondary particle production in tissue-like and
7172 shielding materials for light and heavy ions calculated with the Monte-Carlo code SHIELD-HIT,"
7173 *J. Radiat. Res. (Tokyo)* **43 Suppl** S93-97.
- 7174 Gudowska, I., Sobolevsky, N.,M., Andreo, P., Belkic D., and Brahme, A., (2004). "Ion beam transport in
7175 tissue-like media using the Monte Carlo code SHIELD-HIT," *Phys. Med. Biol.* **49**,1933-1958.
- 7176 Gudowska, I., Kopec, M., and Sobolevsky, N. (2007). "Neutron production in tissue-like media and
7177 shielding materials irradiated with high-energy ion beams," *Radiat. Prot. Dosim.* **126**, 652-656.
- 7178 Gunzert-Marx, K., Schardt, D., and Simon, R.S. (2004). "Fast neutrons produced by nuclear
7179 fragmentation in treatment irradiations with ^{12}C beam," *Radiat. Prot. Dosim.* **110**, 595-600.
- 7180 Gunzert-Marx, K., Iwase, H., Schardt, D., and Simon, R.S. (2008). "Secondary beam fragments produced
7181 by 200MeV/u^{-1} ^{12}C ions in water and their dose contributions in carbon ion radiotherapy," *New*
7182 *Journal of Physics* **10**, 075003.
- 7183 Haberer, T., Becher, W., Schardt, D., and Kraft, G. (1993). "Magnetic scanning system for heavy ion
7184 therapy," *NIM Phys. Res. A* **330**, 296-305.
- 7185 Haettner, E., Iwase, H., and Schardt, D. (2006). "Experimental fragmentation studies with ^{12}C therapy
7186 beams," *Radiat. Prot. Dosim.* **122**, 485-487.

- 7187 Hagan, W.K., Colborn, B.L., Armstrong, T.W., and Allen, M. (1988). "Radiation Shielding Calculations
7188 for a 70- to 350-MeV Proton Therapy Facility," *Nuclear Science and Engineering* **98**, 272-278.
- 7189 Hall, E.J. (2004). "Henry S. Kaplan Distinguished Scientist Award 2003: The crooked shall be made
7190 straight; dose response relationships for carcinogenesis," *Int. J. Radiat. Biol.* **80**, 327-337.
- 7191 Hall, E.J. (2006). "Intensity-modulated radiation therapy, protons, and the risk of second cancers," *Int. J.*
7192 *Radiat. Oncol. Biol. Phys.* **65**, 1-7.
- 7193 Hall, E.J. (2007). "The impact of protons on the incidence of second malignancies in radiotherapy,"
7194 *Technol. Cancer Res. Treat.* **6**, 31-34.
- 7195 Hall, E.J. and Wu C-S. (2003). "Radiation-induced second cancers: The impact of 3D-CRT and IMRT,"
7196 *Int. J. Radiat. Oncol. Biol. Phys.* **56**, 83-88.
- 7197 Hall, E.J., Kellerer, A.M., Rossi, H.H., and Yuk-Ming, P.L. (1978). "The Relative Biological
7198 Effectiveness of 160 MeV Protons. II. Biological Data and Their Interpretation in Terms of
7199 Microdosimetry," *Int. J. Radiat. Oncol. Biol. Phys.* **4**, 1009-1013.
- 7200 Han, A. and Elkind, M.M. (1979). "Transformation of mouse C3H/10T1/2 cells by single and
7201 fractionated doses of X-rays and fission-spectrum neutrons," *Cancer Res.* **39**, 123-130.
- 7202 Hawkins, M.M., Draper, G.J., and Kingston, J.E. (1987). "Incidence of second primary tumours among
7203 childhood cancer survivors," *Br. J. Cancer* **56**, 339-347.
- 7204 Heeg, P., Eickhoff, H., Haberer, T. (2004). "Die Konzeption der Heidelberger Ionentherapieanlage
7205 HICAT," in *Zeitschrift für Medizinische Physik* **14**, 17-24.
- 7206 Heidenreich, W.F., Paretzke, H.G., and Jacob, P. (1997). "No evidence for increased tumor rates below
7207 200 mSv in the atomic bomb survivors data," *Radiat. Environ. Biophys.* **36**, 205-207.
- 7208 Hess, E., Takacs, S., Scholten, B., Tarkanyi, F., Coenen, H.H., and Qaim, S.M. (2001). "Excitation
7209 function of the $^{18}\text{O}(p, n)^{18}\text{F}$ nuclear reaction from threshold up to 30 MeV," *Radiochim. Acta.* **89**,
7210 357-362.

- 7211 Heyes, G.J. and Mill, A.J. (2004). "The neoplastic transformation potential of mammography X rays and
7212 atomic bomb spectrum radiation," *Radiat. Res.* **162**, 120-127.
- 7213 Hirao, Y. (2001). "Results from HIMAC and other therapy facilities in Japan," pp.8-12 in *Proc. of*
7214 *Sixteenth International Conference on Cyclotrons and their Applications 2001, CP600*, 13-17
7215 May 2001, Marti, F., Ed. (American Institute of Physics, East Lansing, MI, USA).
- 7216 Hirao, Y. *et al.* (1992). "Heavy Ion Medical Accelerator in Chiba – A Design Summary and Update –
7217 Division of Accelerator Research," *Report NIRS-M-89, HIMAC-001* (National Institute of
7218 Radiological Sciences, Chiba, Japan).
- 7219 Hofmann, W. and Dittrich, W. (2005). "Use of Isodose Rate Pictures for the Shielding Design of a
7220 Proton Therapy Centre," pp. 181-187 in *Proc. of Shielding Aspects of Accelerators, Targets and*
7221 *Irradiation Facilities (SATIF 7)*, 17-18 May 2004, Portugal.
- 7222 Hranitzky, C., Stadtmann, H., and Kindl, P. (2002). "The use of the Monte Carlo simulation technique
7223 for the design of an H*(10) dosimeter based on TLD-100," *Radiat. Prot. Dosim.*, **101**, 279-282.
- 7224 Hultqvist, M. and Gudowska, I. (2008). "Secondary doses in anthropomorphic phantoms irradiated with
7225 light ion beams," *Nuclear Technology* **10-057-151**.
- 7226 IAEA (1987). International Atomic Energy Agency, *Handbook on Nuclear Activation Data*, IAEA
7227 Technical Report Series 273 (International Atomic Energy Agency, Vienna).
- 7228 IAEA (1988). International Atomic Energy Agency, *Radiological Safety Aspects of the Operation of*
7229 *Proton Accelerators*, Technical Reports Series No. 283 (International Atomic Energy Agency,
7230 Vienna).
- 7231 IAEA (1996). International Atomic Energy Agency, *International Basic Safety Standards for Protection*
7232 *against Ionizing Radiation and for the Safety of Radiation Sources*, IAEA Safety Series No. 115
7233 (International Atomic Energy Agency, Vienna).

- 7234 IAEA (2006). International Atomic Energy Agency, *Radiation Protection in the Design of Radiotherapy*
7235 *Facilities*, IAEA Safety Reports Series No. 47 (International Atomic Energy Agency, Vienna).
- 7236 Iancu, G. and Kraemer, M. (2009). personal communication, Biologie, GSI Helmholtzzentrum für
7237 Schwerionenforschung GmbH, Hessen, Darmstadt.
- 7238 ICRP (1973). International Commission on Radiological Protection, *Data for Protection Against*
7239 *Ionizing Radiation from External Sources* (Supplement to ICRP Publication 15), ICRP
7240 Publication 21, *Annals of the ICRP* **21** (1-3) (Pergamon Press, Oxford, UK).
- 7241 ICRP (1975). International Commission on Radiological Protection, *Reference Man: Anatomical,*
7242 *Physiological and Metabolic Characteristics*, ICRP Publication 23, International Commission on
7243 Radiological Protection (Pergamon Press, Oxford, UK).
- 7244 ICRP (1991). International Commission on Radiological Protection, *Recommendations of the*
7245 *International Commission on Radiological Protection*, ICRP Publication 60, *Annals of ICRP*
7246 **21**(1-3) (Pergamon Press, Oxford, UK).
- 7247 ICRP (1996). International Commission on Radiological Protection, *Conversion Coefficients for use in*
7248 *Radiological Protection against External Radiation*, ICRP Publication 74 (Elsevier Science,
7249 Oxford, UK).
- 7250 ICRP (1998). International Commission on Radiological Protection, *Radiation Dose to Patients from*
7251 *Radiopharmaceuticals*, ICRP Publication 53, *Annals of the ICRP* **18** (Elsevier Science, Oxford,
7252 UK).
- 7253 ICRP (1999). International Commission on Radiological Protection, *Genetic Susceptibility to Cancer,*
7254 ICRP Publication 79, *Annals of the ICRP* **28** (Elsevier Science, Oxford, UK).
- 7255 ICRP (2000). International Commission on Radiological Protection, *Prevention of Accidental*
7256 *Exposures to Patients Undergoing Radiation Therapy*, ICRP Publication 86, *Annals of the ICRP*
7257 **30** (Elsevier Science, Oxford, UK).

- 7258 ICRP (2003a). International Commission on Radiological Protection, *Basic Anatomical and*
7259 *Physiological Data for Use in Radiological Protection: Reference Values*, ICRP Publication 89,
7260 *Annals of the ICRP* **33** (3-4) (Elsevier Science, Oxford, UK).
- 7261 ICRP (2003b). International Commission on Radiological Protection, *Relative Biological Effectiveness*
7262 *(RBE), Quality Factor (Q), and Radiation Weighting Factor (w_R)*, ICRP Publication 92, *Annals of*
7263 *the ICRP* **33** (4) (Elsevier Science, Oxford, UK).
- 7264 ICRP (2007). International Commission on Radiological Protection, *Recommendations of the ICRP*,
7265 ICRP Publication 103, *Annals of the ICRP* (Elsevier Science, Oxford, UK).
- 7266 ICRP (2008). International Commission on Radiological Protection, *Recommendations of the*
7267 *International Commission on Radiological Protection*, ICRP Publication 60, *Annals of the ICRP*
7268 **21** (1-3) (Elsevier Science, Oxford, UK).
- 7269 ICRU (1978). International Commission on Radiation Units and Measurements, *Basic Aspects of High*
7270 *Energy Particle Interaction and Radiation Dosimetry*, ICRU Report 28 (International
7271 Commission on Radiation Measurements and Units, Bethesda, MD).
- 7272 ICRU (1986). International Commission on Radiation Units and Measures, *The Quality Factor in*
7273 *Radiation Protection*, ICRU Report 40 (International Commission on Radiation Units and
7274 Measurements, Bethesda, MD).
- 7275 ICRU (1989). International Commission on Radiation Units and Measures, *Tissue Substitutes in*
7276 *Radiation Dosimetry and Measurement*, ICRU Report 44 (International Commission on
7277 Radiation Units and Measurements, Bethesda, MD).
- 7278 ICRU (1992a). International Commission on Radiation Units and Measures, *Measurement of Dose*
7279 *Equivalents from External Photon and Electron Radiations*, ICRU Report 47 (International
7280 Commission on Radiation Units and Measurements, Bethesda, MD).

- 7281 ICRU (1992b). International Commission on Radiation Units and Measures, *Photon, Electron, Proton*
7282 *and Neutron Interaction Data for Body Tissues*, ICRU Report 46 (International Commission on
7283 Radiation Units and Measurements, Bethesda, MD).
- 7284 ICRU (1993). International Commission on Radiation Units and Measures, *Quantities and Units in*
7285 *Radiation Protection*, ICRU Report 51 (International Commission on Radiation Measurements
7286 and Units, Bethesda, MD).
- 7287 ICRU (1998). International Commission on Radiation Units and Measures, *Conversion Coefficients for*
7288 *Use in Radiological Protection Against External Radiation*, ICRU Report 57 (International
7289 Commission on Radiation Units and Measurements, Bethesda, MD).
- 7290 ICRU (2000). International Commission on Radiation Units and Measures, *Nuclear Data for Neutron*
7291 *and Proton Radiotherapy and for Radiation Protection*, ICRU Report 63 (International
7292 Commission on Radiation Units and Measurements, Bethesda, MD).
- 7293 ICRU (2001). International Commission on Radiation Units and Measurements, *Determination of Dose*
7294 *Equivalent Quantities for Neutrons*, ICRU Report 47 (Nuclear Technology Publishing, Ashford).
- 7295 ICRU (2007). International Commission on Radiation Units and Measures, *Prescribing, Recording, and*
7296 *Reporting Proton-Beam Therapy*, ICRU Report 78 (International Commission on Radiation Units
7297 and Measurements, Bethesda, MD).
- 7298 IEC (1998). International Electrotechnical Commission, *Medical Electrical Equipment - Part 2-1,*
7299 *“Particular requirements for the safety of electron accelerators in the Range 1 MeV to 50 MeV,*
7300 *International Standard IEC 60601-2-1(IHS, Englewood, CO, USA).*
- 7301 IEC (2005). International Electrotechnical Commission, *Functional safety of electrical, electronic, and*
7302 *programmable electronic equipment, International Standard IEC 61508-SER (Ed. 1.0)*
7303 *(International Electrotechnical Commission, Geneva, Switzerland).*

- 7304 IEC (2006) International Electrotechnical Commission, *Medical device software - Software life cycle*
7305 *processes*, IEC 62304 (International Electrotechnical Commission, Geneva, Switzerland).
- 7306 Imaizumi, M., Usa, T., Tominaga, T., Neriishi, K., Akahoshi, M., Nakashima, E., Ashizawa, K., Hida,
7307 A., Soda, M., Fujiwara, S., Yamada, M., Ejima, E., Yokoyama, N., Okubo, M., Sugino, K.,
7308 Suzuki, G., Maeda, R., Nagataki, S., and Eguchi, K. (2006). "Radiation dose-response
7309 relationships for thyroid nodules and autoimmune thyroid diseases in Hiroshima and Nagasaki
7310 atomic bomb survivors 55-58 years after radiation exposure," *JAMA* **295**, 1011-1022).
- 7311 Ipe, N.E. (2008). "Particle accelerators in particle therapy: the new wave," in *Proc. of the 2008 Mid-Year*
7312 *Meeting of the Health Phys. Society on Radiation Generating Devices*, Oakland, CA (Health
7313 Phys. Society, McLean, VA).
- 7314 Ipe, N.E. (2009a). "Transmission of Shielding Materials for Particle Therapy Facilities," in *Proc. of the*
7315 *ICRS-11 International Conference on Radiation Shielding and RPSD-2008 15th Topical Meeting*
7316 *of the Radiation Protection and Shielding Division of the ANS*, 13-18 April 2008, Pine Mountain,
7317 Georgia, USA.
- 7318 Ipe, N.E. and Fasso, A., (2006). "Preliminary computational models for shielding design of particle
7319 therapy facilities," pp. in *Proc. of Shielding Aspects of Accelerators, Targets and Irradiation*
7320 *Facilities (SATIF 8)*, 22-24 May 2006, Gyongbuk, Republic of Korea (Nuclear Energy Agency,
7321 Organization for Economic Co-operation and Development, Paris).
- 7322 IRPL (2000). Italian Radiation Protection Laws, *Decreto Legislativo del Governo n° 230/1995*
7323 *modificato dal 187/2000 e dal 241/2000* (Ministero dell'Ambiente e della Tutela del Territorio,
7324 Italy).
- 7325 Ishikawa, T., Sugita, H., and Nakamura, T. (1991). "Thermalization of accelerator produced neutrons in
7326 concrete," *Health Phys.* **60**, 209-221.

- 7327 ISO (2007). International Organization for Standardization, *Medical devices--Application of risk management*
7328 *to medical devices*, ISO Standard 14791 (International Organization for Standardization, Geneva,
7329 Switzerland).
- 7330 Iwase, H., Niita, K., and Nakamura, T. (2002). "Development of General-Purpose Particle and heavy Ion
7331 Transport Monte Carlo Code," *J. Nucl. Sci. Technol.* **39**, 1142-1151.
- 7332 Iwase, H., Gunzert-Marx, K., Haettner, E., Schardt, D., Gutermuth, F., Kraemer, M., and Kraft, G.
7333 (2007). "Experimental and theoretical study of the neutron dose produced by carbon ion therapy
7334 beams," *Radiat. Prot. Dosim.* **126**, 615-618.
- 7335 Janssen, J.J., Korevaar, E.W., van Battum, L.J., Storchi, P.R., and Huizenga, H. (2001). "A model to
7336 determine the initial phase space of a clinical electron beam from measured beam data," *Phys.*
7337 *Med. Biol.* **46**, 269-286.
- 7338 Jemal, A., Siegel, R., Ward, E., Murray, T., Xu, J., Smigal, C. and Thun, M.J. (2006). "Cancer statistics,
7339 2006," *CA Cancer J. Clin.* **56**, 106-130.
- 7340 Jenkinson, H.C., Hawkins, M.M., Stiller, C.A., Winter, D.L., Marsden, H.B., and Stevens, M.C. (2004).
7341 "Long-term population-based risks of second malignant neoplasms after childhood cancer in
7342 Britain," *Br. J. Cancer* **91**, 1905-1910.
- 7343 Jiang, H., Wang, B., Xu, X.G., Suit, H.D., and Paganetti, H. (2005). "Simulation of Organ Specific
7344 Patient Effective Dose Due to Secondary Neutrons in Proton Radiation Treatment," *Phys. Med.*
7345 *Biol.* **50**, 4337-4353.
- 7346 Jirousek, I. and *et al.* (2003). "The concept of the PROSCAN Patient Safety System," in *Proc. of the IX*
7347 *International Conference on Accelerator and Large Experimental Physics Control Systems*
7348 *(ICALEPCS 2003)*, 13-17 October, 2003, Gyeongju, Republic of Korea.
- 7349 Joiner, M.C., Marples, B., Lambin, P., Short, S.C., and Turesson, I. (2001). "Low-dose hypersensitivity:
7350 current status and possible mechanisms," *Int. J. Radiat. Oncol. Biol. Phys.* **49**, 379-389.

- 7351 Jones, D.G (1998). "A realistic anthropomorphic phantom for calculating specific absorbed fractions of
7352 energy deposited from internal gamma emitters," *Radiat. Prot. Dosim.* **79**, 411-414.
- 7353 JORF (2006). "Arrêté du 15 mai 2006 relatif aux conditions de délimitation et de signalisation des zones
7354 surveillées et contrôlées et des zones spécialement réglementées ou interdites compte tenu de
7355 l'exposition aux rayonnements ionisants, ainsi qu'aux règles d'hygiène, de sécurité et d'entretien
7356 qui y sont imposées," *Journal Officiel de la République Française*, 15 juin 2006.
- 7357 JRPL (2004). Japanese Radiation Protection Laws (Prevention Law), *Law concerning Prevention from
7358 Radiation Hazards due to Radioisotopes etc.* **167**.
- 7359 Kaido, T., Hoshida, T., Uranishi, R., Akita, N., Kotani, A., Nishi, N., and Sakaki, T. (2001).
7360 "Radiosurgery-induced brain tumor. Case report," *J. Neurosurg.* **95**, 710-713.
- 7361 Kaschten, B., Flandroy, P., Reznik, M., Hainaut, H., and Stevenaert, A. (1995). "Radiation-induced
7362 gliosarcoma. Case report and review of the literature," *J. Neurosurg.* **83**, 154-162.
- 7363 Kato, T. and Nakamura, T. (1992). "Estimation of Neutron Yields from thick Targets by high- energy He
7364 Ions for the Design of Shielding for a heavy ion Medical Accelerator," *NIM Phys. Res. A* **311**,
7365 548-557.
- 7366 Kato, T., Kurosawa, K., Nakamura, T. (2002). "Systematic analysis of neutron yields from thick targets
7367 bombarded by heavy ions and protons with moving source model," *NIM Phys. Res. A* **480** 571-
7368 590.
- 7369 Keall, P.J., Siebers, J.V., Libby, B., and Mohan, R. (2003). "Determining the incident electron fluence
7370 for Monte Carlo-based photon treatment planning using a standard measured data set," *Med.*
7371 *Phys.* **30**, 574-582.
- 7372 Kellerer, A.M. (2000). "Risk estimates for radiation-induced cancer - the epidemiological evidence,"
7373 *Radiat. Environ. Biophys.* **39**, 17-24.

- 7374 Kellerer, A.M., Nekolla, E.A., and Walsh, L. (2001). "On the conversion of solid cancer excess relative
7375 risk into lifetime attributable risk," *Radiat. Environ. Biophys.* **40**, 249-257.
- 7376 Kellerer, A.M., Ruhm, W., and Walsh, L. (2006). "Indications of the neutron effect contribution in the
7377 solid cancer data of the A-bomb survivors," *Health Phys.* **90**, 554-564.
- 7378 Kenney, L.B., Yasui, Y., Inskip, P.D., Hammond, S., Neglia, J.P., Mertens, A.C., Meadows, A.T.,
7379 Friedman, D., Robison, L.L., and Diller, L. (2004). "Breast cancer after childhood cancer: a
7380 report from the Childhood Cancer Survivor Study," *Ann. Intern. Med.* **141**, 590-597.
- 7381 Kim, E., Nakamura, T., Uwamino, Y., Nakanishi, N., Imamura, M., Nakao, N., Shibata, S., and Tanaka,
7382 S. (1999). "Measurements of activation cross section on spallation reactions for ^{59}Co and $^{\text{nat}}\text{Cu}$ at
7383 incident neutron energies of 40 to 120 MeV," *J. Nucl. Sci. Technol.*, **36** (1), 29-40.
- 7384 Kim, J. (2003) "Proton Therapy Facility Project in National Cancer Center, Republic of Korea," *Journal*
7385 *of the Republic of Korean Physical Society*, **43**, Sep, 50-54.
- 7386 Kinoshita, N., Masumoto, K., Matsumura, H., Bessho, K., Toyoda, A., Tosaki, Y., Tamari, M.,
7387 Takahashi, T., Sueki, K., Oki, T., Mihara, S., Nagashima, Y., and Matsushi, Y. (2009).
7388 "Measurement and Monte Carlo simulation of radioactivity produced in concrete shield in EP-1
7389 beamline at the 12-GeV proton synchrotron facility, KEK," in *Proc. 5th International Symposium*
7390 *on Radiation Safety and Detection Technology (ISORD-5)*, Kita-Kyushu, Japan.
- 7391 Kirihara, Y., Hagiwara, M., Iwase, H., Ban, S., Itoga, T., and Nakamura, T. (2008). "Comparison of
7392 several Monte Carlo codes with neutron deep penetration experiments," in *Proc. 11th*
7393 *International Conference on Radiation Shielding (ICRS-11)*, Pine Mountain, Georgia, USA.
- 7394 Kitwanga, S.W., Leleux, P., Lipnik, P., and Vanhorenbeeck, J. (1990). "Production of O-14,15, F-18 and
7395 Ne-19 radioactive nuclei from (p, n) reactions up to 30-MeV," *Phys. Rev. C* **42**, 748-752.
- 7396 Klein, E.E., Maserang, B., Wood, R., and Mansur, D. (2006). "Peripheral doses from pediatric IMRT,"
7397 *Med. Phys.* **33**, 2525-2531.

- 7398 Knoll, G.F. (1999). *Radiation Detection and Measurement*, 3rd. ed., (John Wiley & Sons, Hoboken, NJ).
- 7399 Ko, S.J., Liao, X.Y., Molloy, S., Elmore, E., and Redpath, J.L. (2004). "Neoplastic transformation in vitro
7400 after exposure to low doses of mammographic-energy X rays: quantitative and mechanistic
7401 aspects," *Radiat. Res.* **162**, 646-654.
- 7402 Kocher, D.C., Apostolaei, A.I., and Hoffman, F.O. (2005). "Radiation effectiveness factors for use in
7403 calculating probability of causation of radiogenic cancers," *Health Phys.* **89**, 3-32.
- 7404 Komori, M. *et al.* (2004). "Design of Compact Irradiation Port for Carbon Radiotherapy Facility," in
7405 *Proc. of the 3rd Asian Particle Accelerator Conference, 22-26 March 2004, Gyeongju, Republic*
7406 *of Republic of Korea.*
- 7407 Kotegawa, H. *et al.* (1993). "Neutron-Photon Multigroup Cross Sections for Neutron Energies Up to 400
7408 MeV: HIL086R- Revision of HIL086 Library," JAERI-M 93-020 (Japan Atomic Energy
7409 Research Institute).
- 7410 Kraemer, M. *et al.* (2004) "Treatment planning for scanned ion beams," *Radiother. Oncol.* **73**, 80-85.
- 7411 Kraft, G. (2000). "Tumor Therapy with Heavy Charged Particles," *Progress in Particle and Nuclear*
7412 *Physics* **45**.
- 7413 Kramer, R., Zankl, M., Williams, G., and *et al.* (1982). "The calculation of dose from external photon
7414 exposures using reference human phantoms and Monte Carlo methods. Part I: The male (ADAM)
7415 and female (EVA) adult mathematical phantoms," *Gesellschaft fuer Strahlen- und*
7416 *Umweltforschung* **GSF-Bericht-S-885**.
- 7417 Kramer, R., Vieira, J.W., Khoury, H.J., Lima, F.R., and Fuelle, D. (2003). "All about MAX: a male
7418 adult voxel phantom for Monte Carlo calculations in radiation protection dosimetry," *Phys. Med.*
7419 *Biol.* **48**, 1239-1262.
- 7420 Kramer, R., Khoury, H.J., Vieira, J.W., and Lima, V.J. (2006). "MAX06 and FAX06: update of two
7421 adult human phantoms for radiation protection dosimetry," *Phys. Med. Biol.* **51**, 3331-3346.

- 7422 Kry, S.F., Salehpour, M., Followill, D.S., Stovall, M., Kuban, D.A., White, R.A., and Rosen, I.I., (2005).
7423 "The calculated risk of fatal secondary malignancies from intensity-modulated radiation therapy,"
7424 *Int. J. Radiat. Oncol. Biol. Phys.* **62**, 1195-1203.
- 7425 Kry, S.F., Followill, D., White, R.A., Stovall, M., Kuban, D.A., and Salehpour, M. (2007). "Uncertainty
7426 of calculated risk estimates for secondary malignancies after radiotherapy," *Int. J. Radiat. Oncol.*
7427 *Biol. Phys.* **68**, 1265-1271.
- 7428 Kurosawa, T. (1999). "Measurements of secondary neutrons produced from thick targets bombarded by
7429 high-energy neon ions," *J. Nucl. Sci. Technol.* **36**(1), 41-53.
- 7430 Kurosawa, T. (2000). "Neutron yields from thick C, Al, Cu and Pb targets bombarded by 400MeV ar, Fe,
7431 Xe and 800MeV Si ions," *Phys. Rev. C* **62**
- 7432 Kurosawa, T., Nakao, N., Nakamura, T., Uwamino, Y., Shibata, T., Nakanishi, N., Fukamura, A., and
7433 Murakami, K., (1999). "Measurements of secondary neutrons produced from thick targets
7434 bombarded by high-energy helium and carbon ions," *Nucl. Sci. and Eng.* **132**, 30-57.
- 7435 Kuttesch, J.F. Jr., Wexler, L.H., Marcus, R.B., Fairclough, D., Weaver-McClure, L., White, M., Mao, L.,
7436 Delaney, T.F., Pratt, C.B., Horowitz, M.E., and Kun, L.E. (1996). "Second malignancies after
7437 Ewing's sarcoma: radiation dose-dependency of secondary sarcomas," *J. Clin. Oncol.* **14**, 2818-
7438 2825.
- 7439 Lee, C. and Bolch, W. (2003). "Construction of a tomographic computational model of a 9-mo-old and
7440 its Monte Carlo calculation time comparison between the MCNP4C and MCNPX codes," *Health*
7441 *Phys.* **84** S259.
- 7442 Lee, C., Williams, J.L., Lee, C., and Bolch, W.E. (2005). "The UF series of tomographic computational
7443 phantoms of pediatric patients," *Med. Phys.* **32**, 3537-3548.

- 7444 Lee, C., Lee, C., and Bolch, W.E. (2006a). "Age-dependent organ and effective dose coefficients for
7445 external photons: a comparison of stylized and voxel-based paediatric phantoms," *Phys. Med.
7446 Biol.* **51**, 4663-4688.
- 7447 Lee, C., Lee, C., Williams, J.L. and Bolch, W.E. (2006b). "Whole-body voxel phantoms of paediatric
7448 patients--UF Series B," *Phys. Med. Biol.* **51**, 4649-4661.
- 7449 Lee, C., Lee, C., Lodwick, D. and Bolch, W. (2007a). "A series of 4D pediatric hybrid phantoms
7450 developed from the US series B tomographic phantoms [Abstract]," *Med. Phys.* **33**.
- 7451 Lee, C., Lodwick, D., Hasenauer, D., Williams, J.L., Lee, C., and Bolch, W. (2007b). "Hybrid
7452 computational phantoms of the male and female newborn patient: NURBS-based whole-body
7453 models," *Phys. Med. Biol.* **52**, 3309-3333.
- 7454 Lee, C., Lodwick, D., Williams, J.L., and Bolch, W. (2008). "Hybrid computational phantoms of the 15-
7455 year male and female adolescent: Applications to CT organ dosimetry for patients of variable
7456 morphometry," *Med. Phys.* **35**, 2366-2382.
- 7457 Lee, H.S. (2008). personal communication, Radiation Safety Office, Pohang Accelerator Laboratory,
7458 POSTECH, Nam-Gu Pohang, Gyongbuk, Republic of Republic of Korea.
- 7459 Leroy, C. and Rancoita, P.G. (2005). *Principles of Radiation Interaction in Matter and Detection*,
7460 (World Scientific, Singapore).
- 7461 Lim, S.M., DeNardo, G.L., DeNardo, D.A., Shen, S., Yuan, A., O'Donnell, R.T., and DeNardo, S.J.
7462 (1997). "Prediction of myelotoxicity using radiation doses to marrow from body, blood and
7463 marrow sources," *J. Nucl. Med.* **38**, 1374-1378.
- 7464 Little, M.P. (1997). "Estimates of neutron relative biological effectiveness derived from the Japanese
7465 atomic bomb survivors," *Int. J. Radiat. Biol.* **72**, 715-726.

- 7466 Little, M.P. (2000). "A comparison of the degree of curvature in the cancer incidence dose-response in
7467 Japanese atomic bomb survivors with that in chromosome aberrations measured in vitro," *Int. J.*
7468 *Radiat. Biol.* **76**, 1365-1375.
- 7469 Little, M.P. (2001). "Comparison of the risks of cancer incidence and mortality following radiation
7470 therapy for benign and malignant disease with the cancer risks observed in the Japanese A-bomb
7471 survivors," *Int. J. Radiat. Biol.* **77**, 431-464.
- 7472 Little, M.P. and Muirhead, C.R. (2000). "Derivation of low-dose extrapolation factors from analysis of
7473 curvature in the cancer incidence dose response in Japanese atomic bomb survivors," *Int. J.*
7474 *Radiat. Biol.* **76**, 939-953.
- 7475 Liwnicz, B.H., Berger, T.S., Liwnicz, R.G, and Aron, B.S. (1985). "Radiation-associated gliomas: a
7476 report of four cases and analysis of postradiation tumors of the central nervous system,"
7477 *Neurosurgery* **17**, 436-445.
- 7478 Loeffler, J.S., Niemierko, A. and Chapman, P.H. (2003). "Second tumors after radiosurgery: tip of the
7479 iceberg or a bump in the road?" *Neurosurgery* **52**, 1436-1442.
- 7480 Loncol, T., Cosgrove, V., Denis, J.M., Gueulette, J., Mazal, A., Menzel, H.G., Pihet, P., and Sabattier, R.
7481 (1994). "Radiobiological effectiveness of radiation beams with broad LET spectra:
7482 microdosimetric analysis using biological weighting functions," *Radiat. Prot. Dosim.* **52**, 347-
7483 352.
- 7484 Lux, I., and Koblinger, L., (1991). *Monte Carlo particle transport methods: neutron and photon*
7485 *calculations* (CRC Press, Boca Raton, FL).
- 7486 Maisin, J.R., Wambersie, A., Gerber, G.B., Mattelin, G., Lambiet-Collier, M., De Coster, B., and
7487 Gueulette, J. (1991). "Life-shortening and disease incidence in mice after exposure to g rays or
7488 high-energy neutrons," *Radiat. Res.* **128** S117-S23.

- 7489 Mares, V., Leuthold, G., and Schraube, H. (1997). "Organ doses and dose equivalents for neutrons above
7490 20 MeV," *Radiat. Prot. Dosim.*, **70**, 391-394.
- 7491 Marquez, L. (1952). "The yield of F-18 from medium and heavy elements with 420 MeV protons," *Phys.*
7492 *Rev.* **86**, 405-407.
- 7493 Mashnik, S.,G. (2009). "Overview and Validation of the CEM and LAQGSM Event Generators for
7494 MCNP6, MCNPX, and MARS15," in *Proc. of the First International Workshop on Accelerator*
7495 *Radiation Induced Activation (ARIA'08), PSI, Switzerland, PSI Proceedings 09-01*, 20-29.
- 7496 Masumoto, K., Matsumura, H., Bessho, K., and Toyoda, A. (2008). "Role of activation analysis for
7497 radiation control in accelerator facilities," *Journal of Radioanalytical and Nuclear Chemistry*,
7498 **278**, 449-453.
- 7499 Matsufuji, N., Fukumura, A., Komori, M., Kanai, T., and Kohno, T. (2003). "Influence of fragment
7500 reaction of relativistic heavy charged particles on heavy-ion radiotherapy," *Phys. Med. Biol.* **48**,
7501 1605-1623.
- 7502 Mazal, A., Gall, K., Bottollier-Depois, J.F., Michaud, S., Delacroix, D., Fracas, P., Clapier, F.,
7503 Delacroix, S., Nauraye, C., Ferrand, R., Louis, M., and Habrand, J.L. (1997). "Shielding
7504 measurements for a proton therapy beam of 200 MeV: preliminary results," *Radiat. Prot. Dosim.*,
7505 **70**, 429-436.
- 7506 McKinney, G., *et al.* (2006). "Review of Monte Carlo all-particle transport codes and overview of recent
7507 MCNPX features," in *Proc. of the International Workshop on Fast Neutron Detectors* (University
7508 of Cape Town, South Africa).
- 7509 Meier, M.M., Goulding, C.A., Morgan, G.L., and Ullmann, J.L. (1990). "Neutron Yields from Stopping-
7510 and Near-Stopping-Length Targets for 256-MeV Protons," *Nucl. Sci. and Eng.* **104**, 339-363.
- 7511 Mesoloras, G., Sandison, G.A., Stewart, R.D., Farr, J.B., and Hsi, W.C. (2006). "Neutron scattered dose
7512 equivalent to, a fetus from proton radiotherapy of the mother," *Med. Phys.* **33**, 2479-2490.

- 7513 Michel, R., *et al.* (1997). "Cross sections for the production of residual nuclides by low- and medium-
7514 energy protons from the target elements C, N, O Mg, Al, Si, Ca, Ti, V, Mn, Fe, Co, Ni, Cu, Sr, Y,
7515 Zr, Nb, Ba and Au," *NIM Phys. Res.* **B129**, 153-193.
- 7516 Minniti, G., Traish, D., Ashley, S., Gonsalves, A., and Brada, M. (2005). "Risk of second brain tumor
7517 after conservative surgery and radiotherapy for pituitary adenoma: update after an additional 10
7518 years," *J. Clin. Endocrinol. Metab.* **90**, 800-804.
- 7519 Miralbell, R., Lomax, A., Cella, L., and Schneider, U. (2002). "Potential reduction of the incidence of
7520 radiation-induced second cancers by using proton beams in the treatment of pediatric tumors,"
7521 *Int. J. Radiat. Phys. Med. Biol.* **54**, 824-829.
- 7522 Mokhov, N.V. (1995). "The MARS Code System User's Guide," Fermilab-FN-628 (1995).
- 7523 Mokhov, N.V. (2009). "MARS Code System," Version 15 (2009), <http://www-ap.fnal.gov/MARS>,
7524 accessed 20 September 2009.
- 7525 Mokhov, N.V. and Striganov, S.I. (2007). "MARS15 Overview," in *Proc. of the Hadronic Shower
7526 Simulation Workshop 2006, Fermilab 6-8 September 2006*, M., Albrow, R., Raja Eds., *AIP
7527 Conference Proceeding* **896** .
- 7528 Moritz, L.E. (1994). "Summarized experimental results of neutron shielding and attenuation length," pp.
7529 in *Proc. Shielding Aspects of Accelerators, Targets and Irradiation Facilities (SATIF)*, 28-29
7530 April 1998, Arlington, Texas (Nuclear Energy Agency, Organization for Economic Co-operation
7531 and Development, Paris).
- 7532 Moritz, L.E. (2001). "Radiation protection at low energy proton accelerators," *Radiat. Prot. Dosim.*
7533 **96(4)**, 297-309.
- 7534 Morone, M.C., Calabretta, L., Cuttone, G., and Fiorini, F. (2008). "Monte Carlo simulation to evaluate
7535 the contamination in an energy modulated carbon ion beam for hadron therapy delivered by
7536 cyclotron," *Phys. Med. Biol.* **53**, 6045-6053.

- 7537 Morstin, K., and Olko, P. (1994). "Calculation of neutron energy deposition in nanometric sites," *Radiat.*
7538 *Prot. Dosim.* **52**, 89-92.
- 7539 Moyer, B.J. (1957) "University of California Radiation Laboratory Proton Synchrotron", *Rep. TID-7545*,
7540 **38** (U.S. Army Environmental Command, Washington, DC).
- 7541 Moyers, M.F., Benton, E.R., Ghebremedhin, A., and Coutrakon, G. (2008). "Leakage and scatter
7542 radiation from a double scattering based proton beamline," *Med. Phys.* **35**, 128-144.
- 7543 Nakamura, T. (2000). "Neutron production from thin and thick targets by high-energy heavy ion
7544 bombardment," pp. in *Proc. Shielding Aspects of Accelerators, Targets and Irradiation Facilities*
7545 *(SATIF-5)*, 18-21 July 2000, Paris (Nuclear Energy Agency, Organization for Economic Co-
7546 operation and Development, Paris).
- 7547 Nakamura, T. (2002). "Double differential thick-target neutron yields bombarded by high-energy heavy
7548 ions," pp. 19–25 in *Proc. Shielding Aspects of Accelerators, Targets and Irradiation Facilities*
7549 *(SATIF-6)*, 10–12 April 2002, Stanford, CA (Nuclear Energy Agency, Organization for Economic
7550 Co-operation and Development, Paris).
- 7551 Nakamura, T. (2004). "Summarized experimental results of neutron shielding and attenuation length,"
7552 pp. 129-146 in *Proc. Shielding Aspects of Accelerators, Targets and Irradiation Facilities*
7553 *(SATIF-7)*, 17–18 May 2004, Portugal (Nuclear Energy Agency, Organization for Economic Co-
7554 operation and Development, Paris).
- 7555 Nakamura T., and Heilbronn, L. (2006). *Handbook on Secondary Particle Production and Transport by*
7556 *High-Energy Heavy Ions*, (World Scientific, Singapore).
- 7557 Nakamura, T., Nunomiya, T., Yashima, H., and Yonai, S. (2004). "Overview of recent experimental
7558 works on high energy neutron shielding," *Progress in Nuclear Energy*, **44(2)**, 85-187.
- 7559 Nakashima, H., Takada, H., Meigo, S., Maekawa, F., Fukahori, T., Chiba, S., Sakamoto, Y., Sasamoto,
7560 N., Tanaka, S., Hayashi, K., Odano, N., Yoshizawa, N., Sato, O., Suzuoki, Y., Iwai, S., Uehara,

- 7561 T., Takahashi, H., Uwamino, Y., Namito, Y., Ban, S., Hirayama, H., Shin, K. and Nakamura, T.
7562 (1995). "Accelerator shielding benchmark experiment analyses," in *Proc. Shielding Aspects of*
7563 *Accelerators, Targets and Irradiation Facilities (SATIF-2)*, 12-13 October 1995, CERN, Geneva
7564 (Nuclear Energy Agency, Organization for Economic Co-operation and Development, Paris).
- 7565 Nasagawa, H. and Little, J.B. (1999). "Unexpected sensitivity to the induction of mutations by very low
7566 doses of alpha-particle radiation: evidence for a bystander effect," *Radiat. Res.* **152**, 552-557.
- 7567 NCRP (1971). National Council on Radiation Protection and Measurements, *Protection Against Neutron*
7568 *Radiation*, NCRP Report 38 (National Council on Radiation Protection and Measurements,
7569 Bethesda, MD).
- 7570 NCRP (1977). National Council on Radiation Protection and Measurements, *Radiation Protection*
7571 *Design Guidelines for 0.1-100 MeV Particle Accelerator Facilities*, NCRP Report 51 (National
7572 Council on Radiation Protection and Measurements, Bethesda, MD).
- 7573 NCRP (1990). National Council on Radiation Protection and Measurements, *The Relative Biological*
7574 *Effectiveness of Radiations of Different Quality*, NCRP Report 104 (National Council on
7575 Radiation Protection and Measurements, Bethesda, MD).
- 7576 NCRP (1991). National Council on Radiation Protection and Measurements, *Calibration of Survey*
7577 *Instruments Used in Radiation Protection for the Assessment of Ionizing Radiation Fields and*
7578 *Radioactive Surface Contamination*, NCRP Report 112 (National Council on Radiation
7579 Protection and Measurements, Bethesda, MD).
- 7580 NCRP (1993). National Council on Radiation Protection and Measurements, *Limitation of Exposure to*
7581 *Ionizing Radiation (Supersedes NCRP Report No. 91)*, NCRP Report 116 (National Council on
7582 Radiation Protection and Measurements, Bethesda, MD).

- 7583 NCRP (1996). National Council on Radiation Protection and Measurements, *Dosimetry of X-Ray and*
7584 *Gamma-Ray Beams for Radiation Therapy in the Energy Range 10 keV to 50 MeV*, NCRP
7585 Report 69 (National Council on Radiation Protection and Measurements, Bethesda, MD).
- 7586 NCRP (2001). National Council on Radiation Protection and Measurements, *Evaluation of the Linear-*
7587 *Nonthreshold Dose-Response Model for Ionizing Radiation*, NCRP Report 136 (National Council
7588 on Radiation Protection and Measurements, Bethesda, MD).
- 7589 NCRP (2003). National Council on Radiation Protection and Measurements, *Radiation Protection for*
7590 *Particle Accelerator Facilities*, NCRP Report 144 (National Council on Radiation Protection and
7591 Measurements, Bethesda, MD).
- 7592 NCRP (2005). National Council on Radiation Protection and Measurements, *Structural Shielding Design*
7593 *and Evaluation for Megavoltage X- and Gamma-Ray Radiotherapy Facilities*, NCRP Report 151
7594 (National Council on Radiation Protection and Measurements, Bethesda, MD).
- 7595 Neglia, J.P., Meadows, A.T., Robison, L.L., Kim, T.H., Newton, W.A., Ruymann, F.B., Sather, H.N.,
7596 and Hammond, G.D. (1991). "Second neoplasms after acute lymphoblastic leukemia in
7597 childhood," *N. Engl. J. Med.* **325**, 1330-1336.
- 7598 Neglia, J.P., Friedman, D.L., Yasui, Y., Mertens, A.C., Hammond, S., Stovall, M., Donaldson, S.S.,
7599 Meadows, A.T., and Robison, L.L. (2001). "Second malignant neoplasms in five-year survivors
7600 of childhood cancer: childhood cancer survivor study," *J. Natl. Cancer Inst.* **93**, 618-629.
- 7601 Newhauser, W.D., Titt, U., Dexheimer, D., Yan, X. and Nill, S. (2002). "Neutron shielding verification
7602 measurements and simulations for a 235-MeV proton therapy center," *NIM Phys. Res. A* **476**, 80-
7603 84.
- 7604 Newhauser, W.D., Ding, X., Giragosian, D., Nill, S., and Titt, U., (2005a). "Neutron radiation area
7605 monitoring system for proton therapy facilities," *Radiat. Prot. Dosim.* **115**, 149–153.

- 7606 Newhauser, W., Koch, N., Hummel, S., Ziegler, M., and Titt, U. (2005b). "Monte Carlo simulations of a
7607 nozzle for the treatment of ocular tumours with high-energy proton beams," *Phys. Med. Biol.* **50**,
7608 5229-5249.
- 7609 Newhauser, W.D., Fontenot, J.D., Mahajan, A., Kornguth, D., Stovall, M., Zheng, Y., Taddei, P.J.,
7610 Mirkovic, D., Mohan, R., Cox, J.D., and Woo, S. (2009). "The risk of developing a second
7611 cancer after receiving craniospinal proton irradiation," *Phys. Med. Biol.* **54**, 2277-2291.
- 7612 Niita, K., Meigo, S., Takada, H., and Ikeda, Y. (2001). "High energy particle transport code
7613 NMTC/JAM," *NIM Phys. Res.* **B184**, 406-420.
- 7614 Niita, K., Sato, T., Iwase, H., Nose, H., Nakashima, H., and Sihver, L. (2006). "PHITS: a particle and
7615 heavy ion transport code system," *Radiation Measurements* **41**, 1080-1090.
- 7616 Nipper, J.C., Williams, J.L., and Bolch, W.E. (2002). "Creation of two tomographic voxel models of
7617 paediatric patients in the first year of life," *Phys. Med. Biol.* **47**, 3143-3164.
- 7618 Nishimura, H., Miyamoto, T., Yamamoto, N., Koto, M., Sugimura, K., and Tsujii, H. (2003).
7619 "Radiographic pulmonary and pleural changes after carbon ion irradiation," *Int. J. Radiat. Oncol.*
7620 *Biol. Phys.* **55**, 861-866.
- 7621 Noda, K. (2004). "HIMAC and new Facility Design for Widespread Use of Carbon Cancer Therapy," pp
7622 552-556 in *Proc. of the 3rd Asian Particle Accelerator Conference*, 22-26 March 2004,
7623 Gyeongju, Republic of Korea.
- 7624 Noda, K. *et al.* (2006a). "Development for new Carbon Cancer-Therapy Facility and Future Plan of
7625 HIMAC," in *Proc. of EPAC 2006*, 995-957 (Applications of Accelerators, Technology Transfer
7626 and Industrial Relations, Edinburgh, Scotland).
- 7627 Noda, K. *et al.* (2006b). "Design of Carbon Therapy Facility Based on 10 Years Experience at HIMAC,"
7628 *NIM Phys. Res. A* **562**, 1038-1041.

- 7629 Nolte, E., Ruhm, W., Loosli, H.H., Tolstikhin, I., Kato, K., Huber, T.C., and Egbert, S.D. (2006).
7630 "Measurements of fast neutrons in Hiroshima by use of (^{39}Ar) ," *Radiat. Environ. Biophys.* **44**,
7631 261-271.
- 7632 Norosinski, S. (2006). *Erstellung eines Handbuches zur Abschätzung von Abschirmungen*, Diploma
7633 thesis 31 May 2006, Zittau, Görlitz.
- 7634 Numajiri, M. (2007). "Evaluation of the radioactivity of the pre-dominant gamma emitters in components
7635 used at high-energy proton accelerator facilities," *Radiat. Prot. Dosim.* **23 (4)**, 417-425.
- 7636 Oishi, K., Nakao, N., Kosako, K., Yamakawa, H., Nakashima, H, Kawai, M., Yashima, H., Sanami, T.,
7637 Numajiri, M., Shibata, T., Hirayama, H., and Nakamura, T. (2005). "Measurement and analysis
7638 of induced activities in concrete irradiated using high-energy neutrons at KENS neutron
7639 spallation source facility," *Radiat. Prot. Dosim.* **115**, 623–629.
- 7640 Olsen, J.H., Garwicz, S., Hertz, H., Jonmundsson, G., Langmark, F., Lanning, M., Lie, S.O., Moe, P.J.,
7641 Moller, T., Sankila, R., and *et al.* (1993). "Second malignant neoplasms after cancer in childhood
7642 or adolescence. Nordic Society of Paediatric Haematology and Oncology Association of the
7643 Nordic Cancer Registries," *BMJ* **307**, 1030-1036.
- 7644 Olsher, R.H., Hsu, H.H., Beverding, A, Kleck, J.H., Casson, W.H., Vasilik, D.G., and Devine, R.T.
7645 (2000). "WENDI: An improved neutron rem meter," *Health Phys.* **70**, 171-181.
- 7646 Olsher, R.H., Seagraves, D.T., Eisele, S.L., Bjork, C.W., Martinez, W.A., Romero, L.L., Mallett, M.W.,
7647 Duran, M.A., and Hurlbut, C.R. (2004). "PRESCILA: A new, lightweight neutron rem meter,"
7648 *Health Phys.* **86**, 603-612.
- 7649 Paganetti, H. (1998). "Monte Carlo method to study the proton fluence for treatment planning," *Med.*
7650 *Phys.* **25**, 2370-2375.
- 7651 Paganetti, H. (2002). "Nuclear Interactions in Proton Therapy: Dose and Relative Biological Effect
7652 Distributions Originating From Primary and Secondary Particles," *Phys. Med. Biol.* **47**, 747-764.

- 7653 Paganetti, H. (2005). "Changes in tumor cell response due to prolonged dose delivery times in
7654 fractionated radiation therapy," *Int. J. Radiat. Oncol. Biol. Phys.* **63**, 892-900.
- 7655 Paganetti, H. (2006). "Monte Carlo calculations for absolute dosimetry to determine output factors for
7656 proton therapy treatments," *Phys. Med. Biol.* **51**, 2801-2812.
- 7657 Paganetti, H., Olko, P., Kobus, H., Becker, R., Schmitz, T., Waligorski, M.P.R., Filges, D., and Mueller-
7658 Gaertner, H.W. (1997). "Calculation of RBE for Proton beams Using Biological Weighting
7659 Functions," *Int. J. Radiat. Oncol. Biol. Phys.* **37**, 719-729.
- 7660 Paganetti, H., Jiang, H., Lee S-Y., and Kooy, H. (2004). "Accurate Monte Carlo for nozzle design,
7661 commissioning, and quality assurance in proton therapy," *Med. Phys.* **31**, 2107-2118.
- 7662 Paganetti, H., Bortfeld, T., and Delaney, T.F. (2006). "Neutron dose in proton radiation therapy: in
7663 regard to Eric, J. Hall (*Int. J. Radiat. Oncol. Biol. Phys.* 2006;65:1-7)," *Int. J. Radiat. Oncol.*
7664 *Biol. Phys.* **66**, 1594-5; author reply 5.
- 7665 Paganetti, H., Jiang, H., Parodi, K., Slopesma, R., and Engelsman, M. (2008). "Clinical implementation
7666 of full Monte Carlo dose calculation in proton beam therapy," *Phys. Med. Biol.* **53**, 4825-4853.
- 7667 Palm, A. and Johansson, K.A. (2007). "A review of the impact of photon and proton external beam
7668 radiotherapy treatment modalities on the dose distribution in field and out-of-field; implications
7669 for the long-term morbidity of cancer survivors," *Acta. Oncol.* **46**, 462-473.
- 7670 Parodi, K., Ferrari, A., Sommerer, F., and Paganetti, H., (2007). "Clinical CT-based calculations of dose
7671 and positron emitter distributions in proton therapy using the FLUKA Monte Carlo code," *Phys.*
7672 *Med. Biol.* **52**, 3369-3387.
- 7673 Pedroni, E. *et al.* (2005). "The 200 MeV proton therapy project at the Paul Scherrer Institute: conceptual
7674 design and practical realization," *Med. Phys.* **22**, 37-53.

- 7675 Pelliccioni, M. (2000). "Overview of fluence-to-effective dose and fluence-to-ambient dose equivalent
7676 conversion coefficients for high energy radiation calculated using the FLUKA Code," *Radiat.*
7677 *Prot. Dosim.* **88(4)**, 277-297.
- 7678 Pelowitz, D.B., ed. (2005). "MCNPX User's Manual, Version 2.5.0," Los Alamos National Laboratory
7679 report, LA-CP-05-0369, <http://mcnpx.lanl.gov> (accessed 18 September 2009).
- 7680 Perez-Andujar, A., Newhauser, W.D., and Deluca, P.M. (2009). "Neutron production from beam-
7681 modifying devices in a modern double scattering proton therapy beam delivery system," *Phys.*
7682 *Med. Biol.* **54**, 993-1008.
- 7683 Petoussi-Henss, N., Zanki, M., Fill, U., and Regulla, D. (2002). "The GSF family of voxel phantoms,"
7684 *Phys. Med. Biol.* **47**, 89-106.
- 7685 Piegl, L. (1991). "On NURBS: A survey," *IEEE Computer Graphics and Applications* **11**, 55-71.
- 7686 Pierce, D.A. and Preston, D.L. (2000). "Radiation-related cancer risks at low doses among atomic bomb
7687 survivors," *Radiat. Res.* **154**, 178-186.
- 7688 Pierce, D.A., Shimizu, Y., Preston, D.L., Vaeth, M., and Mabuchi, K. (1996). "Studies of the mortality of
7689 atomic bomb survivors. Report 12, Part, I. Cancer: 1950-1990," *Radiat. Res.* **146**, 1-27.
- 7690 Polf, J.C. and Newhauser, W.D. (2005). "Calculations of neutron dose equivalent exposures from range-
7691 modulated proton therapy beams," *Phys. Med. Biol.* **50**, 3859-3873.
- 7692 Polf, J.C., Newhauser, W.D., and Titt, U., (2005). "Patient neutron dose equivalent exposures outside of
7693 the proton therapy treatment field," *Radiat. Prot. Dosim.* **115**, 154-158.
- 7694 Popova, I.I. (2005). "MCNPX vs DORT for SNS shielding design studies," *Radiat. Prot. Dosim.* **115**,
7695 559-563.
- 7696 Porta, A., Agosteo, S., and Campi, F. (2005). "Monte Carlo Simulations for the Design of the Treatment
7697 Rooms and Synchrotron Access Mazes in the CNAO Hadrontherapy Facility," *Rad. Prot. Dosim.*
7698 **113 (3)** 266-274.

- 7699 Porta, A., Agosteo, S., Campi, F., and Caresana, M. (2008). "Double-differential spectra of secondary
7700 particles from hadrons on tissue equivalent targets," *Radiat. Prot. Dosim.* **132** (1), 29-41.
- 7701 Potish, R.A., Dehner, L.P., Haselow, R.E., Kim, T.H., Levitt, S.H., and Nesbit, M. (1985). "The
7702 incidence of second neoplasms following megavoltage radiation for pediatric tumors," *Cancer*
7703 **56**, 1534-1537.
- 7704 Preston, D.L., Shimizu, Y., Pierce, D.A., Suyama, A., and Mabuchi, K. (2003). "Studies of mortality of
7705 atomic bomb survivors. Report 13: Solid cancer and noncancer disease mortality: 1950-1997,"
7706 *Radiat. Res.* **160**, 381-407.
- 7707 Preston, D.L., Pierce, D.A., Shimizu, Y., Cullings, H.M., Fujita, S., Funamoto S., and Kodama, K.
7708 (2004). "Effect of Recent Changes in Atomic Bomb Survivor Dosimetry on Cancer Mortality
7709 Risk Estimates," *Radiat. Res.* **162**, 377-389.
- 7710 Pshenichnov, I., Mishustin, I., and Greiner, W. (2005). "Neutrons from fragmentation of light nuclei in
7711 tissue-like media: a study with the GEANT4 toolkit," *Phys. Med. Biol.* **50**, 5493-5507.
- 7712 Pshenichnov, I., Larionov, A., Mishustin, I., and Greiner, W. (2007). "PET monitoring of cancer therapy
7713 with ^3He and ^{12}C beams: a study with the GEANT4 toolkit," *Phys. Med. Biol.* **52**, 7295-7312.
- 7714 PTCOG (2009). Particle Theory Co-Operative Group, <http://www.psi.org.ch/> Accessed 4 May 09.
- 7715 Raju, M.R. (1980). *Heavy Particle Radiotherapy*, (Academic Press, New York).
- 7716 Reft, C.S., Runkel-Muller, R., and Myriantopoulos, L. (2006). "In vivo and phantom measurements of
7717 the secondary photon and neutron doses for prostate patients undergoing 18 MV IMRT," *Med.*
7718 *Phys.* **33**, 3734-3742.
- 7719 RIBF (2005). "Radiation safety assessment for RI Beam Factory," Promotion Office of RI Beam Factory,
7720 Nishina Center for Accelerator-Based Science, RIKEN (Wako, Japan).
- 7721 Ries, L.A.G., Eisner, M.P., Kosary, C.L., Hankey, B.F., Miller, B.A., Clegg, L., Mariotto, A., Fay, M.P.,
7722 Feuer, E.J., Edwards, B.K., eds. (2003). *SEER Cancer Statistics Review, 1975-2000*,

- 7723 http://seer.cancer.gov/csr/1975_2000/, accessed 20 September 2009 (National Cancer Institute.
7724 Bethesda, MD).
- 7725 Ries, L.A.G., Harkins, D., Krapcho, M., Mariotto, A., Miller, B.A., Feuer, E.J. and *et al.* eds. (2006).
7726 *SEER cancer statistics review, 1975-2003*, http://seer.cancer.gov/csr/1975_2003/, accessed 20
7727 September 2009 (National Cancer Institute. Bethesda, MD).
- 7728 Rijkee, A.G., Zoetelief, J., Raaijmakers, C.P., Van Der Marck, S.C. and Van Der Zee, W. (2006).
7729 "Assessment of induction of secondary tumours due to various radiotherapy modalities," *Radiat.*
7730 *Prot. Dosim.* **118**, 219-226.
- 7731 Rinecker, H. (2005). *Protonentherapie – Neue Chance bei Krebs* ,(F.A. Herbig Verlagsbuchhandlung
7732 GmbH: Munich, Germany).
- 7733 Rogers, J., Stabin, M., and Gesner, J., (2007). "Use of GEANT4 for Monte Carlo studies in voxel-based
7734 anthropomorphic models," *J. Nucl. Med.* **48**, Suppl. 2, 295P.
- 7735 Ron, E. (2006). "Childhood cancer--treatment at a cost," *J. Natl. Cancer Inst.* **98**, 1510-1511.
- 7736 Ron, E. and Hoffmann, F.O. (1997). "Uncertainty in radiation dosimetry and their impact on dose-
7737 response analysis," *National Cancer Institute, National Institute of Health Workshop*
7738 *Proceedings.* 99-4541.
- 7739 Ron, E., Modan, B., Boice, J.D., Alfandary, E., Stovall, M., Chetrit, A., and Katz, L. (1988). "Tumors of
7740 the brain and nervous system after radiotherapy in childhood," *N. Eng. J. Med.* **319**, 1033-1039.
- 7741 Ron, E., Lubin, J.H., Shore, R.E., Mabuchi, K., Modan, B., Pottern, L.M., Schneider, A.B., Tucker,
7742 M.A., and Boice, J.D., Jr. (1995). "Thyroid cancer after exposure to external radiation:, a.pooled
7743 analysis of seven studies," *Radiat. Res.* **141**, 259-277.
- 7744 Roy, S.C. and Sandison, G.A. (2004). "Scattered neutron dose equivalent to a fetus from proton therapy
7745 of the mother," *Radiat. Phys. Chem.* **71**, 997-998.

- 7746 Ruth, T.J. and Wolf, A.P. (1979). "Absolute cross sections for the production of ^{18}F via the ^{18}O (p, n) ^{18}F
7747 reaction," *Radiochim. Acta.* **26**, 21-24.
- 7748 Sadetzki, S., Flint-Richter, P., Ben-Tal, T., and Nass, D. (2002). "Radiation-induced meningioma: a
7749 descriptive study of 253 cases," *J. Neurosurg.* **97**, 1078-1082.
- 7750 Sakamoto, Y., Sato, O., Tsuda, S., Yoshizawa, N., Iwai, S., Tanaka, S., and Yamaguchi, Y. (2003).
7751 "Dose conversion coefficients for high-energy photons, electrons, neutrons and protons," JAERI-
7752 1345 (Japan Atomic Energy Research Institute, Tokai).
- 7753 Sasaki, S. and Fukuda, N. (1999). "Dose-response relationship for induction of solid tumors in female
7754 B6C3F1 mice irradiated neonatally with a single dose of gamma rays," *J. Radiat. Res. (Tokyo)*
7755 **40**, 229-241.
- 7756 Sato, O., Yoshizawa, N., Takagi, S., Iwai, S., Uehara, T., Sakamoto, Y., Yamaguchi, Y., and Tanaka, S.
7757 (1999). "Calculations of effective dose and ambient dose equivalent conversion coefficients for
7758 high energy photons," *J. Nucl. Sci. Tech.*, **36**, 977-987.
- 7759 Sato, T., Endo, A., Zankl, M., Petoussi-Henss, N., and Niita, K. (2009). "Fluence-to-dose conversion
7760 coefficients for neutrons and protons calculated using the PHITS code and ICRP/ICRU adult
7761 reference computational phantoms," *Phys. Med. Biol.* **54**, 1997-2014.
- 7762 Schardt, D., Iwase, H., Simon, R.S., and Gunzert-Marx, K. (2006). "Experimental investigation of
7763 secondary fast neutrons produced in carbon ion radiotherapy," in *Proc. of the International*
7764 *Workshop on Fast Neutron Detectors and Applications*, 3-6 April 2006, University of Cape
7765 Town, South Africa.
- 7766 Scharf, W.H. and Wieszczycka, W. (2001). *Proton Radiotherapy Accelerators* (World Scientific
7767 Publishing Co., London, UK).

- 7768 Schimmerling, W., Miller, J., Wong, M., Rapkin, M., Howard, J., Spieler, H.G., and Jarret, B.V. (1989).
7769 "The fragmentation of 670A MeV neon-20 as a function of depth in water. I Experiment," *Radiat.*
7770 *Res.* **120**, 36-71.
- 7771 Schippers, J.M. *et al.*, (2007). "The SC cyclotron and beam lines of PSI's new proton therapy facility
7772 PROSCAN," *NIM Phys. Res.* **B 261**, 773-776.
- 7773 Schneider, U. and Kaser-Hotz, B. (2005). "Radiation risk estimates after radiotherapy: application of the
7774 organ equivalent dose concept to plateau dose-response relationships," *Radiat. Environ. Biophys.*
7775 **44**, 235-239.
- 7776 Schneider, U., Agosteo, S., Pedroni, E., and Besserer, J. (2002). "Secondary neutron dose during proton
7777 therapy using spot scanning," *Int. J. Radiat. Oncol. Biol. Phys.* **53**, 244-251.
- 7778 Schneider, U., Fiechtner, A., Besserer, J. and Lomax, A. (2004). "Neutron dose from prostheses material
7779 during radiotherapy with protons and photons," *Phys. Med. Biol.* **49**, N119-N24
- 7780 Schneider, U., Lomax, A., Hauser, B. and Kaser-Hotz, B. (2006). "Is the risk for secondary cancers after
7781 proton therapy enhanced distal to the Planning Target Volume? A two-case report with possible
7782 explanations," *Radiat. Environ. Biophys.* **45**, 39-43.
- 7783 Schneider, U., Lomax, A., Besserer, J., Pemler, P., Lombriser, N., and Kaser-Hotz, B. (2007). "The
7784 impact of dose escalation on secondary cancer risk after radiotherapy of prostate cancer," *Int. J.*
7785 *Radiat. Oncol. Biol. Phys.* **68**, 892-897.
- 7786 Schottenfeld, D. and Beebe-Dimmer, J.L. (2006). "Multiple cancers," *Cancer epidemiology and*
7787 *prevention*. Schottenfeld, D. and Fraumeni, J.F., Jr., Eds., 1269-1280.
- 7788 Schultz-Ertner, D. *et al.* (2004). "Results of Carbon Ion Radiotherapy in 152 Patients," *Int. J. Radiation*
7789 *Onc. Biol. Phys.* **58 (2)** 631-640.
- 7790 Schwarz, R., (2008). "Graphical User Interface for High Energy Multi-Particle Transport,"
7791 <http://www.mcnpvised.com>, accessed 20 September 2009.

- 7792 Segars, W.P (2001). "Development and application of the new dynamic NURBS-based cardiac-torso
7793 (NCAT) phantom.," Dissertation in Biomedical Engineering. (University of North Carolina, NC,
7794 USA).
- 7795 Segars, W.P. and Tsui, B.M.W. (2002). "Study of the efficacy of respiratory gating in myocardial
7796 SPECT using the new 4-D NCAT phantom," *IEEE Transactions in Nuclear Science* **49**, 675-679.
- 7797 Segars, W.P., Lalush, D.S., and Tsui, B.M.W. (1999). "A realistic spline-based dynamic heart phantom,"
7798 *IEEE Transactions in Nuclear Science* **46**, 503-506.
- 7799 Shamisa, A., Bance, M., Nag, S., Tator, C., Wong, S., Noren, G., and Guha, A. (2001). "Glioblastoma
7800 multiforme occurring in a patient treated with gamma knife surgery. Case report and review of
7801 the literature," *J. Neurosurg.* **94**, 816-821.
- 7802 Shellabarger, C.J., Chmelevsky, D., and Kellerer, A.M. (1980). "Induction of mammary neoplasms in the
7803 Sprague-Dawley rat by 430keV neutrons and X-rays," *J. Natl. Cancer Inst.* **64**, 821-833.
- 7804 Shi, C. and Xu, X.G. (2004). "Development of a 30-week-pregnant female tomographic model from
7805 computed tomography (CT) images for Monte Carlo organ dose calculations," *Med. Phys.* **31**,
7806 2491-2497.
- 7807 Shi, C.Y., Xu, X.G., and Stabin, M.G. (2004). "Specific absorbed fractions for internal photon emitters
7808 calculated for a tomographic model of a pregnant woman," *Health Phys.* **87**, 507-511.
- 7809 Shin, K, Ono, S., Ishibashi, K., Meigo, S., Takada, H., Sasa, N., Nakashima, H., Tanaka, S., Nakao, N.,
7810 Kurosawa, T., Nakamura, N., and Uwamino, Y. (1997). "Thick target yield measurements in
7811 Tiara, KEK and HIMAC," in *Proc. Shielding Aspects of Accelerators, Targets and Irradiation
7812 Facilities (SATIF-3)*, 12-13 May 1997, Tohoko University, Sendai, Japan (Nuclear Energy
7813 Agency, Organization for Economic Co-operation and Development, Paris).
- 7814 Shin, M., Ueki, K., Kurita, H., and Kirino, T. (2002). "Malignant transformation of a vestibular
7815 schwannoma after gamma knife radiosurgery," *Lancet* **360**, 309-310.

- 7816 Siebers, J.V. (1990). "Shielding Measurements for a 230-MeV Proton Beam," Doctoral Thesis,
7817 Department of Med. Phys. (University of Wisconsin, Madison, WI).
- 7818 Siebers, J.V., DeLuca, P.M., Pearson, D.W., and Coutrakon, G. (1992). "Measurement of Neutron Dose
7819 Equivalent and Penetration in Concrete for 230 MeV Proton Bombardment of Al, Fe and Pb
7820 Targets," *Radiat. Prot. Dosim.* **44** (1), 247-251.
- 7821 Siebers, J.V., DeLuca, P.M., Pearson, D.W., and Coutrakon, G. (1993). "Shielding Measurements for
7822 230-MeV Protons," *Nucl. Sci. and Eng.* **115**, 13-23.
- 7823 Sigurdson, A.J., Ronckers, C.M., Mertens, A.C., Stovall, M., Smith, S.A., Liu, Y., Berkow, R.L.,
7824 Hammond, S., Neglia, J.P., Meadows, A.T., Sklar, C.A., Robison, L.L., and Inskip, P.D. (2005).
7825 "Primary thyroid cancer after a first tumour in childhood (the Childhood Cancer Survivor Study):
7826 a nested case-control study," *Lancet* **365**, 2014-2023.
- 7827 Simmons, N.E. and Laws, E.R., Jr. (1998). "Glioma occurrence after sellar irradiation: case report and
7828 review," *Neurosurgery* **42**, 172-178.
- 7829 Sisterson, J.M., Brooks, F.D., Buffler, A. Allie, M.S., Jones, D.T.L., and Chadwick, M.B. (2005). "Cross-
7830 section measurements for neutron-induced reactions in copper at neutron energies of 70.7 and
7831 110.8 MeV," *NIM Phys. Res.* **B240**, 617-624.
- 7832 Slater, J.M, Archambeau, J.O., Miller, D.W., Notarus, M.I., Preston, W., and Slater, J.D. (1991). "The
7833 Proton Treatment Center at Loma Linda University Medical Center: Rationale for and
7834 Description of its Development," *Int. J. Radiat. Oncol. Biol. Phys.* **22**, 383-389.
- 7835 Smith, A.R. (2009). "Vision 20/20: Proton therapy," *Med. Phys.* **36** (2), 556-568.
- 7836 Snyder, W.S., Fisher, H.L., Jr., Ford, M.R., and Warner, G.G. (1969). "Estimates of absorbed fractions
7837 for monoenergetic photon sources uniformly distributed in various organs of a heterogeneous
7838 phantom," *J. Nucl. Med.* **10** (Suppl 3), 7-52.

- 7839 Sobolevsky, N.M. (2008) "Multipurpose hadron transport code SHIELD," <http://www.inr.ru/shield>,
7840 accessed 20 September 2009.
- 7841 Sorge, H. (1995). "Flavor production in Pb (160A GeV.) on Pb collisions: Effect of color ropes and
7842 hadronic rescattering," *Phys. Rev. C* **52**, 3291-3314.
- 7843 Spitzer, V.M. and Whitlock, D.G. (1998). "The Visible Human Dataset: the anatomical platform for
7844 human simulation," *Anat. Rec.* **253**, 49-57.
- 7845 Stabin, M.G., Watson, E., Cristy, M., and *et al.* (1995). "Mathematical models and specific absorbed
7846 fractions of photon energy in the nonpregnant adult female and at the end of each trimester of
7847 pregnancy," **ORNL/TM-12907**.
- 7848 Stabin, M.G., Yoriyaz, H., Brill, A.B., and Dawant, M. (1999). "Monte Carlo calculations of dose
7849 conversion factors for a new generation of dosimetry phantoms," *J. Nucl. Med.* **40**, 310-311.
- 7850 Stapleton, G.B., O'Brien, K., and Thomas, R.H. (1994). "Accelerator skyshine: Tyger, tiger, burning
7851 bright," *Part. Accel.* **44**.
- 7852 Staton, R.J., Pazik, F.D., Nipper, J.C., Williams, J.L., and Bolch, W.E. (2003). "A comparison of
7853 newborn stylized and tomographic models for dose assessment in paediatric radiology," *Phys.*
7854 *Med. Biol.* **48**, 805-820.
- 7855 Stevenson, G.R. (1999). "The shielding of high-energy accelerators," CERN-TIS-99-RP-CF8 (CERN,
7856 Geneva).
- 7857 Stevenson, G.R. (2001). "Shielding high-energy accelerators," *Radiat. Prot. Dosim.* **96**, 359-371.
- 7858 Stevenson, G.R. and Thomas, R.H. (1984). "A simple procedure for the estimation of neutron skyshine
7859 from proton accelerators," *Health Phys.* **46**, 155.
- 7860 Stichelbaut, F., Canon, T., and Yongen, Y. (2009). "Shielding Studies for a Hadron Therapy Center," in
7861 *Proc. of the ICRS-11 International Conference on Radiation Shielding and RPSD-2008 15th*

- 7862 *Topical Meeting of the Radiation Protection and Shielding Division of the ANS, 13-18 April 2008*
7863 (Pine Mountain, Georgia, USA).
- 7864 Stovall, M., Smith, S.A., and Rosenstein, M. (1989). "Tissue doses from radiotherapy of cancer of the
7865 uterine cervix," *Med. Phys.* **16**, 726-733.
- 7866 Stovall, M., Donaldson, S.S., Weathers, R.E., Robison, L.L., Mertens, A.C., Winther, J.F., Olsen, J.H.,
7867 and Boice, J.D., Jr. (2004). "Genetic effects of radiotherapy for childhood cancer: gonadal dose
7868 reconstruction," *Int. J. Radiat. Oncol. Biol. Phys.* **60**, 542-552.
- 7869 Strong, L.C., Herson, J., Osborne, B.M. and Sutow, W.W. (1979). "Risk of radiation-related subsequent
7870 malignant tumors in survivors of Ewing's sarcoma," *J. Natl. Cancer Inst.* **62**, 1401-1406.
- 7871 Suit, H., Goldberg, S., Niemierko, A., Ancukiewicz, M., Hall, E., Goitien, M., Wong, W., and Paganetti,
7872 H. (2007). "Secondary Carcinogenesis in Patients Treated with Radiation: A Review of Data on
7873 Radiation-Induced Cancers in Human, Non-human Primate, Canine and Rodent Subjects,"
7874 *Radiat. Res.* **167**, 12-42.
- 7875 Sullivan, A.H. (1992). *A Guide to Radiation and Radioactivity Levels Near High-Energy Particle*
7876 *Accelerators*, (Nuclear Technology Publishing, Kent, UK).
- 7877 Sutton, M.R., Hertel, N.E., and Waters, L.S. (2000). "A high-energy neutron depth-dose experiment
7878 performed at the LANSCE/WNR facility," pp. 231-240 in *Proc. 5th Meeting of the Task Force*
7879 *on Shielding Aspects of Accelerators, Targets and Irradiation Facilities*, Paris.
- 7880 Taddei, P.J., Fontenot, J.D., Zheng, Y., Mirkovic, D., Lee, A.K., Titt, U., and Newhauser, W.D. (2008).
7881 "Reducing stray radiation dose to patients receiving passively scattered proton radiotherapy for
7882 prostate cancer," *Phys. Med. Biol.* **53** 2131-2147.
- 7883 Taddei, P.J., Mirkovic, D., Fontenot, J.D., Giebeler, A., Zheng, Y., Kornguth, D., Mohan, R., and
7884 Newhauser, W.D. (2009). "Stray radiation dose and second cancer risk for a pediatric patient
7885 receiving craniospinal irradiation with proton beams," *Phys. Med. Biol.* **54**, 2259-2275.

- 7886 Takacs, S., Tarkanyi, F., Hermanne, A., and Paviotti de Corcuera, R. (2003). "Validation and upgrade of
7887 the recommended cross section data of charged particle reactions used for production pet
7888 radioisotopes," *NIM Phys. Res.* **B 211**, 169-189.
- 7889 Tayama, R., Nakano, H., Handa, H., Hayashi, K., Hirayama, H., Shin, K., Masukawa, H., Nakashima,
7890 H., and Sasamoto, N. (2001). "DUCT-III: A simple Design Code for Duct-Streaming
7891 Radiations," KEK Internal Report (Tsukuba, Japan).
- 7892 Tayama, R., Handa, H., Hayashi, H., Nakano, H., Sasmoto, N., Nakashima, H., and Masukawa, F.
7893 (2002). "Benchmark calculations of neutron yields and dose equivalent from thick iron target fro
7894 52-256 MeV protons," *Nucl. Eng. and Design* **213**, 119-131.
- 7895 Tayama, R., Hayashi, K., and Hirayama, H. (2004) "BULK-I Radiation Shielding Tool for Accelerator
7896 Facilities," KEK Internal, Report, NEA-1727/01 (Tsukuba, Japan).
- 7897 Tayama, R., Fujita, Y., Tadokoro, M., Fujimaki, H., Sakae, T., and Terunuma, T. (2006). "Measurement
7898 of neutron dose distribution for apassive scattering nozzle at the Proton Medical Research Center
7899 (PMRC)," *NIM Phys. Res. A.* **564**, 532-536.
- 7900 Teichmann, S. (2002) "Shielding Calculations for Proscan," *PSI – Scientific and Technical Report* **6**, 58-
7901 59.
- 7902 Teichmann, S. (2006). "Shielding Parameters of Concrete and Polyethylene for the PSI Proton
7903 Accelerator Facilities," in *Proc. Shielding Aspects of Accelerators, Targets and Irradiation
7904 Facilities (SATIF 8)*, 22-24 May 2006, Gyongbuk, Republic of Korea (Nuclear Energy Agency,
7905 Organization for Economic Co-operation and Development, Paris).
- 7906 Tesch, K. (1982) "The attenuation of the neutron dose equivalent in a labyrinth through an accelerator
7907 shield," *Part. Accel.*, **12 (N 3)**, 169-175.
- 7908 Tesch, K. (1985). "A simple estimation of the lateral shielding for proton accelerators in the energy range
7909 50 to 1000 MeV," *Radiat. Prot. Dosim.* **11(3)**, 165-172.

- 7910 Theis, C., Buchegger, K.,H., Brugger, M., Forkel-Wirth, D., Roesler, S., and Vincke, H., (2006).
7911 “Interactive three dimensional visualization and creation of geometries for Monte Carlo
7912 calculations,” *NIM Phys. Res. A* **562**, 827-829, <http://theis.web.cern.ch/theis/simplegeo/>, accessed
7913 20 September 2009.
- 7914 Thomas, R.H. (1993). “Practical Aspects of Shielding High-Energy Particle Accelerators,” Report
7915 UCRL-JC-115068 (U.S. Department of Energy, Washington DC).
- 7916 Titt, U., and Newhauser, W.D. (2005). “Neutron shielding calculations in a proton therapy facility based
7917 on Monte Carlo simulations and analytical models: criterion for selecting the method of choice,”
7918 *Radiat. Prot. Dosim.* **115**, 144–148.
- 7919 Tsoulfanidis, N. (1995). *Measurement and Detection of Radiation*, (Hemisphere Publishing, Washington,
7920 D.C.)
- 7921 Tsui, B.M.W., Zhao, X.D., Gregoriou, G.K., and *et al.* (1994). "Quantitative cardiac SPECT
7922 reconstruction with reduced image degradation due to patient anatomy," *IEEE Transactions in*
7923 *Nuclear Science* **41**, 2838-2844.
- 7924 Tubiana, M. (2005). "Dose-effect relationship and estimation of the carcinogenic effects of low doses of
7925 ionizing radiation: the joint report of the Academie des Sciences (Paris) and of the Academie
7926 Nationale de Medecine," *Int. J. Radiat. Oncol. Biol. Phys.* **63**, 317-319.
- 7927 Tubiana, M. (2009). "Can we reduce the incidence of second primary malignancies occurring after
7928 radiotherapy? A critical review," *Radiother. Oncol.* **91**, 4-15, discussion 1-3.
- 7929 Tubiana, M., Feinendegen, L.E., Yang, C., and Kaminski, J.M. (2009). "The linear no-threshold
7930 relationship is inconsistent with radiation biologic and experimental data," *Radiology* **251**, 13-22.
- 7931 Tucker, M.A., Meadows, A.T., Boice, J.D., Jr., and *et al.* (1984). "Cancer risk following treatment of
7932 childhood cancer," *Radiation carcinogenesis: Epidemiology and biological significance*. Boice,
7933 J.D., Jr., and Fraumeni, J.F., Jr., Eds. 211-224.

- 7934 Tucker, M.A., D'Angio, G.J., Boice, J.D., Jr., Strong, L.C., Li, F.P., Stovall, M., Stone, B.J., Green,
7935 D.M., Lombardi, F., Newton, W., and *et al.* (1987). "Bone sarcomas linked to radiotherapy and
7936 chemotherapy in children," *N. Engl. J. Med.* **317** 588-593.
- 7937 Tujii, H., Akagi, T., Akahane, K., Uwamino, Y., Ono, T., Kanai, T., Kohno, R., Sakae, T., Shimizu, M.,
7938 Urakabe, E., Nakayama, T., Nakamura, T., Nishio, T., Nishizawa, Ka., Nishizawa, Ku., Fukuda,
7939 S., Matsufuji, N., Yamashita, H., and Yonai, S. (2009). "Research on radiation protection in the
7940 application of new technologies for proton and heavy ion radiotherapy," *Jpn., J. Med. Phys.*, **28**,
7941 172-206.
- 7942 Turner, J.E. (1986). *Atoms, Radiation, and Radiation Protection*, (Pergamon Press, New York).
- 7943 Ueno, A.M., Vannais, D.B., Gustafson, D.L., Wong, J.C., and Waldren, C.A. (1996). "A low, adaptive
7944 dose of gamma-rays reduced the number and altered the spectrum of S1-mutants in human-
7945 hamster hybrid AL cells," *Mutat. Res.* **358**, 161-169.
- 7946 Ullrich, R.L. (1980). "Effects of split doses of x rays or neutrons on lung tumor formation in RFM mice,"
7947 *Radiat. Res.* **83**, 138-145.
- 7948 Ullrich, R.L. and Davis, C.M. (1999). "Radiation-induced cytogenetic instability in vivo," *Radiat. Res.*
7949 **152**, 170-173.
- 7950 Ullrich, R.L., Jernigan, M.C., Satterfield, L.C., and Bowles, N.D. (1987). "Radiation carcinogenesis:
7951 time-dose relationships," *Radiat. Res.* **111**, 179-184.
- 7952 Upton, A.C. (2001). "Radiation hormesis: data and interpretations," *Crit. Rev. Toxicol.* **31**, 681-695.
- 7953 USNRC (2009). United States Nuclear Regulatory Commission, *Standards for Protection Against*
7954 *Radiation 10CFR20, Code of Federal Regulations*, [www.nrc.gov/reading-rm/doc-](http://www.nrc.gov/reading-rm/doc-collections/cfr/part020/)
7955 [collections/cfr/part020/](http://www.nrc.gov/reading-rm/doc-collections/cfr/part020/), accessed 18 September 2009.
- 7956 Uwamino, Y. (2007) personal communication, RIKEN, Safety Management Group (RIKEN, Japan).

- 7957 Uwamino, Y. and Nakamura, T. (1985). "Two types of multi-moderator neutron spectrometers: gamma-
7958 ray insensitive type and high-efficiency type," *NIM Phys. Res.* **A239**, 299-309.
- 7959 Uwamino, Y., Fujita, S., Sakamoto, H., Ito, S., Fukunishi, N., Yabutani, T., Yamano, T., and Fukumura,
7960 A. (2005). "Radiation protection system at the Riken RI Beam Factory," *Radiat. Prot. Dosim.*,
7961 **115**, 279-283.
- 7962 van Leeuwen, F.E. and Travis, L.B. (2005). "Second cancers," *Cancer: Principles and practice of*
7963 *oncology, 7th edition*. Devita, V.T. *et al.* (Eds.) 2575-2602.
- 7964 Verellen, D. and Vanhavere, F. (1999). "Risk assessment of radiation-induced malignancies based on
7965 whole-body equivalent dose estimates for IMRT treatment in the head and neck region,"
7966 *Radiother. Oncol.* **53**, 199-203.
- 7967 Vlachoudis, V., (2009). "FLAIR: FLUKA Advanced Interface," <http://www.fluka.org/flair/>, accessed 20
7968 September 2009.
- 7969 Wang, Q.B., Masumoto, K., Bessho, K., Matsumura, H., Miura, T., and Shibata, T. (2004). "Tritium
7970 activity induced in the accelerator building and its correlation to radioactivity of gamma-
7971 nuclides," *Journal of Radioanalytical and Nuclear Chemistry*, **262**, 587-592.
- 7972 Weber, U. (2007). "The Particle Therapy Centre of Rhön Klinikum AG at the University Hospital
7973 Marburg," pp. 242-243 in *Ion Beams in Biology and Medicine, 39. Annual Conference of the*
7974 *German-Swiss Association for Radiation Protection and 11th Workshop of Heavy Charged*
7975 *Particles in Biology and Medicine* (IRPA Fachverband für Strahlenschutz, Switzerland and
7976 Germany).
- 7977 White, R.G., Raabe, O.G., Culbertson, M.R., Parks, N.J., Samuels, S.J., and Rosenblatt, L.S. (1993).
7978 "Bone sarcoma characteristics and distribution in beagles fed strontium-90," *Radiat. Res.* **136**,
7979 178-189.

- 7980 Wiegel, B. and Alevra, A.V. (2002). "NEMUS – the PTB neutron multisphere spectrometer: Bonner
7981 spheres and more," *NIM Phys. Res.* **A476**, 36-41.
- 7982 Wolff, S. (1998). "The adaptive response in radiobiology: evolving insights and implications," *Environ.*
7983 *Health Perspect.* **106 (Suppl 1)**, 277-283.
- 7984 Wood, D.H. (1991). "Long-term mortality and cancer risk in irradiated rhesus monkeys," *Radiat. Res.*
7985 **126**, 132-140.
- 7986 Wroe, A., Rosenfeld, A., and Schulte, R. (2007). "Out-of-field dose equivalents delivered by proton
7987 therapy of prostate cancer," *Med. Phys.* **34**, 3449-3456.
- 7988 Wroe, A., Clasio, B., Kooy, H., Flanz, J., Schulte, R., and Rosenfeld, A. (2009). "Out-of-field dose
7989 equivalents delivered by passively scattered therapeutic proton beams for clinically relevant field
7990 configurations," *Int. J. Radiat. Oncol. Biol. Phys.* **73**, 306-313.
- 7991 Xu, X.G., Chao, T.C., and Bozkurt, A. (2000). "VIP-MAN: an image-based whole-body adult male
7992 model constructed from color photographs of the Visible Human Project for multi-particle Monte
7993 Carlo calculations," *Health Phys.* **78**, 476-485.
- 7994 Xu, X.G., Chao, T.C., and Bozkurt, A. (2005). "Comparison of effective doses from various
7995 monoenergetic particles based on the stylised and the VIP-Man tomographic models," *Radiat.*
7996 *Prot. Dosim.* **115**, 530-535.
- 7997 Xu, X.G., Taranenko, V., Zhang, J., and Shi, C. (2007). "A boundary-representation method for
7998 designing whole-body radiation dosimetry models: pregnant females at the ends of three
7999 gestational periods—RPI-P3, -P6 and -P9," *Phys. Med. Biol.* **52**, 7023-7044.
- 8000 Xu, X.G., Bednarz, B., and Paganetti, H. (2008). "A Review of Dosimetry Studies on External-Beam
8001 Radiation Treatment with Respect to Second Cancer Induction," *Phys. Med. Biol.* **53**, R193-
8002 R241.

- 8003 Yan, X., Titt, U., Koehler, A.M., and Newhauser, W.D. (2002). "Measurement of neutron dose
8004 equivalent to proton therapy patients outside of the proton radiation field," *NIM Phys. Res. A* **476**,
8005 429-434.
- 8006 Yashima, H., Uwamino, Y., Sugita, H., Nakamura, T., Ito, S., and Fukumura, A. (2002). "Projectile
8007 dependence of radioactive spallation products induced in copper by high-energy heavy ions,"
8008 *Phys. Rev. C* **66**, 044607-1 to 11.
- 8009 Yashima, H., Uwamino, Y., Iwase, H., Sugita, H., Nakamura, T., Ito, S., and Fukumura, A. (2003).
8010 "Measurement and calculation of radioactivities of spallation products by high-energy heavy
8011 ions," *Radiochim. Acta*, **91**, 689-696.
- 8012 Yashima, H., Uwamino, Y., Iwase, H., Sugita, H., Nakamura, T., Ito, S., and Fukumura, A. (2004a).
8013 "Cross sections for the production of residual nuclides by high-energy heavy ions," *NIM Phys.*
8014 *Res.* **B226**, 243-263.
- 8015 Yashima, H., Uwamino, Y., Sugita, H., Ito, S., Nakamura, T., and Fukumura, A. (2004b). "Induced
8016 radioactivity in Cu targets produced by high-energy heavy ions and the corresponding estimated
8017 photon dose rates," *Radiat. Protec. Dosim.* **112**, 195-208.
- 8018 Yonai, S., Matsufuji, N., Kanai, T., Matsui, Y., Matsushita, K., Yamashita, H., Numano, M., Sakae, T.,
8019 Terunuma, T., Nishio, T., Kohno, R., and Akagi, T. (2008). "Measurement of neutron ambient
8020 dose equivalent in passive carbon-ion and proton radiotherapies," *Med. Phys.* **35**, 4782-4792.
- 8021 Yu, J.S., Yong, W.H., Wilson, D., and Black, K.L. (2000). "Glioblastoma induction after radiosurgery
8022 for meningioma," *Lancet* **356**, 1576-1577.
- 8023 Zacharatou Jarlskog, C. and Paganetti, H. (2008a). "Sensitivity of different dose scoring methods on
8024 organ specific neutron doses calculations in proton therapy," *Phys. Med. Biol.* **53**, 4523-4532.

- 8025 Zacharatou Jarlskog, C. and Paganetti, H. (2008b). "The risk of developing second cancer due to neutron
8026 dose in proton therapy as a function of field characteristics, organ, and patient age," *Int. J. Radiat.*
8027 *Oncol. Biol. Phys.* **69**, 228-235.
- 8028 Zacharatou Jarlskog, C., Lee, C., Bolch, W., Xu, X.G., and Paganetti, H. (2008). "Assessment of organ
8029 specific neutron doses in proton therapy using whole-body age-dependent voxel phantoms,"
8030 *Phys. Med. Biol.* **53**, 693-714.
- 8031 Zaidi, H. and Xu, X.G. (2007). "Computational anthropomorphic models of the human anatomy: the path
8032 to realistic monte carlo modeling in radiological sciences," *Ann. Rev. Biomed. Eng.* **9**, 471-500.
- 8033 Zankl, M., Veit, R., Williams, G., Schneider, K., Fendel, H., Petoussi, N., and Drexler, G. (1988). "The
8034 construction of computer tomographic phantoms and their application in radiology and radiation
8035 protection," *Radiat. Environ. Biophys.* **27**, 153-164.
- 8036 Zhang, G., Liu, Q., Zeng, S., and Luo, Q. (2008). "Organ dose calculations by Monte Carlo modeling of
8037 the updated VCH adult male phantom against idealized external proton exposure," *Phys. Med.*
8038 *Biol.* **53**, 3697-3722.
- 8039 Zheng, Y., Newhauser, W., Fontenot, J., Taddei, P., and Mohan, R. (2007). "Monte Carlo study of
8040 neutron dose equivalent during passive scattering proton therapy," *Phys. Med. Biol.* **52**, 4481-
8041 4496.
- 8042 Zheng, Y., Fontenot, J., Taddei, P., Mirkovic, D., and Newhauser, W. (2008). "Monte Carlo simulations
8043 of neutron spectral fluence, radiation weighting factor and ambient dose equivalent for a
8044 passively scattered proton therapy unit," *Phys. Med. Biol.* **53**, 187-201.
- 8045 Zubal, I.G. and Harell, C.H. (1992). "Voxel based Monte Carlo calculations of nuclear medicine images
8046 and applied variance reduction techniques," *Image and Vision Computing* **10**, 342-348.
8047